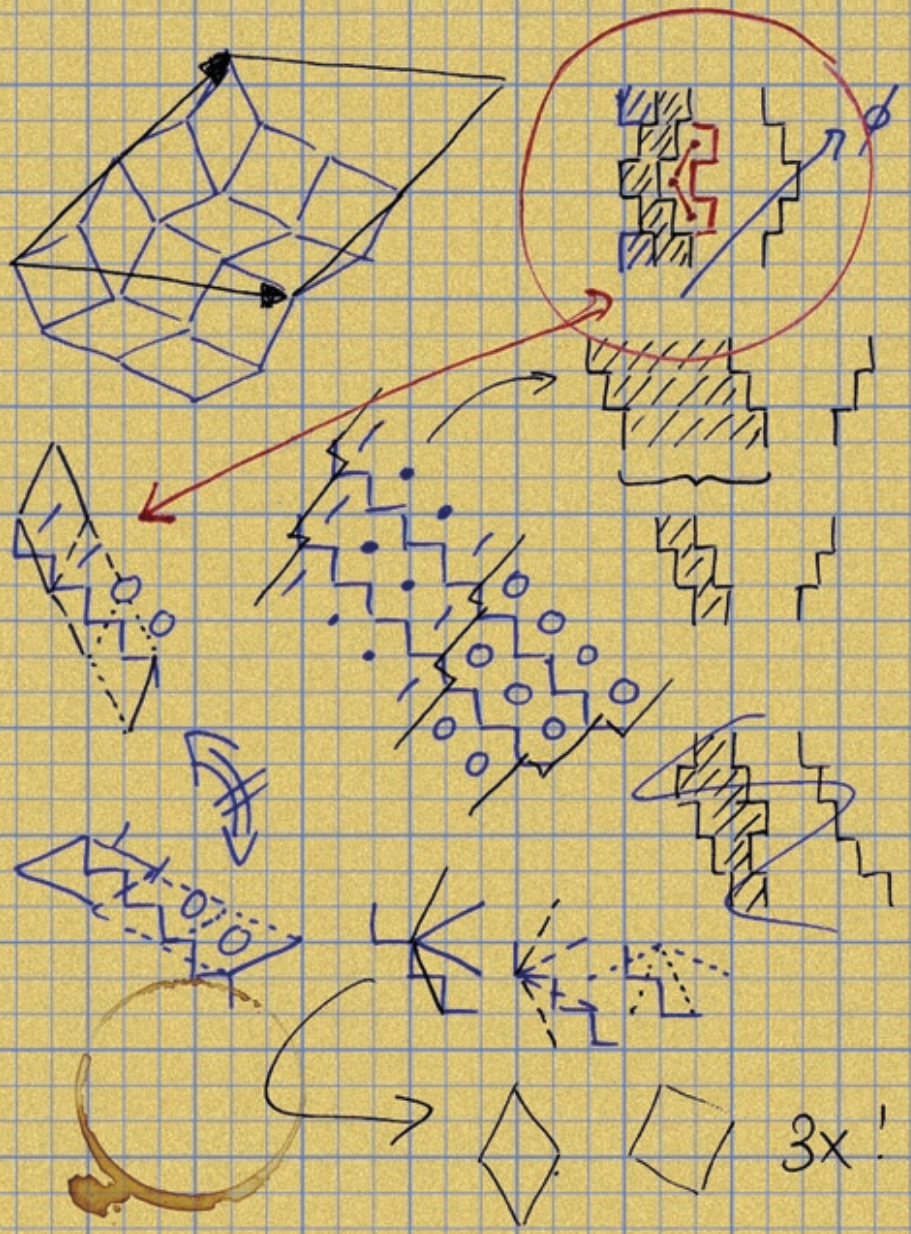


A supersymmetric model for lattice fermions Liza Huijse 2010

# A supersymmetric model for lattice fermions

Liza Huijse

2010

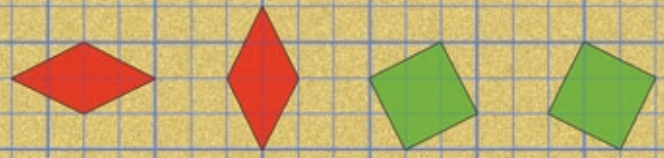

# A supersymmetric model for lattice fermions

# A supersymmetric model for lattice fermions

ACADEMISCH PROEFSCHRIFT

ter verkrijging van de graad van doctor
aan de Universiteit van Amsterdam
op gezag van de Rector Magnificus
prof. dr. D.C. van den Boom
ten overstaan van een door het college voor promoties ingestelde
commissie, in het openbaar te verdedigen in de Agnietenkapel
op vrijdag 18 juni, te 12:00 uur

door

Liza Huijse

geboren te Amsterdam, Nederland

Promotiecommissie:

| | |
|---|---|
| Promotor: | prof. dr. C.J.M. Schoutens |
| Overige leden: | prof. dr. F.A. Bais |
| | prof. dr. J. de Boer |
| | prof. dr. P. Fendley |
| | dr. J. Jonsson |
| | dr. M. Mostovoy |
| | prof. dr. B. Nienhuis |

Faculteit der Natuurwetenschappen, Wiskunde en Informatica

The work described in this thesis was carried out
under supervision of Prof. C.J.M. Schoutens, at the
Instituut voor Theoretische Fysica of the Universiteit van Amsterdam,
Valckenierstraat 65, 1018 XE Amsterdam, The Netherlands,
where a limited number of copies of this thesis is available.
Or: `http://dare.uva.nl`

# Contents

# Chapter 1
# Introduction

## 1.1 Strongly interacting electron systems

The complexity of many-body systems and the richness of the emerging physics makes condensed matter physics a highly inspiring and challenging field. The constituent particles of condensed matter materials, electrons, protons and neutrons, are well-known. They interact via the electro-magnetic Coulomb force and are governed by the laws of quantum mechanics. In principle we can formulate matter in terms of a many-particle hamiltonian describing the interactions of the constituent particles. Nevertheless, it is hopelessly naive to expect that any relevant information about the material can be extracted from this hamiltonian. Instead many a simplification should, and as we shall see, can be made to describe condensed matter materials.
The success of band theory for conventional conductors and insulators, shows that the physics of condensed matter is governed by the valence electrons. The valence electrons feel a lattice potential coming from the attractive interaction with the crystallized ions. Where band theory concerns non-interacting electrons, Landau's Fermi liquid theory [1] enjoys unparalleled success in describing interacting electron systems. In fact, it is said that Fermi liquid theory is unreasonably successful, since despite its perturbative nature it does very well, way outside the perturbative regime. The reason for this lies in *adiabatic continuity* [2], the principle that the quantum numbers that characterize a system are determined by fundamental symmetries. It follows that the physics of the interacting system can be found from a non-interacting system as long as they share the same symmetries. This will typically not be true when the interactions are strong enough to induce a phase transition.
As is well-known, nature presents us with numerous examples of materials in which the quasi-particle excitations have little or nothing to do with the microscopic degrees of freedom (the valence electrons). A beautiful example is the fractional quantum Hall system [3, 4, 5], where the quasi-particles carry a charge which is a fraction of the electron charge. Another famous example of a strongly interacting electron system showing 'non-Fermi liquid' behavior is formed by the high temperature superconductors. Examples of the poorly understood phases present in these systems are the pseudo gap phase [6, 7, 8, 9, 10] and the strange metal phase [11, 12, 13].

## 1.2 The Hubbard model

A widely used simplification in condensed matter physics is to study quantum many-body systems on a lattice. The simplification is motivated by the tight-binding approximation, which describes the valence electrons in a crystal by approximating the electron orbitals around the ions by points located at the positions of the ions in the crystal: the lattice sites. The tight-binding model, which is the simplest lattice model since the electrons are non-interacting, is used in band theory to derive the band structure of conducting solids. This model can be improved by incorporating effects of the electrostatic repulsion

between the electrons. In the Hubbard model this repulsive interaction is approximated by an on-site repulsion assuming that the ions are well separated and the overlap between neighboring orbitals is negligible. The hamiltonian consists of a nearest-neighbor hopping term parameterized by $t$ and an on-site interaction for electrons with opposite spin with interaction strength $U$. Despite its simplicity, the Hubbard model poses theoretical physicists with a challenge for over 40 years. The model is believed to have a rich phase diagram which shows remarkable resemblance with that of the high $T_c$ cuprates.
For low particle density or filling fraction $n$ the inter-particle distance is large and the system is dominated by the kinetic term in the hamiltonian. In this regime, Fermi liquid theory is valid and the Hubbard model is believed to exhibit a metallic phase. For the half-filled system, that is on average one particle per site, with strong interactions $U/t >> 1$, the electrons get jammed, since double occupancy is energetically highly unfavorable. This results in an unconventional insulating phase, known as the Mott insulator. This phase is characterized by an anti-ferromagnetic ordering of the electron spins and is believed to be present in the undoped cuprate systems. Upon doping away from half-filling the anti-ferromagnetic order will be destroyed and the system is found to form stripe-like domains with spin- and charge order [14].
As of today the question whether the rich phenomenology of the cuprates is captured by the Hubbard model remains a subject of debate. The strongly interacting regime at intermediate filling is still a black box. Here both analytic as well as numerical techniques face the challenges posed by the Fermi sign problem. The Fermi statistics of the electrons renders both quantum field theoretical methods as well as quantum Monte-Carlo techniques into trouble. The fact that the Fermi sign problem falls into the class of NP hard problems [15], is a great incentive to propose drastically different approaches to the study of strongly interacting fermion systems (see for example [16, 17]).

## 1.3 Hard-core spinless fermions

Where the Hubbard model is already a dramatic simplification of the true interactions in the system, we now propose an even stronger simplification. Instead of electrons we consider hard-core spinless fermions. By the Pauli exclusion principle double occupancy is forbidden for spinless fermions. This is extended by the hard-core character of the particles, which imposes nearest neighbor exclusion. At low enough densities this system will exhibit a metallic phase described by (spinless) Fermi liquid theory. For this system on the square lattice the half-filled phase, that is one particle on every two sites, is trivial: there are two ordered patterns in which the fermions are completely jammed. However, for small hole-doping there is strong evidence for a stripe phase, where domain walls between the different orders favor being parallel [18, 19, 20]. So even though this system seems to violently oversimplify the problem, it can still exhibit non-trivial physics. Moreover, it has proven to be one of the few higher than $D = 1$ dimensional lattice models for which exact results can be obtained in the strongly interacting regime at intermediate filling [21]. Instrumental for these results was the idea to incorporate supersymmetry in the system [22].
In a remarkable series of work [22, 23, 21] P. Fendley and K. Schoutens together with J. de Boer and B. Nienhuis introduce and investigate a specific model for hard-core spinless fermions (see [24] for a review). They show that by turning on a next-nearest neighbor

repulsive term for the hard-core fermions, the model can be tuned to a supersymmetric point. The supersymmetry turns out to induce a subtle interplay between the kinetic and interaction terms at intermediate filling, leading to quantum criticality in D = 1 and a novel feature, called superfrustration, in D = 2 and D = 3.
Quantum criticality typically refers to a second order phase transition, not due to temperature fluctuations, but caused by quantum fluctuations [25]. Even though a quantum phase transition strictly speaking occurs at absolute zero temperature, it is often accompanied by a line of second order classical phase transitions at low, but non-zero, temperatures. Experiments on the superconducting cuprates [26] and heavy fermion materials [27], have induced a tremendous effort on the theory side, to try and understand the nature of quantum criticality for strongly interacting systems. It is widely believed that the physics of unconventional phases, such as the pseudo gap phase, is dominated by the nearby presence of a quantum critical point. The past decades has seen substantial progress in understanding and classifying quantum criticality in D = 1 [28] and the hard-core spinless fermions at the supersymmetric point nicely fit into this framework.
The phenomenon of frustration in lattice systems is best known in the context of spin degrees of freedom [29], the standard example being the anti-ferromagnet on the triangular lattice. As a result of the competition between different terms in the hamiltonian, the system cannot find one way to minimize its energy, instead the lowest energy state is (highly) degenerate. Although less familiar, frustration can also arise in systems with spinless charge degrees of freedom. An example is given in [30], where spinless fermions on a checkerboard lattice with repulsive interactions are shown to have a ground state degeneracy, exponential in the system size, in the absence of kinetic terms. In [21] P. Fendley and K. Schoutens show that the supersymmetric model on two dimensional lattices exhibits a strong form of quantum charge frustration. The competition between the kinetic and interaction terms in the model leads to an exponential number of quantum ground states, resulting in an extensive ground state entropy. This phenomenon is called superfrustration.

## 1.4 Supersymmetric models for lattice fermions

Supersymmetry has been instrumental in unravelling the properties described above and will also play an important role in this thesis. Supersymmetry is a symmetry between fermionic and bosonic degrees of freedom (see [31] for a general reference). It plays an important role in theoretical high energy physics, where various theories that go beyond the standard model require supersymmetry for a consistent formulation. In these theories all the known elementary particles are accompanied by yet to be discovered superpartners. In the lattice model discussed here the physical particles are spin-less lattice fermions and the supersymmetry relates fermionic and bosonic many particle states with an odd and even number of the lattice fermions respectively. A central role is played by the operators $Q$ and $Q^\dagger$, called supercharges, which have the following properties

- $Q$ adds one fermion to the system and $Q^\dagger$ takes out one fermion from the system.
- The supercharges are fermionic operators and thus nilpotent: $Q^2 = (Q^\dagger)^2 = 0$.
- The hamiltonian is the anti-commutator of the supercharges, $H = \{Q, Q^\dagger\}$, and

as a consequence it commutes with the supercharges and conserves the number of fermions in the system.

Imposing this structure has some immediate consequences for the spectrum. This is illustrated in figure 1.1, where we show the spectrum for the hard-core fermions on a 6-site chain with no interactions, arbitrary next-nearest neighbor interactions and tuned interactions to the supersymmetric point. The key features at the supersymmetric point, which hold by definition are the following. The energy is positive definite, $E > 0$. States with a positive energy are paired into doublets: each state with energy $E > 0$ has a superpartner with the same energy with one fermion less (or more), that is obtained from the original state by acting with $Q^\dagger$ (or $Q$). The unpaired states are annihilated by both supercharges, which implies that they have zero energy. If zero energy states exist, supersymmetry is said to be unbroken.

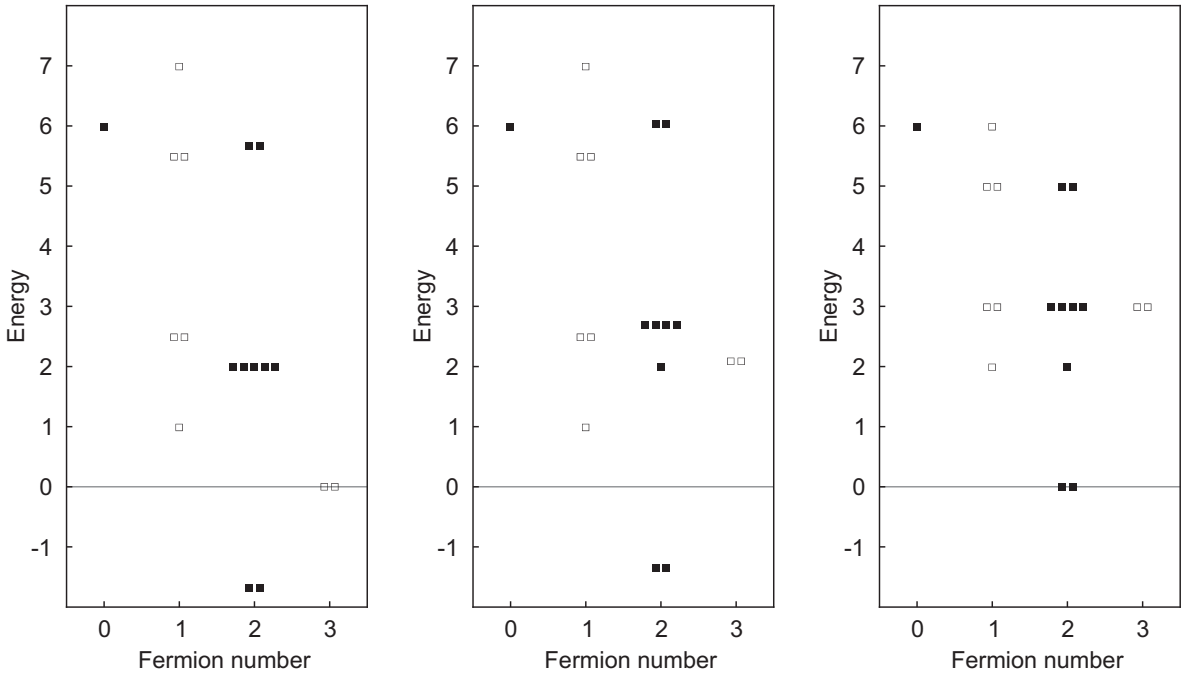


(a) $V_2 = 0$ (b) $t/V_2 = 2.14$ (c) $t/V_2 = 1$

**Figure 1.1:** We show the spectra (energy versus fermion number) for hard-core spinless fermions on a periodic chain with $L = 6$ sites. The filled squares denote bosonic states and the empty squares denote fermionic states. From left to right we show the spectra for the fermions with no next-nearest neighbor interactions ($V_2 = 0$), arbitrary next-nearest neighbor interactions and tuned interactions to the supersymmetric point. At the supersymmetric point $t/V_2 = 1$, there are two $E = 0$ ground states, and every state with energy $E > 0$ and fermion number $f$ can be paired to a state with the same energy $E$ and with fermion number $f \pm 1$.

As was pointed out above, supersymmetric models allow for a certain degree of analytic control. In particular, there are two important tools to study the ground state structure of these models. One is the Witten index [32] which defines a lower bound to the number of zero-energy ground states. Precisely, it is the number of bosonic ground states minus the number of fermionic ground states. This tool is very powerful, because the doublet structure of the positive energy states allows one to compute this index for the lattice

model in a purely combinatorial way. Further analytic control follows from the fact that zero energy ground states are in one-to-one correspondence with elements of the cohomology of the supercharges. Using a spectral sequence technique [33] the cohomology of $Q$ can be obtained analytically for various one and two dimensional lattices. From such computations one obtains the total number of ground states (bosonic plus fermionic) and the number of particles in each ground state.

## 1.5 This thesis

In this thesis we present a follow-up study of the supersymmetric model for hard-core spinless fermions [34, 35]. At the time this project started, a variety of results for the model on one and two dimensional lattices was known [21, 36, 37, 38].
As was mentioned before, in D = 2 the system typically shows superfrustration, leading to an extensive ground state entropy. A heuristic understanding of this frustration was given by the "3-rule" [21]: to minimize the energy, fermions prefer to be mostly 3 sites apart (with details depending on the lattice). For generic two dimensional lattices the 3-rule can be satisfied in an exponential number of ways. This picture was supported by a remarkable relation found by J. Jonsson [39, 37] between zero energy ground states of the supersymmetric model and tilings of the lattice.
One of the main results presented in this thesis, is the proof of an explicit one-to-one relation between the quantum mechanical ground states of the supersymmetric model on the square lattice and certain tilings of that lattice. As we will see, this relation implies that the number of ground states grows exponentially with the linear size of the system, leading to a sub-extensive ground state entropy.
In D = 1 it was shown that the supersymmetric model on the chain is quantum critical, with the low energy continuum limit described by an $\mathcal{N} = (2, 2)$ superconformal field theory. In this thesis we present a detailed study of this system providing further insight in the relation between the lattice model and the continuum theory. In particular, this insight allows us to develop a technique to probe for critical modes in the supersymmetric lattice model on general one dimensional lattices. By applying this analysis to ladder realizations of the square lattice, we find convincing evidence for criticality in these systems.
The main goal of studying ladder models, although interesting in their own right, is to gather insight in the physics of the full two dimensional system. By combining the ground state-tiling relation with our findings for the ladder models, we arrive at a picture in which the tilings not only count the number of ground states, but actually dominate the ground state wavefunctions. This picture allows us to propose the existence of critical edge modes in the supersymmetric model on the two dimensional square lattice with a boundary.

## 1.6 Outline

In chapter 2 we introduce the supersymmetric model in detail. We elaborate on the general properties of the spectrum that follow from imposing supersymmetry and make the relation between the quantum ground states and cohomology elements precise by relating the model to an independence complex. In the next chapter, we briefly summarize some aspects of (super) conformal field theory, necessary for the discussion of criticality in the supersymmetric model on one dimensional lattices. In chapter 4 we present a detailed

discussion of the supersymmetric model for spinless fermions on the one dimensional chain. We give a (complete) overview of known results and the relation of this model to other models, before we move on to an in depth analysis relating the lattice model spectrum and operators to the operator content of the continuum theory.
In chapter 5, we shift gears and discuss the model for two dimensional lattices. Again we aim at giving a more or less complete overview of the known results and important open questions. We close by interpreting the theorem that relates the quantum mechanical ground states of the supersymmetric model on the square lattice to tiling configurations. The proof of the theorem can be found in chapter 6.
In chapter 7 we discuss a variety of ladder models, whose ground state structure is also related to tilings. Employing the spectral flow analysis developed in chapter 4 we present convincing evidence for critical modes in these ladder systems. We continue by presenting analytic results for the ground states of certain ladders and numerical and analytic results on entanglement entropy and one-point functions to support the idea that the tilings not only count the number of ground states, but actually dominate the ground state wavefunctions. Also here, we will discuss various interesting open problems. Finally, we close this thesis with a discussion of the presented results in chapter 8. Apart from a brief summary and interpretation, we also allow ourselves to speculate on a variety of topics, such as the existence of a supertopological phase, characterized by a sub-extensive ground state entropy and edge modes, for certain two dimensional systems and possible bulk criticality for other two dimensional systems, the relation between criticality and the imposed supersymmetry and finally a possible connection between superfrustration and zero temperature entropy of extremal black holes.

# Chapter 2
# A supersymmetric model for lattice fermions

In this chapter we define the supersymmetric model for lattice fermions which was first introduced in [22] and which is the subject of study in this thesis. In the first section, we discuss the general properties of the spectrum of this model that follow from imposing supersymmetry. In section 2.2, we define an independence complex and its cohomology and show how these are related to the Hilbert space and the ground states of the model.

## 2.1 The model

In this section, we first introduce quantum mechanical supersymmetry and derive some basic properties for the spectrum of a supersymmetric theory. We then introduce hard-core lattice fermions and write down the model. Finally, we illustrate the basic properties of this model with a simple example.

### 2.1.1 Supersymmetry

An $\mathcal{N} = 2$ supersymmetric quantum mechanical theory is constructed from a basic algebra, defined by two nilpotent supercharges $Q$ and $Q^\dagger$ (complex conjugation is implied) [32],

$$\{Q, Q\} = \{Q^\dagger, Q^\dagger\} = 0 \tag{2.1}$$

and the hamiltonian given by

$$H = \{Q^\dagger, Q\}. \tag{2.2}$$

It satisfies

$$[H, Q] = [H, Q^\dagger] = 0. \tag{2.3}$$

The eigenvalues and eigenvectors of the hamiltonian give the energy spectrum and the corresponding quantum states. The definition of the hamiltonian has some immediate consequences for the energy spectrum. First of all, it is positive definite:

$$\begin{aligned} \langle\psi|H|\psi\rangle &= \langle\psi|(Q^\dagger Q + QQ^\dagger)|\psi\rangle \\ &= |Q|\psi\rangle|^2 + |Q^\dagger|\psi\rangle|^2 \geq 0 \end{aligned} \tag{2.4}$$

for all choices of the quantum state $|\psi\rangle$. Second of all, the fact that both $Q$ and $Q^\dagger$ commute with the hamiltonian, gives rise to a twofold degeneracy in the energy spectrum. In other words, all eigenstates of the hamiltonian with an energy $E_s > 0$ form doublet representations of the supersymmetry algebra. To see this we first note that due to the

nilpotency of the supercharges the eigenstates of the hamiltonian decompose into quadruplets $(|s'\rangle, Q|s'\rangle, Q^\dagger|s'\rangle, QQ^\dagger|s'\rangle)$ (the state $Q^\dagger Q|s'\rangle$ is not linearly independent, since it can be written as $Q^\dagger Q|s'\rangle = (H - QQ^\dagger)|s'\rangle = E_s|s'\rangle + QQ^\dagger|s'\rangle$). However, this four dimensional representation is reducible. Let us define

$$|s\rangle \equiv |s'\rangle - \frac{1}{E_s} QQ^\dagger|s'\rangle. \tag{2.5}$$

It follows that $Q^\dagger|s\rangle = 0$, so the quadruplet reduces to the doublets $(|s\rangle, Q|s\rangle)$ and $(Q^\dagger|s'\rangle, QQ^\dagger|s'\rangle)$. A doublet thus consists of two states, $|s\rangle$ and $Q|s\rangle$, such that $Q^\dagger|s\rangle = 0$[1]. The states $|s\rangle$ and $Q|s\rangle$ are said to be superpartners. Finally, all states with zero energy must be singlets: $Q|g\rangle = Q^\dagger|g\rangle = 0$ and conversely, all singlets must be zero energy states [32]. In addition to supersymmetry our models will also have a particle-number symmetry generated by the operator $F$ with

$$[F, Q^\dagger] = -Q^\dagger \quad \text{and} \quad [F, Q] = Q. \tag{2.6}$$

Consequently, $F$ commutes with the hamiltonian. Furthermore, this tells us that superpartners differ in their fermion number by one (let $F|s\rangle = f_s|s\rangle$, then $F(Q|s\rangle) = Q(F+1)|s\rangle = (f_s+1)(Q|s\rangle)$).

### 2.1.2 Witten index

An important issue is whether or not supersymmetric ground states at zero energy occur, that is, whether there are singlet representations of the algebra. For this one considers the Witten index [32]

$$W = \mathrm{tr}\left[(-1)^F e^{-\beta H}\right] \ , \tag{2.7}$$

where the trace is over the entire Hilbert space. Remember that all excited states come in doublets with the same energy and differing in their fermion-number by one. This means that in the trace all contributions of excited states will cancel pairwise, and that the only states contributing are the zero energy ground states. We can thus evaluate $W$ in the limit of $\beta \to 0$, where all states contribute $(-1)^F$. It also follows that $|W|$ is a lower bound to the number of zero energy ground states.

### 2.1.3 Lattice fermions

We now make the model more concrete by defining the supercharges in terms of lattice particles. The particles we will consider are spin-less electrons, also called spin-less fermions. Their key property is that the wavefunction is antisymmetric under the exchange of two fermions. It follows that the operator $c_i^\dagger$ that creates a fermion on site $i$ in the lattice and the operator $c_j$ that annihilates a fermion on site $j$ in the lattice, satisfy the following anti-commutation relations:

$$\{c_i^\dagger, c_j\} = \delta_{ij}$$
$$\{c_i, c_j\} = \{c_i^\dagger, c_j^\dagger\} = 0.$$

[1] Note that the choice $(|s\rangle, Q^\dagger|s\rangle)$, with $Q|s\rangle = 0$ is completely equivalent.

The particle-number operator for fermions is defined as $F = \sum_i c_i^\dagger c_i$, where the sum is over all lattice sites. This operator counts the total number of particles in a state. A simple choice for the supercharges would be $Q = \sum_i c_i^\dagger$ and $Q^\dagger = \sum_i c_i$. It is readily verified that both obey the nilpotency condition and that the commutation relations with $F$ (2.6) are satisfied. However, this choice leads to a trivial hamiltonian: $H = L$, where $L$ is the total number of sites of the lattice. To obtain a non-trivial hamiltonian, we dress the fermion with a projection operator: $P_{<i>} = \prod_{j \text{ next to } i}(1 - c_j^\dagger c_j)$, which requires all sites adjacent to site $i$ to be empty. We can now formulate the supercharges in terms of these hard-core fermions: $Q = \sum c_i^\dagger P_{<i>}$ and $Q^\dagger = \sum c_i P_{<i>}$. Again the nilpotency condition and the commutation relations (2.6) are satisfied, but now the hamiltonian of these hard-core fermions reads

$$H = \{Q^\dagger, Q\} = \sum_i \sum_{j \text{ next to } i} P_{<i>} c_i^\dagger c_j P_{<j>} + \sum_i P_{<i>}.$$

The first term is a nearest neighbor hopping term, that is, the fermions can hop from site $j$ to site $i$ as long as $i$ and $j$ are connected by an edge and provided that the neighboring sites are empty. The second term contains a next-nearest neighbor repulsion, a chemical potential and a constant. The details of the latter terms will depend on the lattice we choose.
Note that all the parameters in the hamiltonian (the hopping $t$, the nearest neighbor repulsion $V_1$, the next-nearest neighbor repulsion $V_2$ and the chemical potential $\mu$) are fixed by the choice of the supercharges and the requirement of supersymmetry and eventually the lattice.

### 2.1.4 Example: 6-site chain

Let us consider as an example of all the above, the chain of six sites with periodic boundary conditions. The first thing we note is that the hamiltonian for an $L$-site chain with periodic boundary conditions can be rewritten in the following form:

$$H = H_{\text{kin}} + H_{\text{pot}}, \tag{2.8}$$

where

$$H_{\text{kin}} = \sum_{i=1}^{L} \left[ P_{i-1} \left( c_i^\dagger c_{i+1} + c_{i+1}^\dagger c_i \right) P_{i+2} \right], \tag{2.9}$$

$$\begin{aligned} H_{\text{pot}} &= \sum_{i=1}^{L} P_{i-1} P_{i+1} \\ &= \sum_{i=1}^{L} \left[ 1 - 2n_i + n_i n_{i+2} \right] \\ &= \sum_{i=1}^{L} (n_i n_{i+2}) + L - 2F. \end{aligned}$$

Here $P_i = 1 - n_i$, $n_i = c_i^\dagger c_i$ is the usual number operator and $F = \sum_i n_i$ is the total number of fermions. (We shall denote eigenvalues of this operator by $f$ and write the

fermion density or filling fraction as $\nu = f/L$.) The form of the hamiltonian makes clear that the hopping parameter $t$ is tuned to be equal to the next-nearest neighbor repulsion $V_2$, which is tuned to unity. The nearest neighbor repulsion $V_1$ is by definition infinite and the chemical potential $\mu$ is 2. Finally, there is a constant contribution $L$ to the hamiltonian. Note that the second term in the hamiltonian $H_{\rm pot}$ suggests that the energy is minimized when the hard-core fermions are three sites apart.

Let us consider the possible configurations of the 6-site chain. In addition to the empty state, there are six configurations with one fermion, nine with two fermions and two with three fermions (see Fig. 2.1). Because of the hard-core character of the fermions, half-filling is the maximal density. Clearly, the operator $Q$ gives zero on these maximally filled states. On the other hand, $Q^\dagger$ acts non-trivially on these states, so two of the nine states with two fermions are superpartners of the maximally filled states. The empty state $|0\rangle$ has an energy $E = 6$ and $Q^\dagger|0\rangle = 0$, whereas $Q|0\rangle = \sum_i c_i^\dagger|0\rangle$, so $(|0\rangle, Q|0\rangle)$ make up a doublet. The other five states with one fermion are annihilated by $Q^\dagger$ and $Q$ acts non-trivially on them, so they form supersymmetry doublets with five two-fermion-states. At this point, seven of the nine two-fermion-states are paired up in doublets, either with one- or three-fermion-states. The remaining two states cannot be part of a doublet, which implies that they must be singlet states and thus have zero energy. So we find that the 6-site chain has a twofold degenerate zero energy ground state at filling $\nu = f/L = 1/3$. The full spectrum of the 6-site chain is shown in Fig. 2.1.

We observe that the ground state filling fraction of 1/3 agrees with the expectation that fermions tend to be three sites apart. This geometric rule suggests three possible ground states; in the full quantum theory two are realized as zero-energy states. Note that the actual ground state wavefunctions are superpositions of many different configurations. In particular, the ground states of the 6-site periodic chain can be written as

$$\begin{aligned} |\psi_1\rangle &= |14\rangle - |15\rangle - |24\rangle + 2|25\rangle - |26\rangle - |35\rangle + |36\rangle, \\ |\psi_2\rangle &= -|13\rangle + 3|14\rangle - 2|15\rangle - 2|24\rangle + 3|25\rangle - |26\rangle - |35\rangle + |46\rangle, \end{aligned}$$

where $|ij\rangle \equiv c_i^\dagger c_j^\dagger|0\rangle$ denotes a configuration with sites $i$ and $j$ occupied.

Since the hamiltonian commutes with the fermion number operator $F$ and the translation operator $T$, we can block diagonalize the hamiltonian. In the two particle sector, diagonalizing the translation operator gives $|\phi_k\rangle = \sum_{l=0}^5 t_k^{-l} T^l|13\rangle$, where $t_k = \exp(2\pi\imath k/6)$, with $k = 1, \ldots, 6$ and $|\chi_k\rangle = \sum_{l=0}^5 t_k^{-l} T^l|14\rangle$, where $t_k = \exp(2\pi\imath k/6)$, with $k = 1, 3, 5$. It follows that the hamiltonian reads $H = 3$ in the sectors with $k = 2, 4, 6$ and

$$H = \begin{pmatrix} 3 & \sqrt{2}(1-t^2) \\ \sqrt{2}(1-t^{-2}) & 2 \end{pmatrix}, \tag{2.10}$$

with eigenvalues $E_\pm = (5 \pm \sqrt{17 - 16\cos(2\pi k/3)})/2$. For $k = 3$ this gives $E_+ = 3$ and $E_- = 2$ and for $k = 1$ and $k = 5$ we find $E_+ = 5$ and $E_- = 0$. It follows that the ground states have eigenvalues $\exp(\pm\pi i/3)$ under translation by one site.

Now let us compute the Witten index for this example. Remember that for a supersymmetric theory it simply reads

$$W = \mathrm{tr}(-1)^F. \tag{2.11}$$

Note that we can take any basis of states we like to compute the trace. Above we have specified a basis by considering all the possible configurations of up to three fermions on

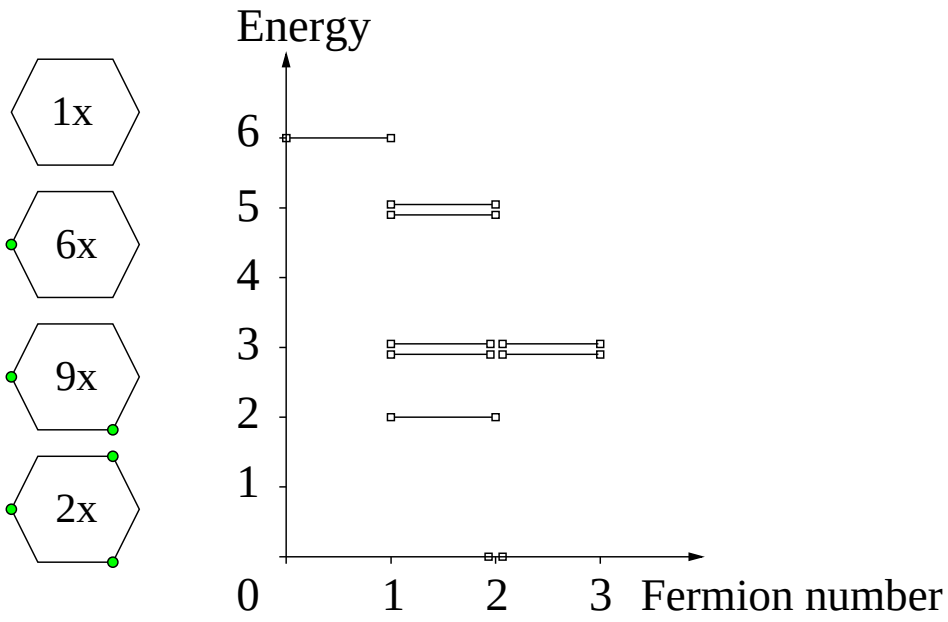


**Figure 2.1:** On the left we show the 6-site chain and the possible configurations of hard-core fermions on this lattice. The numbers give the number of possible configurations with a given number of fermions. On the right we show the spectrum, energy versus fermion number, of the 6-site chain.

the chain. It immediately gives $W = 1 - 6 + 9 - 2 = 2$ in agreement with the existence of the two ground states that we found.

We close this section with two comments. First, we stress that the extremely simple computation of $W$ alone guarantees the existence of at least two ground states at zero energy. Similar results are easily established for much larger systems, where a direct evaluation of the ground state energies is way out of reach, showing the power of supersymmetry. Second, we observe that here the Witten index is exactly equal to the number of ground states. We will encounter examples where ground states exist at more than one fermion number $f$, leading to cancellations in the Witten index so that $|W|$ is strictly smaller than the number of ground states.

## 2.2 Relation to independence complex and (co)homology theory

In this section we define independent sets, an independence complex and its (co)homology. We show that these are related to hard-core fermion configurations, the Hilbert space and the zero energy ground states of the lattice model. These relations have proven to be extremely powerful in the study of the ground state structure of the lattice model. Central in these studies is the 'tic-tac-toe' lemma of [33]. This technique will be illustrated at the end of this section in a few simple examples.

### 2.2.1 Independence complex

An independent set on a graph is a subset of the vertex set of the graph with the property that no two vertices are adjacent. Since hard-core fermions cannot occupy adjacent sites, it is clear that each allowed configuration of hard-core fermions forms an independent set. In the following we will use the term lattice (i.e. a grid) instead of the more general term graph, since in the physics context it is most natural to study fermions on a lattice. However, the correspondences we establish in this section hold for graphs in general. The family of independent sets of a lattice forms the independence complex $\Sigma$ of the lattice. We can define the partition sum in the asymptotic (thermodynamic) limit for the independence complex $\Sigma$ as

$$Z(\Sigma, z) \equiv \sum_{\sigma \in \Sigma} z^{|\sigma|}, \tag{2.12}$$

where $z$ is called the activity. Until recently there were essentially no exact results for independence complexes on two dimensional lattices, with one important exception. Baxter [40] gave an analytic expression for the partition sum of the independence complex on the triangular lattice with positive activity in the thermodynamic limit. This is also referred to as the exact solution for hard hexagons (hard-core fermions on the triangular lattice can, in this context, be viewed as hexagons that share, at most, a side or a corner).
Now observe that the coefficient of $z^k$ in (2.12) is the number of sets in $\Sigma$ with size $k$ or, in other words, the number of configurations with $k$ hard-core fermions. Consequently, $Z(\Sigma, 1)$ gives the dimension of the full Hilbert space $\mathcal{H}$; the space spanned by all possible hard-core fermion configurations. What is even more interesting, however, is that $Z(\Sigma, -1)$ coincides with the Witten index (2.7)

$$Z(\Sigma, -1) = \sum_{\sigma \in \Sigma} (-1)^{|\sigma|} = \mathrm{tr}(-1)^F.$$

### 2.2.2 Cohomology and homology theory

It should be clear from the previous that the Hilbert space is a graded vector space, where the grading is defined by the particle-number operator $F$. That is, the Hilbert space can be written as $\mathcal{H} = \oplus C_n$, where $C_n$ is a subspace spanned by all the possible configurations with $n$ particles. From the definitions of $F$ and $Q$ and their commutation relations (2.6) it is clear that $Q$ is a map from $C_n$ to $C_{n+1}$. Since $Q$ squares to zero, we can define its cohomology. On the other hand, $Q^\dagger$ is a map from $C_n$ to $C_{n-1}$ and also nilpotent, so we can define the homology of $Q^\dagger$.

$$C_0 \underset{Q^\dagger}{\overset{Q}{\rightleftarrows}} C_1 \underset{Q^\dagger}{\overset{Q}{\rightleftarrows}} C_2 \underset{Q^\dagger}{\overset{Q}{\rightleftarrows}} C_3 \dots$$

It turns out that the zero energy ground states of the model are in one-to-one correspondence with the non-trivial classes of the cohomology of $Q$ and the homology of $Q^\dagger$. Remember that all states with zero energy must be singlets: $Q|g\rangle = Q^\dagger|g\rangle = 0$ and conversely, all singlets must be zero energy states. Clearly, all singlets, and thus all (zero

energy) ground states, are in the kernel of $Q$: $Q|g\rangle = 0$ and not in the image of $Q$, because if we could write $|g\rangle = Q|f\rangle$, then $(|f\rangle, |g\rangle)$, would be a doublet. Equivalently, we can say that a ground state with $n$ fermions is a cycle but not a boundary in $C_n$. This is precisely the definition of an element of the $n$-th cohomology of $Q$, $H_Q^{(n)} = \ker Q/\mathrm{Im}\ Q$ within $C_n$. Two states $|s_1\rangle$ and $|s_2\rangle$ are said to be in the same cohomology-class if $|s_1\rangle = |s_2\rangle + Q|s_3\rangle$ for some state $|s_3\rangle$. Since a ground state is annihilated by both $Q$ and $Q^\dagger$, different (i.e. linearly independent) ground states must be in different cohomology-classes[2] of $Q$. Finally, the number of independent ground states is precisely the dimension of the cohomology of $Q$ and the fermion-number of a ground state is the same as the grade of the corresponding cohomology-class. Thus the ground states of a supersymmetric theory are in one-to-one correspondence with the cohomology of $Q$. With the same line of reasoning we may also conclude that the ground states are in one-to-one correspondence with the homology of $Q^\dagger$. Finally, the Euler characteristic, defined in cohomology theory as

$$\chi \equiv \sum_n \left[(-1)^n \mathrm{dim} H_Q^{(n)}\right],$$

is precisely the Witten index.

### 2.2.3 The 'tic-tac-toe' lemma

Central to the computation of the cohomology of $Q$ for the lattice models presented in this thesis is the 'tic-tac-toe' lemma of [33]. Let us decompose the lattice $S$ into two sublattices $S_1$ and $S_2 = S \setminus S_1$ and we write $Q = Q_1 + Q_2$, where $Q_1$ and $Q_2$ act on $S_1$ and $S_2$ respectively. We can then consider the double complex $\oplus_n C_n = \oplus_n \oplus_{p+q=n} K_{p,q}$, where $p$ ($q$) is the size of the vertex set on $S_1$ ($S_2$). Equivalently, if we define $f_i$ as the number of particles on $S_i$, we have $f_1 = p$ and $f_2 = q$. Finally, we have $Q_1 : K_{p,q} \to K_{p+1,q}$ and $Q_2 : K_{p,q} \to K_{p,q+1}$. The 'tic-tac-toe' lemma now tells us that the cohomology of $Q$, $H_Q$, is the same as the cohomology of $Q_1$ acting on the cohomology of $Q_2$, i.e. $H_Q = H_{Q_1}(H_{Q_2}) \equiv H_{12}$, provided that $H_{12}$ has entries only in one row. That is, $H_{12}$ is non-vanishing only for one value of $q$ (or $f_2$). So a sufficient condition for the lemma to hold is that all non-trivial elements of $H_{12}$ have the same $f_2$ (the fermion-number on $S_2$).

$$\begin{array}{ccccccc}
\vdots & & \vdots & & \vdots & & \\
\uparrow Q_2 & & \uparrow Q_2 & & \uparrow Q_2 & & \\
K_{0,2} & \xrightarrow{Q_1} & K_{1,2} & \xrightarrow{Q_1} & K_{2,2} & \xrightarrow{Q_1} & \cdots \\
\uparrow Q_2 & & \uparrow Q_2 & & \uparrow Q_2 & & \\
K_{0,1} & \xrightarrow{Q_1} & K_{1,1} & \xrightarrow{Q_1} & K_{2,1} & \xrightarrow{Q_1} & \cdots \\
\uparrow Q_2 & & \uparrow Q_2 & & \uparrow Q_2 & & \\
K_{0,0} & \xrightarrow{Q_1} & K_{1,0} & \xrightarrow{Q_1} & K_{2,0} & \xrightarrow{Q_1} & \cdots
\end{array}$$

[2] Let $|s_1\rangle$ and $|s_2\rangle$ be two linearly independent ground states. It follows that $Q|s_1\rangle = Q|s_2\rangle = Q^\dagger|s_1\rangle = Q^\dagger|s_2\rangle = 0$. If we now write $|s_1\rangle = |s_2\rangle + Q|s_3\rangle$, we find that $Q^\dagger|s_1\rangle = Q^\dagger|s_2\rangle + Q^\dagger Q|s_3\rangle$ and thus $Q^\dagger Q|s_3\rangle = 0$. From this we find $\langle s_3|Q^\dagger Q|s_3\rangle = |Q|s_3\rangle|^2 = 0$ and thus $Q|s_3\rangle = 0$. With this we obtain $|s_1\rangle = |s_2\rangle$, which contradicts our assumption that $|s_1\rangle$ and $|s_2\rangle$ are linearly independent, so we conclude that $|s_1\rangle$ and $|s_2\rangle$ must be in different cohomology classes.

### 2.2.4 Examples: 6-site periodic and 4-site open chain

As an example we compute the cohomology of the 6-site periodic and 4-site open chain. The first example is relatively simple: We will find that the non-trivial elements in the cohomology $H_{12}$ will all have the same number of fermions on the sublattice $S_2$. This is a sufficient condition for the 'tic-tac-toe' lemma to hold, that is, we directly find the full cohomology $H_Q = H_{12}$. In the second example this condition will not be satisfied. However, with some extra work one can still obtain the full cohomology from $H_{12}$. In particular we will see that $H_Q$ is contained in $H_{12}$, but they are not equal.
For the 6-site chain we choose sites 3 and 6 as sublattice $S_2$ and the rest as sublattice $S_1$. We now consider $H_{Q_2}$. If both sites next to site 3 are empty, $H_{Q_2}$ is trivial: $Q_2$ acting on the empty site 3 does not vanish, while the filled site 3 is $Q_2$ acting on the empty site. The same holds for site 6 independently. It follows that the only non-trivial elements of $H_{Q_2}$ have at least one site next to site 3 and one site next to site 6 occupied. There are only 2 such configurations: the one with site 2 and 5 occupied and the one with site 4 and 1 occupied. Both states belong to $H_{12}$: they are closed because $Q_1$ gives zero on them, and not exact because there are no elements in $H_{Q_2}$ with 1 fermion. By the tic-tac-toe lemma, there must be precisely two different cohomology classes in $H_Q$, and therefore exactly two ground states with $f = 2$.
We now consider the 4-site chain with open boundary conditions chain as a simple example of the case where $H_Q$ is contained in $H_{12}$ but not exactly equal to it. Take site 2 and 3 as the sublattice $S_2$. This is a 2-site chain and it is easily verified that it has one ground state with one particle (the state $|2\rangle - |3\rangle$, where $|i\rangle$ is the configuration with the $i$-th site occupied). Solving $H_{Q_2}$ thus gives two configurations: the one with site 1 and 4 empty and the configuration $|2\rangle - |3\rangle$ on $S_2$ and the one with both sites 1 and 4 occupied and $S_2$ empty.
Now, *within* $H_{Q_2}$, $Q_1$ gives zero on both configurations, so they are both closed and consequently not exact. So we find two different cohomology classes in $H_{12}$. However, their particle number on $S_2$ differs and thus $H_Q = H_{12}$ does not necessarily hold. That is, within $H_{12}$, there may be configurations that are not in the kernel of $Q$ and there may be configurations that are in the image of $Q$. To check this we must perform the tic-tac-toe procedure. We start from the configuration with sites 1 and 4 empty. We act on this configuration with $Q$ without restricting ourselves to $H_{Q_2}$. We find the following: $Q(|2\rangle - |3\rangle) = Q_1(|2\rangle - |3\rangle) = -|24\rangle - |13\rangle$. Remember that the fermionic creation operators anticommute, hence $|42\rangle = -|24\rangle$. Now since $H_{Q_2}$ was empty at $f_1 = f_2 = 1$ and the newly obtained state belongs to the kernel of $Q_2$, it must also belong to the image of $Q_2$. Indeed we can write $-|24\rangle - |13\rangle = Q_2(-|4\rangle + |1\rangle)$. So we find that $(|2\rangle - |3\rangle)$ does not belong to the kernel of $Q$, but maybe $(|2\rangle - |3\rangle) - (-|4\rangle + |1\rangle)$ does. Let us check this:

$$\begin{aligned} Q(|2\rangle - |3\rangle + |4\rangle - |1\rangle) &= Q_1(|2\rangle - |3\rangle) - Q_2(-|4\rangle + |1\rangle) - Q_1(-|4\rangle + |1\rangle) \\ &= -Q_1(-|4\rangle + |1\rangle) \\ &= -(-|14\rangle - |14\rangle) = 2|14\rangle. \end{aligned}$$

Remember that $|14\rangle$ also belongs to $H_{12}$. Thus we have found that none of the elements in $H_{12}$ belong to $H_Q$, since $|2\rangle - |3\rangle$ is not closed and $|14\rangle$ is exact. Thus we have found that the number of ground states on the 4-site open chain is zero. It can be shown that this result generalizes to all open chains with length $3s + 1$.

# Chapter 3
# Superconformal field theory

## 3.1 Continuum theory

Identifying critical behavior in the supersymmetric lattice models is an important part of this thesis. Since the models we describe in this thesis have an exact supersymmetry by definition, this property will persist in the continuum limit. For quantum critical lattice models the continuum limit typically exhibits conformal invariance. This can roughly be understood from the fact that a critical lattice model has no scale except for the lattice spacing. At a critical point the gap or mass vanishes or, equivalently, the correlation length diverges. Upon sending the lattice spacing to zero in the continuum limit the conformal invariance emerges. Consequently, one expects the continuum limit of a *supersymmetric, quantum critical* lattice model to be described by a supersymmetric conformal field theory (SCFT). For various (quasi) one dimensional systems we compare the properties of finite size systems to the properties one expects for a system that is described by a supersymmetric conformal field theory in the continuum limit.
In this chapter we briefly introduce supersymmetric conformal field theory (for a nice review see [41]), where we will emphasize that it is an extension of the more familiar conformal field theory [42].

## 3.2 Conformal field theory

A conformal field theory is a theory that is invariant under the conformal transformations: translations, rotations, scale transformations and the so-called special conformal transformations. These transformations are generated by the stress-energy tensor $T$. Restricting the discussion to $d = 2$ dimensions, the holomorphic and anti-holomorphic parts of the stress-energy tensor have the following operator product expansions (OPE) on the complex plane:

$$\begin{aligned} T(z)T(w) &= \frac{c/2}{(z-w)^4} + \frac{2}{(z-w)^2}T(w) + \frac{1}{(z-w)}\partial T(w) + \dots \\ \overline{T}(\overline{z})\overline{T}(\overline{w}) &= \frac{c/2}{(\overline{z}-\overline{w})^4} + \frac{2}{(\overline{z}-\overline{w})^2}\overline{T}(\overline{w}) + \frac{1}{(\overline{z}-\overline{w})}\overline{\partial T}(\overline{w}) + \dots \end{aligned}$$

here $c$ is the central charge or conformal anomaly of the theory. As usual in OPEs, we indicated the terms that are finite in the limit that $z \to w$ by $+\dots$. In the following we will restrict the discussion to the holomorphic part of the theory and assume that the anti-holomorphic sector has a structure directly parallel to the holomorphic sector. The stress-energy tensor is a quasi-primary field of conformal dimension 2 and its mode expansion reads

$$T(z) = \sum_{n=-\infty}^{\infty} L_n z^{-n-2}.$$

From the OPE and the mode expansion one derives the following commutation relations

$$[L_m, L_n] = (m-n)L_{m+n} + \frac{1}{12}c(m^3 - m)\delta_{m+n,0}. \tag{3.1}$$

This is called the Virasoro algebra and the modes, $L_m$, are called the Virasoro generators. Representations of the Virasoro algebra are given by highest weight states defined by primary fields and their descendants. A primary field $\phi(z)$ of conformal dimension $h$ is a field that under the transformation $z \to f(z)$, transforms as

$$\phi(z) \to \Big(\frac{\partial f(z)}{\partial z}\Big)^h \phi(f(z)). \tag{3.2}$$

Its OPE with the stress-energy tensor reads

$$T(z)\phi(w) \;=\; \frac{h}{(z-w)^2}\phi(w) + \frac{1}{(z-w)}\partial\phi(w) + \dots \tag{3.3}$$

If we define the vacuum as the state that has $L_m|0\rangle = 0$ for $m \geq -1$, then the state $|h\rangle = \phi(0)|0\rangle$ created from the vacuum by this primary field is called a highest weight state. It satisfies

$$L_0|h\rangle = h|h\rangle \quad L_m|h\rangle = 0,\ m > 0. \tag{3.4}$$

The descendants of the highest weight state are generated by the Virasoro generators $L_m$ with $m < 0$. Since $L_0 + \overline{L}_0$ generates translations, the eigenvalue of $L_0$ is related to the energy of the state. From the Virasoro algebra it follows that the highest weight state has the lowest energy and the descendant states form a so-called tower of higher energy states.

## 3.3 $\mathcal{N} = 2$ Superconformal field theory

In an $\mathcal{N} = 2$ superconformal field theory [43, 44] there are three generators besides the stress-energy tensor: two supercharges, $G^+(z)$ and $G^-(z)$ , and a $U(1)$ current, $J(z)$. They satisfy the following OPEs

$$\begin{aligned}
G^\pm(z)G^\mp(w) &= \frac{2c/3}{(z-w)^3} \pm \frac{2}{(z-w)^2}J(w) + \frac{1}{(z-w)}(2T(w) \pm \partial J(w)) + \dots \\
J(z)G^\pm(w) &= \pm\frac{1}{(z-w)}G^\pm(w) + \dots \\
J(z)J(w) &= \frac{c/3}{(z-w)^2} + \dots \\
T(z)J(w) &= \frac{1}{(z-w)^2}J(w) + \frac{1}{(z-w)}\partial J(w) + \dots \\
T(z)G^\pm(w) &= \frac{3/2}{(z-w)^2}G^\pm(w) + \frac{1}{(z-w)}\partial G^\pm(w) + \dots
\end{aligned} \tag{3.5}$$

In this thesis, we will mostly consider models with an $\mathcal{N} = (2,2)$ type supersymmetry, which means that there is an analog of (3.5) for the anti-holomorphic fields. It is custom

to concentrate only on the holomorphic fields, since many of the arguments are identical for the anti-holomorphic fields. This strategy is also adopted here. We will, however, also encounter models with $\mathcal{N} = (2,0)$ (or simply $\mathcal{N} = 2$) supersymmetry in which case we will mention this explicitly.
By comparing the latter two OPEs in (3.5) with the OPE of a primary field (3.3), we conclude that the supercharges and the current are primary fields with the conformal dimensions $\frac{3}{2}$, $\frac{3}{2}$ and 1 respectively. As for the stress-energy tensor, we can write the mode expansions for the supercharges and the current

$$\begin{aligned} G^{\pm}(z) &= \sum_r G_r^{\pm} z^{-r-3/2} \\ J(z) &= \sum_{n=-\infty}^{\infty} J_n z^{-n-1}, \end{aligned} \tag{3.6}$$

where $r$ runs over all values in $\mathbb{Z} + \alpha$, with $\alpha$ a real number which determines the branch cut properties of $G^{\pm}(z)$. For $\alpha = 0$ the theory is said to be in the Ramond sector and for $\alpha = 1/2$ it is said to be in the Neveu-Schwarz sector. This will be discussed in more detail in section 4.8.
From the mode expansions, we obtain the superconformal algebra. The superconformal algebra is defined by the Virasoro algebra (3.1) together with a $U(1)$ Kac-Moody algebra for the current

$$[J_m, J_n] = \frac{c}{3} m \delta_{m+n,0} \quad [L_m, J_n] = -n J_{m+n}, \tag{3.7}$$

and the algebra of the supercharges

$$\left[L_m, G_r^{\pm}\right] = (\frac{1}{2}m - r) G_{m+r}^{\pm}, \tag{3.8}$$

$$\left[J_m, G_r^{\pm}\right] = \pm G_{m+r}^{\pm}, \tag{3.9}$$

$$\{G_r^{\pm}, G_s^{\mp}\} = 2L_{r+s} \pm (r-s) J_{r+s} + \frac{1}{3} c (r^2 - \frac{1}{4}) \delta_{r+s,0}. \tag{3.10}$$

Like in CFT, representations of the superconformal algebra are formed by the primary fields and their descendants. A primary field $\psi(z)$ satisfies

$$\begin{aligned} J(z)\psi(w) &= \frac{q}{(z-w)} \psi(w) + \dots \\ G^{\pm}\psi(w) &= \frac{1}{(z-w)} \Lambda^{\pm}(w) + \dots \end{aligned}$$

where the fields $\Lambda^{\pm}(w)$ are the superpartners of $\psi(w)$. In terms of modes, this gives for the highest weight state corresponding to $\psi(z)$ ($|h,q\rangle = \psi(0)|0\rangle$)

$$\begin{aligned} L_n|h,q\rangle = J_n|h,q\rangle = 0, \ n > 0 \\ L_0|h,q\rangle = h|h,q\rangle, \ J_0|h,q\rangle = q|h,q\rangle, \\ G_r^{\pm}|h,q\rangle = 0, \ r \geq 1/2 \\ G_{-\frac{1}{2}}^{\pm}|h,q\rangle = \Lambda^{\pm}(0)|0\rangle. \end{aligned} \tag{3.11}$$

So $h$ is related to the energy of the state and $q$ is related to the charge of the state under the $U(1)$ current.

## 3.4 Minimal series

In conformal field theories with central charge $c < 1$, the unitarity constraint leads to a discrete series called the minimal series [45, 46]. Below $c = 1$ one can only have a unitary theory for

$$c = 1 - \frac{6}{m(m+1)}, \ m = 3, 4, \ldots \tag{3.12}$$

Furthermore, there is a finite set of primary fields or highest weight states with conformal dimensions

$$h_{p,r}(m) = \frac{[(m+1)p - mr]^2 - 1}{4m(m+1)} \tag{3.13}$$

where $p, r$ are integers satisfying $1 \leq p \leq m-1$, $1 \leq r \leq p$.
In supersymmetric theories, the unitarity constraint leads to a discrete series for theories with $c < 3$ [47, 48]. The allowed values for the central charge are

$$c = 3 - \frac{6}{(k+2)}, \ k = 1, 2, \ldots \tag{3.14}$$

For each of these supersymmetric minimal models there is again a finite set of primary fields. Their conformal dimensions and corresponding $U(1)$ charges are

$$h_{p,r}(k) = \frac{p(p+2) - r(r-2) - 4r\alpha + 2k(1/2-\alpha)^2}{4(k+2)} \quad q_r(k) = \frac{r + k/2 - k\alpha}{k+2}, \tag{3.15}$$

with $p = 0, 1, \ldots, k$ and $r = -p, -p+2, \ldots, p-2, p$. Remember that $\alpha$ is a real number connected to the boundary conditions imposed on the supercharges. For $\alpha = 0$ ($\alpha = 1/2$) the theory the Ramond (Neveu-Schwarz) sector.

## 3.5 Superpartners and Witten index

Let us now try to relate the above to the properties of our models that we derived from supersymmetry. That is, a positive definite energy spectrum, and a decomposition of the spectrum in singlets and doublets, the notion of a Witten index, etc. We start by noting that the hamiltonian $H$, i.e. the energy operator, is the generator of translations in the time direction. On the plane we have $H = L_0 + \overline{L}_0$ and on the cylinder this is $H = L_0 + \overline{L}_0 - \frac{c}{12}$. If we now define two supercharges as

$$G = \frac{1}{\sqrt{2}}(G_0^+ - \overline{G}_0^+) \quad G^\dagger = \frac{1}{\sqrt{2}}(G_0^- - \overline{G}_0^-), \tag{3.16}$$

we find that we can write the hamiltonian on the cylinder as

$$H = L_0 + \overline{L}_0 - \frac{c}{12} = \{G, G^\dagger\}. \tag{3.17}$$

Note that these supercharges are defined in the Ramond sector. Indeed it turns out that the supersymmetric structure as we discussed it in section 2.1.1 is only fully realized in the

Ramond sector of the superconformal algebra. From the commutator of the supercharges with the Virasoro generators (3.8), one easily verifies that the hamiltonian commutes with $G$ and $G^\dagger$. Furthermore, from the commutation relation with the U(1) current, we find that the hamiltonian also commutes with $F = J_0 - \overline{J}_0$. Note that for $F$ to be a well defined fermion number operator we must have $q - \overline{q} \in \mathbb{Z}$. The supercharges satisfy

$$[F, G] = -G \quad \left[F, G^\dagger\right] = G^\dagger. \tag{3.18}$$

These are precisely the relations we found for the supersymmetric model (see section 2.1.1). It thus follows that the spectrum of the hamiltonian in the Ramond sector will indeed have the properties mentioned above.
We now focus on the minimal models for a moment. One can see directly from the definition of the hamiltonian that the state with $h = \overline{h} = 0$ has negative energy. From the allowed conformal dimensions of the minimal models, however, one quickly finds that this state, with energy $-\frac{c}{12}$, is in the Neveu-Schwarz sector. Let us now check that for the minimal models the energy is positive definite for all states in the Ramond sector. In the Ramond sector the highest weight states have conformal dimension

$$h_{p,r}(k) = \frac{p(p+2) - r(r-2) + k/2}{4(k+2)}, \tag{3.19}$$

which is minimized if $p(p+2) - r(r-2)$ is minimized. If we write $r = -p + 2m$, where $m = 0, 1, \ldots, p$, we find

$$h_{p,-p+2m}(k) = \frac{4m(p-m+1) + k/2}{4(k+2)}, \tag{3.20}$$

which is minimal for $m = 0$. In this case the conformal dimension does not depend on $p$ so there are $k+1$ fields with the lowest conformal dimension given by

$$h_{p,-p}(k) = \frac{k}{8(k+2)} = \frac{c}{24}. \tag{3.21}$$

One can check that the corresponding values of the $U(1)$ charges satisfy $q_{-p}(k) = \frac{k/2-p}{k+2}$. Consequently, $q \in (-\frac{1}{2}, \frac{1}{2})$ and the condition that $q - \overline{q} \in \mathbb{Z}$ then implies $q = \overline{q}$. It follows that in the Ramond sector there are $k+1$ states with $h = \overline{h} = c/24$ and thus zero energy. All other states have an energy larger than zero.
As we have seen before, the Witten index is simply the partition sum with an extra factor $(-1)^F$ in the trace. We have to define however in which sector we take the trace. In the Ramond sector, we have found that the manifestly supersymmetric structure is realized. It follows that the states with energy greater than zero do not contribute to the trace. The number of zero energy states is $k+1$ for the $k$-th minimal model. Since these states all have $q - \overline{q} = 0$, their contribution to the Witten index is positive: $(-1)^F = (-1)^{J_0 - \overline{J}_0} = +1$. It thus follows that we find for the Witten index of the $k$-th minimal model

$$W_k = k + 1. \tag{3.22}$$

## 3.6 Spectral flow

An important tool in the analysis of superconformal field theories is the spectral flow [49] (see also [50, 41]). It follows from an operator that shifts the $U(1)$ charge of any field. Since the current is a bosonic field of conformal dimension 1 we can write it as

$$J(z) = \imath\sqrt{\frac{2gc}{3}}\partial\Phi(z), \tag{3.23}$$

where $\Phi(z,\overline{z}) = \Phi(z) + \overline{\Phi}(\overline{z})$ is just the free boson with action $S = \frac{g}{\pi}\int \partial\Phi\overline{\partial}\Phi$, where $g$ is the coupling. We can now define the spectral flow operator as

$$U(z,\overline{z}) = \exp\left[\imath\sqrt{\frac{2gc}{3}}\theta(\Phi - \overline{\Phi})\right]. \tag{3.24}$$

The action of this operator on a field with charge $q$ is that it changes it to a field with charge $q + \theta c/3$. It can be shown that the generators of the superconformal algebra transform as follows under this map [49]

$$\begin{aligned} L_n^\theta &= L_n + \theta J_n + \frac{c}{6}\theta^2\delta_{n,0} \\ J_n^\theta &= J_n + \frac{c}{3}\theta\delta_{n,0} \\ G_r^{\theta,+} &= G_{r-\theta}^+ \\ G_r^{\theta,-} &= G_{r+\theta}^-. \end{aligned}$$

First of all, one can check that for $\theta$ integer the algebra maps back to itself. Second, we find that if $r$ is integer, the spectral flow maps the superconformal algebra of the Ramond sector onto a representation with $\alpha = \theta$. In particular, for $\theta = \frac{1}{2}$ it maps the Ramond sector onto the Neveu-Schwarz sector.
This mapping will turn out to be particularly powerful in the study of the supersymmetric lattice models. As we mentioned before, representations with different values of $\alpha$ correspond to theories with different boundary conditions. It turns out that these boundary conditions are directly related to the boundary conditions in the lattice model.

# Chapter 4
# The supersymmetric model on the one dimensional chain

## 4.1 Introduction

In this chapter we discuss the supersymmetric model on the one dimensional chain. The supersymmetric model was first introduced for this lattice [22]. Its ground state structure was investigated and the model was foud to be integrable and solved via Bethe Ansatz. The continuum limit is described by an $\mathcal{N} = (2,2)$ superconformal field theory with central charge $c = 1$. In follow up work, a precise mapping of this model onto the antiferromagnetic critical XXZ Heisenberg spin chain was presented [23] and the chain with open boundary conditions was investigated, both analytically and numerically [51].
Here we will not only briefly review these results, but we will also present a detailed analysis relating the lattice model spectrum and operators to the operator content of the continuum theory. We will see that this model forms a textbook example of how a superconformal field theory can be identified studying the finite size lattice model properties. Apart from finite size scaling of the spectrum, we will study a boundary twist, one-point functions and entanglement entropy. The boundary twist in the lattice model is related to a spectral flow in the continuum theory. The power of this type of analysis is that it does not require a comparison between models on lattices with different size (length). This will prove very useful in chapter 7.

## 4.2 Hamiltonian

For convenience, we restate the hamiltonian for the supersymmetric model on the one dimensional periodic chain of length $L$:

$$\begin{aligned} H = \{Q^\dagger, Q\} &= \sum_i \sum_{j \text{ next to } i} P_{<i>} c_i^\dagger c_j P_{<j>} + \sum_i P_{<i>} \\ &= \sum_{i=1}^{L} \Big[ P_{i-1} \big( c_i^\dagger c_{i+1} + c_{i+1}^\dagger c_i \big) P_{i+2} \Big] + \sum_{i=1}^{L} (n_i n_{i+2}) + L - 2F. \end{aligned}$$

Here $P_i = 1 - n_i$, $n_i = c_i^\dagger c_i$ is the usual number operator and $F = \sum_i n_i$ is the total number of fermions.

## 4.3 Witten index

In the example of the 6-site chain (section 2.1.4) we saw that the Witten index can be computed by simply summing over all possible configurations with the appropriate sign. However, because of the hard-core character of the fermions this is not a trivial problem

for larger sizes. To compute the Witten index for chains of arbitrary length we use the following method [22]. First divide the lattice into two sublattices $S_1$ and $S_2$. Then fix the configuration on $S_1$ and sum $(-1)^F$ for the configurations on $S_2$. Finally, sum the results over the configurations of $S_1$. Of course the trick is to make a smart choice for the sublattices. For the periodic chain with $L = 3j$ sites, we take $S_2$ to be every third site. All the sites on $S_2$ are disconnected and thus every site can be either empty or occupied given that its neighboring sites on $S_1$ are empty. This means that the sum of $(-1)^F$ for the configurations on $S_2$ vanishes as soon as at least one site on $S_2$ can be both empty and occupied. Consequently, the only non-zero contribution comes from the configurations such that at least one of the adjacent sites on $S_1$ is occupied for each site on $S_2$. There are only two such configurations:

$$\begin{aligned} |\alpha\rangle &\equiv \cdots \bullet \square \circ \bullet \square \circ \bullet \square \circ \bullet \square \circ \bullet \square \circ \bullet \square \circ \bullet \square \circ \ldots \\ |\gamma\rangle &\equiv \cdots \circ \square \bullet \circ \square \bullet \circ \square \bullet \circ \square \bullet \circ \square \bullet \circ \square \bullet \circ \square \bullet \ldots \end{aligned} \tag{4.1}$$

where the square represents an empty site on $S_2$. The final step is to sum $(-1)^F$ for these two configurations, and since both configurations have $f = L/3 = j$, we find that the Witten index is $W = 2(-1)^j$. Note that this agrees with the result we obtained for the 6-site chain. One can also use this method of splitting the lattice in sublattices to compute the cohomology, i.e. the total number of ground states. We will come back to this in section 4.4. First, however, we discuss a different method to compute the Witten index that nicely generalizes to arbitrary chain lengths and open boundary conditions.

### 4.3.1 Transfer matrix

There is an alternative way of computing the Witten index by using the transfer matrix. Let us write the partition function as

$$Z = \sum_{\text{states}} z^f e^{-\beta E}, \tag{4.2}$$

where $z \equiv e^{\beta\mu}$ is the fugacity, $\beta$ is the inverse temperature, $\mu$ is the chemical potential and $E$ and $f$ are the energy and fermion number, respectively. If we take the limit where $\beta E \to 0$, but $\beta\mu$ finite, the partition function becomes an important combinatorial tool. In this limit we obtain

$$Z(z) = \sum_{\text{states}} z^f. \tag{4.3}$$

It follows that $Z(z = 1)$ is the size of the Hilbert space. More importantly, $Z(z = -1)$ is precisely the Witten index. Remember that because of the nearest neighbor exclusion rule, the occupation number $n_i$ of a site $i$ depends on the occupation numbers of the neighboring sites. It follows that we can write the partition function of a periodic chain of $L$ sites as

$$Z(z) = \sum_{\text{states}} z^f = \sum_{\text{states}} \prod_i z^{n_i} = \text{Tr } \mathcal{T}^L, \tag{4.4}$$

where $\mathcal{T}$ is the transfer matrix given by

$$\mathcal{T}_{ij} = (1 - \delta_{2,n_i+n_j}) z^{n_i} \Rightarrow \mathcal{T} = \begin{pmatrix} 1 & 1 \\ z & 0 \end{pmatrix}$$

where we chose the basis $n_1 = 0$ and $n_2 = 1$. The eigenvalues of the transfer matrix are $\frac{1}{2} \pm \frac{1}{2}\sqrt{1+4z}$. From this we obtain the following expression for the Witten index for a periodic chain of $L$

$$W = Z(z=-1) = (\frac{1}{2} + \frac{1}{2}\imath\sqrt{3})^L + (\frac{1}{2} - \frac{1}{2}\imath\sqrt{3})^L. \tag{4.5}$$

Rewriting this we get

$$W = e^{\pi\imath L/3} + e^{-\pi\imath L/3} = 2\cos(\pi L/3). \tag{4.6}$$

For $L \mod 6 = 0, 1, 2, 3, 4, 5$ we find $W = 2, 1, -1, -2, -1, 1$ respectively.
One can also obtain the Witten index for open boundary conditions. In that case, the first and last site both have just one neighbor and the partition function can be written as

$$Z(z) = \sum_{i,j=1}^{2} (\mathcal{T}^{L-1})_{ij} c_j, \tag{4.7}$$

where $c_1 = 1$ and $c_2 = z$. One can verify that this gives

$$W = -\frac{2}{\sqrt{3}} \sin(\pi(L-1)/3). \tag{4.8}$$

It follows that for the chain with open boundary conditions with length $L \mod 6 = 0, 1, 2, 3, 4, 5$ the Witten index is $W = 1, 0, -1, -1, 0, 1$ respectively. Clearly, the transfer matrix is a very powerful tool to obtain the Witten index.

### 4.3.2 Ground state momenta

For the periodic chain the hamiltonian commutes with the translation operator $T$. A nice way to compute the momenta of the ground states of the periodic chain, is to compute the Witten index per momentum sector, characterized by the eigenvalues of $T$ [23]. Unfortunately, there is not an obvious way to do this for general system size. For small system sizes, however, it is a very simple computation. One writes down all configurations modulo translations, determines the possible eigenvalues of $T$ for each configuration and computes the Witten index per sector. The procedure is illustrated for the 6-site chain in table 4.1. One easily reads off that the Witten index is unity in the momentum sectors with translation eigenvalues $t = e^{\pi\imath/3}$ and $t = e^{5\pi\imath/3}$. The two zero energy ground states of the 6-site periodic chain thus have momenta $\pi/3$ and $5\pi/3$.
By doing this computation for various small system sizes one can figure out the systematics. It was found that [23] for periodic chains of length $L = 3j$ the Witten index $W_t$ at fixed translation eigenvalue $t$ reads

$$W_t = \begin{cases} (-1)^L & \text{for } t = (-1)^{L+1} e^{2\pi\imath k/3} \text{ with } k = 1, 2 \\ 0 & \text{otherwise,} \end{cases} \tag{4.9}$$

and for all other lengths $L$

$$W_t = \begin{cases} (-1)^{L+1} & \text{for } t = (-1)^{L+1} \\ 0 & \text{otherwise.} \end{cases} \tag{4.10}$$

**Table 4.1:** We show the procedure to compute the Witten index per momentum sector for the 6-site chain. In the first column we show the possible configurations modulo translation for the 6-site chain. We use the notation where we write $c_1^\dagger c_3^\dagger|0\rangle$ for example as $|101000\rangle$, so that the translation eigenvalues can easily be read of. In the second column, we show the possible eigenvalues $t_k$ of the translation operator $T$ in terms of $k$, where $t_k = e^{\pi\imath k/3}$. In columns 3 through 8, we give $(-1)^F$ for the different configurations. If a configuration does not occur in a given sector we write a zero. Finally, in the bottom row, we compute the Witten index in the momentum sectors corresponding to $k = 1, \ldots, 6$ by adding the entries in columns 3 through 8. That is, we compute $W_k = \mathrm{Tr}_k(-1)^F$, where the trace is restricted to states with translation eigenvalue $t_k$.

| configurations "mod $T$" | eigenvalues of $T$: possible values of $k$ for $t_k = e^{\pi\imath k/3}$ | $(-1)^F$ for $k=1$ | $(-1)^F$ for $k=2$ | $(-1)^F$ for $k=3$ | $(-1)^F$ for $k=4$ | $(-1)^F$ for $k=5$ | $(-1)^F$ for $k=6$ |
|---|---|---|---|---|---|---|---|
| $\|000000\rangle$ | $t^1 = 1 \Rightarrow k = 6$ | 0 | 0 | 0 | 0 | 0 | 1 |
| $\|100000\rangle$ | $t^6 = 1 \Rightarrow k = 1, \ldots, 6$ | -1 | -1 | -1 | -1 | -1 | -1 |
| $\|101000\rangle$ | $t^6 = 1 \Rightarrow k = 1, \ldots, 6$ | 1 | 1 | 1 | 1 | 1 | 1 |
| $\|100100\rangle$ | $t^3 = -1 \Rightarrow k = 1, 3, 5$ | 1 | 0 | 1 | 0 | 1 | 0 |
| $\|101010\rangle$ | $t^2 = 1 \Rightarrow k = 3, 6$ | 0 | 0 | -1 | 0 | 0 | -1 |
| Witten index per sector: | | 1 | 0 | 0 | 0 | 1 | 0 |

## 4.4 Cohomology

To find the exact number of ground states we compute the cohomology by using the 'tic-tac-toe' lemma of [33] (see section 2.2.3). This says that under certain conditions, the cohomology $H_Q$ for $Q = Q_1 + Q_2$ is the same as the cohomology of $Q_1$ acting on the cohomology of $Q_2$. In an equation, $H_Q = H_{Q_1}(H_{Q_2}) \equiv H_{12}$, where $Q_1$ and $Q_2$ act on different sublattices $S_1$ and $S_2$. We find $H_{12}$ by first fixing the configuration on all sites of the sublattice $S_1$, and computing the cohomology $H_{Q_2}$. Then one computes the cohomology of $Q_1$, acting not on the full space of states, but only on the classes in $H_{Q_2}$. A sufficient condition for the lemma to hold is that all non-trivial elements of $H_{12}$ have the same $f_2$ (the fermion-number on $S_2$). For the periodic chain with $L = 3j$ we choose the sublattice as before (see section 4.3: $S_2$ is every third site). Now consider a single site on $S_2$. If both of the adjacent $S_1$ sites are empty, $H_{Q_2}$ is trivial: $Q_2$ acting on the empty site does not vanish, while the filled site is $Q_2$ acting on the empty site. Thus $H_{Q_2}$ is non-trivial only when every site on $S_2$ is forced to be empty by being adjacent to an occupied site. The elements of $H_{Q_2}$ are just the two states $|\alpha\rangle$ and $|\gamma\rangle$ pictured above in equation (4.1). Both states $|\alpha\rangle$ and $|\gamma\rangle$ belong to $H_{12}$: they are closed because $Q_1|\alpha\rangle = Q_1|\gamma\rangle = 0$, and not exact because there are no elements of $H_{Q_2}$ with $f_1 = f - 1$. By the tic-tac-toe lemma, there must be precisely two different cohomology classes in $H_Q$, and therefore exactly two ground states with $f = L/3$. Applying the same arguments to the periodic chain with $3j \pm 1$ sites and to the open chain yields in all cases exactly one $E = 0$ ground state, except in open chains with $3j + 1$ sites, where there are none [23] (see also section 6.3).

## 4.5 Bethe Ansatz solution in continuum limit

The supersymmetric model on the chain can be solved exactly through a Bethe Ansatz [22]. In the continuum limit one can derive the thermodynamic Bethe Ansatz equations. The model has the same thermodynamic equations as the XXZ Heisenberg spin chain at a specific value of the anisotropy parameter $\Delta$. There is indeed a mapping between the supersymmetric model on the chain and the Heisenberg spin chain with special boundary conditions [23]. The hamiltonian of the XXZ chain is defined in terms of the usual Pauli matrices as

$$H_{\mathrm{XXZ}} = \frac{1}{2}\sum_{i=1}^{L}\left[\sigma_i^x\sigma_{i+1}^x + \sigma_i^y\sigma_{i+1}^y - \Delta\sigma_i^z\sigma_{i+1}^z\right]. \tag{4.11}$$

The continuum limit of the XXZ chain is described by the massless Thirring model [52], or equivalently a free massless boson $\Phi$ with action [53]

$$S = \frac{g}{4\pi}\int dx\,dt\ \left[(\partial_t\Phi)^2 - (\partial_x\Phi)^2\right]. \tag{4.12}$$

The coupling constant $g$ is related to the anisotropy parameter $\Delta$ in the XXZ chain. On the conformal field theory side the coupling constant $g$ is related to the compactification radius $R$ of the free boson theory via $g = 2/R^2$. The free boson theory is characterized by a central charge $c = 1$ and a set of highest weight states which depend on the compactification radius. At a compactification radius $R = \sqrt{3}$, the conformal algebra is enhanced to an $\mathcal{N} = (2,2)$ superconformal algebra [54, 53]. The $(2,2)$ means that both the holomorphic as well as the anti-holomorphic fields satisfy an $\mathcal{N} = 2$ superconformal algebra. More specifically, the free boson at compactification radius $R = \sqrt{3}$ is the simplest field theory with $\mathcal{N} = (2,2)$, namely the first in the series of minimal supersymmetric models. It turns out that the compactification radius $R = \sqrt{3}$ corresponds to an anisotropy parameter of $\Delta = -1/2$ (see for example [55]) which is precisely the value one obtains upon mapping the supersymmetric model onto the XXZ chain.
The fact that the low-energy spectrum of the supersymmetric model on the chain is described by a superconformal theory in the continuum limit, tells us that the model is quantum critical.

## 4.6 Relation to other models

Before we explore the continuum limit of the supersymmetric model on the chain in great detail in the following sections, we would like to mention the relation between this model and three other models. The models are, firstly, a generalization of the supersymmetric model discussed here [23], secondly, the XXZ Heisenberg spin chain, a famous integrable model without explicit supersymmetry, and finally, the supersymmetric matrix model [56] at strong coupling, an explicitly supersymmetric model that arose as a toy-model in the context of high energy physics. Both our supersymmetric model on the chain as well as the supersymmetric matrix model in the strong coupling limit can be mapped explicitly onto the XXZ Heisenberg spin chain [23, 57], making the models equivalent under certain conditions.

### 4.6.1 A family of supersymmetric models

In [23] a generalization of the supersymmetric model was presented, generating a whole family of supersymmetric lattice models. Interestingly, all these models can be tuned to be quantum critical. The lattice models can be labelled by an index $k$ and it was shown that in the continuum limit their low-energy spectrum is described by the $k$-th superconformal field theory in the minimal series (see section 3.4). The generalization follows from allowing no more than $k$ consecutive sites to be occupied on the chain. Clearly, the supersymmetric model discussed in this chapter has $k = 1$. For the model with $k = 1$ we can define the supercharge $Q$ as a sum over the hard-core fermion creation operators $d_i^\dagger \equiv P_{i-1}c_i^\dagger P_{i+1}$. For $k = 2$ a second type of creation operator $e_i^\dagger \equiv P_{i-2}c_{i-1}^\dagger c_{i-1}c_i^\dagger P_{i+1} + P_{i-1}c_i^\dagger c_{i+1}^\dagger c_{i+1}P_{i+2}$ is introduced, which creates a particle on site $i$ if precisely one of its neighbors is occupied and both neighbors of the occupied site are empty. The supercharge $Q$ is now defined as

$$Q = \sum_i [y_1 d_i^\dagger + y_2 e_i^\dagger].$$

The nilpotency condition of the supercharges is satisfied for all values of $y_1$ and $y_2$, so the ratio $x_1 = y_1/y_2$ is a non-trivial adjustable parameter in the model. The quantum critical point is reached by setting $x_1 = \sqrt{2}$. For general $k$ the supersymmetric model can be constructed in a similar manner and has $k-1$ adjustable parameters. For further details and a full analysis of these models we refer to [23].

### 4.6.2 The XXZ Heisenberg spin chain

The hamiltonian of the XXZ Heisenberg spin chain is given in (4.11). The mapping can be found in detail in [23] (see also [58]), here we will sketch the main idea. To map the supersymmetric model onto a spin chain, we identify a site, occupied by a fermion, including its adjacent edges with a down-spin and an edge between two empty sites with an up-spin (see figure 4.1). The length $L$ of the spin chain can therefore be written as $L = N - f$, where $N$ is the length of the original fermion chain and $f$ is the number of fermions. From this map one finds that a fermion that hops from one site to the next, corresponds to a spin flip between two neighboring spins. More precisely, we find

$$\begin{gathered} \textstyle\sum_i \left[P_{i-1}\left(c_i^\dagger c_{i+1} + c_{i+1}^\dagger c_i\right)P_{i+2}\right] \\ \Longleftrightarrow \\ \textstyle\sum_j \left[\sigma_j^+\sigma_{j+1}^- + \sigma_j^-\sigma_{j+1}^+\right] \end{gathered}$$

where the spin-flip operators are defined in terms of the usual Pauli matrices, $\sigma^\pm \equiv (\sigma^x \pm \imath\sigma^y)/2$. The diagonal term in the supersymmetric hamiltonian counts the number of empty next-nearest neighbor pairs. Under the mapping such a pair either translates into a down-spin or into a pair of neighboring up-spins. We thus find

$$\sum_i P_{<i>} \Longleftrightarrow \sum_j (1-\sigma_j^z)/2 + (1+\sigma_j^z)(1+\sigma_{j+1}^z)/4. \tag{4.13}$$

Working out the latter for a periodic spin chain, we find $(3L + \sum_j \sigma_j^z\sigma_{j+1}^z)/4$. Combining the results for the diagonal and off-diagonal terms we find that the supersymmetric model

maps onto the XXZ Heisenberg spin chain up to an additive constant

$$H_{\text{SUSY}} = \sum_{i=1}^{N} \left[ P_{i-1} \left( c_i^\dagger c_{i+1} + c_{i+1}^\dagger c_i \right) P_{i+2} + P_{<i>} \right]$$
$$\Longleftrightarrow$$
$$H_{\text{XXZ}} + \tfrac{3L}{4} = \tfrac{1}{2} \sum_{j=1}^{L} \left[ \sigma_j^x \sigma_{j+1}^x + \sigma_j^y \sigma_{j+1}^y + \tfrac{1}{2} \sigma_j^z \sigma_{j+1}^z \right] + \tfrac{3L}{4} \quad .$$

Note that since $L = N - f$, the supercharges do note preserve the length of the spin chain. This explains why supersymmetry is not explicit in the spin chain. Furthermore, note that the supersymmetric model maps unto the XXZ spin chain with anisotropy parameter $\Delta = -1/2$ (4.11).

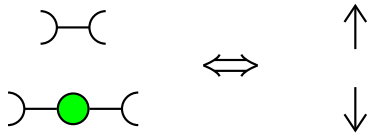

**Figure 4.1:** To map the supersymmetric model onto a spin chain, we identify an edge between two empty sites (top left) with an up-spin (top right) and a site, occupied by a fermion, including its adjacent edges (bottom left) with a down-spin (bottom right).

In spite of this mapping, the two hamiltonians do not have entirely the same spectrum when periodic boundary conditions are imposed (for open boundary conditions these subtleties do not occur and the two spectra are indeed equal). It turns out that for periodic boundary conditions the sizes of the Hilbert spaces at corresponding sectors do not agree due to an ambiguity in the mapping. Furthermore, due to the anti-commutation relations satisfied by the fermions, a state acquires a minus sign when a fermion hops over the boundary in a state with an even number of fermions. These differences can be overcome by restricting to sectors with translation eigenvalue $t$ and introducing twisted boundary conditions in the spin chain (for details see [23]).

### 4.6.3 A supersymmetric matrix model

In a series of papers [56, 59, 57] Veneziano and Wosiek introduce and investigate a supersymmetric matrix model. The model was introduced in the context of high energy physics, where it was proposed as a toy model to study a claimed equivalence [60] between a non-supersymmetric theory, such as quantum chromo dynamics, and a supersymmetric "parent" theory. It turns out, however, that the model is quite interesting in its own right. In particular, investigations of the model in a special limit independently led to the observation that the XXZ Heisenberg spin chain has a hidden supersymmetry at $\Delta = -1/2$ [57]. This observation followed from an explicit mapping to the spin chain. Since both the supersymmetric model discussed in this thesis as well as the supersymmetric matrix model, can be mapped to the XXZ spin chain, there may be a direct relation between the two. Exploiting this relation may lead to further insights for both models.
In a matrix model the usual quantum mechanical creation and annihilation operators for bosons and fermions are replaced by $N \times N$ matrices. It follows that there are $N^2$ bosonic and $N^2$ fermionic degrees of freedom. The usual (anti-)commutation relations are replaced by

$$\begin{aligned} [a_{ij}, a_{kl}^\dagger] &= \delta_{jk}\delta_{il} \quad \text{for the bosons and} \\ \{f_{ij}, f_{kl}^\dagger\} &= \delta_{jk}\delta_{il} \quad \text{for the fermions.} \end{aligned}$$

Veneziano and Wosiek choose to define the supercharges as

$$Q = \mathrm{Tr}[fa^\dagger(1+ga^\dagger)], \quad Q^\dagger = \mathrm{Tr}[f^\dagger a(1+ga)] \tag{4.14}$$

and the hamiltonian reads

$$H = \{Q^\dagger, Q\}. \tag{4.15}$$

Note that the hamiltonian conserves the number of fermions $F = \mathrm{Tr}(f^\dagger f)$, whereas, is can change the number of bosons $B = \mathrm{Tr}(a^\dagger a)$ by 0,1 or -1.
The model is studied in the large $N$ limit. In the limit of $N \to \infty$, while keeping the 't Hooft coupling $\lambda = g^2 N$ fixed, the so-called single trace states

$$|n_1, \ldots, n_F\rangle = \mathrm{Tr}[(a^\dagger)^{n_1} f^\dagger \ldots (a^\dagger)^{n_F} f^\dagger]|0\rangle \tag{4.16}$$

are invariant under the action of the hamiltonian. The action of the hamiltonian on other states can be shown to generate terms which are subleading in $N$. The other states can thus simply be discarded in the large $N$ limit, since the single-trace states form a closed subspace under the action of the hamiltonian.
In a remarkable series of papers [56, 59, 57] Veneziano and Wosiek show that this model is far from trivial. Since the hamiltonian conserves the total number of fermions, the model can be studied in sectors with fixed $F$. For the sectors with $F = 0, 1, 2, 3, 4$ various interesting analytical and numerical results were obtained. These results include Witten index computations as a function of the 't Hooft coupling, clear evidence of a phase transition at 't Hooft coupling $\lambda = 1$ accompanied by a jump in the Witten index (see also [61]), an exact strong-weak coupling duality and a mapping to the XXZ Heisenberg spin chain in the strong coupling limit. In [62] these results are extended with an analytic expression for the ground state in sectors with $F = 2, 4$, by computing the harmonic representatives of the cohomology of $Q$.
Let us briefly discuss the mapping to the XXZ Heisenberg spin chain (4.11). In the strong coupling limit, that is $\lambda \to \infty$, the hamiltonian reduces to $H_{\mathrm{SC}}$, which conserves both $F$ and $B$. Veneziano and Wosiek find the following relations [57]

- for $F$ odd $H_{\mathrm{SC}} \Leftrightarrow H_{\mathrm{XXZ}} + \frac{3}{4}L$, with anisotropy parameter $\Delta = -\frac{1}{2}$,
- for $F$ even and $B$ odd $H_{\mathrm{SC}} \Leftrightarrow -H_{\mathrm{XXZ}} + \frac{3}{4}L$, with anisotropy parameter $\Delta = \frac{1}{2}$,
- for $F$ *and* $B$ even no equivalence was found.

The length of the spin chain is $L = F + B$ and the conserved component of the total spin is $S_z = \frac{1}{2}(F - B)$. Also here the spectrum on the spin side should be computed for fixed values of the translation eigenvalue.
These mappings suggest that there is a direct relation between the supersymmetric model on the chain and the supersymmetric matrix model in the strong coupling limit with $F$ odd.

## 4.7 Free boson with $\mathcal{N} = (2, 2)$ supersymmetry

The continuum limit of the supersymmetric model on the chain is described by the free boson (4.12) with $\mathcal{N} = (2, 2)$ supersymmetry [22]. The supersymmetry arises as an enhanced symmetry for a specific compactification radius or, equivalently, a specific coupling

$g$. In this section we will discuss this theory in some detail and in particular its relation to the lattice model. Let us first see how the $\mathcal{N} = (2,2)$ supersymmetry arises at compactification radius $R = \sqrt{3}$, and thus $g = 2/3$.
The free boson field $\Phi$ can be decoupled into left and right movers: $\Phi = \Phi_L + \Phi_R$ and the dual is defined as $\tilde{\Phi} = g(\Phi_L - \Phi_R)$. The left moving field obeys the following OPEs

$$\Phi_L(z)\Phi_L(w) \sim -\frac{1}{2g}\ln(z-w), \quad \partial\Phi_L(z)\partial\Phi_L(w) \sim -\frac{1}{2g}\frac{1}{(z-w)^2},$$

and similarly for the right moving field

$$\Phi_R(\overline{z})\Phi_R(\overline{w}) \sim -\frac{1}{2g}\ln(\overline{z}-\overline{w}), \quad \partial\Phi_R(\overline{z})\partial\Phi_R(\overline{w}) \sim -\frac{1}{2g}\frac{1}{(\overline{z}-\overline{w})^2}.$$

The operators

$$V_{m,n} = :\exp(\imath m\Phi + \imath n\tilde{\Phi}):\,,$$

are called vertex operators. Here the semicolons imply normal ordering, in the following we will drop this notation and tacitly assume that normal ordering is taken care of. The vertex operators are primary fields (see (3.3)) and their conformal dimensions are

$$h_{L,R} = (m \pm gn)^2/(4g), \tag{4.17}$$

with $m \in \mathbb{Z}$ and $n \in \mathbb{Z}/2$. Note that we label holomorphic and anti-holomorphic dimensions with $L$ and $R$, for left and right movers, respectively. Remember that in an $\mathcal{N} = 2$ superconformal field theory there are two supercharges of conformal dimension 3/2 and a $U(1)$ current of dimension 1. From (4.17) we find that for $R = \sqrt{3}$, and thus $g = 2/3$, the operators $V_{\pm1,\pm3/2}$ have conformal dimensions $(h_L, h_R) = (3/2, 0)$ and the operators $V_{\pm1,\mp3/2}$ have conformal dimensions $(h_L, h_R) = (0, 3/2)$. These four operators are the two left mover supercharges and two right mover supercharges. Finally, the $U(1)$ currents of dimensions $(1,0)$ and $(0,1)$ are proportional to $\partial\Phi_L$ and $\partial\Phi_R$ respectively. The proportionality factor follows from comparing the OPEs of $\partial\Phi_{L,R}$ with the OPE of the U(1) current (see (3.5))

$$J(z)J(w) \sim \frac{c/3}{(z-w)^2} \Rightarrow J_{L,R}(z) = \pm\imath\sqrt{2gc/3}\partial\Phi_{L,R} = \pm\imath 2/3\partial\Phi_{L,R}. \tag{4.18}$$

So these operators, together with the stress-energy tensor form an $\mathcal{N} = (2,2)$ superconformal algebra.

### 4.7.1 Spectrum

The spectrum of a superconformal field theory can be generated from the highest weight states by acting with the Virasoro generators and the supercharges. The effect of the Virasoro generators on a highest weight state $|h_L, h_R\rangle$ is well known

$$\begin{aligned}
L_{L,R;0}|h_L,h_R\rangle &= h_{L,R}|h_L,h_R\rangle,\\
L_{L,R;n}|h_L,h_R\rangle &= 0,\\
L_{L,-n}|h_L,h_R\rangle &= |h_L+n,h_R\rangle,\\
L_{R,-n}|h_L,h_R\rangle &= |h_L,h_R+n\rangle,
\end{aligned}$$

with $n > 0$. The vacuum is defined as the state with $L_{L,R;0}|0\rangle = 0$. Remember that the hamiltonian is given by

$$H = L_{L,0} + L_{R,0} - c/12. \tag{4.19}$$

It follows that for $c = 1$ the energy of a state is given by $E = h_R + h_L - 1/12$.
Let us now see what the effect of the supercharges is. We write the supercharges as

$$G_L^{\pm} = V_{\pm 1,\pm 3/2} \quad \text{and} \quad G_R^{\pm} = V_{\pm 1,\mp 3/2}. \tag{4.20}$$

As an example we consider the action of the supercharge $G_L^+$ on a state $V_{m,n}|0\rangle$. Remember that $G_L^+$ has conformal weight $(h_L, h_R) = (3/2, 0)$. The mode expansion for a purely holomorphic (purely left moving) field $\phi$ of conformal weight $(h, 0)$ is given by

$$\phi(z) = \sum_l z^{-l-h}\phi_l, \tag{4.21}$$

which is chosen such that $\phi_{-l}$ has conformal weight $l$ (under $z \to z/\lambda$ we have $\phi(z) \to \lambda^h\phi(z/\lambda)$ from which it follows that $\phi_{-l} \to \lambda^l\phi_{-l}$). The modes satisfy

$$\phi_l = \oint \frac{dz}{2\pi\imath} z^{l+h-1}\phi(z). \tag{4.22}$$

So we find the following mode expansion for $G_L^+$

$$G_{L,l}^+ = \oint \frac{dz}{2\pi\imath} z^{l+1/2} G_L^+ = \oint \frac{dz}{2\pi\imath} z^{l+1/2} V_{1,3/2}, \tag{4.23}$$

where $l \in \mathbb{Z}$ in the Ramond sector and $l \in (\mathbb{Z} + 1/2)$ in the NS sector. Consequently, we have

$$G_{L,l}^+ V_{m,n}|0\rangle = \oint \frac{dz}{2\pi\imath} z^{l+1/2} V_{1,3/2} V_{m,n}|0\rangle. \tag{4.24}$$

We can also compute the OPE for $G_L^+(z)V_{m,n}(w,\overline{w})$. We use that for a vertex operator $V_\alpha(z) = \exp(\imath\alpha\phi(z))$ of conformal weight $h = \alpha^2/(4g)$ the OPE is given by (see [42])

$$V_\alpha(z)V_\beta(w) \sim (z-w)^{\alpha\beta/(2g)} V_{\alpha+\beta}(w).$$

Using $\alpha_{L,R} = (m \pm 2n/3)$, we find

$$\begin{aligned} G_L^+(z)V_{m,n}(w,\overline{w}) &\sim (z-w)^{(2)(m+2n/3)3/4} \times (\overline{z}-\overline{w})^{(0)(m-2n/3)3/4} \\ &\quad \times \exp(\imath[(1+m)\Phi(w,\overline{w}) + (3/2+n)\tilde{\Phi}(w,\overline{w})]) \\ &= (z-w)^{3/2m+n} V_{m+1,n+3/2}(w,\overline{w}). \end{aligned} \tag{4.25}$$

Finally, combining (4.24) and (4.25) gives

$$G_{L,l}^+ V_{m,n}(0,0)|0\rangle = \oint \frac{dz}{2\pi\imath} z^{3/2m+n+l+1/2} V_{m+1,n+3/2}|0\rangle. \tag{4.26}$$

Similarly, we obtain

$$\begin{aligned} G^-_{L,l} V_{m,n}(0,0)|0\rangle &= \oint \frac{dz}{2\pi\imath} z^{-3/2m-n+l+1/2} V_{m-1,n-3/2}|0\rangle, \\ G^+_{R,l} V_{m,n}(0,0)|0\rangle &= \oint \frac{dz}{2\pi\imath} \overline{z}^{3/2m+n+l+1/2} V_{m+1,n-3/2}|0\rangle, \\ G^-_{R,l} V_{m,n}(0,0)|0\rangle &= \oint \frac{dz}{2\pi\imath} \overline{z}^{-3/2m-n+l+1/2} V_{m-1,n+3/2}|0\rangle. \end{aligned}$$

For the contour integrals to be well-defined the power of $z$ or $\overline{z}$ has to be integer. Since $l$ is integer (half-integer) in the Ramond (NS) sector, we find $3/2m + n$ is half-integer (integer) in the Ramond (NS) sector. This condition can be reformulated by saying that $(-1)^{m+2n}$ is 1 in the Neveu-Schwarz sector and $-1$ in the Ramond sector.
Furthermore, we see that the first mode $G^+_{L,l}$ of $G^+_L$ that gives a non-zero contribution must obey $3/2m + n + l + 1/2 \leq -1$, i.e. $l \leq -3/2 - 3/2m - n$. Equivalently, we find for $G^-_{L,l}$: $l \leq -3/2 + 3/2m + n$ and for $G^\pm_{R,l}$: $l \leq -3/2 \mp 3/2m \pm n$.
From the above relations it also follows that by acting on a vertex operator with certain combinations of the supercharges we can raise or lower $n$ by multiples of 3 while keeping $m$ fixed. At the same time, the supercharges change $m$ by $\pm 1$, while leaving $(-1)^{m+2n}$ unchanged. From this, it follows that we need only three vertex operators per sector, since all other vertex operators can be generated from these states with the supercharges. For example, one can easily check that $V_{0,-5/2}|0\rangle = G^+_{R,-1} G^-_{L,-1} V_{0,1/2}|0\rangle$ and $V_{-1,-1}|0\rangle = G^-_{L,-1} V_{0,1/2}|0\rangle$.
In the Ramond sector, we choose the highest weight states $V_{0,\pm 1/2}|0\rangle$ and $V_{0,3/2}|0\rangle$, since these are the states with lowest energy. Their conformal dimensions are $h_{L,R} = 1/24$ and $h_{L,R} = 3/8$, respectively, and thus their energies are $E = 0$ and $E = 2/3$. Clearly, the same reasoning applies in the Neveu-Schwarz sector and the highest weight states are $V_{0,0}|0\rangle$ and $V_{0,\pm 1}|0\rangle$ with $h_{L,R} = 0$ and $h_{L,R} = 1/6$ respectively.
We can now compare this to the conformal dimensions of the minimal model in the supersymmetric minimal series given in section 3.4. The free boson has central charge $c = 1$, which corresponds to the first ($k = 1$) minimal model (see (3.14)). The highest weight states of the first minimal model in the supersymmetric minimal series can be found from (3.15) with $k = 1$ and $\alpha = 0, 1/2$ in the Ramond and Neveu-Schwarz sector, respectively:

$$\begin{aligned} h &= \frac{1}{24}, \frac{1}{24}, \frac{3}{8} \qquad \text{(R)} \\ h &= 0, \frac{1}{6}, \frac{1}{6} \qquad \text{(NS)}. \end{aligned}$$

This agrees nicely with the highest weight states we identified above. Finally, remember that the two states with $h = 1/24$ are the zero energy states, corresponding to the Witten index of the first ($k = 1$) minimal model: $W_1 = 2$.
To obtain the corresponding $U(1)$ charges, we consider the OPE of $\partial\Phi$ and a vertex operator $V_\alpha$ with conformal dimension $h = \alpha^2/(4g)$

$$\partial\Phi(z) V_\alpha(w) \sim -\frac{\imath\alpha}{2g} \frac{V_\alpha}{(z-w)}. \tag{4.27}$$

The $U(1)$ current, however, satisfies the following OPE with a primary field $\psi$

$$J(z)\psi(w) \sim \frac{q}{(z-w)}\psi(w). \tag{4.28}$$

Using (4.18) and the fact that the vertex operators $V_{m,n}$ have $\alpha_{L,R} = (m \pm 2n/3)$, we find

$$\begin{aligned} J_L(z)V_{m,n}(0,0) &\sim (m/2+n/3)\frac{V_{m,n}}{z} \equiv q_L\frac{V_{m,n}}{z}, \\ J_R(\overline{z})V_{m,n}(0,0) &\sim -(m/2-n/3)\frac{V_{m,n}}{\overline{z}} \equiv q_R\frac{V_{m,n}}{\overline{z}}, \end{aligned}$$

where we defined the $U(1)$ charges

$$q_{L,R} = n/3 \pm m/2. \tag{4.29}$$

For the highest weight states in the Ramond and Neveu-Schwarz sector, we readily verify that $q_{L,R}$ are in accordance with the values for the first minimal model (see (3.15))

$$q_{L,R} = \frac{-1/2+\alpha}{3}, \frac{1/2+\alpha}{3}, \frac{3/2+\alpha}{3}. \tag{4.30}$$

Note that $\alpha$ here refers to the sector of the theory ($\alpha = 0$ in the Ramond sector and $\alpha = 1/2$ in the Neveu-Schwarz sector) and should not be confused with $\alpha_{L,R}$ which are related to the conformal dimensions of the vertex operators.
Supersymmetry implies that the zero energy states in the Ramond sector do not have superpartners. Consequently, they must be annihilated by the zero modes of the supercharges, that is $G^{\pm}_{R,L,0}$. From the inequalities relating the mode $l$ to $m$ and $n$ given above, we find that indeed $G^{\pm}_{R,L,0}V_{0,\pm 1/2}|0\rangle = 0$. The third highest weight state in the Ramond sector, $h_{L,R} = 3/8$, has non-zero energy, so we would expect this state to have a superpartner. In fact, since the left and right movers completely decouple in the continuum limit, the continuum theory has two $\mathcal{N} = 2$ supersymmetries. Consequently, the third highest weight state forms a quadruplet instead of a doublet. We find that there are four states with $h_{L,R} = 3/8$ and energy $E = 3/8 + 3/8 - 1/12 = 2/3$, which are all related via the supercharges

$$\begin{aligned} G^{-}_{L,0}V_{0,3/2}|0\rangle &= V_{-1,0}|0\rangle, \\ G^{+}_{R,0}V_{0,3/2}|0\rangle &= V_{1,0}|0\rangle, \\ G^{-}_{L,0}G^{+}_{R,0}V_{0,3/2}|0\rangle &= G^{+}_{R,0}G^{-}_{L,0}V_{0,3/2}|0\rangle = V_{0,-3/2}|0\rangle. \end{aligned}$$

A pictorial summary of the above can be found in figure 4.2.
This concludes this section, since one can now construct all states in the spectrum from the three highest weight states in a given sector using the Virasoro operators and the supercharges.

### 4.7.2 Lattice operators: fermion number and momentum

In the previous section we discussed the energy spectrum. In the lattice model a state can be characterized, not only by its energy, but also by momentum and fermion number.

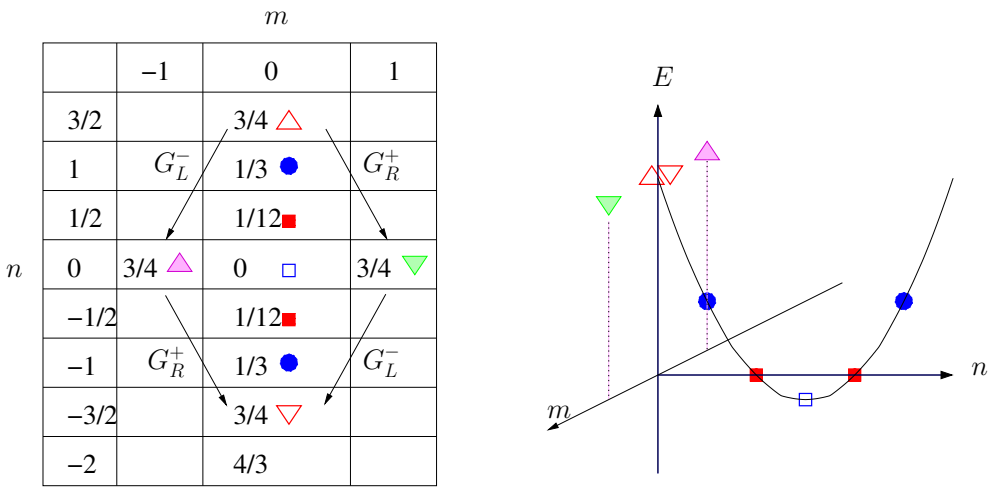


**Figure 4.2:** The table shows $h_L + h_R = 3/4m^2 + 1/3n^2$, where $(-1)^{m+2n}$ is $+1$ in the NS and $-1$ in the R sector. The big arrows point at the superpartners of the state with $h_L + h_R = 3/4$. The symbols can be found in the 3D plot, where the energy $E = h_L + h_R - c/12$ is plotted against $n$ and $m$.

In this section we will identify the corresponding properties in the superconformal field theory.
Remember that the model on the one dimensional periodic chain with length $L = 0$ mod 3 has two $E = 0$ ground states. The ground states have fermion number $f_{GS} = L/3$. In the lattice model each non-zero energy state always has a superpartner with one fermion less or more. Inspection of the action of the supercharges, allows us to identify the index $m$ of a vertex operator $V_{m,n}$ as the charge difference with respect to the ground state charge (or fermion number) in the lattice model: $m = f - f_{GS} = f - L/3$. Using the definition of the $U(1)$ charges (4.29) we can write

$$f - f_{GS} = q_L - q_R = m \tag{4.31}$$

and identify the fermion number operator on the lattice with the difference of the $U(1)$ currents:

$$F = J_{L,0} - J_{R,0} + f_{GS}. \tag{4.32}$$

In the lattice model the translation operator $T$ commutes with both the hamiltonian $H$ and fermion number operator $F$. The eigenvalues $t$ of the translation operator satisfy $t^L = 1$. In the field theory the operator that generates translations in the space direction corresponds to rotations on the complex plane. The momentum operator on the lattice is thus proportional to $L_{L,0} - L_{R,0}$. All highest weight states in the field theory have $h_L = h_R$, which would thus imply zero momentum. However, we know (see 4.3.2) that the zero-energy states in the Ramond sector do not have zero momentum. In the following we will identify the operator that gives the momenta of the highest weight states.
Let us introduce the boundary condition that the wavefunction picks up a factor $\exp(2\pi\imath\alpha)$ when a fermion hops over the end of the chain, i.e. between site $L$ and site 1. This boundary condition is called a twisted boundary condition. For $\alpha = 0$ we have periodic boundary conditions, which corresponds to the Ramond sector (see 3.5), whereas for

$\alpha = 1/2$ we have anti-periodic boundary conditions, corresponding to the Neveu-Schwarz sector. Consequently, the boundary twist in the lattice model corresponds to a spectral flow in the continuum theory (see section 3.6).
In the following we will show, on the one hand, that the momentum of a state in the lattice model depends linearly on the boundary twist and, on the other hand, that also the index $n$ of a vertex operator $V_{m,n}$ will change linearly under spectral flow. These observations will allow us to relate the two.
Momentum, $p \mod 2\pi$, can be defined by writing the eigenvalues of the translation operator as $t = e^{\imath p}$. The boundary twist can be implemented by replacing the term that hops a particle over the boundary $c_L^\dagger c_1 +$ h.c. by $e^{2\pi\imath\alpha}(c_L^\dagger c_1 +$ h.c.). The eigenvalues of the translation operator for general $\alpha$ then follow from

$$T_\alpha^L|\psi\rangle \;=\; e^{\imath p_0 L} e^{2\pi\imath\alpha f}|\psi\rangle \equiv e^{\imath p_\alpha L}|\psi\rangle, \tag{4.33}$$

where $p_0$ is the momentum of $|\psi\rangle$ for $\alpha = 0$, $L$ is the length of the system and $f$ is the total number of particles in the state $|\psi\rangle$. It follows that momentum indeed depends linearly on the boundary twist: $p_\alpha = p_0 + 2\pi\alpha f/L \mod 2\pi$. In the ground state sector we have $f = L/3$ and thus $p = p_0 + 2\pi\alpha/3 \mod 2\pi$.
Now let us consider the continuum theory. In the previous section we have seen that $(-1)^{m+2n} = \pm 1$ in the Neveu-Schwarz and Ramond sector respectively. In the ground state sector we have $m = 0$. It follows that $n$ is half-integer in the Ramond sector and integer in the Neveu-Schwarz sector. We can thus identify the spectral flow operator that conserves fermion number $m$, and takes us from the Ramond sector to the Neveu-Schwarz sector, as the operator $V_{0,1/2}$. More generally, the operator $V_{0,\alpha}$ corresponds to the lattice model operator that introduces the boundary twist $\alpha$.
If we now combine the fact that $p_\alpha = p_0 + 2\pi\alpha/3 + 2\pi\alpha m/L \mod 2\pi$ for a state in the lattice model and $n = n_0 + \alpha$ for an operator in the field theory, we find that $p$ is proportional to $n$. By eliminating $\alpha$ and using the known results for the zero energy ground states in the lattice model we obtain

$$p = 2\pi n/3 + 2\pi n m/L + f_{GS}\pi \mod 2\pi. \tag{4.34}$$

For the Ramond vacua $V_{0,\pm 1/2}|0\rangle$ we can easily check this relation. We know that the two ground states of the periodic chain of length $L = 3j$ have momenta $p_0 = \pm\pi/3 + \pi f_{GS} \mod 2\pi$. Since the Ramond vacua have $n = \pm 1/2$ and $m = 0$, we find that this indeed nicely agrees with the equation above. Note that the middle term is precisely $2\pi(h_R - h_L)/L$. Finally, using the definition of the $U(1)$ charges (4.29) we can write momentum as

$$p = (q_L + q_R)\pi + 2\pi(h_R - h_L)/L + f_{GS}\pi \mod 2\pi \tag{4.35}$$

and we find that the momentum operator on the lattice can be expressed as

$$P \;=\; (J_{L,0} + J_{R,0})\pi + (L_{L,0} - L_{R,0})2\pi/L + f_{GS}\pi \mod 2\pi. \tag{4.36}$$

### 4.7.3 Highest weight state and descendants

We are now fully equipped to construct the entire energy spectrum of the superconformal field theory. We start from the highest weight states and build the spectrum by acting

**Table 4.2:** In this table we show the descendants of the highest weight state $V_{0,1/2}|0\rangle$. This is one of the two zero energy states in the Ramond sector. We order the descendants by their energy, also called level, in the first column. The energy is given by $E = h_L + h_R - 1/12$. In the second column we give the state $L_{L,-l_1} \dots L_{L,-l_s} L_{R,-r_1} \dots L_{R,-r_q} V_{n,m}|0\rangle_{NS} \equiv |h_L - 1/24 + \sum_{i=1}^{s} l_i, h_R - 1/24 + \sum_{i=1}^{q} r_i\rangle$. In the third column we give $h_L - h_R$, which is directly related to the change in momentum with respect to the highest weight state. In the fourth column we give all the fields that correspond to the state given in the second column and finally, in the last column we give the charge $m$. The charge gives the change in fermion number with respect to the highest weight state.

| Energy | State | $h_L - h_R$ | Fields | Charge |
|---|---|---|---|---|
| 0 | $\|0,0>$ | 0 | $V_{0,1/2}$ | 0 |
| 1 | $\|1,0>$ | 1 | $L_{L,-1}V_{0,1/2}$ | 0 |
| | | | $G^-_{L,-1}V_{0,1/2} = V_{-1,-1}$ | -1 |
| | $\|0,1>$ | -1 | $L_{R,-1}V_{0,1/2}$ | 0 |
| | | | $G^+_{R,-1}V_{0,1/2} = V_{1,-1}$ | 1 |
| 2 | $\|2,0>$ | 2 | $L_{L,-1}L_{L,-1}V_{0,1/2}$ | 0 |
| | | | $L_{L,-2}V_{0,1/2}$ | 0 |
| | | | $G^+_{L,-2}V_{0,1/2} = V_{1,2}$ | 1 |
| | | | $L_{L,-1}G^-_{L,-1}V_{0,1/2} = L_{L,-1}V_{-1,-1}$ | -1 |
| | $\|1,1>$ | 0 | $L_{L,-1}L_{R,-1}V_{0,1/2}$ | 0 |
| | | | $L_{R,-1}G^-_{L,-1}V_{0,1/2} = L_{R,-1}V_{-1,-1}$ | -1 |
| | | | $L_{L,-1}G^+_{R,-1}V_{0,1/2} = L_{L,-1}V_{1,-1}$ | 1 |
| | | | $G^+_{R,-1}G^-_{L,-1}V_{0,1/2} = V_{0,-5/2}$ | 0 |
| | $\|0,2>$ | -2 | $L_{R,-1}L_{R,-1}V_{0,1/2}$ | 0 |
| | | | $L_{R,-2}V_{0,1/2}$ | 0 |
| | | | $G^-_{R,-2}V_{0,1/2} = V_{-1,2}$ | -1 |
| | | | $L_{R,-1}G^+_{R,-1}V_{0,1/2} = L_{R,-1}V_{1,-1}$ | 1 |
| ... | | | | |

on these states with the operators $L_{(R,L),-n}$ and $G^{\pm}_{(R,L),-l}$, with $l, n > 0$. Let us work out an example. We start from one of the Ramond vacua: $V_{0,1/2}|0\rangle$. It is now convenient to write a highest weight state as $V_{n,m}|0\rangle_{NS} = |h_L - 1/24, h_R - 1/24\rangle$, so for the Ramond vacuum under consideration we write $V_{0,1/2}|0\rangle = |0,0\rangle$. The action of $L_{L,-n}$ is now simply $L_{L,-n}|h_L - 1/24, h_R - 1/24\rangle = |h_L - 1/24 + n, h_R - 1/24\rangle$ and similarly for $L_{R,-n}$. Putting everything together, we summarize the spectrum that follows from this particular highest weight state in table 4.2 and in figure 4.3. The energy follows from $E = h_L + h_R - 1/12$, momentum is given by $P = 2\pi(h_L - h_R)/L + p$, with $p = 2\pi n/3 + f\pi \mod 2\pi$ and the charge is simply $m$. Since $p$ is left unchanged by both the Virasoro operators as well as the supercharges, all states generated from the Ramond vacuum $V_{0,1/2}|0\rangle$ have momentum $P = 2\pi(h_L - h_R)/L + \pi/3 + f_{GS}\pi \mod 2\pi$. To save space, we just give $h_L - h_R$ in the table.

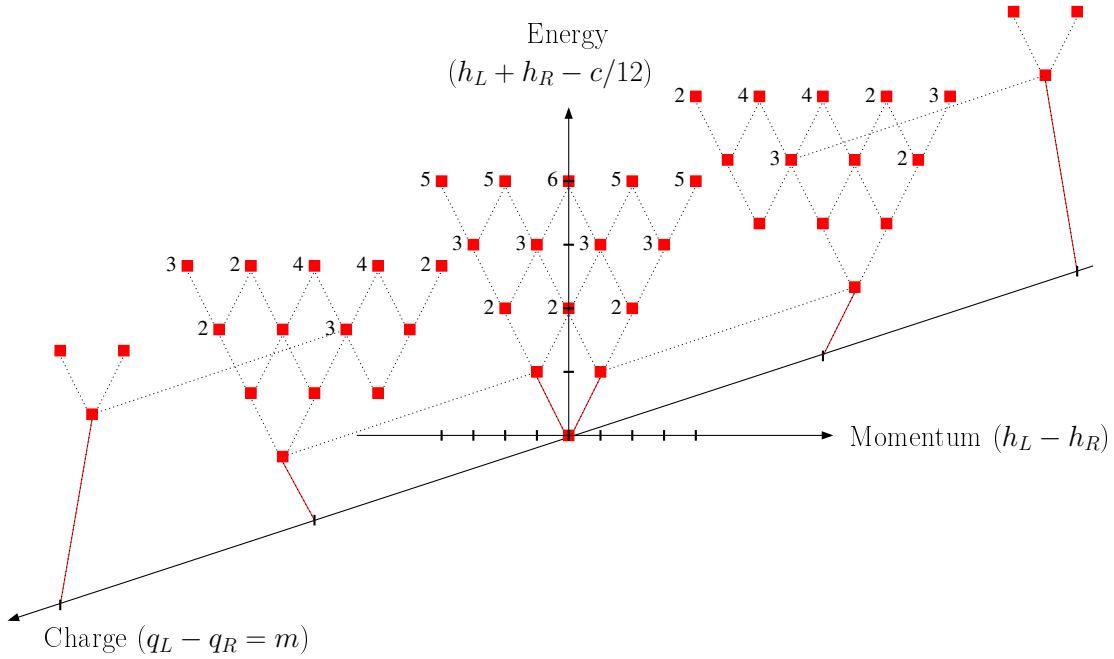


**Figure 4.3:** We depict the highest weight state $V_{0,1/2}|0\rangle$ and its descendants in a 3D plot. The energy (first column in table 4.2) runs on the vertical axis. Horizontally, we plot the momentum $h_L - h_R$ and the fermion number $m$ relative to the highest weight state (third and last column in table 4.2). The labels indicate the degeneracy of the state (states with no label are non-degenerate). Finally, the dotted lines serve as guides to the eye.

### 4.7.4 Partition sum

In this section we briefly discuss the partition sum and character formula's. Remember that computing the partition sum at finite temperature is equivalent to computing the path integral with the imaginary time direction compactified. Let $w$ be the complex coordinate parametrizing the cylinder, where time runs along the cylinder. We know that translations in the time direction are generated by the hamiltonian, whereas translations in the space direction are generated by the momentum operator. To compactify the time direction we need to identify two periods in $w$ defining a torus: $w \equiv w + 2\pi\omega_1$ and $w \equiv w + 2\pi\omega_2$. Because of conformal invariance this can be rescaled, so that there is only one parameter characterizing the torus, the modular parameter, $\tau = \omega_2/\omega_1$. Clearly, the modular parameter is a complex parameter and can be written as $\tau = \tau_1 + \imath\tau_2$, with $\tau_1$ and $\tau_2$ real parameters. It now follows that a translation in space-time along the $\tau$ direction over a distance $a$ is given by the operator

$$\exp\left[-\frac{a}{2\pi|\tau|}(2\pi H\tau_2 - 2\pi\imath P\tau_1)\right]. \tag{4.37}$$

If we now consider $a$ as the lattice spacing in a two dimensional statistical mechanical model, the above parameter is simply the transfer matrix from one row in the model to the next. It follows that we can write the partition sum as the trace over this operator to the power $l$ (see also section 4.3.1), such that $al = 2\pi|\tau|$, the period of the system. So we find

$$Z = \mathrm{Tr}\ \exp\left[-2\pi H\tau_2 + 2\pi\imath P\tau_1\right]. \tag{4.38}$$

Using the expressions of $H$ and $P$ on the cylinder in terms of the Virasoro generators, we find

$$\begin{aligned} Z &= \text{Tr } \exp\left[-2\pi(L_0 - c/24 + \overline{L}_0 - \overline{c}/24)\tau_2 + 2\pi\imath(L_0 - c/24 - \overline{L}_0 + \overline{c}/24)\tau_1\right] \\ &= \text{Tr } \exp\left[2\pi\imath\tau(L_0 - c/24)\right] \exp\left[-2\pi\imath\overline{\tau}(\overline{L}_0 - \overline{c}/24)\right] \\ &= \text{Tr } q^{L_0 - c/24}\overline{q}^{\overline{L}_0 - \overline{c}/24}, \end{aligned} \tag{4.39}$$

where $q \equiv e^{2\pi\imath\tau}$.
To find an explicit expression for the partition sum, we thus have to compute the traces of $q^{L_0-c/24}$ and $\overline{q}^{\overline{L}_0-\overline{c}/24}$. Since the spectrum decomposes in highest weight states and their descendants, it is convenient to also decompose the trace this way. A highest weight state of conformal dimension $h$ has $L_0|h\rangle = h|h\rangle$ and its descendants have $L_0 L_{-n_k} \dots L_{-n_2} L_{-n_1}|h\rangle = (h + n_k + \dots + n_2 + n_1) L_{-n_k} \dots L_{-n_2} L_{-n_1}|h\rangle$, with all $n_i$ positive. The trace of $q^{L_0-c/24}$ restricted to this highest weight state and its descendants is called the character, usually denoted by $\chi_h(q)$. We find that

$$\chi_h(q) = \sum_n \dim(h+n) q^{h+n-c/24}, \tag{4.40}$$

where $\dim(h+n)$ denotes the number of linearly independent states at level $n$. It can be shown that this number is precisely $p(n)$, the number of integer partitions of $n$. Since the generating function of $p(n)$ is given by

$$\sum_n p(n) x^n = \prod_{k=1}^{\infty} (1 - x^k)^{-1}, \tag{4.41}$$

we find

$$\begin{aligned} \chi_h(q) &= \sum_n p(n) q^{h+n-c/24} \\ &= q^{h-c/24} \prod_{k=1}^{\infty} (1 - q^k)^{-1}. \end{aligned} \tag{4.42}$$

In the literature one usually defines $\eta(q) \equiv q^{c/24} \prod_{k=1}^{\infty}(1-q^k)$, such that the character can be written as $\chi_h(q) = q^h/\eta(q)$.
Remembering that for the free boson we have $c = \overline{c} = 1$ and conformal dimensions $h_{L,R}(m,n) = (m \pm gn)^2/(4g)$, we can write the partition sum as

$$\begin{aligned} Z &= \text{Tr } q^{L_0 - 1/24}\overline{q}^{\overline{L}_0 - 1/24} \\ &= \frac{1}{\eta\overline{\eta}} \sum_{m,n} q^{h_L(m,n)} \overline{q}^{h_R(m,n)} \\ &= \frac{1}{\eta\overline{\eta}} \sum_{m,n} q^{(m+gn)^2/(4g)} \overline{q}^{(m-gn)^2/(4g)}, \end{aligned} \tag{4.43}$$

with $\overline{\eta} = \eta(\overline{q})$ and $\eta(q) = q^{1/24} \prod_{k=1}^{\infty}(1-q^k)$. Finally, the coupling $g$ is related to the compactification radius as $g = 2/R^2$.

### 4.7.5 Fermi velocity

The finite-size scaling of the energy depends on the boundary conditions. For (anti-) periodic boundary conditions, which corresponds to the cylinder on the field theory side, the scaling is given by [63, 64]

$$E_{\text{num}} = 2\pi E_{\text{SCFT}} v_F / N + \mathcal{O}(1/N^2), \tag{4.44}$$

where $N$ is the length of the finite system and $v_F$ the Fermi velocity. It follows that by comparing the finite size spectra with the spectrum of the field theory one can extract the Fermi velocity. In this case, however we can also obtain the Fermi velocity using the mapping of the supersymmetric model onto the XXZ chain. For the XXZ chain (4.11) the Fermi velocity is given by

$$v_F(\Delta) = \pi \sin\theta/\theta, \tag{4.45}$$

with $\cos\theta = -\Delta$. The supersymmetric model maps to the XXZ chain with $\Delta = -1/2$, so we find $\theta = \pi/3$ and the Fermi velocity of the corresponding XXZ chain is $v_F = (3\sqrt{3})/2$. To find the Fermi velocity for the supersymmetric model, we note that the length $N$ of XXZ chain is related to the length $L$ of the supersymmetric chain via $N = L - f$, where $f$ is the number of fermions in the supersymmetric model [23]. In the continuum limit the low energy states have approximately $f = L/3$, so $N = 2L/3$. Combining all this, we find for the supersymmetric model that

$$E_{\text{num}} = 2\pi E_{\text{SCFT}} v_F / L + \mathcal{O}(1/L^2), \tag{4.46}$$

with Fermi velocity $v_F = 3/2 v_{F,XXZ} = (9\sqrt{3})/4$.

### 4.7.6 Chain of length $L = \pm 1 \mod 3$

In the previous sections we have identified the Ramond sector of the field theory to correspond to the lattice model on a chain with length $L = 0 \mod 3$ with periodic boundary conditions. For the chain of length $L = 3j$, the fermion number in the ground state sector is $f_{GS} = L/3 = j$. For a chain of length $L = 3j \pm 1$, we would correspondingly find $f_{GS} = L/3 = j \pm 1/3$. We know, however, that for a chain of length $L = 3j \pm 1$ the ground state has fermion number $f_{GS} = j$. It follows that, compared to the chain of length $L = 3j$, the chain of length $L = 3j \pm 1$ has a slightly lower/higher charge density in the ground state sector. Now remember that $m$ gives the charge compared to the charge in the ground state sector of the chain of length $L = 3j$, that is $L/3$. Suppose that instead of $m = f - f_{GS}$, we now write $m = f - L/3$. For the chain of length $L = 3j$, the two definition are completely equivalent. However, for a chain of length $L = 3j \pm 1$ we now find that $m = f_{GS} - L/3 = \mp 1/3$ in the ground state sector. The supersymmetry in the lattice model tells us that the chain with periodic boundary conditions corresponds to the Ramond sector in the field theory. Now that $m$ takes values in $\mathbb{Z} \mp 1/3$, it follows that in the Ramond sector, which has $3m/2 + n \in \mathbb{Z} + 1/2$, $n$ is now integer. In fact, we find that adding or subtracting one site from a chain of length $L = 3j$ corresponds in the field theory to acting with the operator $V_{\mp 1/3,-1/2}$. Upon acting with this operator the highest weight states in the Ramond sector become

$$V_{\mp 1/3,-1}|0\rangle, V_{\mp 1/3,0}|0\rangle \text{ and } V_{\mp 1/3,1}|0\rangle, \tag{4.47}$$

for the chains of length $L = 3j \pm 1$. The corresponding energies are respectively $E = 1/3, 0$ and $1/3$. This agrees with the fact that these chain lengths only have one zero energy ground state. Furthermore, we see that, since the ground state has $n = 0$, it has the correct momentum $p = 0 + j\pi \mod 2\pi$.

### 4.7.7 Finite size spectra

In this section we analyze the numerically obtained spectra for the supersymmetric model on the chain with periodic and anti-periodic boundary conditions. We consider lengths up to $L = 27$. Since the hamiltonian commutes with the fermion number operator $F$ and translation operator $T$, we can block diagonalize the hamiltonian. To do this we construct a basis of eigenstates of $F$ and $T$. The first is straightforward since each configuration is an eigenstate of $F$, since it has a well defined particle number. The latter requires a bit more work. An eigenstate of $T$ clearly obeys

$$T|\Psi\rangle = t|\Psi\rangle. \tag{4.48}$$

Given a certain configuration $|C\rangle$, we can construct an eigenstate of $T$ by writing

$$|\Psi\rangle = \sum_{l=1}^{L} t^{-l}(T)^l|C\rangle. \tag{4.49}$$

The slightly subtle part now concerns the possible values of $t$. Remember that for a state with $f$ fermions the eigenvalues of $T$ satisfy $t^L = e^{2\pi\imath\alpha f}$, with $\alpha = 0$ for periodic bc and $\alpha = 1$ for anti-periodic bc. It follows that in principle $t$ can take all values $t_k = e^{2\pi\imath(\alpha f+k)/L}$, with $k = 1, 2, \ldots, L$. This is not true, however, if the configuration $|C\rangle$ maps onto itself under the action of $T^n$, with $n < L$, that is

$$T^n|C\rangle = (-1)^s e^{2\pi\imath\alpha f n/L}|C\rangle, \tag{4.50}$$

with $s = f^2 n(L-n)/L^2$, is the sign that comes from the Fermi statistics of the particles ($nf/L$ fermions hop over $(L-n)f/L$ fermions). It then follows that $t$ can only take the values $t_k = e^{2\pi\imath(\alpha f/L + s/2n + k/n)}$, with $k = 1, 2, \ldots, n$.
Upon using these symmetries the hamiltonian block diagonalizes into blocks $H_{f,t}$. At length $L = 27$ the largest block has $f = 8$ and $t = e^{2\pi\imath(\alpha 8+k)/27}$, with $k = 1, \ldots, 27$. The dimension of the Hilbert space in this sector is 4000. This matrix size can be effectively handled by the built-in diagonalization scheme of Matlab.
We have concluded in the previous sections that chains of length $L = 3j$ with anti-periodic bc correspond to the vacuum sector of the superconformal field theory. Indeed numerically, we find that for these systems there is one negative energy state with fermion number $f = L/3$ (see figure 4.4(f) for an example). In figure 4.5(a) the energy of this state is plotted for various system sizes as a function of one over the length of the system. Remember that the scaling is given by [63, 64]

$$E_{\text{num}} = 2\pi E_{\text{SCFT}} v_F/L + \mathcal{O}(1/L^2), \tag{4.51}$$

where $E_{\text{SCFT}} = h_L + h_R - c/12$ and $v_F = 9\sqrt{3}/4$. For the vacuum we have $h_L = h_R = 0$ and since $c = 1$, we find that the energy of these states scales as $E_{\text{num}} = -3\sqrt{3}\pi/(8N) \approx$

$-2.041/N$. The function that gives the best fit to the numerics is $f(L) = a/L+b/L^2+c/L^3$ with $a = -2.038$, $b = -0.056$ and $c = -6.509$. Clearly, the value of $a$ agrees well with the theoretical value.

We perform this scaling analysis for all highest weight states and some descendants for all boundary conditions, that is periodic and anti-periodic and lengths $L = 3j$ and $L = 3j \pm 1$. In the field theory these boundary condition correspond to the Ramond and Neveu-Schwarz sectors and the untwisted ($L = 3j$) and twisted ($L = 3j \pm 1$) sectors. By twisted sectors, we mean the sectors where $m$ takes values in $\mathbb{Z} \pm 1/3$ (see section 4.7.6). We have plotted the spectra of the largest system sizes for the particle numbers at which the highest weight states occur and indicated for which states we performed the scaling analysis (fig. 4.4). The scaling data and the fits are shown in figure 4.5. The results are summarized in table 4.3.

An interesting point is that for the periodic chain of length $L = 3j$, the two states that correspond to the fields $V_{0,\pm 3/2}$ are not degenerate at finite size (in figure 4.4(e)) these are the states with labels 3 and 4). The same is true for the states with labels 5 and 6 in 4.4(e) which correspond to the fields $L_{-1;L/R}V_{0,1/2}$. Since the model is exactly solvable, we know that this must be a finite size effect and should thus vanish in the continuum limit (see also [65]). For the two states that correspond to the fields $V_{0,\pm 3/2}$, we checked this explicitly by verifying that the energy difference between the two states goes to zero faster than one over the length of the system. Indeed, we find that the energy difference scales as $a/L^2 + b/L^3$, with $a = 52$ and $b = -86$.

Remarkably, we find that the states with the higher energy have superpartners at $f = j+1$, whereas the states with lower energy have superpartners at $f = j - 1$. This is probably explained as follows. The continuum limit holds for systems of infinite size close to or at 1/3 filling. In the continuum limit there is a particle-hole symmetry corresponding to the mapping $m, n \to -m, -n$. In a finite size system, however, the particle-hole symmetry is not realized, because of the nearest-neighbor exclusion rule. At 1/3 filling it thus costs more energy to add a particle than to take out a particle, since one is closer to the completely full system than the completely empty system.

Another way to see this is via the mapping to the XXZ chain. The supersymmetric model on a chain of length $L$ at 1/3 filling corresponds to the XXZ chain of length $N$ at zero magnetization. The two chain lengths are related via $N = L - f$, where $f$ is the number of fermions in the supersymmetric model. It follows that the supercharges which add or remove a fermion in the supersymmetric model translate into operators on the spin chain which change the length of the chain. Since the energy scales as one over the length, a states with more particles in the supersymmetric model, which has a shorter length in the XXZ chain, will thus have a higher energy. Conversely, a state with less particles will have a lower energy.

## 4.8 Spectral flow

In superconformal field theory one can define a spectral flow operator that maps the Ramond sector to a sector with $r \in \mathbb{Z}+\alpha$, where $r$ labels the modes in the mode expansion of the supercharge (3.6). In this section we will discuss the effect of this operator on the states, first for a general superconformal field theory (see also section 3.6) and later for the first supersymmetric minimal model in particular. In the lattice model the spectral

**Table 4.3:** This table contains a summary of the data extracted from the finite size spectra and the scaling fits. The first column contains the labels which can be found in figures 4.4 and 4.5. In the last column, we defined $P'_{\text{num}} \equiv P_{\text{num}} + \pi j \mod 2\pi$.

$L = 3j$

| label | BC | $n$ | field | $E_{\text{SCFT}}$ | $h_L - h_R$ | $(q_L + q_R)\pi$ | $E_{\text{num}}L/(2\pi v_F)$ | $P'_{\text{num}}$ |
|---|---|---|---|---|---|---|---|---|
| 1 | $R$ | $-\frac{1}{2}$ | $V_{0,-\frac{1}{2}}$ | 0 | 0 | $\frac{5\pi}{3}$ | 0 | $\frac{5\pi}{3}$ |
| 2 | $R$ | $\frac{1}{2}$ | $V_{0,\frac{1}{2}}$ | 0 | 0 | $\frac{\pi}{3}$ | 0 | $\frac{\pi}{3}$ |
| 3 | $R$ | $-\frac{3}{2}$ | $V_{0,-\frac{3}{2}}$ | $\frac{2}{3}$ | 0 | $\pi$ | 0.670 | $\pi$ |
| 4 | $R$ | $\frac{3}{2}$ | $V_{0,\frac{3}{2}}$ | $\frac{2}{3}$ | 0 | $\pi$ | 0.666 | $\pi$ |
| 5 | $R$ | $\frac{1}{2}$ | $L_{L,-1}V_{0,\frac{1}{2}}$ | 1 | 1 | $\frac{\pi}{3}$ | 1.004 | $\frac{\pi}{3} + \frac{2\pi}{L}$ |
| 6 | $R$ | $\frac{1}{2}$ | $L_{R,-1}V_{0,\frac{1}{2}}$ | 1 | $-1$ | $\frac{\pi}{3}$ | 0.997 | $\frac{\pi}{3} - \frac{2\pi}{L}$ |
| 7 | NS | 0 | $V_{0,0}$ | $-\frac{1}{12}$ | 0 | 0 | $-0.0832$ | 0 |
| 8 | NS | 1 | $V_{0,1}$ | $\frac{1}{4}$ | 0 | $\frac{2\pi}{3}$ | 0.250 | $\frac{2\pi}{3}$ |
| 9 | NS | $-1$ | $V_{0,-1}$ | $\frac{1}{4}$ | 0 | $\frac{4\pi}{3}$ | 0.250 | $\frac{4\pi}{3}$ |

$L = 3j + 1$

| label | BC | $n$ | field | $E_{\text{SCFT}}$ | $h_L - h_R$ | $(q_L + q_R)\pi$ | $E_{\text{num}}L/(2\pi v_F)$ | $P'_{\text{num}}$ |
|---|---|---|---|---|---|---|---|---|
| 1 | $R$ | 0 | $V_{-\frac{1}{3},0}$ | 0 | 0 | 0 | 0 | 0 |
| 2 | $R$ | $-1$ | $V_{-\frac{1}{3},-1}$ | $\frac{1}{3}$ | 0 | $\frac{4\pi}{3}$ | 0.333 | $\frac{4\pi}{3} + \frac{2\pi}{9j}$ |
| 3 | $R$ | 1 | $V_{-\frac{1}{3},1}$ | $\frac{1}{3}$ | 0 | $\frac{2\pi}{3}$ | 0.333 | $\frac{2\pi}{3} - \frac{2\pi}{9j}$ |
| 4 | $R$ | 0 | $L_{L,-1}V_{-\frac{1}{3},0}$ | 1 | 1 | 0 | 1.001 | $\frac{2\pi}{L}$ |
| 5 | $R$ | 0 | $L_{R,-1}V_{-\frac{1}{3},0}$ | 1 | $-1$ | 0 | 1.001 | $-\frac{2\pi}{L}$ |
| 6 | NS | $\frac{1}{2}$ | $V_{-\frac{1}{3},\frac{1}{2}}$ | $\frac{1}{12}$ | 0 | $\frac{\pi}{3}$ | 0.0831 | $\frac{\pi}{3} - \frac{\pi}{9j}$ |
| 7 | NS | $-\frac{1}{2}$ | $V_{-\frac{1}{3},-\frac{1}{2}}$ | $\frac{1}{12}$ | 0 | $\frac{5\pi}{3}$ | 0.0831 | $\frac{5\pi}{3} + \frac{\pi}{9j}$ |
| 8 | NS | $\frac{3}{2}$ | $V_{-\frac{1}{3},\frac{\pm 3}{2}}$ | $\frac{3}{4}$ | 0 | $\pi$ | 0.752 | $\pi \pm \frac{\pi}{3j}$ |

$L = 3j - 1$

| label | BC | $n$ | field | $E_{\text{SCFT}}$ | $h_L - h_R$ | $(q_L + q_R)\pi$ | $E_{\text{num}}L/(2\pi v_F)$ | $P'_{\text{num}}$ |
|---|---|---|---|---|---|---|---|---|
| 1 | $R$ | 0 | $V_{\frac{1}{3},0}$ | 0 | 0 | 0 | 0 | 0 |
| 2 | $R$ | $-1$ | $V_{\frac{1}{3},-1}$ | $\frac{1}{3}$ | 0 | $\frac{4\pi}{3}$ | 0.333 | $\frac{4\pi}{3} - \frac{2\pi}{9j}$ |
| 3 | $R$ | 1 | $V_{\frac{1}{3},1}$ | $\frac{1}{3}$ | 0 | $\frac{2\pi}{3}$ | 0.333 | $\frac{2\pi}{3} + \frac{2\pi}{9j}$ |
| 4 | $R$ | 0 | $L_{L,-1}V_{\frac{1}{3},0}$ | 1 | 1 | 0 | 1.002 | $\frac{2\pi}{L}$ |
| 5 | $R$ | 0 | $L_{R,-1}V_{\frac{1}{3},0}$ | 1 | $-1$ | 0 | 1.002 | $-\frac{2\pi}{L}$ |
| 6 | NS | $\frac{1}{2}$ | $V_{\frac{1}{3},\frac{1}{2}}$ | $\frac{1}{12}$ | 0 | $\frac{\pi}{3}$ | 0.0835 | $\frac{\pi}{3} + \frac{\pi}{9j}$ |
| 7 | NS | $-\frac{1}{2}$ | $V_{\frac{1}{3},-\frac{1}{2}}$ | $\frac{1}{12}$ | 0 | $\frac{5\pi}{3}$ | 0.0835 | $\frac{5\pi}{3} - \frac{\pi}{9j}$ |
| 8 | NS | $\frac{3}{2}$ | $V_{\frac{1}{3},\frac{\pm 3}{2}}$ | $\frac{3}{4}$ | 0 | $\pi$ | 0.753 | $\pi \pm \frac{\pi}{3j}$ |

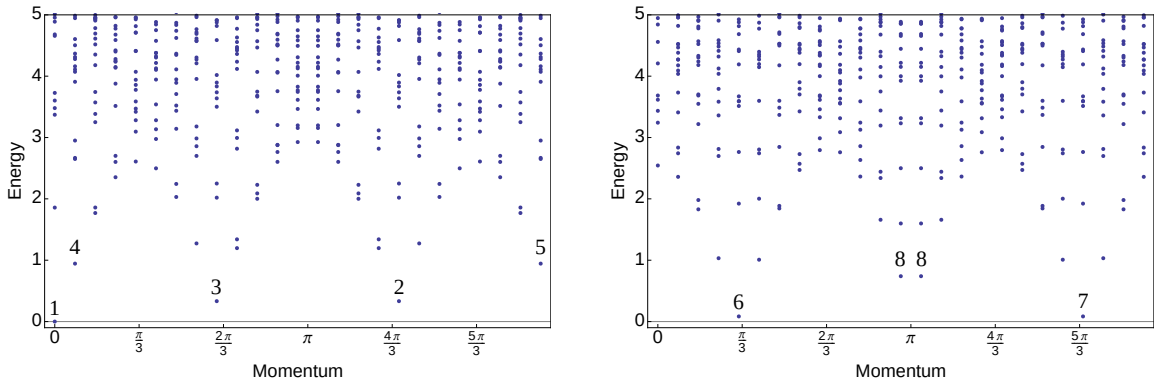


(a) $L = 25,\ f = 8,\ \alpha = 0$ (b) $L = 25,\ f = 8,\ \alpha = 1/2$

(c) $L = 26,\ f = 9,\ \alpha = 0$ (d) $L = 26,\ f = 9,\ \alpha = 1/2$

(e) $L = 27,\ f = 9,\ \alpha = 0$ (f) $L = 27,\ f = 9,\ \alpha = 1/2$

**Figure 4.4:** Energy versus momentum for chains of lengths $L = 25, 26, 27$ with periodic ($\alpha = 0$) and anti-periodic ($\alpha = 1/2$) boundary conditions and fermion number $f = \text{int}(L/3)$. The labels of the states refer to the numbers in the first column in table 4.3.

flow operator corresponds to the boundary twist operator. This correspondence will prove very powerful in identifying critical modes in supersymmetric models on ladders. Since the supersymmetric model on the chain is exactly solvable, we know that the spectral flow should correctly describe the boundary twist. We have already seen that the scaling behavior of the finite size spectra nicely corresponds to the behavior one expects from the field theory. However, for more complicated systems extracting the scaling behavior can be very challenging, whereas boundary twists are easily carried out. For this reason we

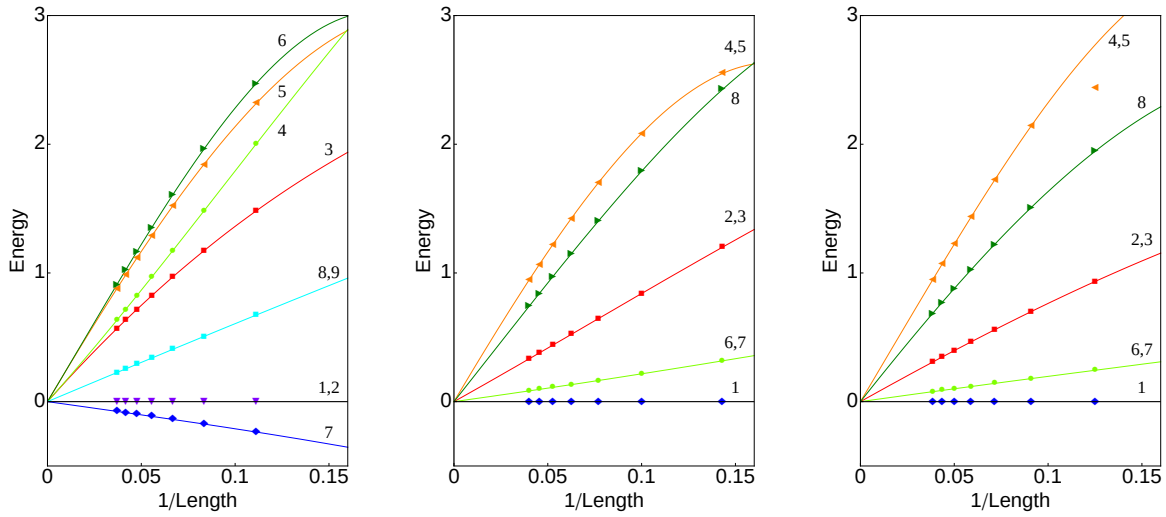


(a) $L = 3j$ (b) $L = 3j + 1$ (c) $L = 3j - 1$

**Figure 4.5:** Energy versus the inverse chain length for chains with periodic and anti-periodic boundary conditions. The numerical data and fits are shown. The fit function is $f(L) = a/L + b/L^2 + c/L^3$. The labels of the fits refer to the numbers in the first column in table 4.3.

will discuss the spectral flow and boundary twist for the chain here in quite some detail. In general we have that a spectral flow characterized by the parameter $\alpha$ in a superconformal field theory with central charge $c$ has the following effect on the conformal dimensions and charges [49]

$$\begin{aligned} h^{\alpha}_{L,R} &= h^{0}_{L,R} + \alpha q^{0}_{L,R} + \frac{c}{6}\alpha^2 \\ q^{\alpha}_{L,R} &= q^{0}_{L,R} + \frac{c}{3}\alpha. \end{aligned} \tag{4.52}$$

It follows that energy changes parabolically with $\alpha$ under spectral flow

$$E_{\alpha} = E_0 + \alpha(q_L + q_R) + \frac{c}{3}\alpha^2. \tag{4.53}$$

If we define $Q = q_L - q_R$ and $\tilde{Q} = q_L + q_R$, which are related to charge and momentum respectively, we find that under spectral flow

$$\begin{aligned} Q_{\alpha} &= Q_0, \\ \tilde{Q}_{\alpha} &= \tilde{Q}_0 + \frac{2c}{3}\alpha, \end{aligned} \tag{4.54}$$

that is $Q$ is invariant and $\tilde{Q}$ changes linearly with $\alpha$ under spectral flow.
In the lattice model we can go from periodic to anti-periodic boundary conditions continuously by replacing the term that hops a particle over the boundary $c^{\dagger}_{L}c_1 +$ h.c. by $e^{2\pi\imath\alpha}c^{\dagger}_{L}c_1 +$ h.c. The eigenvalues of the translation operator $p_{\alpha}$ will then depend linearly on the twist parameter:

$$T^{L}_{\alpha}|\psi\rangle = e^{\imath p_0 L}e^{2\pi\imath\alpha f}|\psi\rangle \equiv e^{\imath p_{\alpha} L}|\psi\rangle, \tag{4.55}$$

so $p_\alpha = p_0 + 2\pi\alpha f/L \mod 2\pi$ where $L$ is the length of the system and $f$ is the total number of particles in the state $|\psi\rangle$.
To compare the numerical values we obtain for the energy of finite size systems of length $L$ with a boundary twist we use $E_{\text{num}}(\alpha) = 2\pi E_\alpha v_F/L$, where $v_F$ is the Fermi velocity. Using the linear relation between momentum in the lattice model and the twist $\alpha$, we can express the energy as a parabolic function of momentum

$$E_{\text{num}}(p_\alpha) = 2\pi E_0 v_F/L + \frac{(p_\alpha - p_0)\tilde{Q}_0 v_F}{f} + \frac{c(p_\alpha - p_0)^2 v_F L}{6\pi f^2}$$

It follows that in a finite size system we should be able to fit the energies to the following curve

$$E_{\text{num}}(p_\alpha) = a + bp_\alpha + dp_\alpha^2, \tag{4.56}$$

where the fit parameters $b$ and $d$ will satisfy

$$\begin{aligned} b &= \frac{\tilde{Q}_0 v_F}{f} - \frac{cp_0 L v_F}{3\pi f^2}, \\ d &= \frac{cLv_F}{6\pi f^2}. \end{aligned} \tag{4.57}$$

If we combine this with $E_{\text{num}}(p_{\alpha=0}) = 2\pi E_0 v_F/L$, we have three equations for four parameters in the continuum theory: the central charge $c$, the energy in the Ramond sector $E_0$, the sum of the $U(1)$ charges $\tilde{Q}$ and finally the Fermi velocity $v_F$. It follows that from the energy dependence on a boundary twist, one can extract $c$, $E_0$ and $\tilde{Q}$ as functions of the Fermi velocity.
Let us now go back to the supersymmetric model on the chain and thus the first supersymmetric minimal model. In section 4.7.2, we identified the operator $V_{0,\alpha}$ as the operator that corresponds to the boundary twist in the lattice model. Upon comparison with the general expression for the spectral flow operator (3.24) we find that this boundary twist operator is indeed the spectral flow operator:

$$\begin{aligned} U(z,\bar{z}) &= \exp\left[\imath\sqrt{\frac{2gc}{3}}\alpha(\Phi_L - \Phi_R)\right] \\ &= \exp\left[\imath\alpha\tilde{\Phi}\right] \\ &= V_{0,\alpha}. \end{aligned} \tag{4.58}$$

We can easily derive expressions for the energy, momentum and fermion number of the highest weight states under the action of this operator. The operator $V_{0,\alpha}$ leaves $m$ unchanged and sends $n$ to $n+\alpha$, so we find

$$\begin{aligned} f_\alpha &= f_0, \\ E_\alpha &= E_0 + \frac{2n\alpha + \alpha^2}{3}, \\ p_\alpha &= p_0 + \frac{2\pi\alpha}{3} \mod 2\pi. \end{aligned}$$

where $f_0, E_0$ and $p_0$ are the values of fermion number, energy and momentum of the highest weight states in the Ramond sector. To check that this agrees with the general spectral flow equations given in (4.53) and (4.54), remember that $f$ and $p$ can be expressed in terms of $Q$ and $\tilde{Q}$ as $f = Q + f_{GS}$ and $p = (\tilde{Q} + f)\pi \mod 2\pi$.

### 4.8.1 Spectral flow in finite size spectra

In this section we present the data for periodic chains of lengths up to $L = 27$ with a boundary twist. In the lattice model the boundary twist is implemented by replacing the term in the hamiltonian that hops a particle over the boundary $c_L^\dagger c_1 +$ h.c. by $e^{2\pi\imath\alpha}(c_L^\dagger c_1 +$ h.c.). We compute the spectra for various values of $\alpha$ to extract the behavior of the energy as a function of the twist parameter $\alpha$. Note that the spectrum of the system with twist parameter $-\alpha$ can be obtained from the spectrum with $+\alpha$ using symmetry arguments. To see this we first note that the hamiltonian commutes with $T$. The eigenvalues of $T$ are $t_k(\alpha) = \exp(2\pi\imath(k+\alpha f)/L)$ with $k = 1, \ldots, L$. Furthermore, the hamiltonian is Hermitian. Since we have $(t_k(\alpha))^\dagger = t_{-k}(-\alpha)$, we find that $E_k(\alpha) = E_{-k}(-\alpha)$, where $E_k(\alpha)$ denotes the energy of a state with momentum $p_k(\alpha) = 2\pi(k + \alpha f)/L \mod 2\pi$. For $2\alpha \in \mathbb{Z}$, we find that $p_k(\alpha) = 2\pi(k + \alpha f)/L \mod 2\pi = \pi k'/L$ and $p_{-k}(-\alpha) = -2\pi(k + \alpha f)/L \mod 2\pi = \pi(2L - k')/L$, with $k'$ between 0 and $2L$. It follows that the spectrum is symmetric around $p = \pi$. However, for $2\alpha \notin \mathbb{Z}$ we find that the spectrum at momentum $p_k(\alpha) = 2\pi(k + \alpha f)/L \mod 2\pi$ for a system with twist parameter $\alpha$ is equal to the spectrum at momentum $p_{-k}(-\alpha) = -2\pi(k + \alpha f)/L \mod 2\pi$ for a system with twist parameter $-\alpha$.

We compute the spectrum of the system for $\alpha = \frac{s}{8}$, with $s = 0, \ldots, 4$. For $s = 0$ ($s = 4$) we have periodic (anti-periodic) boundary conditions. An example is shown in figure 4.6, for the chain of length $L = 27$ and particle number $f = 9$. For the low lying states one can easily see how the energy changes under the boundary twist. The drawn lines are parabolic fits to the energies $E_{\text{num}}$ as a function of the momenta $p_\alpha$. For the two lowest lying states, with $E_{\text{num}} = 0$ for $p_{\alpha=0} = 2\pi/3$ and $p_{\alpha=0} = 4\pi/3$ we find the fits $f(x) = a + bx + dx^2$, with $(a, b, d) = (0.607, -0.435, 0.069)$ and $(a, b, d) = (0.579, -0.422, 0.068)$ respectively. Using equations (4.57) and the usual finite size scaling for the energy, we find

$$\frac{E_\alpha}{c} = \frac{E_{\text{num}}(p_\alpha)L^2}{d12\pi^2 f^2} \tag{4.59}$$

$$\frac{\tilde{Q}_\alpha}{c} = \frac{b + 2dp_\alpha L}{d6\pi f}. \tag{4.60}$$

For the first fit we find $(E_0/c, \tilde{Q}_0/c) = (0, -0.334)$ and $(E_{1/2}/c, \tilde{Q}_{1/2}/c) = (-0.083, 0.000)$ and for the second fit we find $(E_0/c, \tilde{Q}_0/c) = (0, 0.334)$ and $(E_{1/2}/c, \tilde{Q}_{1/2}/c) = (0.254, 0.675)$. It is clear that both fits correspond quite accurately with the theoretically predicted values of $(E_0/c, \tilde{Q}_0/c) = (0, \pm 1/3)$ in the Ramond sector and $(E_{1/2}/c, \tilde{Q}_{1/2}/c) = (-1/12, 0)$ and $(E_{1/2}/c, \tilde{Q}_{1/2}/c) = (1/4, 2/3)$ in the Neveu-Schwarz sector.

Note that the two fits are almost the same, as they should since the fields $V_{0,-1/2}$ and $V_{0,1/2}$ flow into each other under spectral flow, so their energies lie on the same parabola.

In table 4.4 we summarize the values we extract from the parabola fits for $(E_{1/2}/c, \tilde{Q}_{1/2}/c)$ for various system sizes. It is important to note, first of all, that the values are quite accurate already for very small system sizes and, second of all, that we do not have to compare systems of different lengths. These two properties make this analysis very powerful, also for systems for which we do not know what the continuum limit is.

**Table 4.4:** In this table we summarize the values we extract from the parabola fits for $E_{1/2}/c$ and $\tilde{Q}_{1/2}/c$ for various system sizes. Note that for each chain length we give two pairs of extracted values. They correspond to two different highest weight states in the Neveu-Schwarz sector. Furthermore, the values are extracted from two different fits, namely a fit to the flow of that particular highest weight state to the Ramond sector. To be precise, for the chains with length $L = 3j$ the middle two columns are extracted from a fit to the flow of state 1 in figure 4.4(e) to state 7 in figure 4.4(f), whereas the last two columns are extracted from a fit to the flow of state 2 in figure 4.4(e) to state 8 in figure 4.4(f). For the chains with length $L = 3j + 1$ the middle two columns are extracted from a fit to the flow of state 1 in figure 4.4(a) to state 6 in figure 4.4(b), and the last two columns are extracted from a fit to the flow of state 2 in figure 4.4(a) to state 7 in figure 4.4(b). For the chains with length $L = 3j - 1$ the middle two columns are extracted from a fit to the flow of state 1 in figure 4.4(c) to state 7 in figure 4.4(d), and the last two columns are extracted from a fit to the flow of state 3 in figure 4.4(c) to state 6 in figure 4.4(d).

| chain length | fermion number | $E_{1/2}/c$ from first fit | $\tilde{Q}_{1/2}/c$ from first fit | $E_{1/2}/c$ from second fit | $\tilde{Q}_{1/2}/c$ from second fit |
|---|---|---|---|---|---|
| 6 | 2 | -0.085 | -0.004 | 0.339 | 0.846 |
| 9 | 3 | -0.084 | -0.002 | 0.285 | 0.738 |
| 12 | 4 | -0.084 | -0.001 | 0.270 | 0.706 |
| 15 | 5 | -0.084 | -0.001 | 0.263 | 0.692 |
| 18 | 6 | -0.084 | 0.000 | 0.259 | 0.685 |
| 21 | 7 | -0.083 | 0.000 | 0.257 | 0.680 |
| 24 | 8 | -0.083 | 0.000 | 0.255 | 0.677 |
| 27 | 9 | -0.083 | 0.000 | 0.254 | 0.675 |
| 5 | 2 | 0.086 | 0.338 | 0.138 | -0.560 |
| 8 | 3 | 0.084 | 0.335 | 0.101 | -0.407 |
| 11 | 4 | 0.084 | 0.334 | 0.093 | -0.372 |
| 14 | 5 | 0.084 | 0.334 | 0.089 | -0.357 |
| 17 | 6 | 0.084 | 0.334 | 0.087 | -0.350 |
| 20 | 7 | 0.083 | 0.334 | 0.086 | -0.346 |
| 23 | 8 | 0.083 | 0.334 | 0.086 | -0.343 |
| 26 | 9 | 0.083 | 0.334 | 0.085 | -0.341 |
| 7 | 2 | 0.085 | 0.336 | 0.108 | -0.436 |
| 10 | 3 | 0.084 | 0.335 | 0.095 | -0.381 |
| 13 | 4 | 0.084 | 0.334 | 0.09 | -0.362 |
| 16 | 5 | 0.084 | 0.334 | 0.088 | -0.352 |
| 19 | 6 | 0.084 | 0.334 | 0.087 | -0.347 |
| 22 | 7 | 0.083 | 0.334 | 0.086 | -0.344 |
| 25 | 8 | 0.083 | 0.334 | 0.085 | -0.342 |

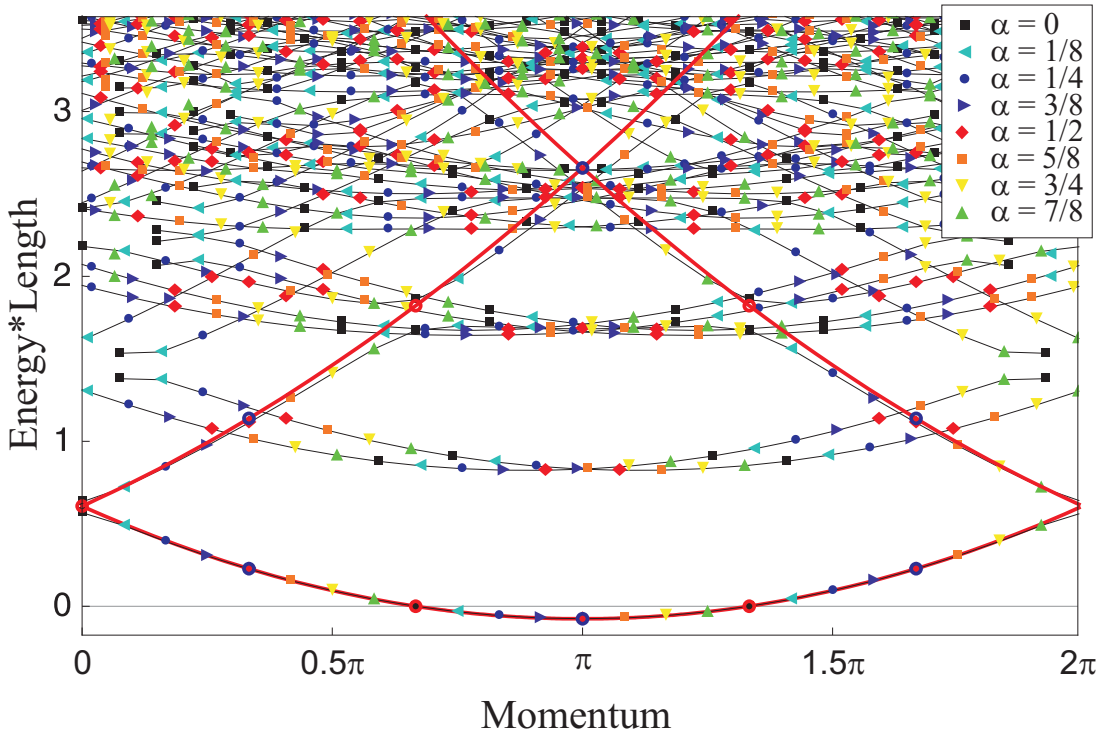


**Figure 4.6:** We show the spectra (energy times chain length versus momentum) of the 27-site periodic chain with 9 fermions for $\alpha = 0, \frac{1}{8}, \frac{1}{4}, \frac{3}{8}, \frac{1}{2}, \frac{5}{8}, \frac{3}{4}, \frac{7}{8}$. It follows that the spectrum given by the black squares is precisely the spectrum plotted in figure 4.4(e) and the spectrum given by the red diamonds is also plotted in figure 4.4(f). The black line connects the levels for different values of the twist parameter. The red line is the parabola obtained from a fit to the flow of one of the Ramond vacua (state 1 in figure 4.4(e)) to the Neveu-Schwarz vacuum (state 7 in figure 4.4(f)). The open red (blue) circles on this parabola correspond to $\alpha = 0 \mod 1$ ($\alpha = 1/2 \mod 1$). The two lowest energy states follow the parabola very nicely as a function of the twist parameter. For the higher energy states, we see that there are avoided level crossings (see also the end of section 4.7.7) at integer values of $\alpha$, but for intermediate values of $\alpha$ they still qualitatively follow the parabola. By eye one can also clearly distinguish the parabola's through the first descendants of the Neveu-Schwarz vacuum, again interrupted by occasional avoided crossings.

## 4.9 Open boundary conditions

In the previous sections, we have discussed the continuum limit of the supersymmetric model on the periodic chain in great detail. In this section we will discuss the chain with open boundary conditions. We will first identify the continuum theory (the $\mathcal{N} = 2$ superconformal field theory at $c = 1$) and the three sectors corresponding to the three possible chain lengths modulo three. In the second part, we discuss some results by Beccaria and De Angelis [51] on one-point functions in the chain with open boundary conditions.

### 4.9.1 Continuum theory

In the previous sections, we have discussed the continuum limit of the supersymmetric model on the periodic chain in great detail. In this section we will discuss the chain with

open boundary conditions. A first guess is that the open boundary conditions couple the left- and right-moving modes, so that the continuum field theory becomes the $\mathcal{N} = 2$ superconformal field theory with central charge $c = 1$. By comparing the spectrum of this theory with numerical computations of finite size spectra, we concluded that this is indeed the correct guess. Let us first discuss the $\mathcal{N} = 2$ superconformal field theory with central charge $c = 1$ in some detail.
The states of the field theory are given by the vertex operators

$$V_m = e^{(\imath m\Phi/\sqrt{3})}, \tag{4.61}$$

where the $\sqrt{3}$ comes from the compactification radius $R = \sqrt{3}$ and $m \in Z$ in the Neveu-Schwarz sector and $m \in Z + 1/2$ in the Ramond sector. The conformal dimension $h_m$ corresponding to $V_m$ is

$$h_m = m^2/6. \tag{4.62}$$

For $m = \pm 3$ we find the supercharges, given by

$$G^{\pm} = e^{(\pm\imath\sqrt{3}\Phi)}, \tag{4.63}$$

with conformal dimension $h = 3/2$.
In the following we only consider the Ramond sector, since this is the sector that is realized in the lattice model. There are three highest weight states that we need to consider. They correspond to the primary fields: $V_{-1/2}$, $V_{1/2}$ and $V_{3/2}$. All other states are generated by the supercharges and the Virasoro algebra. The fields $V_{-1/2}$ and $V_{1/2}$ both have conformal dimension $h = 1/24$. Since the hamiltonian is given by $H = L_0 - c/24$, they correspond to zero energy states. The state $V_{3/2}|0\rangle$, however, has energy $E = 9/24 - 1/24 = 1/3$ and also has a superpartner $(V_{-3/2}|0\rangle)$.
Since the supercharges change $m$ by $\pm 3$, we infer that $m/3$ corresponds to the fermion number in the lattice model. It thus quickly follows that the three sectors; $m = 1/2, 3/2, 5/2 \mod 3$, are related to the three sectors in the lattice model with chain lengths $L = 0, 1, 2 \mod 3$. Indeed from section 4.4, we know that chains of length $L = 0, 2 \mod 3$ have one zero energy ground states and chains of length $L = 1 \mod 3$ have all energies larger than zero. It follows that chains with length $L = 1 \mod 3$ correspond to the sector with $m = 3/2 \mod 3$. To identify the sector of the other two chain lengths, we look at the first excited state and its superpartner. The first excited state is given by $L_{-1}V_{\pm 1/2}|0\rangle$ and the respective superpartners are $G^{\mp}_{-1}V_{\pm 1/2}|0\rangle = V_{\mp 5/2}|0\rangle$. One easily checks that the superpartners indeed have energy $E = m^2/6 - 1/24 = 1$. The difference is that one occurs at $f = f_{GS} + 1$ and the other at $f = f_{GS} - 1$. If we compare this with the finite size spectra we quickly conclude that open chains with length $L = 3j$ correspond to the sector with $m = 5/2 \mod 3$ and chains with length $L = 3j - 1$ correspond to the sector with $m = 1/2 \mod 3$.
Finally, we find the following relation between fermion number $f$, chain length $L$ and the quantum number $m$:

$$\tilde{f} \equiv f - L/3 = (m + 1/2)/3. \tag{4.64}$$

For $m = -1/2$ this relation gives $\tilde{f} = 0$, which agrees with $f = j$ and $L = 3j$. For $m = 1/2$ this relation gives $\tilde{f} = 1/3$, which agrees with $f = j$ and $L = 3j - 1$. Finally, for $L = 3j + 1$ the two lowest energy states are found at $f = n$ and $f = n + 1$, which matches with $m = -3/2$ and $m = 3/2$.

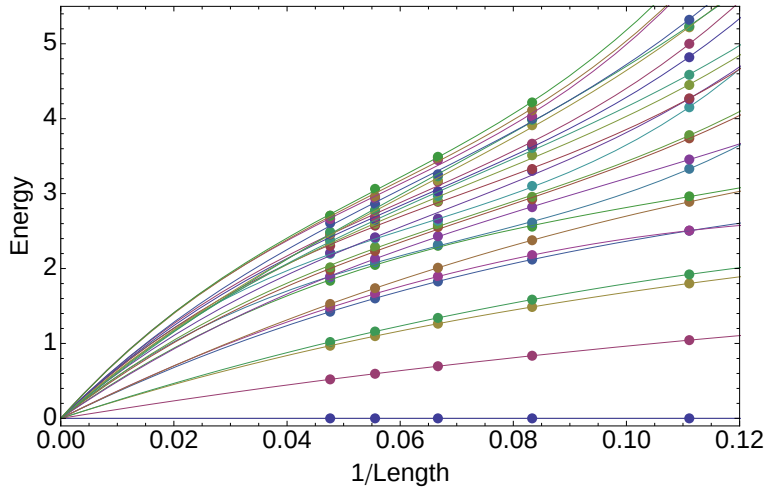


**Figure 4.7:** The numerically obtained energies are plotted against the inverse chain length. The fits are obtain by fitting the function $f(L) = a/L + b/L^2 + c/L^3$. The energy in the continuum limit then follows from $E = a/(\pi v_F)$.

**Table 4.5:** The degeneracy at level $n$ is given by the number of partitions $p(n)$. The energy at level $n$ is given by $E = m^2/6 - 1/24 + n$.

| level | 0 | 1 | 2 | 3 | 4 | 5 | 6 | 7 | 8 | 9 | 10 | 11 | 12 |
|---|---|---|---|---|---|---|---|---|---|---|---|---|---|
| degeneracy | 1 | 1 | 2 | 3 | 5 | 7 | 11 | 15 | 22 | 30 | 42 | 56 | 77 |

The spectrum per sector now simply follows from the highest weight states and their descendants. The character formula is given by (see 4.42)

$$\begin{aligned} \chi_h(q) &= q^h/\eta(q) \\ &= q^{m^2/6}/\eta(q). \end{aligned} \tag{4.65}$$

From this formula we obtain the degeneracies at each level. For the first few levels the degeneracies are summarized in the table below (Tab. 4.5). The energy of the $n$-th level is given by $E = m^2/6 - 1/24 + n$. The spectra are plotted for the three different sectors in figures 4.8(a), 4.9(a) and 4.10(a).
We now compare the theory explained above to the numerics. We perform a scaling analysis for the numerically obtained energies for chains of lengths up to $L = 23$. The low lying levels are nicely fitted with the function $f(L) = a/L + b/L^2 + c/L^3$. As an example we show the raw data and the fits for chain lengths $L = 3j$ and fermion number $f = j$ in figure 4.7. For open boundary conditions the scaling is given by

$$E_{\text{num}} = \pi E_{\text{SCFT}} v_F / L + \mathcal{O}(1/L^2), \tag{4.66}$$

where the Fermi velocity is given by $v_F = 9\sqrt{3}/4$. It follows that the energies in the continuum limit can be extracted from the fits via $E = a/(\pi v_F)$. The continuum limit spectra that we extracted in this way for the various chain lengths $L = 0, 1, 2 \mod 3$ are plotted in figures 4.8(b), 4.9(b) and 4.10(b). Clearly, for the first few levels, we find a very nice agreement with the theoretically obtained spectra. For the higher levels, the fits are not very reliable. We indicate two reasons for this. First of all, there is a large degeneracy

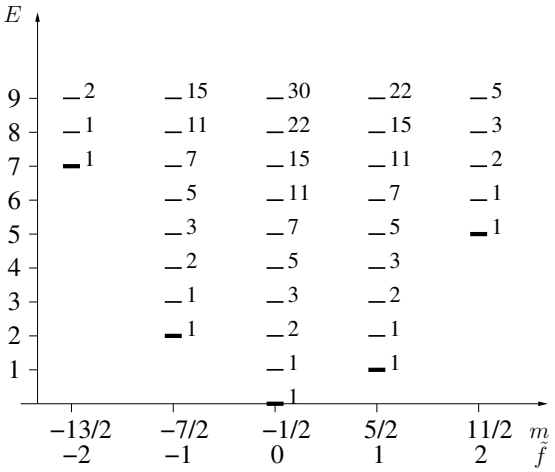


(a) The energy levels $E = m^2/6 - 1/24 + n$ are plotted versus $m$ for $m = 5/2 \mod 3$ which corresponds to chains of length $L = 3j$. On the horizontal axis we also indicate the shifted fermion number $\tilde{f} \equiv f - L/3 = (m + 1/2)/3$. The level corresponding to the highest weight state and the levels that are generated from this field by the supercharge operators, that is the levels with energy $E = m^2/6 - 1/24$, are indicated by a thick bar. The descendants are indicated by thinner bars. The labels indicate the degeneracy of the levels.

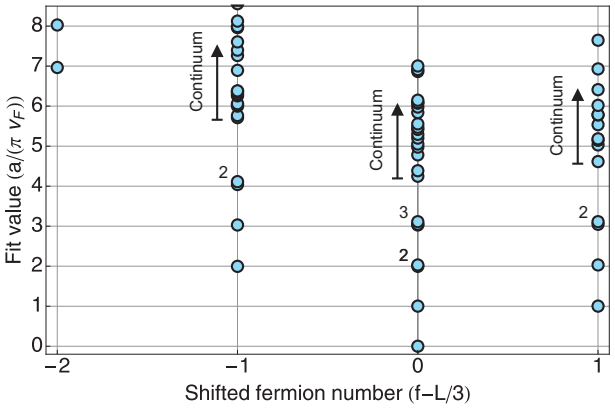


(b) The numerically fitted values of the energy are plotted versus the shifted fermion number $\tilde{f} \equiv f - L/3$ for chains of length $L = 3j$. The fit values are obtained by fitting the numerically obtained energies as a function of the chain length $L$ with the function $f(L) = a/L + b/L^2 + c/L^3$. The energy is then given by $E = a/(\pi v_F)$. The labels indicate the number of overlapping data points.

**Figure 4.8:** On the left we show the theoretically predicted spectrum and on the right the spectrum obtained from fits to the numerically obtained spectra. These spectra are for chains of length $L = 3j$.

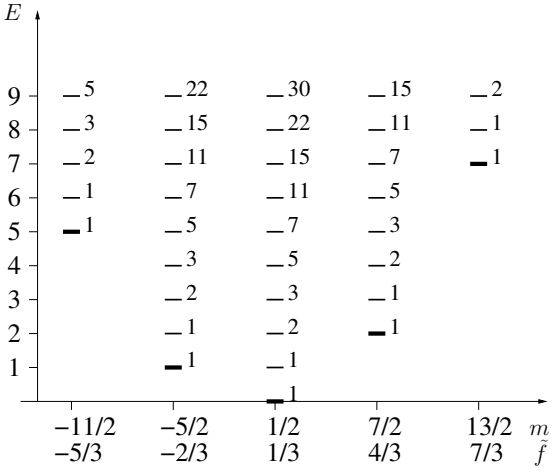


(a) The energy levels $E$ are plotted versus $m$ and $\tilde{f}$ for $m = 5/2 \mod 3$ which corresponds to chains of length $L = 3j - 1$.

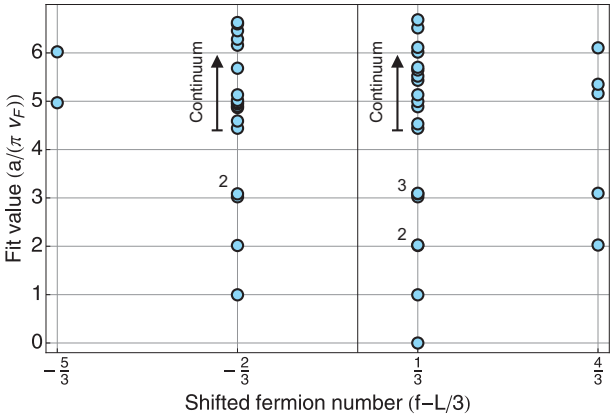


(b) The numerically fitted values of the energy are plotted versus the shifted fermion number $\tilde{f} \equiv f - L/3$ for chains of length $L = 3j - 1$.

**Figure 4.9:** On the left we show the theoretically predicted spectrum and on the right the spectrum obtained from fits to the numerically obtained spectra. These spectra are for chains of length $L = 3j - 1$.

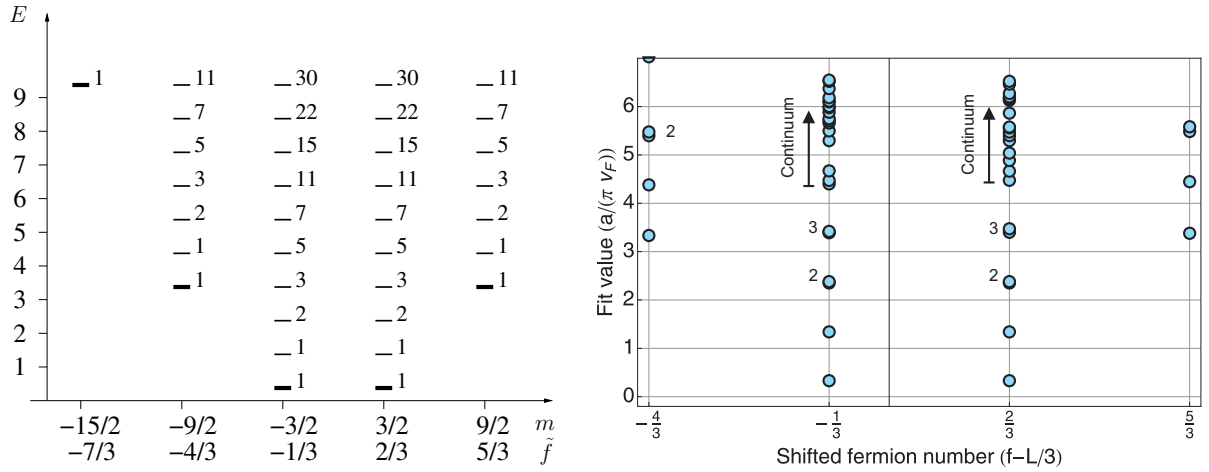


(a) The energy levels $E$ are plotted versus $m$ and $\tilde{f}$ for $m = 5/2 \mod 3$ which corresponds to chains of length $L = 3j + 1$.

(b) The numerically fitted values of the energy are plotted versus the shifted fermion number $\tilde{f} \equiv f - L/3$ for chains of length $L = 3j + 1$.

**Figure 4.10:** On the left we show the theoretically predicted spectrum and on the right the spectrum obtained from fits to the numerically obtained spectra. These spectra are for chains of length $L = 3j + 1$.

of these levels in the continuum limit. However, in the finite size spectra the degeneracies are not realized, since for finite size matrices the eigenvalues tend to spread. Second of all, since there are corrections of order $1/L^p$ with $p \geq 2$, there can be level crossings as a function of the length. Numerically, however, we simply connect the $n$-th level at different lengths, so we do not take possible level crossings into account. The latter argument also explains why supersymmetry may appear to be broken in the spectra extracted from the fits. Clearly, this is not the case in the original numerical spectra.
Using density renormalization group methods, one can obtain the low lying levels for much larger system sizes. In figure 4.11 we show the spectrum for the 120-site chain with open boundary conditions [66]. The spectrum and level degeneracies are, at least up to level 7, in excellent agreement with the continuum theory in the sector with $m = -1/2 \mod 3$.

### 4.9.2 One-point functions

In [51] Beccaria and De Angelis discuss the supersymmetric model on the chain with open boundary conditions and length $L \mod 3 = 0$. In particular, they use non standard number theoretical methods to obtain exact expressions for the ground state wave function, on the one hand, and on the other hand, they study the finite size scaling behavior of some simple correlation functions using exact diagonalization. In this section we present and interpret their results for the one point-function $\langle n_k \rangle = \langle \psi_0 | c_k^\dagger c_k | \psi_0 \rangle$. Their results can be summarized as follows. They find that $\langle n_k \rangle$ has a clear $\mathbb{Z}_3$ substructure. The one-point functions $\langle n_{k,k=1 \mod 3} \rangle$ and $\langle n_{k,k=0 \mod 3} \rangle$ are not symmetric under $k \mapsto L - k$. The one-point function $\langle n_{k,k=2 \mod 3} \rangle$ *is* symmetric under this map, however, it shows a very different behavior from the other two. For the different branches they extract the following finite size scaling behavior

- $\langle n_k \rangle - 1/3 = f_+ \left( (k - k_+)/\tilde{L} \right) \tilde{L}^{-\nu}$ for $k \mod 3 = 2$,

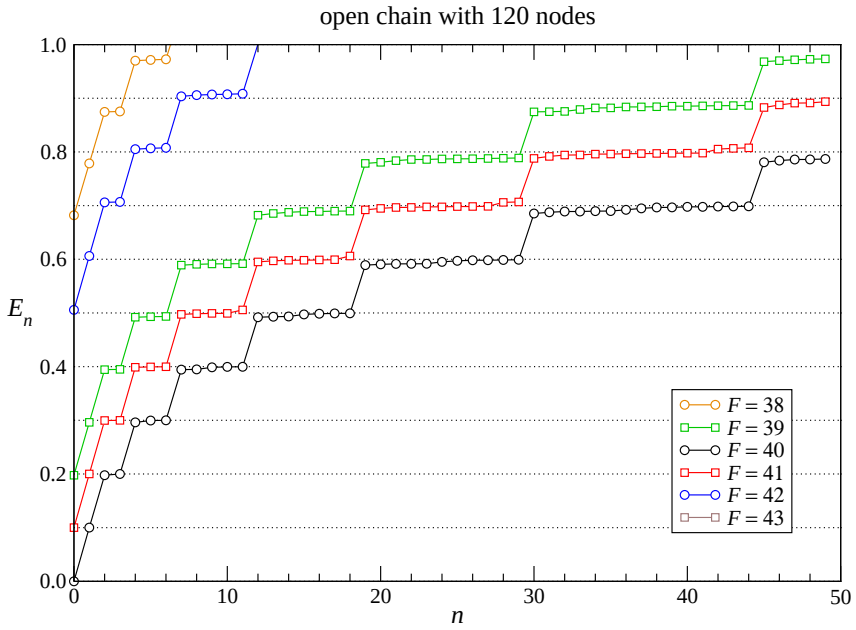


**Figure 4.11:** We show the spectrum of an open chain with 120 sites obtained by Campostrini [66] using DMRG methods. The energy is plotted as a function of the level number for the different fermion numbers. The different curves correspond to different fermion numbers. It is easily verified that, at least up to level 7, the degeneracies are in excellent agreement with the values in the field theory in the sector with $m = -1/2 \mod 3$ (compare with table 4.5).

- $\langle n_k + n_{k+2} \rangle - 2/3 = f_- \left( (k - k_-)/\tilde{L} \right) \tilde{L}^{-\nu}$ for $k \mod 3 = 1$,

where $\tilde{L} = L/3 + 1$, $k_\pm = (L \pm 1)/2$. They obtain the best fit for $\nu = 0.33(2)$.

In the following we will use the observed $\mathbb{Z}_3$ substructure to propose an identification of the one-point functions and expectation values of operators in the superconformal field theory on the strip. We show how these expectation values can be computed analytically by mapping the strip onto the plane and introducing the mirror images to ensure the boundary conditions are preserved. The formulae we obtain are in nice agreement with the finite size scaling behavior found in [51].

Let us first identify the $\mathbb{Z}_3$ operator in the superconformal field theory on the strip. Remember that the boson is compactified: $\Phi \equiv \Phi + 2\pi R$, with $R = \sqrt{3}$. It follows that the operator $T$ that acts as follows $T : \Phi \mapsto \Phi + 2\pi\sqrt{3}/3$ satisfies $T^3 = 1$. We now consider the action of this operator on the vertex operators $V_{\pm 1} = e^{\pm \imath \Phi/\sqrt{3}}$

$$T V_{\pm 1} = e^{\pm \imath (\Phi + 2\pi\sqrt{3}/3)/\sqrt{3}} = e^{\pm 2\pi \imath/3} V_{\pm 1}. \tag{4.67}$$

Furthermore, we trivially have $T V_0 = V_0$ and clearly $V_0$ is just the identity. It follows that $V_0$ and $V_{\pm 1}$ are eigenfunctions of the $\mathbb{Z}_3$ operator with eigenvalues $\omega_0 = 1$ and $\omega_{\pm 1} = e^{\pm 2\pi\imath/3}$ respectively.

In the lattice the one-point function $\langle n_k \rangle$ shows strong oscillations with period three in $k$. It follows that we can identify the inverse translation operator which sends $k$ to $k - 1$

as the $\mathbb{Z}_3$ operator[1]. We thus find that the functions,

$$\omega_l^{-1} n_{k-1} + n_k + \omega_l n_{k+1}, \tag{4.68}$$

are eigenfunctions of the inverse translation operator with eigenvalues $\omega_l = e^{2\pi\imath l/3}$. In the following, we will assume[2] $k \mod 3 = 2$.
Combining these observations we find

$$\begin{aligned} A_0 V_0 &= n_{k-1} + n_k + n_{k+1} \\ A_1 V_{\pm 1} &= e^{\mp 2\pi\imath/3} n_{k-1} + n_k + e^{\pm 2\pi\imath/3} n_{k+1}, \end{aligned}$$

where $A_0$ and $A_1$ are constants. From the fact that the ground state has filling $1/3$, we immediately find that $A_0 = 1$. Solving the above equations for the $n_k$ we obtain

$$\begin{aligned} 3n_k &= V_0 + A_1(V_1 + V_{-1}) \\ 3n_{k+1} &= V_0 + A_1(e^{-2\pi\imath/3} V_1 + e^{2\pi\imath/3} V_{-1}) \\ 3n_{k-1} &= V_0 + A_1(e^{2\pi\imath/3} V_1 + e^{-2\pi\imath/3} V_{-1}). \end{aligned}$$

Now we wish to compute the expectation values of these operators. To do that however, we have to map the strip onto the plane, where the correlator of vertex operators $V_\alpha = \exp(\pi\imath\alpha\Phi)$ gives

$$\langle V_{\alpha_1}(z_1) V_{\alpha_2}(z_2) \dots V_{\alpha_n}(z_n) \rangle = \prod_{i<j} (z_i - z_j)^{\alpha_i \alpha_j}. \tag{4.69}$$

To illustrate how we go from the strip to the plane we compute the expectation value of the vertex operator $V_1 = e^{\pi\imath\Phi/\sqrt{3}}$ in the Neveu-Schwarz vacuum. To compute this we have to do two steps. First we extend the strip of length $L$ to a cylinder with radius $2L$, where we use the image-technique to ensure that the boundary conditions are unchanged. Then we use a conformal map to map the cylinder onto the complex plane, where we can compute the expectation value. The first step gives

$$\langle 0|V_1(x)|0\rangle_{\text{strip}} = \langle 0|V_1(x) V_{-1}(2L - x)|0\rangle_{\text{cyl}}, \tag{4.70}$$

where the image of $V_1(x)$, $V_{-1}(2L - x)$, is included when going from the strip of length $L$ to the cylinder with radius $2L$. The two-point function is an equal time correlator, so the coordinates on the cylinder are $u_1 = x + \imath t$ and $u_2 = 2L - x + \imath t$. Mapping the cylinder to the plane we get $z = e^{\pi\imath u/L}$. We thus find

$$\begin{aligned} \langle 0|V_1(x) V_{-1}(2L - x)|0\rangle_{\text{cyl}} &= \left(\frac{\partial z_1}{\partial u_1}\right)^{h_1} \left(\frac{\partial z_2}{\partial u_2}\right)^{h_2} \langle 0|V_1(z_1) V_{-1}(z_2)|0\rangle_{\text{plane}} \\ &= \left(\frac{\pi\imath}{L} z_1\right)^{1/6} \left(\frac{\pi\imath}{L} z_2\right)^{1/6} (z_1 - z_2)^{-1/3} \\ &= \left(\frac{\pi\imath}{L}\right)^{1/3} \left(e^{\pi\imath(u_1+u_2)/L}\right)^{1/6} \left(e^{\pi\imath u_1/L} - e^{\pi\imath u_2/L}\right)^{-1/3} \\ &= \left(\frac{\pi\imath}{L}\right)^{1/3} \left(e^{-2\pi t/L}\right)^{1/6} e^{-\pi t/3L} \left(e^{\pi\imath x/L} - e^{\pi\imath(2L-x)/L}\right)^{-1/3} \\ &= \left(\frac{\pi}{2L}\right)^{1/3} \sin^{-1/3}(\pi x/L). \end{aligned}$$

[1] Note that there is an ambiguity here: we could just as well have identified the translation operator, which sends $k$ to $k + 1$ with the $\mathbb{Z}_3$ operator. However, this ambiguity is fixed by comparison with the numerical results of [51].

[2] There is again an ambiguity here, since we could also take $k \mod 3 = 0, 1$. This choice, however, is again fixed by comparison with the numerical results of [51] (see also the end of this section).

Now remember that we identified the ground state of the chain of length $L = 3j$ and open boundary conditions with the Ramond vacuum $V_{-1/2}|0\rangle$. To compute an expectation value we define the in-state as $|R\rangle \equiv \lim_{z\to 0} V_{-1/2}(z)|0\rangle$ and the out-state as $\langle R| \equiv \lim_{z\to\infty}\langle 0|V_{1/2}(z)z^{1/12}$. These definitions ensure that

$$\begin{aligned}\langle R|R\rangle &= \lim_{z_2\to 0, z_1\to\infty}\langle 0|V_{1/2}(z_1)z_1^{1/12}V_{-1/2}(z_2)|0\rangle \\ &= \lim_{z_2\to 0, z_1\to\infty} z_1^{1/12}(z_1-z_2)^{-1/12} \\ &= 1.\end{aligned}$$

It thus follows that

$$\begin{aligned}\langle R|V_1(x)|R\rangle_{\text{strip}} &= \langle R|V_1(x)V_{-1}(2L-x)|R\rangle_{\text{cyl}} \\ &= \left(\frac{\pi\imath}{L}\right)^{1/3}(z_2z_3)^{1/6}\lim_{z_4\to 0, z_1\to\infty}\langle 0|V_{1/2}(z_1)z_1^{1/12}V_1(z_2)V_{-1}(z_3)V_{-1/2}(z_4)|0\rangle \\ &= \left(\frac{\pi\imath}{L}\right)^{1/3} z_2^{1/3}(z_2-z_3)^{-1/3},\end{aligned}$$

where $z_2 = e^{\pi\imath(x+\imath t)/L}$ and $z_3 = e^{\pi\imath(2L-x+\imath t)/L}$. In the last step we used (4.69). Equivalently we find

$$\begin{aligned}\langle R|V_{-1}(x)|R\rangle_{\text{strip}} &= \left(\frac{\pi\imath}{L}\right)^{1/3} z_3^{1/3}(z_3-z_2)^{-1/3} \\ &= \left(\frac{\pi\imath}{L}\right)^{1/3} e^{-\pi\imath/3}z_3^{1/3}(z_2-z_3)^{-1/3}.\end{aligned} \tag{4.71}$$

Combining all the above, we obtain

$$\begin{aligned}3\langle n_k\rangle &= 1 + A_1 2\left(\frac{\pi}{2L}\right)^{1/3} e^{\pi\imath/6}\frac{\cos(\pi(x-L/2)/3L)}{\sin^{1/3}(\pi x/L)} \\ 3\langle n_{k+1}\rangle &= 1 + A_1 2\left(\frac{\pi}{2L}\right)^{1/3} e^{\pi\imath/6}\frac{\sin(\pi(x-L)/3L)}{\sin^{1/3}(\pi x/L)} \\ 3\langle n_{k-1}\rangle &= 1 - A_1 2\left(\frac{\pi}{2L}\right)^{1/3} e^{\pi\imath/6}\frac{\sin(\pi x/3L)}{\sin^{1/3}(\pi x/L)}\end{aligned} \tag{4.72}$$

These equations clearly reproduce the observed scaling behavior. Comparison with the numerics suggests that we should choose $e^{\pi\imath/6}A_1 \approx 0.77$. Finally, we argue that we should identify the width of the strip $L$ with $L_c + 3$, where $L_c$ is the length of the chain. The way we understand this, is that the open chain can be obtained from a periodic chain with three sites extra, by pinning one particle to a certain site. Due to the hard-core character of the particles, the neighboring two sites must be empty. One thus effectively takes out three sites from the system and is left with an open chain. Finally, this implies that the sites -1 and $L_c + 2$ are identified with the boundaries of the strip: $x = 0$ and $x = L$. Consequently, an arbitrary site $p$ of the chain should be identified with the point $x = p + 1$ on the strip. In figure 4.12(a) we show the one-point functions for a chain of length $L_c = 30$, this plot can be compared directly to the data presented in figure 1 in [51]. In figure 4.12(b) we plot the finite size scaling functions to be compared with figure 2 in [51]. The agreement with the data of Beccaria et. al. is quite convincing, however, it

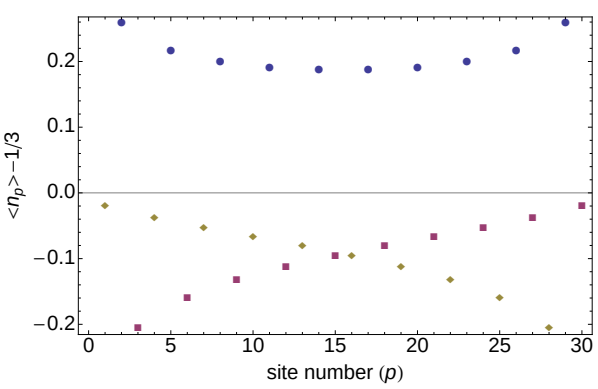


(a) One-point functions for chain length $L_c = 30$.

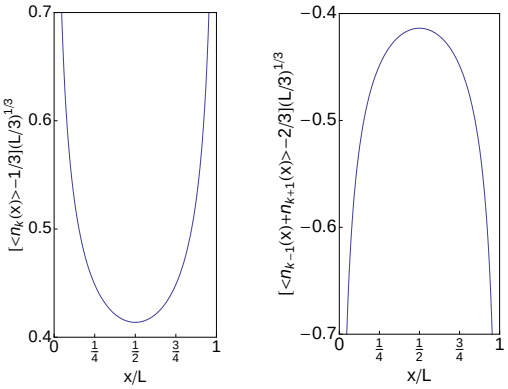


(b) Finite size scaling functions versus the normalised position on the strip (which is related to the site number, $p$, via $x = p + 1$).

**Figure 4.12:** On the left we show the one-point functions for a chain of length $L_c = 30$, this plot can be compared directly to the data presented in figure 1 in [51]. On the right we plot the finite size scaling functions, $(\langle n_k \rangle - 1/3)(L/3)^{1/3}$ and $(\langle n_{k+1} + n_{k+2} \rangle - 2/3)(L/3)^{1/3}$, to be compared with figure 2 in [51].

seems to get poorer upon approaching the boundary of the system. In particular, the value for $\langle n_1 \rangle$, which they obtain analytically using sophisticated number theoretical methods, cannot be reproduced from the field theory.

We can use the scaling functions to compute $F_i \equiv \sum_{k,k \mod 3=i} \langle n_k \rangle$, which is the average fermion number in the three branched distinguished by the site number modulo three. Replacing the sum by an integral and using that

$$\begin{aligned} \int_0^1 \frac{\cos(\pi(x-1/2)/3)}{\sin^{1/3}(\pi x)} dx &= 2^{1/3}, \\ \int_0^1 \frac{\sin(\pi x/3)}{\sin^{1/3}(\pi x)} dx &= -2^{-2/3}, \end{aligned}$$

we find

$$\begin{aligned} F_2 &= L/9 + A_1 \frac{2}{3} \left(\frac{\pi}{2L}\right)^{1/3} e^{\pi\imath/6} \frac{L}{3} 2^{1/3} \approx F/3 + 0.52\ F^{2/3}, \\ F_1 = F_0 &= L/9 - A_1 \frac{2}{3} \left(\frac{\pi}{2L}\right)^{1/3} e^{\pi\imath/6} \frac{L}{3} 2^{-2/3} \approx F/3 - 0.26\ F^{2/3}, \end{aligned}$$

where we used $e^{\pi\imath/6} A_1 \approx 0.77$ and $F = L/3$. Consequently, the oscillation in occupation number with period three in the site number, does not lead to a difference in the average fermion number in the three branches. Nevertheless, since the subleading term goes as $F^{2/3}$ it is very hard to distinguish numerically. Even for $F = 1000$ they still only differ by one order of magnitude.

On a qualitative level the $\mathbb{Z}_3$ substructure can probably be interpreted as follows. Remember that on the periodic chain we have two ground states, which are plane waves with opposite momenta differing by $2\pi/3$. It seems that for open boundary conditions these two ground states combine into a standing wave, which explains the observed density fluctuations.

An obvious follow-up on this work, is to extend it to two-point functions (see also [51]), chains of length $L \neq 0 \mod 3$ and periodic boundary conditions.

## 4.10 Entanglement entropy

Before closing this chapter, we wish to touch upon a last, very powerful technique to study criticality in finite size systems. Entanglement entropy is often used as a measure for the entanglement between two spatially separated parts of the system. Let $\rho$ be the density matrix of a system in a pure quantum state $|\Psi\rangle$: $\rho = |\Psi\rangle\langle\Psi|$. Let us now divide the system in two parts $A$ and $B$, such that the Hilbert space can be written as $\mathcal{H} = \mathcal{H}_A \otimes \mathcal{H}_B$ and thus $|\Psi\rangle = |\Psi_A\rangle|\Psi_B\rangle$. We then define the reduced density matrix of subsystem $A$ as

$$\rho_A = \mathrm{Tr}_B \rho = \langle\Psi_B|\Psi\rangle\langle\Psi|\Psi_B\rangle. \tag{4.73}$$

The entanglement entropy is now defined as the Von Neumann entropy of the reduced density matrix

$$S_A = -\mathrm{Tr}\rho_A \ln \rho_A, \tag{4.74}$$

and equivalently for $S_B$. For a system in a pure quantum state we have $S_A = S_B$.
For a system with a gap and thus a finite correlation length, the entanglement entropy typically saturates at a certain value when the size of the subsystem exceeds a certain length related to the correlation length. For a critical system, which can be described by a conformal field theory in the continuum limit, the entanglement entropy does not saturate. In fact, it shows a universal scaling law at a conformal critical point [67, 68, 69]

$$S(l_A) = \frac{c}{3} \ln(l_A) + b, \tag{4.75}$$

where $c$ is the central charge of the conformal field theory and $b$ is a non-universal constant. Finally, for a one dimensional quantum critical system of finite size $L$, the entanglement entropy scales as [69, 70]

$$S(l_A) = \frac{c}{3} \ln(\frac{L}{\pi} \sin(\frac{l_A \pi}{L})) + b, \tag{4.76}$$

which reduces to the expression above for $L \to \infty$.
It is now clear, that if one can compute the entanglement entropy of a one dimensional system, this can be a very powerful way of studying the system. It can be used to, first of all, determine whether the system is critical or not and, second of all, if it is critical, to determine the central charge of the continuum theory. An important boundary condition for this method to work, is that one is able to determine the entanglement entropy for a subsystem larger than the correlation length if the system is gapped. For exact diagonalization this is clearly not always the case. However, if the system is studied using density matrix renormalization group (DMRG) methods [71, 72, 73], this condition is often met. Moreover, the entanglement entropy comes out essentially for free if one determines the ground state of the system with DMRG.
For the supersymmetric model on the chain, the entanglement entropy has been studied using DMRG methods [66]. The results were fitted very well by (4.76) and always in

good agreement with central charge $c = 1$ (with errors $\ll 1\%$) for the ground state of chains with periodic boundary conditions and $L = 3j \pm 1$ or with anti-periodic boundary conditions and $L = 3j$. As can be seen from figure 4.4, the ground state for the other cases, that is periodic boundary conditions and $L = 3j$ or anti-periodic boundary conditions and $L = 3j \pm 1$, is degenerate. To determine the central charge reliably in these cases one would have to construct translational invariant ground states. Finally, for the chain with open boundary conditions it is difficult to obtain a precise determination of the central charge since the entanglement entropy is plagued by very strong oscillations of period 3. Clearly, these oscillations are strongly related to the oscillations in the fermion number densities (see section 4.9.2).
Using exact diagonalization, we determined the entanglement entropy for the ground state of chains with periodic boundary conditions and $L = 3j \pm 1$, for $L$ up to 23. The systems are too small to get a good determination of the central charge. They are, however, in reasonable agreement with $c = 1$. Excluding the values for $l_A < 3$ and $l_A > L - 3$, we obtain $c \approx 1.05$ for $L = 22$ and $c \approx 1.04$ for $L = 23$ (see figure 4.13).

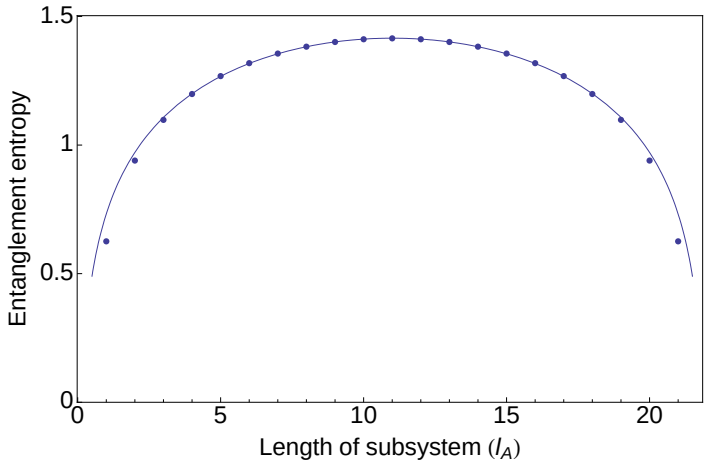


(a) $L = 22$ and $f = 7$.

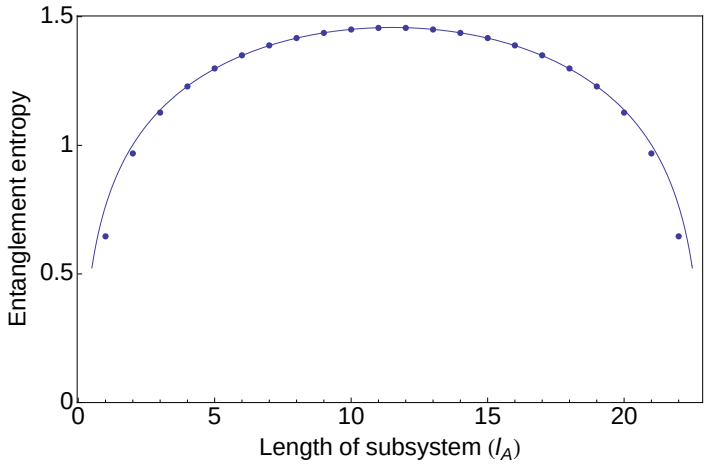


(b) $L = 23$ and $f = 8$.

**Figure 4.13:** Entanglement entropy versus subsystems size $l_A$ for the ground state of the chain of length $L = 22$ with $f = 7$ fermions (left) and the chain of length $L = 23$ with $f = 8$ fermions (right).

# Chapter 5
# The supersymmetric model on two dimensional lattices

## 5.1 Superfrustration

In the previous chapter we studied the supersymmetric model on the chain in great detail. In particular, we investigated the continuum limit properties of the system. For two-dimensional systems this kind of analysis is still out of reach, however, one can obtain (exact) results for the Witten index and the total number of ground states for various two-dimensional systems. In recent years, there has been quite some activity in this field, both in the physics as well as the mathematics literature. On the physics side, these questions arise not only in the context of the supersymmetric lattice model, but also in the context of statistical mechanics. In the latter case one studies the partition sum of, for example, hard squares or hard hexagons [74, 36, 37, 38, 40]. For negative activity there is a direct relation with the Witten index of the supersymmetric model on the square and triangular lattice respectively (see section 2.2.1 for the details). On the mathematics side, these questions arise in the studies of partition sums, (co)homology and homotopy of independence complexes [39, 75, 76, 77]. In sections 2.2.1 and 2.2.2 we discuss the relation between these studies and the supersymmetric lattice model in some detail.

In this chapter we will summarize the results that have been obtained for the supersymmetric model on two-dimensional lattices [21, 36, 78, 37, 38, 35]. These results all show that ground state degeneracy is a generic feature of the model. In fact, in two spatial dimensions the number of ground states typically grows exponentially with the system size. This characteristic of having an extensive ground state entropy $S_{\mathrm{GS}}$ goes under the name of superfrustration [21].

A heuristic way of understanding the superfrustration is from the "3-rule": to minimize the energy, fermions prefer to be mostly 3 sites apart (with details depending on the lattice). For generic two-dimensional lattices the 3-rule can be satisfied in an exponential number of ways.

Superfrustration, in particular if it leads to an extensive ground state entropy, is in contradiction with the third law of thermodynamics, which says that as the temperature goes to zero, the entropy vanishes. A well-known counter example is formed by glasses, which have a frozen-in disorder that can lead to a zero temperature entropy of the order of the number of atoms. More recently this feature has also been observed experimentally in highly pure $Sr_3Ru_2O_7$ single crystals at magnetic field strengths for which the compound is believed to have a zero temperature quantum critical point [79] (see also [80] for a nice perspective). For the supersymmetric model, the exact ground state degeneracy is an artifact of the imposed supersymmetry. That is, all parameters in the hamiltonian are tuned, such that the ground states have zero energy precisely and are thus exactly degenerate. The frustration, however, arises due to a subtle interplay between the kinetic and interaction terms and could persist even for modest perturbations around the supersymmetric

point. We expect that the exact degeneracy will be lifted, but that for sufficiently small perturbations the ground states will form a low lying band with a non-trivial contribution to the entropy at small temperatures. We thus like to take the point of view that fine tuning to the supersymmetric point allows us to analyze the model, but that the features of the supersymmetric system may well be exhibited by more generic strongly correlated itinerant fermion systems.
On a side note, the term superfrustration also arises in the context of frustrated spin models [81], which also exhibit an extensive ground state entropy. For the spin models, however, the term superfrustration is reserved for models in which the frustration is so strong that it explicitly causes all correlations to decay exponentially at any temperature. For the models discussed here, we believe that this is typically not the case. Apart from explicit examples such as the chain and various ladder models (chapters 4 and 7), the intuition is in general that the supersymmetry is not only related to superfrustration but also to quantum criticality.
In this chapter we aim at giving an up to date overview of the known results for the supersymmetric model on two-dimensional lattices and graphs. Exact results for the number of ground states were obtained for various lattices [21, 35], which will be summarized in sections 5.2 and 5.4. Numerical studies of the Witten index have shown that even this lower bound is typically extensive [78] (see section 5.3.1). For certain two-dimensional lattices it was proven that zero-energy ground states exist at various fillings [39] (see section 5.3), indicating a flat band in the energy as a function of the fermion density. The filling is defined as the number of particles per lattice site. For the square, triangular and hexagonal lattice there exist zero-energy ground states for all rational fillings $\nu$ within the range $[1/5, 1/4]$, $[1/7, 1/5]$ and $[1/4, 5/18]$, respectively.
The final section discusses the square lattice [37, 35]. The solution of the cohomology problem for this lattice on the torus is one of the main results of this thesis. We find a theorem that relates elements of the cohomology to tilings of the lattice [35]. This relation between ground states and tilings seems to be more generic [39]. The implications of the theorem are discussed here, the proof, however, is postponed to chapter 6.

## 5.2 Exact results for the cohomology of $Q$ on two-dimensional lattices

In chapter 2, we discussed the relation between ground states of the supersymmetric model and elements of the cohomology of the supercharge $Q$. In particular, we stated the 'tic-tac-toe'-lemma for a double complex (2.2.3). This lemma is very powerful for the supersymmetric model, since one can easily construct a double complex by dividing the lattice into two sublattices. Using this method, Fendley and Schoutens computed the cohomology and thus the number of ground states analytically for various two-dimensional lattices [21]. In figure 5.1 we show the enneagon-triangle lattice, also known as the martini lattice, the octagon-square lattice and the square lattice with two additional sites on every link. In the following sections, we will explicitly compute the cohomology of $Q$ for these lattices. Here we first summarize the results. For the martini lattice, the number of ground states is found to grow exponentially with the number of lattice sites. For the octagon-square lattice with $4MN$ sites, the number of ground states grows as $2^M + 2^N - 1$. For the square lattice with two additional sites on every link, one finds that there are just

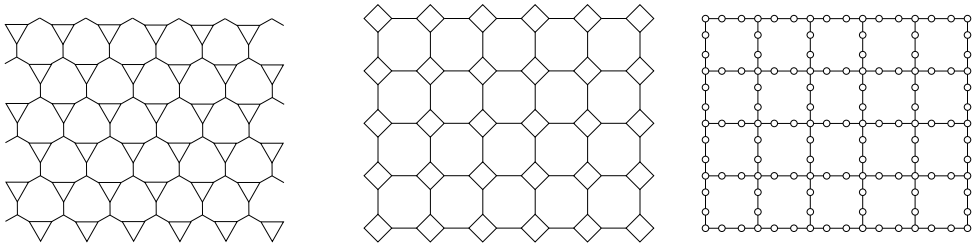

**Figure 5.1:** From left to right we show the martini lattice, the octagon-square lattice and the square lattice with two additional sites per link.

two ground states. Finally, in section 5.4 we will see that for the square lattice of $MN$ sites, for which an exact solution of the cohomology of $Q$ also exists, the ground state degeneracy roughly grows as $2^{M+N}$.
It follows that for all lattices, for which the exact ground state degeneracy was found, only the martini lattice has an extensive ground state entropy. This may seem in contradiction with our claim, at the start of this chapter, that an extensive ground state entropy is a generic property of two-dimensional lattices. However, solving the cohomology problem is in general very difficult and the fact that an exact solution can be found for these lattices is probably related to the fact that they have a relatively simple ground state structure. For the martini lattice and the octagon-square lattice, for example, all ground states have the same particle number. The square lattice with two additional sites on every link has ground states at different fillings, but there are just one or two at each filling. A way to interpret these simplifications is that the lattices for which an exact solution exists, typically accommodate the 3-rule better. This property, in turn, often leads to a reduction in the frustration.

### 5.2.1 Martini lattice

For the martini lattice, which is formed by replacing every other site on a hexagonal lattice by a triangle (see 5.1), the number of zero-energy ground states was found to equal the number of dimer coverings of the hexagonal lattice [21]. The argument is as follows. Let us define sublattice $S_1$ as the collection of sites on the corners of the triangles. The remaining sites belong to sublattice $S_2$. We define $Q = Q_1 + Q_2$, where $Q_1$ and $Q_2$ act on different sublattices $S_1$ and $S_2$. The 'tic-tac-toe'-lemma says that the cohomology, $H_Q$, is the same as the cohomology of $Q_1$ acting on the cohomology of $Q_2$, that is $H_Q = H_{Q_1}(H_{Q_2})$, given that all non-trivial elements of $H_{12}$ have the same fermion-number, $f_2$, on $S_2$. To compute the cohomology of $Q_2$ we consider a single site on $S_2$. If both of the adjacent $S_1$ sites are empty, $H_{Q_2}$ is trivial: $Q_2$ acting on the empty site does not vanish, while the filled site is $Q_2$ acting on the empty site. Thus $H_{Q_2}$ is non-trivial only when every site on $S_2$ is forced to be empty by being adjacent to an occupied site. Note that there can be at most one particle on each triangle in $S_1$ and that there are as many sites in $S_2$ as there are triangles in $S_1$ (for appropriate boundary conditions). It follows that an element in $H_{Q_2}$ must have precisely one particle per triangle, each adjacent to a different site in $S_2$. The number of such configurations equals the number of dimer coverings on the original hexagonal lattice. This can be seen by thinking of the dimers as stretching between the $S_2$ site and the site replaced by the triangle whose occupied site is adjacent to the $S_2$ site. A dimer covering is such that each site is connected to precisely one link containing a dimer. This

is equivalent to having precisely one particle per triangle in the martini lattice. Since all elements in $H_{Q_2}$ have the same number of particles on $S_1$, they are automatically also in $H_{12}$. Finally, since all elements have $f_2 = 0$, we find that $H_Q = H_{12}$. The number of ground states for the supersymmetric model on the martini lattice, thus equals the number of dimer coverings on the original hexagonal lattice. This problem was solved in the context of statistical mechanics [82, 83]. For large systems (number of sites $N \to \infty$) this gives a closed expression for the ground state entropy, $S_{\rm GS}$, per site

$$\frac{S_{\rm GS}}{N} = \frac{1}{\pi}\int_0^{\pi/3} d\theta \ln[2\cos\theta] = 0.16153\ldots$$

We conclude that the ground state entropy is an extensive quantity. This is closely related to the fact that for the martini lattice, due to its structure, the 3-rule can be implemented in many ways.

### 5.2.2 Octagon-square lattice

The $M \times N$ octagon-square lattice is obtained from the $M \times N$ square lattice by replacing every site by a square (see figure 5.1). The $M \times N$ octagon-square lattice thus contains $4MN$ sites. For this lattice the total number of ground states can be obtained analytically [21], again by using the 'tic-tac-toe' lemma. We will consider the case with doubly periodic boundary conditions. For this case, we take $S_1$ to consist of all left-most sites of the squares. Consequently, $S_2$ is a collection of $N$ periodic chains of length $3M$. Now remember that the periodic chain of length $3M$ has two ground states with $M$ fermions. It follows that if we leave $S_1$ completely empty, we obtain $2^N$ non-trivial elements of $H_2$ at grade $MN$, that is, with $MN$ fermions. To find the other elements of $H_2$ we note that if we occupy a site on $S_1$, we block two sites on the $S_2$ chain to its right. Consequently, the $S_2$ chain effectively reduces to an isolated site and an open chain of length $3(M-1)$. It follows that a configuration with a single site on $S_1$ occupied, does not belong to $H_2$, since it will contain an isolated site that can be both empty and occupied. Upon inspection of the lattice, one quickly sees that if all $S_1$ sites on a row are occupied, the $S_2$ sublattice effectively becomes a collection of open chains of length $3(M-1)$. Consequently, this gives an element of $H_2$ at grade $N(M-1)+N = MN$. It follows that $H_2$ is trivial unless *all* $S_1$ sites on a row are either empty or occupied. This gives $2^N - 1$ non-trivial elements of $H_2$ corresponding to the configurations with at least one row of $S_1$ sites occupied and finally $2^M$ non-trivial elements of $H_2$ corresponding to the configuration with all $S_1$ sites empty. One easily checks that all non-trivial elements in $H_2$ are at grade $MN$ and thus with $MN$ fermions. From this it follows that all elements in $H_2$ are automatically also in $H_{12}$. Finally, the fact that all elements in $H_{12}$ have the same fermion number $f = MN$, implies that $Q$ cannot map one element to another. From this it follows that $H_Q = H_{12}$, even though, the condition that all elements have equal $f_2$, does not hold for this case. We conclude that the supersymmetric model on the octagon-square lattice has $2^N + 2^M - 1$ zero energy ground states with $MN$ particles.

For completeness, we mention that using the same arguments as above, we find that the number of ground states for the octagon-square lattice with periodic boundary conditions only in the horizontal (vertical) direction is $2^N$ ($2^M$). For open boundary conditions in both directions the ground state is unique.

### 5.2.3 Graphs with extra sites on the links

In the previous two examples, we clearly saw that the 'tic-tac-toe' lemma could be exploited because the lattices naturally break up into sublattices. In this section, we discuss a class of graphs where this property is again crucial. We introduce graphs of type $\Lambda_n$, which are obtained from the original graph $\Lambda$ by adding $n-1$ additional vertices on every link. In the following the only restriction on the graph $\Lambda$ is that it does not contain any isolated sites. This is because for that type of graph the cohomology of $Q$ is always trivial.

Let us start with the case $\Lambda_3$, which was discussed in [21]. That is, we put two additional sites on every link. Now consider the original graph $\Lambda$ as the subgraph $S_1$ and the additional sites as the subgraph $S_2$. The graph $S_2$ is a collection of two site chains. The non-trivial elements in $H_2$ have the $S_1$ sites neighboring a two site chain on $S_2$ either both empty or both occupied. It follows that there are only two non-trivial elements in $H_2$, one with $S_1$ completely empty and one with $S_1$ completely filled. If we leave $S_1$ completely empty, we obtain one non-trivial element of $H_2$ at grade $L_\Lambda$, where $L_\Lambda$ denotes the number of links in the original graph $\Lambda$. The element with $S_1$ completely filled, clearly sits at grade $N_\Lambda$, where $N_\Lambda$ denotes the number of vertices in the original graph $\Lambda$. It now quickly follows that these two elements are also in $H_{12}$ and in $H_Q$ provided that $N_\Lambda \neq L_\Lambda \pm 1$.

As an example consider the square lattice with doubly periodic boundary conditions as the original graph $\Lambda$. The lattice $\Lambda_3$ is shown in figure 5.1. We find that $L_\Lambda = 2N_\Lambda$ and the total number of sites in $\Lambda_3$ is $N = 2L_\Lambda + N_\Lambda$. Consequently, this lattice has one ground state at 1/5 filling and one at 2/5 filling.

We can extend this result for the graphs of type $\Lambda_3$ to the general case of $\Lambda_{3m}$, with $m$ integer, using the cohomology results for the chain with open boundary conditions (see section 4.4). Remember that open chains of length $3m$ and $3m-1$ have one ground state with $f = m$ fermions and an open chain of length $3m+1$ has no zero-energy ground state. If we take $S_2$ again to consists of all the added sites in $\Lambda_{3m}$, it is a collection of chains of length $3m-1$. It follows that there are again two non-trivial elements in $H_2$, one at grade $mL_\Lambda$ and one at grade $N_\Lambda + (m-1)L_\Lambda$. Again we find that these two elements are also in $H_{12}$ and in $H_Q$ provided that $N_\Lambda \neq L_\Lambda \pm 1$.

For graphs of type $\Lambda_{3m\pm1}$ there is no general solution to the cohomology problem, however, one can relate it to the cohomology problem of the original lattice $\Lambda$.

For the graph $\Lambda_{3m+1}$ the subgraph, $S_2$, is a collection of chains of length $3m$. For this case, two $S_1$ sites that are neighbors in the original graph, cannot be both occupied, because then the $S_2$ chain between these two sites effectively reduces to an open chain of length $3m-2$, which has no zero-energy ground state. However, if the two $S_1$ sites are both empty or if one of them is occupied, the $S_2$ chain accommodates one ground state with $m$ fermions in all cases. It follows that all allowed configurations on the original graph $\Lambda$ are non-trivial elements of $H_2$. Clearly, we then find that $H_{12}$ is directly related to the cohomology of the original graph. Finally, since all elements in $H_{12}$ have $f_2 = mL_\Lambda$ we find that $H_Q = H_{12}$ holds. We thus find that the cohomology of $Q$ on $\Lambda_{3m+1}$ at grade $n + mL_\Lambda$ is directly related to the cohomology of $Q$ on $\Lambda$ at grade $n$. In particular, we find that the Witten indices are related via $W_{\Lambda_{3m+1}} = (-1)^{mL_\Lambda} W_\Lambda$.

For the graph $\Lambda_{3m-1}$ the subgraph, $S_2$, is a collection of chains of length $3m-2$. For this case, two $S_1$ sites that are neighbors in the original graph, cannot be both *empty*, because then the $S_2$ chain between these two sites has no zero-energy ground state. However, if the two $S_1$ sites are both occupied or if one of them is occupied, the $S_2$ chain accommodates

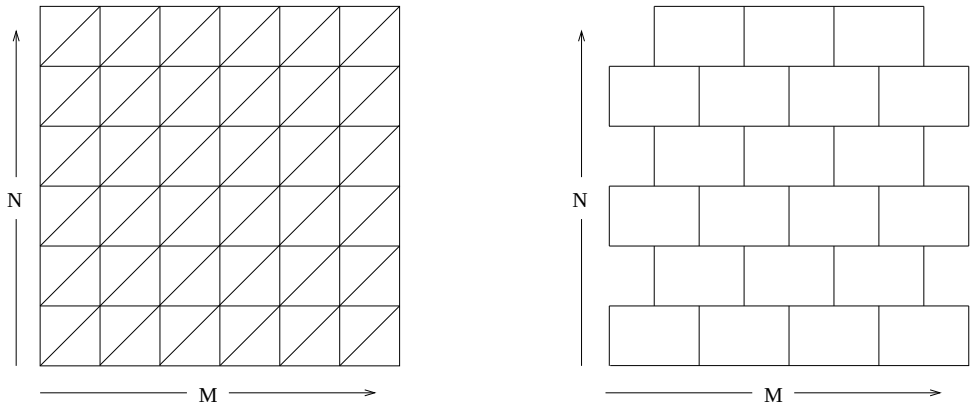


**Figure 5.2:** The $M \times N$ triangular (left) and hexagonal (right) lattice with periodic boundary conditions along the directions of the two arrows.

one ground state with $m-1$ fermions in all cases. We can again relate all the elements in $H_2$ to configurations on the original graph $\Lambda$, but now we have to use a particle-hole symmetry. Following the same arguments as for the previous case, we conclude that the cohomology of $Q$ on $\Lambda_{3m-1}$ at grade $n+mL_\Lambda$ is directly related to the cohomology of $Q$ on $\Lambda$ at grade $N_\Lambda - n$. In particular, the Witten indices are related via $W_{\Lambda_{3m-1}} = (-1)^{mL_\Lambda - N_\Lambda} W_\Lambda$.
The results we derived in this section for graphs of type $\Lambda_n$ with general $n$ were also obtained on a homotopy level using Alexander dualities in [77].

## 5.3 Triangular and hexagonal lattice

In this section, we discuss the triangular and hexagonal lattice. For these lattices, the ground state structure is not fully understood. Nevertheless, it is clear that ground states occur in a finite window of filling fractions $\nu = f/L$ [39] and that there is extensive ground state entropy [78]. The latter result, stems from a numerical analysis of the Witten index for finite size systems (see 5.3.1). The former result, is an analytic result, which we discuss in section 5.3.2, where we also discuss an analytic upper bound on the number of ground states [76].

### 5.3.1 Numerical results for Witten index

In tables 5.1 and 5.2 respectively, we show the Witten indices for the $M \times N$ triangular and hexagonal lattices, with periodic boundary conditions applied along two axes of the lattice [78] (see figure 5.2). The exponential growth of the index is clear from the table. To quantify the growth behavior, one may determine the largest eigenvalue $\lambda_N$ of the row-to-row transfer matrix for the Witten index on size $M \times N$. For the triangular lattice this gives [78]

$$|W_{M,N}| \sim (\lambda_N)^M + (\bar{\lambda}_N)^M \ , \quad \lambda_N \sim \lambda^N$$
$$|\lambda| \sim 1.14 \ , \quad \arg(\lambda) \sim 0.18 \times \pi$$

leading to a ground state entropy per site of

$$\frac{S_{\mathrm{GS}}}{MN} \geq \frac{1}{MN} \log |W_{M,N}| \sim \log |\lambda| \sim 0.13 \ .$$

The argument of $\lambda$ indicates that the asymptotic behavior of the index is dominated by configurations with filling fraction around $\nu = 0.18$. Similarly, one obtains for the hexagonal lattice [78]

$$\frac{S_{\mathrm{GS}}}{MN} \gtrsim 0.18 \ .$$

For this case the data is insufficient to determine the argument of $\lambda$.

**Table 5.1:** Witten index for $M \times N$ triangular lattice (taken from [78]).

| | 1 | 2 | 3 | 4 | 5 | 6 | 7 | 8 | 9 | 10 |
|---|---|---|---|---|---|---|---|---|---|---|
| 1 | 1 | 1 | 1 | 1 | 1 | 1 | 1 | 1 | 1 | 1 |
| 2 | 1 | -3 | -5 | 1 | 11 | 9 | -13 | -31 | -5 | 57 |
| 3 | 1 | -5 | -2 | 7 | 1 | -14 | 1 | 31 | -2 | -65 |
| 4 | 1 | 1 | 7 | -23 | 11 | 25 | -69 | 193 | -29 | -279 |
| 5 | 1 | 11 | 1 | 11 | 36 | -49 | 211 | -349 | 811 | -1064 |
| 6 | 1 | 9 | -14 | 25 | -49 | -102 | -13 | -415 | 1462 | -4911 |
| 7 | 1 | -13 | 1 | -69 | 211 | -13 | -797 | 3403 | -7055 | 5237 |
| 8 | 1 | -31 | 31 | 193 | -349 | -415 | 3403 | 881 | -28517 | 50849 |
| 9 | 1 | -5 | -2 | -29 | 881 | 1462 | -7055 | -28517 | 31399 | 313315 |
| 10 | 1 | 57 | -65 | -279 | -1064 | -4911 | 5237 | 50849 | 313315 | 950592 |
| 11 | 1 | 67 | 1 | 859 | 1651 | 12607 | 32418 | 159083 | 499060 | 2011307 |
| 12 | 1 | -47 | 130 | -1295 | -589 | -26006 | -152697 | -535895 | -2573258 | -3973827 |
| 13 | 1 | -181 | 1 | -77 | -1949 | 67523 | 330331 | -595373 | -10989458 | -49705161 |
| 14 | 1 | -87 | -257 | 3641 | 12611 | -139935 | -235717 | 5651377 | 4765189 | -232675057 |
| 15 | 1 | 275 | -2 | -8053 | -32664 | 272486 | -1184714 | -1867189 | 134858383 | -702709340 |

**Table 5.2:** Witten index for $M \times N$ hexagonal lattice (taken from [78]).

| | 2 | 4 | 6 | 8 | 10 | 12 | 14 | 16 | 18 |
|---|---|---|---|---|---|---|---|---|---|
| 2 | -1 | -1 | 2 | -1 | -1 | 2 | -1 | -1 | 2 |
| 4 | 3 | 7 | 18 | 47 | 123 | 322 | 843 | 2207 | 5778 |
| 6 | -1 | -1 | 32 | -73 | 44 | 356 | -1387 | 2087 | 2435 |
| 8 | 3 | 7 | 18 | 55 | 123 | 322 | 843 | 2215 | 5778 |
| 10 | -1 | -1 | 152 | -321 | -171 | 7412 | -26496 | 10079 | 393767 |
| 12 | 3 | 7 | 156 | 1511 | 6648 | 29224 | 150069 | 1039991 | 6208815 |
| 14 | -1 | -1 | 338 | 727 | -5671 | 1850 | 183560 | -279497 | -4542907 |
| 16 | 3 | 7 | 1362 | 12183 | 31803 | 379810 | 5970107 | 55449303 | 327070578 |

### 5.3.2 Bounds on the size and dimension of the homology of $Q$

There are two main results for bounds on the full cohomology problem for the triangular and hexagonal lattices. Here we briefly sketch how they were obtained. The first result, obtained by Jonsson [39], is a certain type of homology cycle for these lattices called cross-cycles. The size of a cross-cycle refers to the number of vertices in the cycle, that is the number of occupied sites. A bound on the size of these cross-cycles is obtained and this results in a bound on the grade of the vector spaces for which the homology is

non-vanishing. That is, there is a set of rational numbers $r$, such that there exist cross-cycles of size $rN$, where $N$ is the number of vertices of the two-dimensional lattice. For the triangular lattice it is found that $r \in [\frac{1}{7}, \frac{1}{5}] \cap \mathbb{Q}$ and for the hexagonal lattice $r \in [\frac{1}{4}, \frac{5}{18}] \cap \mathbb{Q}$ (and $r \in [\frac{1}{5}, \frac{1}{4}] \cap \mathbb{Q}$ for the square lattice, see section 5.4). Let us give the specific form of a cross-cycle $z$ of size $k$:

- $z = \prod_{i=1}^{k}(|a_i\rangle - |b_i\rangle)$ such that $z \in C_k$, that is the $a_i$ and $b_i$ obey the hard-core condition.
- Furthermore, there is at least one configuration in $z$ such that all sites in the lattice are either occupied or adjacent to at least one occupied site. This is called a maximal independent set.
- Finally, $a_i$ is adjacent to $b_i$.

Note that, in this case, we consider the homology and not the cohomology. It is easily verified that $z$ belongs to the kernel of $Q^\dagger$, since $Q^\dagger$ gives zero on each term in the product:

$$Q^\dagger(|a_i\rangle - |b_i\rangle) = |\emptyset\rangle - |\emptyset\rangle = 0.$$

The latter two conditions ensure that $z$ is not exact. The second condition ensures that there is no site $c$ such that $Q^\dagger|c\rangle \prod_{i=1}^{k}(|a_i\rangle - |b_i\rangle) = z$ and the third condition ensures that $|a_j\rangle|b_j\rangle \prod_{i\neq j}(|a_i\rangle - |b_i\rangle)$ violates the hard-core condition.
Clearly, the latter two conditions, combined with the hard-core condition, also impose certain bounds on the size of a cross-cycle. For the triangular lattice the size of the cross-cycles is at most a fifth of all the sites in the lattice and at least a seventh [39]. In fact, the cross-cycles are found to induce tilings of the triangular lattice with paralellogram-shaped tiles of area 5 and area 7. See figure 5.3 for a specific tiling and its corresponding cross-cycle. The black dots are the $a_i$ sites, whereas the white dots are the $b_i$ sites. Note that both $\{a_i\}$ and $\{b_i\}$ are a maximal independent set. For the square lattice the cross-cycles also induce a tiling (see figure 5.7). This will be discussed in more detail in the next section. For further details and the specific form of the cross-cycles for the hexagonal lattice we refer to [39].
The second result that imposes a bound on the (co)homology on the triangular and hexagonal lattices, was obtained by Engström [76]. He finds an upper bound to the total dimension of the cohomology and thus to the Euler characteristic for general graphs $G$ using discrete Morse theory: if $G$ is a graph and $D$ a subset of its vertex set such that $G \setminus D$ is a forest, then $\sum_i \dim(H_Q^{(n)}) \leq |\mathrm{Ind}(G[D])|$. Here $H_Q^{(n)}$ is the n-th cohomology class of $Q$ on the independence complex on the graph $G$ and $\mathrm{Ind}(G[D])$ is the induced independence complex on the subset $D$. Thus finding the minimal set of vertices that should be removed from $G$ to obtain a forest, gives an upper bound on the total dimension of $H_Q$ and thus on the total number of zero energy ground states for the supersymmetric model on the graph $G$.
As an example we show the hexagonal lattice of size $2m \times 2n$. The subset $D$ contains $mn$ disconnected sites (see figure 5.4). Each site can be empty or occupied in $\mathrm{Ind}(G[D])$ and thus $|\mathrm{Ind}(G[D])| = 2^{mn}$. Finally, also the triangular lattice is shown (figure 5.5). For the triangular lattice of size $2m \times n$ the upper bound was found to be approximately $\phi^{mn}$, with $\phi = \frac{1}{2}(1 + \sqrt{5})$, the golden ratio.

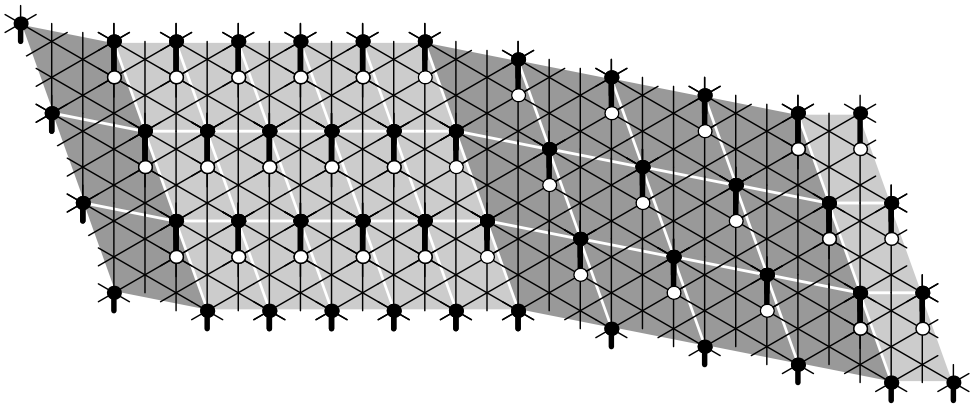

**Figure 5.3:** An example of a cross-cycle on the triangular lattice (taken from [39]). The black dots are the $a_i$ sites, the white dots are the $b_i$ sites. Both sets $\{a_i\}$ and $\{b_i\}$ are maximal independent sets. Notice the induced tiling.

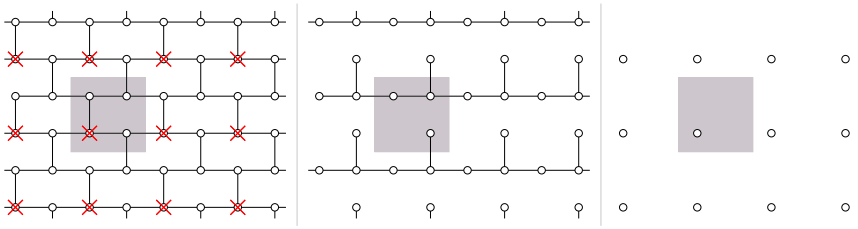

**Figure 5.4:** For the hexagonal lattice we show from left to right: the graph $G$, the forest $G \setminus D$ and the subset $D$ (taken from [76]).

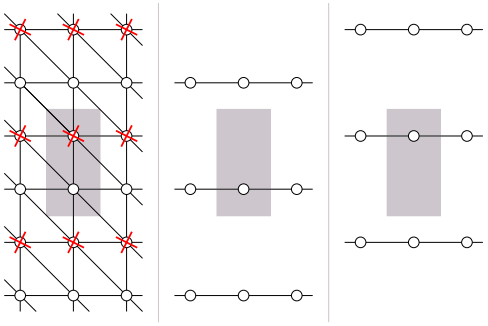

**Figure 5.5:** For the triangular lattice we show from left to right: the graph $G$, the forest $G \setminus D$ and the subset $D$ (taken from [76]).

**Table 5.3:** Witten Index for $M \times N$ square lattice with periodic boundary conditions along the horizontal and vertical direction (taken from [36]).

| | 1 | 2 | 3 | 4 | 5 | 6 | 7 | 8 | 9 | 10 | 11 | 12 |
|---|---|---|---|---|---|---|---|---|---|---|---|---|
| 1 | 1 | 1 | 1 | 1 | 1 | 1 | 1 | 1 | 1 | 1 | 1 | 1 |
| 2 | 1 | -1 | 1 | 3 | 1 | -1 | 1 | 3 | 1 | -1 | 1 | 3 |
| 3 | 1 | 1 | 4 | 1 | 1 | 4 | 1 | 1 | 4 | 1 | 1 | 4 |
| 4 | 1 | 3 | 1 | 7 | 1 | 3 | 1 | 7 | 1 | 3 | 1 | 7 |
| 5 | 1 | 1 | 1 | 1 | -9 | 1 | 1 | 1 | 1 | 11 | 1 | 1 |
| 6 | 1 | -1 | 4 | 3 | 1 | 14 | 1 | 3 | 4 | -1 | 1 | 18 |
| 7 | 1 | 1 | 1 | 1 | 1 | 1 | 1 | 1 | 1 | 1 | 1 | 1 |
| 8 | 1 | 3 | 1 | 7 | 1 | 3 | 1 | 7 | 1 | 43 | 1 | 7 |
| 9 | 1 | 1 | 4 | 1 | 1 | 4 | 1 | 1 | 40 | 1 | 1 | 4 |
| 10 | 1 | -1 | 1 | 3 | 11 | -1 | 1 | 43 | 1 | 9 | 1 | 3 |
| 11 | 1 | 1 | 1 | 1 | 1 | 1 | 1 | 1 | 1 | 1 | 1 | 1 |
| 12 | 1 | 3 | 4 | 7 | 1 | 18 | 1 | 7 | 4 | 3 | 1 | 166 |
| 13 | 1 | 1 | 1 | 1 | 1 | 1 | 1 | 1 | 1 | 1 | 1 | 1 |
| 14 | 1 | -1 | 1 | 3 | 1 | -1 | -27 | 3 | 1 | 69 | 1 | 3 |
| 15 | 1 | 1 | 4 | 1 | -9 | 4 | 1 | 1 | 4 | 11 | 1 | 4 |

## 5.4 Square lattice

In this section, we discuss the square lattice which plays a central role in this thesis. For this lattice we really tried to push our understanding of both the ground state properties as well as the low lying excitations for the two-dimensional system. In this section we summarize the results that were obtained for the ground state counting. For the square lattice with various types of boundary conditions the cohomology problem can be fully solved [35, 75, 84], however, the proofs, especially for the square lattice wrapped around the torus, are rather involved and are presented separately in chapter 6. The discussion of the low lying excitations is postponed to chapter 8.
A first study of the Witten index for the square lattice with doubly periodic boundary conditions revealed various interesting properties [36]. First of all, numerical studies of the Witten index does not show the exponential growth as was found for various other lattices. Instead, at first glance it clearly shows a very different behavior (see table 5.3). A more detailed investigation of these results led to two conjectures [36] for which a proof was found by Jonsson [37].
We state these results here:

- The eigenvalues of the transfer matrix with periodic boundary conditions are all roots of unity.
- For an $M \times N$ square lattice with periodic boundary conditions in both directions, $W = 1$ when $M$ and $N$ are coprime.

Extending this work, Jonsson found a general expression for the Witten index $W_{u,v}$ of hard-core fermions on the square lattice with periodic boundary conditions given by the vectors $u = (u_1, u_2)$ and $v = (v_1, v_2)$. The $M \times N$ square lattice is now a specific case with $u = (M, 0)$ and $v = (0, N)$ [37]. A crucial step in [37] is the introduction of rhombus tilings

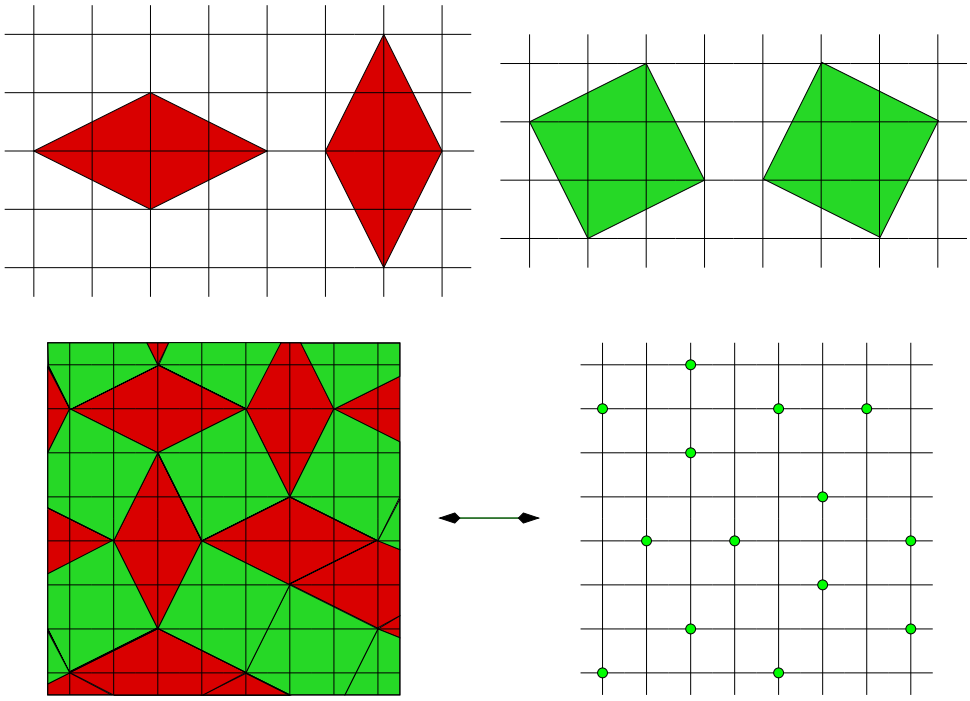

**Figure 5.6:** Tilings of the 2D square lattice. Above: the four different rhombi. Below: mapping between tiles and hard-core fermions.

of the square lattice. It is shown that the trace in the Witten index can be restricted to configurations that can be mapped to coverings of the plane with the four rhombi or tiles shown in figure 5.6. A rhombus tiling is obtained by tiling the plane with the rhombi depicted in figure 5.6, such that the entire plane is tiled and the rhombi do not overlap (they can have only a corner or a side in common). We call the tiles with area 4 diamonds and the ones with area 5 squares. Note that the sides of these rhombi, which connect the hard-core fermions, are in agreement with the heuristic 3-rule.
To state Jonsson's results for the Witten index we introduce the following notations. We denote by $R_{u,v}$ the family of tilings of the plane with boundary conditions given by $u = (u_1, u_2)$ and $v = (v_1, v_2)$. Furthermore $|R^+_{u,v}|$ and $|R^-_{u,v}|$ are the number of tilings of this plane with an even and an odd number of tiles, respectively. Finally, we define

$$\theta_d \equiv \begin{cases} 2 & \text{if } d = 3k, \text{ with } k \text{ integer} \\ -1 & \text{otherwise.} \end{cases}$$

Jonsson's result then reads

**Theorem 1 (Jonsson, 2006)** *The Witten index for the square lattice with periodicities* $u = (u_1, u_2)$ *and* $v = (v_1, v_2)$ *is given by*

$$W_{u,v} = -(-1)^d \theta_d \theta_{d^*} + |R^+_{u,v}| - |R^-_{u,v}|,$$

*where* $d \equiv \gcd(u_1 - u_2, v_1 - v_2)$ *and* $d^* \equiv \gcd(u_1 + u_2, v_1 + v_2)$.

It can be shown that the Witten index grows exponentially with the linear size (not the area) of the 2D lattice. Detailed results for the case of diagonal boundary conditions have been given in [38]. Further studies of the Witten index transfermatrix for the square lattice

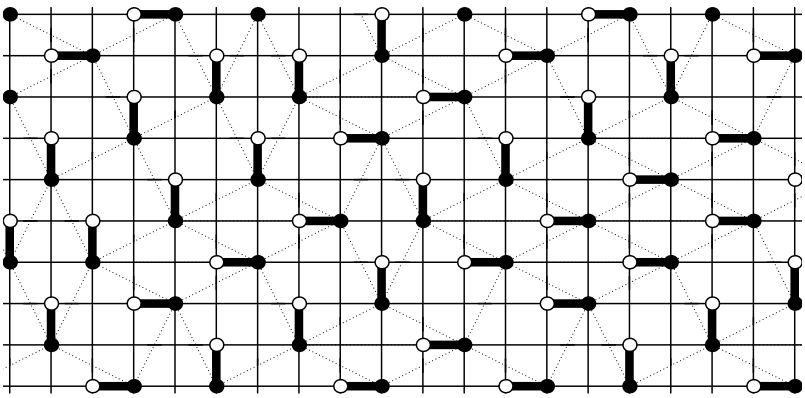

**Figure 5.7:** An example of a tiling on the square lattice and its corresponding cross-cycle. The black dots are the $a_i$ sites, the white dots are the $b_i$ sites. Both sets $\{a_i\}$ and $\{b_i\}$ are maximal independent sets. (Figure source: [39])

with diagonal and free boundary conditions by Baxter [74] have led to an additional set of conjectures.

We should stress that this result was obtained by studying the purely combinatorial problem of configurations of hard-core fermions or, equivalently, of hard squares with negative activity. For the square lattice the condition that two particles cannot occupy two adjacent sites readily translates to the hard square condition if we define the squares to be tilted by 45° and to have a particle at their center. It follows that the squares cannot overlap, however they can have a corner or a side in common.

In a follow-up study Jonsson presents the first results on the homology problem for the square lattice with doubly periodic boundary conditions [39]. He shows that at certain grades the homology must be non-vanishing since there exist non-trivial elements of the homology. These cross-cycles were discussed in section 5.3.2. Jonsson finds that for the square lattice the size of the cross-cycles is at most a quarter of all the sites in the lattice and at least a fifth. In fact, he finds that all the possible cross-cycles are one-to-one with the tiling configurations of the rhombi of figure 5.6. See figure 5.7 for a specific tiling and its corresponding cross-cycle $z = \prod_{i=1}^{k}(|a_i\rangle - |b_i\rangle)$. The black dots are the $a_i$ sites, whereas the white dots are the $b_i$ sites. Note that both $\{a_i\}$ and $\{b_i\}$ are a maximal independent set.

A natural extension of the results by Jonsson, is to relate the full cohomology problem to tiling configurations. This relation was first conjectured by Fendley [34]. Using the 'tic-tac-toe' lemma and a spectral sequence, we were able to prove this relation explicitly when $\vec{u} = (m, -m)$ and $v_1 + v_2 = 3p$ [35] (see chapter 6).

**Theorem 2** *For the square lattice with periodicities $\vec{v} = (v_1, v_2)$, $v_1 + v_2 = 3p$ with $p$ a positive integer and $\vec{u} = (m, -m)$, we find for the cohomology $H_Q$*

$$N_n = \dim(H_Q^{(n)}) = t_n + \Delta_n \tag{5.1}$$

*where $N_n$ is the number of zero energy ground states with $n$ fermions, $t_n$ is the number of rhombus tilings with $n$ tiles, and*

$$\Delta_n = \begin{cases} \Delta \equiv -(-1)^{(\theta_m+1)p}\theta_d\theta_{d*} & \text{if } n = [2m/3]p \\ 0 & \text{otherwise,} \end{cases} \tag{5.2}$$

*with* $[a]$ *the nearest integer to* $a$. *Finally,* $d = \gcd(u_1 - u_2, v_1 - v_2)$, $d^* = \gcd(u_1 + u_2, v_1 + v_2)$ *and*

$$\theta_d \equiv \begin{cases} 2 & \text{if } d = 3k, \text{ with } k \text{ integer} \\ -1 & \text{otherwise.} \end{cases} \tag{5.3}$$

Although, the proof is restricted to a certain set of periodicities, the theorem is expected to hold for general $\vec{u}$ and $\vec{v}$. Compelling evidence stems, on the one hand, from the fact that Jonsson's result for the Witten index holds for general periodicities and on the other hand, from numerical and analytic results for small systems (see chapter 7).
Clearly, as an immediate consequence of this theorem, we obtain for the Euler characteristic, or equivalently, the Witten index

$$\chi \equiv \sum_n \left[ (-1)^n \dim H_Q^{(n)} \right] = \sum_n (-1)^n (t_n + \Delta_n).$$

which is precisely the result obtained by Jonsson for the hard squares at activity $z = -1$ [37].
Another direct consequence follows from the area of the tiles. The diamonds have area 4, and thus a tiling with solely diamonds will contain $L/4$ tiles. This corresponds to an element in the $L/4$-th cohomology and a ground state with $L/4$ particles. Conversely, a tiling consisting of squares only corresponds to an element in the $L/5$-th cohomology and a ground state with $L/5$ particles. Continuing this argument for general tilings with the diamonds and squares, we find on the infinite plane that for all rational numbers $r \in [\frac{1}{5}, \frac{1}{4}] \cap \mathbb{Q}$ the cohomology at grade $rL$ is non vanishing, or, equivalently, there exists a zero energy ground state with $rL$ particles. Clearly, this nicely agrees with the bounds on the size of the homology of $Q^\dagger$ obtained by Jonsson using the cross-cycles. However, for the cross-cycles it was an open question whether they are independent, i.e. in different homology classes, and whether they constitute a basis. A comparison with our result, theorem 2, suggests that the cross-cycles are indeed independent and span the full homology with the exception of $\Delta_n$ elements at the $n$-th grade.
Finally, the theorem provides insight in the growth behavior of the number of ground states, since this is now directly related to the growth behavior of the number of tilings. In [38] various results on the number of tilings on the doubly periodic square lattice are reported (see also section 6.6). Here we mention two of these results for the case that $\vec{u} = (m, -m)$ and $\vec{v} = (k, k)$.

1 For $m$ and $k$ such that $\gcd(m, k) = 1$, there are no rhombus tilings that satisfy the periodicities given by $\vec{u}$ and $\vec{v}$.

2 For $m = 3\mu q$ and $k = 3\lambda q$, with $\mu$ and $\lambda$ positive integers and $q$ large, the total number of rhombus tilings $t$ grows as

$$t \equiv \sum_n t_n \sim \frac{9}{2} \frac{4^{\mu q + \lambda q}}{\pi q \sqrt{\mu \lambda}}. \tag{5.4}$$

In the first case, it follows that the number of ground states with $n$ particles is given by $\Delta_n$, which is non-zero only for $n = [2m/3]p$ given that $2k = 3p$. In the second case, the number of ground states shows the same growth behavior as the number of tilings.

This number turns out to be dominated entirely by the number of tilings with $2L/9$ tiles. Furthermore, it is noteworthy that the number of tilings grows exponentially with the linear dimensions, instead of the area, of the system. It follows that, even though the system is highly frustrated, this leads only to a sub-extensive ground state entropy. This is in contrast with results discussed in the previous sections for the triangular, hexagonal and martini lattices, for which the ground state entropy was found to be extensive.
We finish this chapter by stating the results for the square lattice on the plane and on the cylinder. For open boundary conditions in either one or both of the diagonal directions along the square lattice ($(m,-m)$ and $(n,n)$) the number of ground states reduces dramatically [37, 75, 34]. One finds that it is either one or zero, except for the cylindrical case periodic in the $(m,-m)$-direction with $m=3p$ and $n=3q+2$ or $n=3q+3$. In that case the number of ground states is $4^{(q+1)}$. These results are fairly easily obtained using the 'tic-tac-toe' lemma. The proofs are given in section 6.4. Finally, there is a result for the Witten index for the square lattice of $M\times N$ sites with periodic boundary conditions along the $(N,0)$-direction and $N$ odd [84]. It was proven that for odd $N$

$$W=\begin{cases} 2 & \text{if 3 divides } \gcd(M-1,N) \\ -1 & \text{otherwise.} \end{cases}$$

# Chapter 6
# Ground states of the 2D square lattice on the torus related to rhombus tilings

## 6.1 Introduction

In this chapter we give the proof for theorem 2, which can be formulated both in physical as well as mathematical terminology [35]. We prove the theorem in the mathematics context, namely we find the dimensions of the cohomology for the independence complex on the square lattice wrapped around a torus. In the physics context this translates to the statement that we found the total number of ground states for the supersymmetric model on the square lattice wrapped around a torus. For the interpretation and consequences of the theorem we refer to chapters 5, 7 and 8.

The solution is found by relating ground states, or equivalently elements of the cohomology, to tilings of the plane with two types of rhombi. As was mentioned before, this relation is inspired by the work of Jonsson [37, 39]. He first introduced the rhombi when he related the partition sum of hard squares with activity $z = -1$ to these rhombus tilings. This is precisely the Witten index for our model on the square lattice, and also the Euler characteristic of $H_Q$. The Witten index is a lower bound to the number of ground states. The result presented here gives us, not just this bound, but the total number of ground states with their respective fermion number in terms of rhombus tilings. A rhombus tiling is obtained by tiling the plane with the rhombi depicted in figure 6.1, such that the entire plane is tiled and the rhombi do not overlap (they can have only a corner or a side in common). We call the tiles with area 4 diamonds and the ones with area 5 squares.

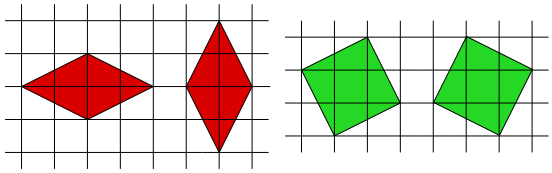

**Figure 6.1:** The diamonds on the left and squares on the right.

Although, the proof of the theorem is restricted to a certain class of periodicities on the square lattice, there is strong evidence that the theorem holds in general. This evidence comes from, on the one hand, the fact that Jonsson's result for the Witten index holds for general periodicities and on the other hand, numerical and analytic evidence for small systems (see chapter 7).

## 6.2 Outline of the proof

The proof presented in this chapter is quite involved and consists of several intermediate steps. Here we will give a brief outline of these steps. In section 2.2.3 we discussed the 'tic-tac-toe' lemma which plays a crucial role in the proof. The lemma relates $H_Q$ to $H_{Q_1}$ and $H_{Q_2}$ when $Q$ is written as $Q_1+Q_2$. This is achieved by writing the lattice $S$ as $S_1 \cup S_2$ and letting $Q_i$ act solely on $S_i$. The crucial step is to choose the right sublattices. It turns out that for the square lattice one should pick a set of disconnected points for $S_1$ and a set of (disconnected) chains for $S_2$ (for the details see definition 2).
First, in section 6.3, we will discuss the cohomology results for a single chain with various boundary conditions. These results are crucial in the first step of the 'tic-tac-toe' lemma, i.e. computing the cohomology of $Q_2$, since $Q_2$ acts on a set of chains.
Second, in section 6.4, we consider the square lattice on the plane and on the cylinder, to illustrate the power of the 'tic-tac-toe' lemma for a relatively simple case. We choose the boundary conditions in such a way that $H_{Q_2}$ is non-vanishing only for one value of $f_1$ and $f_2$. Consequently, $H_{12}$ and $H_Q$ are trivially obtained from $H_{Q_2}$.
Finally, we wrap the square lattice around the torus. We then apply the same strategy as in section 6.4, and $H_{Q_2}$ is easily obtained. Unfortunately, however, it has entries in several rows and columns of the double complex and computing $H_{12}$ is highly non trivial.
As a first step (section 6.5.1), we compute $H_{12}$ for a thin torus, such that the $S_2$ sublattice consists of one chain only. For this case, we then show that $H_Q = H_{12}$, even though $H_{12}$ has entries in multiple rows. The final step for this simple case is to relate the elements of $H_Q$ to periodic sequences of tiles and identify the elements that give rise to the small number $\Delta$ in (5.1).
In the last step (section 6.5.2), we finally present the proof of theorem 2. Here the sublattice $S_2$ consists of an arbitrary number of chains. We proceed as in section 6.5.1 to obtain $H_{12}$ and each step will be similar, but slightly more involved. Again we find that $H_{12}$ does not have entries only in one row. In contrast to the thin torus case, however, we find that here $H_Q$ is contained in but not equal to $H_{12}$. Using the 'tic-tac-toe' procedure, we reduce $H_{12}$ to obtain $H_Q$. What we find is that all the elements of $H_Q$ can be obtained by concatenating so-called building blocks and in the final step we map each building block to a sequence of tiles. It follows from this mapping, that the elements of $H_Q$ map to all possible tilings, again with a small discrepancy $\Delta$, which is computed in the very last step.
Finally, in section 6.6 we present a counting formula for the number of tilings given the periodicities for which theorem 2 is proven to hold.

## 6.3 The cohomology of $Q$ on the chain

In the following sections we will often use the cohomology results for the supersymmetric model on the chain. These results can be found in [23, 22] (see also section 4.4), but will be restated here for completeness.

**Definition 1** *An open chain of length $L$ is the graph $G(V,E)$ with vertices $V = \{v_j | j \in \mathbb{N}, j \leq L\}$ and edges $E = \{(v_j, v_{j+1}) | j \in \mathbb{N}, j < L\}$. A periodic chain of length $L$ is a cycle defined by the graph $G(V,E')$ where $E' = E \cup \{(v_L, v_1)\}$.*

In the following $j \in \mathbb{N}$ ($j$ can also be zero as long as the number of sites $L$ is positive).

**Theorem 3** *The cohomology of $Q$ on the periodic chain with $L$ sites has:*

- *2 non-trivial cohomology classes with $j$ fermions if $L = 3j$,*
- *1 non-trivial cohomology class with $j$ fermions if $L = 3j \pm 1$.*

*The cohomology of $Q$ on the open chain with $L$ sites has:*

- *1 non-trivial cohomology class with $j$ fermions if $L = 3j$ or $L = 3j - 1$,*
- *0 non-trivial cohomology classes if $L = 3j + 1$.*

*Proof.* We prove this result for the periodic chain with $L = 3j$ sites. We take $S_2$ to be every third site and the remaining sites $S_1$. Remember that $f_i$ is the number of fermions on sublattice $S_i$. Consider a single site on $S_2$. If both of the adjacent $S_1$ sites are empty, $H_{Q_2}$ is trivial: $Q_2$ acting on the empty site does not vanish, while the filled site is $Q_2$ acting on the empty site. So the empty site does not belong to the kernel of $Q_2$, whereas the filled site belongs to the image of $Q_2$. This leads to a vanishing $H_{Q_2}$, unless every site on $S_2$ is forced to be empty by being adjacent to an occupied site. There are only two such configurations:

$$\begin{aligned} |\alpha\rangle &\equiv \cdots \bullet \square \circ \bullet \square \circ \bullet \square \circ \bullet \square \circ \bullet \square \circ \bullet \square \circ \ldots \\ |\gamma\rangle &\equiv \cdots \circ \square \bullet \circ \square \bullet \circ \square \bullet \circ \square \bullet \circ \square \bullet \circ \square \bullet \ldots \end{aligned} \tag{6.1}$$

where the square represents an empty site on $S_2$. Both states $|\alpha\rangle$ and $|\gamma\rangle$ belong to $H_{12}$: they are closed because $Q_1|\alpha\rangle = Q_1|\gamma\rangle = 0$, and not exact because there are no elements of $H_{Q_2}$ with $f_1 = f - 1$ fermions, where $f = L/3 = j$. By the 'tic-tac-toe' lemma, there must be precisely two different cohomology classes in $H_Q$, and therefore exactly two ground states with $j$ fermions. □

The proofs for the other cases are completely analogous. In the main proof we will need the representatives of the non-trivial cohomology classes of $Q$ on the open chain. We will use the following notation: to denote a configuration with fermions on sites $a$, $b$, $c$, etc. we write $|a, b, c \ldots\rangle$.

**Lemma 1** *A representative of the non-trivial cohomology classes of $Q$ on the open chain with $L = 3j$ or $L = 3j - 1$ sites is*

$$|\phi\rangle \equiv |2, 5, 8 \ldots 3j - 1\rangle, \tag{6.2}$$

*where on the dots the numbers always increase by three.*

*Proof.* From theorem 3 we know that the representative has $j$ fermions. In the case that $L = 3j$ it follows that $|\phi\rangle$ is the only configuration with $j$ fermions that belongs to the kernel of $Q$. Since the dimension of $H_Q$ is one, $|\phi\rangle$ must be a representative of the non-trivial cohomology class.
When $L = 3j - 1$ there are two configurations that belong to the kernel of $Q$: $|1, 4, 7 \ldots 3j - 2\rangle$ and $|2, 5, 8 \ldots 3j - 1\rangle$, however the dimension of $H_Q$ is again just one. It follows that a linear combination of these two configurations will be in the image

of $Q$. In general, two states $|s_1\rangle$ and $|s_2\rangle$ are in the same cohomology class if one can write $|s_1\rangle = |s_2\rangle + Q|s_3\rangle$ for some state $|s_3\rangle$. In that case both $|s_1\rangle$ and $|s_2\rangle$ are good representatives of the cohomology class. Since $|\phi\rangle$ itself is not in the image of $Q$ it is thus a good representative. □

## 6.4 The cohomology of $Q$ on the square lattice. Part I: Tilted rectangles and cylinders

Let us define $\mathcal{R}(M,N)$ with $M,N \geq 1$ as the subset of $\mathbb{Z}^2$ given by the points $(x,y)$ such that

$$y \leq x \leq y+M-1 \quad \text{and} \quad -y+1 \leq x \leq -y+N. \tag{6.3}$$

This defines a tilted rectangular part of the square lattice. We can also define $\tilde{\mathcal{R}}(M,N)$ with $M,N \geq 1$ as the subset of $\mathbb{Z}^2$ given by the points $(x,y)$ such that

$$y \leq x \leq y+M-1 \quad \text{and} \quad -y \leq x \leq -y+N-1. \tag{6.4}$$

Whereas $\tilde{\mathcal{R}}(M,N)$ contains the point $(0,0)$, it is excluded in $\mathcal{R}(M,N)$. The lattice $\tilde{\mathcal{R}}(M,N)$ can be mapped to a lattice of the former type except when $M$ and $N$ are both odd. Finally, for $M$ even the cylindrical version $\mathcal{R}_c(M,N)$ can be obtained from $\mathcal{R}(M+1,N)$ by identifying the vertices $(i,i)$ and $(i+M/2, i-M/2)$.
For the lattices $\mathcal{R}(M,N)$, $\tilde{\mathcal{R}}(M,N)$ and $\mathcal{R}_c(M,N)$ the full cohomology problem has been solved using Morse theory [75]. These cases can also be solved using the 'tic-tac-toe' lemma. The crucial step is to choose the right sublattices. We take a set of disconnected sites for $S_1$ and a set of (open or periodic) chains for $S_2$ (see fig. 6.2).

**Definition 2** *More formally, for $\mathcal{R}(M,N)$ $S_1$ is the set of points $(x,y)$ that satisfy*

$$\begin{aligned} y \leq x \leq y+M-1 \quad &\textit{and} \quad -y \leq x \leq -y+N-1 \\ &\textit{and} \quad x = -y+3s, \end{aligned} \tag{6.5}$$

*with $3 \leq 3s \leq N-1$ and $S_2$ is the set of points $(x,y)$ that satisfy*

$$\begin{aligned} y \leq x \leq y+M-1 \quad &\textit{and} \quad -y \leq x \leq -y+N-1 \\ &\textit{and} \quad -y+3p+1 \leq x \leq -y+3p+2, \end{aligned} \tag{6.6}$$

*with $0 \leq 3p \leq N-3$. The sublattices can be defined similarly for $\tilde{\mathcal{R}}(M,N)$.*

To solve $H_{Q_2}$ we start from the bottom-left chain. If a site on $S_1$ directly above this chain is occupied, we are left with an isolated site on the bottom-left chain (see fig. 6.3), leading to a vanishing $H_{Q_2}$ (see section 6.3). It follows that all sites directly above the bottom-left chain must be empty. Continuing this argument for subsequent chains one finds that all sites on $S_1$ must be empty. However, in the case that $N = 3l+1$ we have a set of disconnected sites at the top-right that belong to $S_2$. From the previous argument we obtained that the sites of $S_1$ directly below the top-right sites of $S_2$ have to be empty. This implies that for $N = 3l+1$ $H_{Q_2}$ vanishes. When $N \neq 3l+1$ we find that all elements in

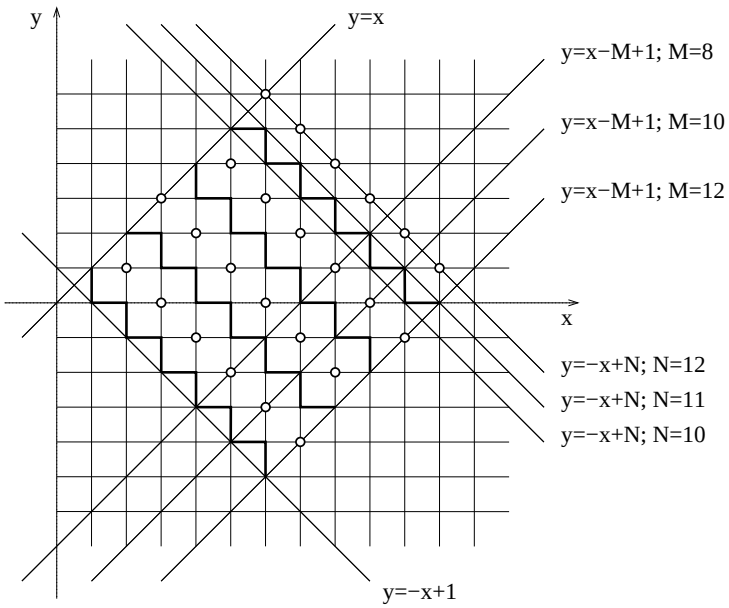


**Figure 6.2:** Sublattice $S_1$ is indicated by circles and sublattice $S_2$ is indicated by the fat lines. The bounding lines of $\mathcal{R}(M,N)$ defined in (6.3) are drawn for various values of $M$ and $N$. For the cylinder $M$ should be even, but for the rectangle it can be odd as well. One easily checks that the length of the $S_2$ chain is $M$. Note that for $N = 3n+1$ only half of the upper-right $S_2$ chain is included in $\mathcal{R}(M,N)$.

$H_{Q_2}$ have all sites in $S_1$ empty, thus computing $H_{Q_1}(H_{Q_2})$ is a trivial step. The dimension of $H_Q$ is related to the number of ground states, or equivalently, the number of non-trivial cohomology classes of $Q$ on the chains that constitute $S_2$. Note that the length of these chains is $M$ both for the tilted rectangles as well as for the cylinder. In the first case the chains have open boundary conditions, whereas in the latter the chains are periodic. Now, the number of non-trivial cohomology classes of $Q$ for all these cases can be found in theorem 3.

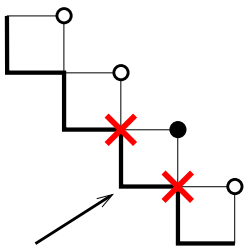

**Figure 6.3:** A site directly above the bottom-left chain is occupied. This generates an isolated site on the bottom-left chain.

It follows that for the tilted rectangles, $\mathcal{R}(M,N)$ and $\tilde{\mathcal{R}}(M,N)$, with $N \neq 3l+1$ we have

i) no non-trivial cohomology classes for $M = 3p+1$

ii) one non-trivial cohomology class for $M \neq 3p+1$.

For the cylinder, $\mathcal{R}_c(M,N)$, with $N \neq 3l+1$ and $M$ even we have

i) one non-trivial cohomology class for $M = 3p \pm 1$

ii) $2^K$ non-trivial cohomology classes for $M = 3p$, with $K$ the nearest integer to $N/3$.

For $N = 3l+1$ the non-trivial cohomology vanishes for both the rectangle and the cylinder.

## 6.5 The cohomology of $Q$ on the square lattice. Part II: The torus

We now define the doubly periodic lattices via two linearly independent vectors $\vec{u} = (u_1, u_2)$ and $\vec{v} = (v_1, v_2)$. We wrap the square lattice around the torus by identifying all points $(i, j)$ with $(i + ku_1 + lv_1, j + ku_2 + lv_2)$. The main result of [35] is the solution of the full cohomology of $Q$ on the square lattice with doubly periodic boundary conditions defined by $\vec{u} = (m, -m)$ and $\vec{v} = (v_1, v_2)$ such that $v_1 + v_2 = 3p$. In particular, we obtain a direct relation between elements of $H_Q$ and tiling configurations. This relation allows us to prove theorem 2, that was first conjectured by P. Fendley and is strongly inspired by the work of Jonsson [37, 39]. It is restated here for convenience.

*For the square lattice with periodicities $\vec{v} = (v_1, v_2)$, $v_1 + v_2 = 3p$ with $p$ a positive integer and $\vec{u} = (m, -m)$, we find for the cohomology $H_Q$*

$$N_n = dim\ H_Q^{(n)} = t_n + \Delta_n \tag{6.7}$$

*where $N_n$ is the number of zero energy ground states with $n$ fermions, $t_n$ is the number of rhombus tilings with $n$ tiles, and*

$$\Delta_n = \begin{cases} \Delta \equiv -(-1)^{(\theta_m+1)p}\theta_d\theta_{d*} & \text{if } n = [2m/3]p \\ 0 & \text{otherwise,} \end{cases} \tag{6.8}$$

*with $[a]$ the nearest integer to $a$. Finally, $d = \gcd(u_1 - u_2, v_1 - v_2)$, $d^* = \gcd(u_1 + u_2, v_1 + v_2)$ and*

$$\theta_d \equiv \begin{cases} 2 & \text{if } d = 3k, \text{ with } k \text{ integer} \\ -1 & \text{otherwise.} \end{cases} \tag{6.9}$$

Computing the cohomology for these tori is far from trivial. First of all, computing $H_{Q_2}$ does not imply that all sites on $S_1$ are empty, instead there are many allowed configurations on $S_1$. Secondly, because of this, computing $H_{Q_1}(H_{Q_2})$ becomes much more involved. Finally, we will see that, generally, $H_Q$ will be contained in $H_{12}$, but not equal to $H_{12}$.
We will divide the proof into two parts. We start by proving the theorem for a specific torus, defined by $\vec{u} = (m, -m)$ and $\vec{v} = (1, 2)$. This proof will already contain many steps that we use in the proof for the more general case, however, it will be deprived of certain complications. For instance, here we will find $H_Q = H_{12}$. As we said, this is not true in general, and in the second part of the proof a substantial part will be concerned with obtaining $H_Q$ once we have found $H_{12}$.

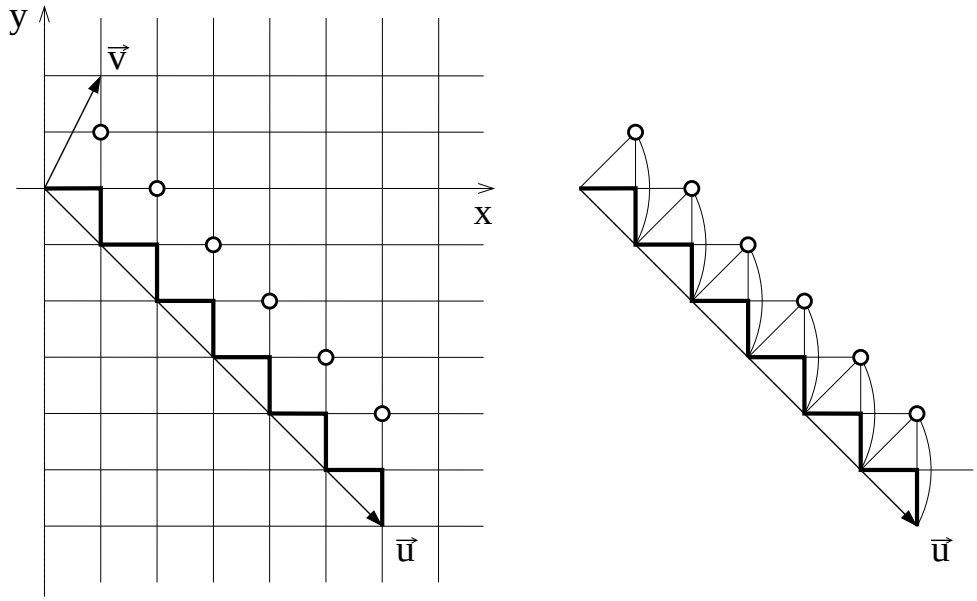


**Figure 6.4:** The square lattice is wrapped around the torus by imposing periodicities $\vec{v}$ and $\vec{u}$. Here $\vec{v} = (1, 2)$ and $\vec{u} = (m, -m)$, consequently $S_2$ consists of 1 chain. On the right we have drawn the cylinder, where periodicity in the $\vec{u}$-direction is still implied.

### 6.5.1 A special case: $S_2$ consisting of 1 chain

In this section we consider the case where $\vec{v} = (1, 2)$ and $\vec{u} = (m, -m)$. It follows that $S_2$ consists of exactly one periodic chain (see fig. 6.4).
The proof of theorem 2 for this case will consist of 4 steps:

1. We compute $H_{Q_2}$.
2. We compute $H_{12} = H_{Q_1}(H_{Q_2})$ and show that its elements can be constructed from a finite number of building blocks, called motifs. A motif is characterized by a certain configuration on a finite number of subsequent $S_1$ sites.
3. We show that $H_Q = H_{12}$.
4. We relate the elements of $H_Q$ to tiling configurations by relating each motif to a small series of tiles.

#### Step 1

First we compute $H_{Q_2}$ and we find the following:

**Lemma 2** *The cohomology of $Q_2$ consists of all possible configurations on $S_1$ except for configurations with a multiple of three $S_1$ sites empty between two occupied $S_1$ sites.*

*Proof.* The proof is relatively simple. First note that when a site on $S_1$ is occupied, it blocks four subsequent sites on the $S_2$ chain (see fig. 6.4). By occupying sites on $S_1$ the periodic $S_2$ chain is cut into smaller pieces of chain with open boundary conditions.

Consequently, $H_{Q_2}$ vanishes when at least one of these smaller pieces has length $3p+1$. This happens when the number of empty sites between two occupied sites on $S_1$ is a multiple of three. We conclude that all configurations on $S_1$ are allowed except for configurations with a multiple of three sites empty between two occupied sites. □

**Step 2**

This step in the proof is the most involved. In the next section, where we prove theorem 2 in all generality, we will often refer back to the results obtained in this step. In this step we compute $H_{Q_1}(H_{Q_2})$, where $H_{Q_2}$ was obtained in the previous step. Let us define $f_1$ and $f_2$ as the number of fermions on $S_1$ and $S_2$ respectively. Furthermore we shall adopt the following notation: an empty site on $S_1$ is denoted by 0 and an occupied site is denoted by 1. A configuration on $S_1$ can then be written as a series of 1's and 0's. In the following we shall consider all possible types of configurations on $S_1$ that belong to $H_{Q_2}$ and we shall investigate if they also belong to $H_{12}$.
If we consider a configuration on $S_1$, we note that there have to be at least two adjacent, empty $S_1$ sites to allow for $f_2 > 0$. This is because two adjacent empty sites leave an open chain of two sites unblocked on $S_2$ and this has an element in $H_{Q_2}$ with $f_2 = 1$. A typical configuration will thus consist of alternating segments, where a segment is a sequence of $S_1$ sites. The segments are characterized by the number of fermions on the part of the $S_2$ chain corresponding to the segment, this is either zero or greater than zero. In a segment with $f_2 > 0$ all $S_1$ sites are empty and it contains at least two sites. On the other hand, a segment with $f_2 = 0$ can have empty sites on $S_1$, but the empty sites cannot be adjacent. Finally, a segment with $f_2 = 0$ will always start and end with an occupied $S_1$ site. We will call this pair of occupied sites a pair of bounding sites. Note that a segment with $f_2 = 0$ can consist of a single occupied site, in that case the bounding sites fall on top of each other and the pair of bounding sites is just this one site.

**Example 1** *Consider the configuration "1101101010000100", there are two segments with $f_2 = 0$, formed by the first nine sites and the fourteenth site respectively. There are also two segments with $f_2 > 0$ constituted by the rest of the sites. Finally, the first and the ninth site form a pair of bounding sites.*

First, we consider the segments with $f_2 > 0$.

**Lemma 3** *$Q_1$ acting on a segment with $f_2 > 0$ gives zero within $H_{Q_2}$.*

*Proof.* Suppose this segment between a pair of bounding sites consists of $l$ empty $S_1$ sites. The corresponding $S_2$ chain then has length $L = 2l - 2$. Since $l = 3k \pm 1$, we find $L = 6k$ or $L = 6k - 4$. For these chain lengths the elements of the cohomology of $Q_2$ have $2k$ and $2k - 1$ fermions respectively. We now distinguish two cases: a) $Q_1$ acts on a site at the boundary of the segment, b) $Q_1$ acts on a site away from the boundary.
a) In this case the length of the $S_2$ chain in the new configuration is $L' = L - 2$. Thus $L' = 6k - 2$ or $L' = 6k - 6$. On the new chain there are still $2k$ or $2k - 1$ fermions respectively. However, theorem 3 states that the cohomology for chain length $6k - 2$ ($6k - 6$) vanishes at all fermion numbers except $f = 2k - 1$ ($f = 2k - 2$). Thus the new

configuration does not belong to $H_{Q_2}$ and it follows that this action of $Q_1$ within $H_{Q_2}$ gives zero.
b) In this case the action of $Q_1$ cuts the $S_2$ chain into two smaller chains of lengths $L_1'$ and $L_2'$. Their total length is $L_1' + L_2' = L - 4$, since the occupied $S_1$ site now blocks 4 sites on the $S_2$ chain. For $L = 6k$ we have $L_1' = 3k_1$ and $L_2' = 3k_2 + 2$ or $L_1' = 3k_1 + 1$ and $L_2' = 3k_2 + 1$, where in both cases $k_1 + k_2 = 2k - 2$. For the latter case $H_{Q_2}$ vanishes at all grades. In the first case $H_{Q_2}$ is non-vanishing only for $f = k_1 + k_2 + 1 = 2k - 1$. However, the number of fermions on the $S_2$ chains in the new configuration is $f = 2k$ and thus is does not belong to $H_{Q_2}$. Similarly, one finds that for $L = 6k - 4$, the new configuration does not belong to $H_{Q_2}$. Again we obtain that this action of $Q_1$ within $H_{Q_2}$ gives zero.
Finally, if the segment with $f_2 > 0$ extends over the entire system, we are always in the case considered under b). However, the original chain length can now also be $L = 6k - 2$ with $2k - 1$ fermions on it. Under the action of $Q_1$ we obtain a new chain of length $L' = 6k - 6$, which has a non-vanishing cohomology if and only if $f = 2k - 2$. So also in this case we find that the action of $Q_1$ gives zero within $H_{Q_2}$.

□

Second, we consider the segments with $f_2 = 0$.

**Lemma 4** *$H_{Q_1}(H_{Q_2})$ vanishes when the number of $S_1$ sites between any pair of bounding sites in a segment with $f_2 = 0$, is $3p + 1$ and it contains one element otherwise.*

**Example 2** *Consider a configuration with one empty site between a pair of bounding sites: "101", this is not an element of $H_{Q_1}(H_{Q_2})$, since $Q_1$ on this configuration gives "111", which is also in $H_{Q_2}$. Now consider two sites between a pair of bounding sites. Then there are two configuration with one empty site: "1011" and "1101" and one configuration with all sites occupied "1111" (remember that the configuration "1001" does not have $f_2 = 0$). It follows that $Q_1$ acting on ("1101" − "1011") gives 2"1111", whereas $Q_1$ acting on ("1101" + "1011") gives zero*[1]*. Consequently, we find that $H_{Q_1}(H_{Q_2})$ consists of one element: the sum of the configurations with $f_1 = 3$.*

*Proof.* We can solve $H_{Q_1}(H_{Q_2})$ for an arbitrary number of sites between a pair of bounding sites, by realizing that this problem can be mapped to the normal chain. For the normal chain no two fermions can be adjacent, whereas here no two empty $S_1$ sites can be adjacent. So we can map empty $S_1$ sites to fermions on the chain and occupied $S_1$ sites to empty sites in the normal chain. Finally, $Q_1$ is mapped to $Q^\dagger$ on the normal chain. For the chain $H_{Q^\dagger}$ (which has the same dimension as $H_Q$) vanishes when the length of the chain is $3p+1$ and it contains one element otherwise. So here we have that $H_{Q_1}(H_{Q_2})$ vanishes when the number of sites between two occupied sites is $3p+1$ and it contains one element otherwise.

□

For a segment with $f_2 = 0$, let us denote the representative of $H_{Q_1}(H_{Q_2})$ by the pair of bounding sites with dots in between, for example we denote ("1101" + "1011") by "$1 \cdot\cdot 1$". Even though, this is now a sum of configurations, we will still refer to this simply

[1] Note that the fermionic character of the particles is reflected in the sign here: $Q_1$ acting on "1011" gives −"1111", whereas $Q_1$ acting on "1101" gives +"1111". In the first case the particle is created on position 2 and has to hop over the particle at position 1, this gives a minus sign, in the second case the new particle is created at position 3 and thus has to hop over two particles, giving rise to no overall sign change. Also note that the states are not properly normalized, but this is not important for the argument.

as a configuration. It follows that, for a segment with $f_2 = 0$, two types of configurations are allowed. The two types can be distinguished by containing $3s-1$ dots or $3s$ dots. Examples of the first type are: "1", "1 $\cdot\cdot$1", "1 $\cdot\cdot\cdot\cdot\cdot$ 1", etc. Note that the configuration with $s = 0$, and thus with -1 dots between the pair of bounding sites, is "1". Examples of the second type are: "11", "1 $\cdot\cdot\cdot$ 1", "1 $\cdot\cdot\cdot\cdot\cdot\cdot$1", etc.
Combining lemma's 3 and 4, we find that $H_{Q_1}(H_{Q_2})$ is spanned by all configurations that can be formed by concatenating the following motifs:
"000"
"1 $\cdot_{3s-1}$ 100"
"1 $\cdot_{3s}$ 100"
"1 $\cdot_{3s-1}$ 10000"
"1 $\cdot_{3s}$ 10000"
where $\cdot_{3s}$ means $3s$ dots and, as before, "1 $\cdot_{3s-1}$ 1" with $s = 0$ means "1".
Finally one can also have all zeroes for any length and all dots for any length. Note that if the number of $S_1$ sites is a multiple of three, that both the configuration with all zeroes and the one with all dots account for two linearly independent elements of $H_{12}$. This is because the cohomology of $Q$ acting the periodic chain with length a multiple of three has dimension two (see theorem 3).

**Example 3** *As an example, suppose we have $\vec{v} = (1, 2)$ as always and $\vec{u} = (10, -10)$. This implies that $S_1$ consists of 10 sites and with the defined motifs it follows that the following 12 elements belong to $H_{12}$: "1100000000", "1100000100", "1100100000", "1100100100", "1100110000", "1100 1$\cdot\cdot$100", "1$\cdot\cdot$ $\cdots$ $\cdot\cdot$100", "1$\cdot\cdot$ $\cdot\cdot$100 000", "1$\cdot\cdot$ $\cdot\cdot$100 100", "1000010000", "0000000000" and "$\cdot\cdot\cdot\cdot\cdot\cdot\cdot\cdot\cdot\cdot$". Note that the first nine motifs have periodicity 10 and thus account for ten elements of $H_{12}$ each, whereas the motif "1000010000" has periodicity 5 and the last two motifs have periodicity 1. For each element one can easily compute the number of fermions and it follows that the first nine motifs have 7 fermions, the motif "1000010000" has 6 fermions and the last two motifs have again 7 fermions. So in total we have 92 elements in $H_{12}$ with 7 fermions and 5 elements with 6 fermions.*

### Step 3

In the previous step we have obtained $H_{12}$ for $\vec{v} = (1, 2)$. In this step we show that in this case this is equal to the cohomology of $Q$. We do this via the 'tic-tac-toe' procedure [33]. That is, we act on a configuration, say $|\psi\rangle$, with $Q$. The $Q_2$ part will automatically give zero, but the $Q_1$ part not necessarily, since we no longer restrict ourselves to the subspace $H_{Q_2}$. If it does give zero, we know that the configuration belongs to the kernel of $Q$. The configuration will thus belong to $H_Q$ unless it also belongs to the image of $Q$. In that case, another configuration will map to this configuration at the end of the 'tic-tac-toe' procedure. So we continue with the configurations, $|\psi_0\rangle$, that do not belong to the kernel of $Q_1$. Since the image of $|\psi_0\rangle$ does not belong to $H_{Q_2}$ and it does belong to the kernel of $Q_2$, it must also belong to the image of $Q_2$. So we can write $Q|\psi_0\rangle = Q_2|\phi\rangle$, for some configuration $|\phi\rangle$. Now let us define a new state $|\psi_1\rangle \equiv |\psi_0\rangle - |\phi\rangle$. It then follows that $Q|\psi_1\rangle = -Q_1|\phi\rangle$. If this is zero, we have found that the state $|\psi_1\rangle$ belongs to the kernel of $Q$. If it is non-zero we proceed as before: we try to find a configuration $|\chi\rangle$, such that $Q_1|\phi\rangle = Q_2|\chi\rangle$ and define a new state $|\psi_2\rangle \equiv |\psi_0\rangle - |\phi\rangle + |\chi\rangle$, etc. This procedure ends,

either when we have found a state $|\psi_n\rangle$ such that $Q|\psi_n\rangle = 0$, or when $Q|\psi_n\rangle = |\tilde{\psi}\rangle$ with $|\tilde{\psi}\rangle$ an element of $H_{Q_1}(H_{Q_2})$. In the latter case, we say $|\psi_0\rangle$ maps to $|\tilde{\psi}\rangle$ at the end of the 'tic-tac-toe' procedure and we conclude that neither $|\psi_0\rangle$ nor $|\tilde{\psi}\rangle$ belong to $H_Q$.
For the case we consider in this section, we will show that for each element $|\psi_0\rangle$, there is an element $|\psi_n\rangle$ that belongs to the kernel of $Q$. So for each element in $H_{12}$ we can find a corresponding element in $H_Q$, thus we obtain $H_Q = H_{12}$. In the next section, however, we will see that this is not true for general boundary conditions. We will then find that after several steps in the 'tic-tac-toe' procedure we map certain configurations in $H_{12}$ to other configurations in $H_{12}$. It follows that the first do not belong to the kernel of $Q$ and the latter belong to the image of $Q$. In that case $H_Q$ is strictly smaller than $H_{12}$.

**Lemma 5** *$H_Q = H_{12}$ for $\vec{v} = (1, 2)$ and $\vec{u} = (m, -m)$.*

*Proof.* For the segments with $f_2 = 0$, we found that $Q_1$ vanishes if we choose the states represented by the dots such that they are ground states of the normal chain with empty and occupied sites exchanged (see lemma 4). For the segments with $f_2 > 0$, we know from lemma 3 that the new configuration always belongs to the image of $Q_2$. That is, $Q_1|\psi_0\rangle = Q_2|\phi\rangle$, for some configuration $|\phi\rangle$ if $Q_1$ acts on a segment with $f_2 > 0$. So we can define a new configuration $|\psi_1\rangle \equiv |\psi_0\rangle - |\phi\rangle$, such that $Q|\psi_1\rangle = -Q_1|\phi\rangle$. Now $Q_1$ either acts on a different segment with $f_2 > 0$, in which case the new configuration again belongs to the image of $Q_2$, or it acts on the same segment. In the latter case the new configuration is cancelled by the same configuration in which the two $S_1$ sites are occupied in the reverse order due to the fermionic character of the particles. It thus follows that the 'tic-tac-toe' procedure always gives zero after as many steps as there are segments with $f_2 > 0$. □

### Step 4

In this final step we will show that the dimension of $H_Q$ (and the fermion number of each state) can be computed by counting all tiling configurations (and the number of tiles per configuration) with the four types of tiles depicted in figure 6.1. For the boundary conditions we consider here, the tilings reduce to a single layer sequence of only two types of tiles. Namely the two tiles that respect the boundary condition $\vec{v} = (1, 2)$. These tiles have two edges parallel to $(1, 2)$ and then the diamond has the other two edges parallel to $(1, -2)$ whereas the square has the other edges parallel to $(2, -1)$ (see fig. 6.5(a)). Given the sublattices $S_1$ and $S_2$ there are three types of vertices: the ones that belong to $S_1$, the lower left sites of the $S_2$-chain and the upper right sites of the $S_2$ chain. It follows that the diamond has one of three types of edges along the $(1, -2)$ direction and a matching type of edge along the $(1, 2)$ direction, the square can have one of three different types of edges along the $(2, -1)$ direction and a matching type of edge along the $(1, 2)$ direction. We conclude that we have 6 types of tiles, depicted in figure 6.5(b).
To establish theorem 2 we map each of the motifs obtained in step 2 to a unique sequence of tiles. The mapping for the four basis motifs, "100", "1100", "10000" and "110000", is shown in figure 6.6. Remember that each motif is modulo the addition of 3 zeroes and modulo the insertion of 3 dots. In terms of tilings, we find that each basis motif can be followed by an arbitrary repetition of the tiling corresponding to the 3 zeroes (see

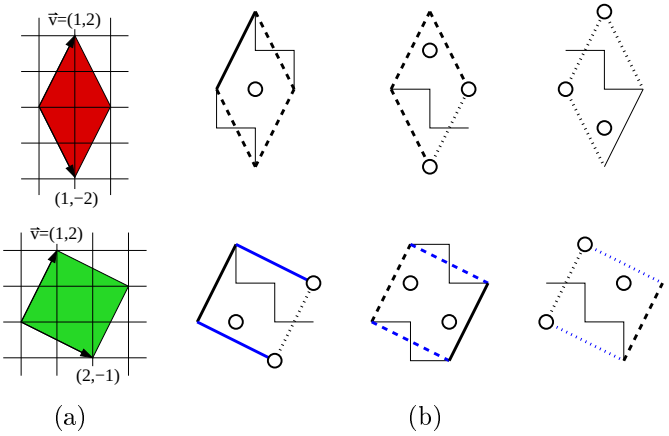


**Figure 6.5:** Types of tiles we use to tile the square lattice with periodicities $\vec{v} = (1, 2)$ and $\vec{u} = (m, -m)$. 6.5(a) Shows the diamond and square that respect $\vec{v} = (1, 2)$. 6.5(b) Shows the three types of diamonds and squares given the sublattices $S_1$ and $S_2$.

fig. 6.7(a)). On the other hand, insertions of multiples of 3 dots correspond to inserting multiples of the tiling shown in figure 6.7(a) at the dotted line along the $(1, 2)$ direction in the basis motifs. Some examples are shown in figure 6.7(b). Note that here we cannot easily write the motif of dots directly in the tiles (see fig. 6.7(b)), however, the mapping is still unambiguous.

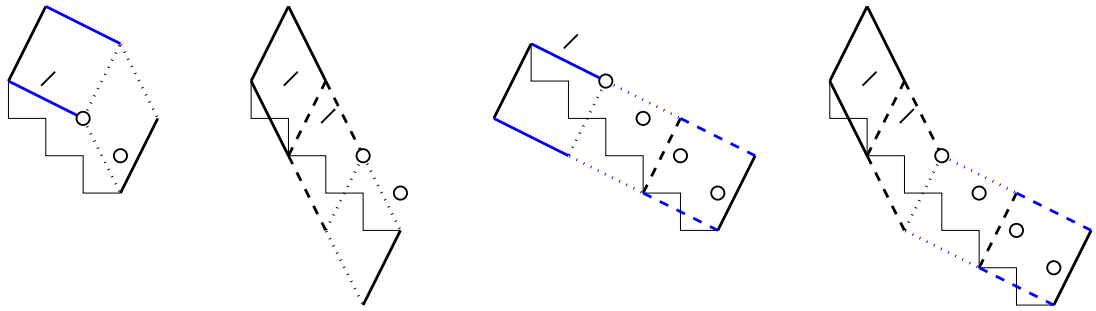

**Figure 6.6:** The four basis motifs and the corresponding sequences of tiles.

Let us determine the number of fermions per motif. First of all, in a segment with $f_2 > 0$, the number of fermions is determined by the length of the corresponding $S_2$ chain. It is easily verified, that for a segment with $n$ empty $S_1$ sites the corresponding chain has length $2n-2$. Moreover, from theorem 3, we know that an element in the cohomology of $Q$ on a chain with length $L = 2n - 2$ contains $[(2n - 2)/3]$ fermions, where $[a]$ is the nearest integer to $a$. Similarly, we find that a segment with $k$ dots contains $[2k/3]$ fermions. Thus a segment with $f_2 = 0$, consisting of $k$ dots and a the pair of bounding sites, contains $[2k/3] + 2$ fermions. From these formulae we find for the four basis motifs "100", "1100", "10000" and "110000", that they contain 2, 3, 3 and 4 fermions respectively. Furthermore, an insertion of 3 zeroes, corresponds to increasing $n$ by 3, and thus increasing the number of fermions, $[(2n - 2)/3]$, by 2. Equivalently, inserting 3 dots corresponds increasing $k$ by 3, and thus again increasing the number of fermions, $[2k/3]$, by 2. If we compare this

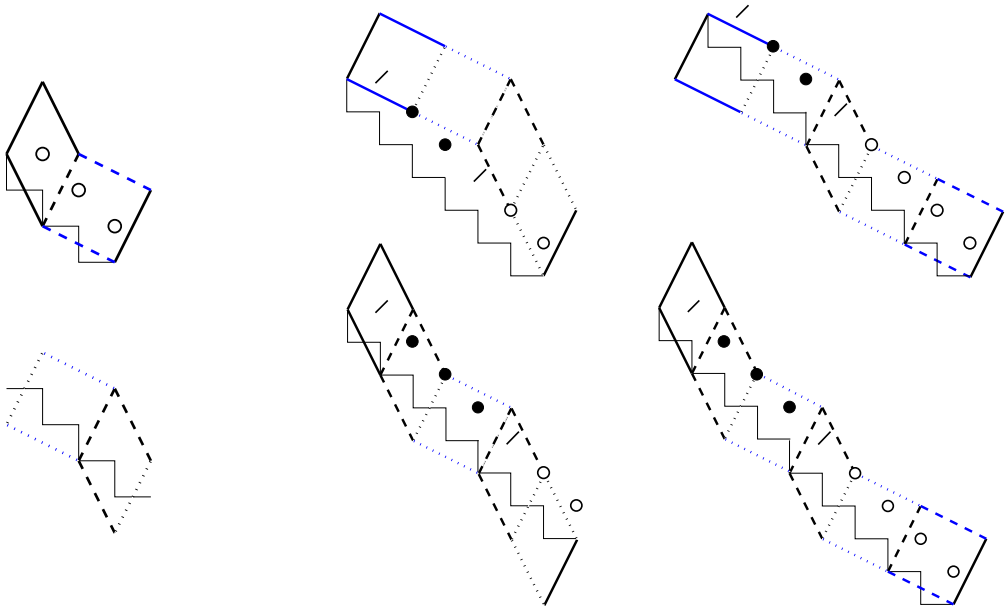

(a) (b)

**Figure 6.7:** On the left we show the sequences of tiles that correspond to the motifs with 3 zeroes (top) and 3 dots (bottom). The addition of 3 zeroes to a basis motif corresponds to attaching the sequence of tiles corresponding to the 3 zeroes to the sequence of tiles corresponding to the basis motif. An insertion of 3 dots in a basis motif corresponds to inserting the sequence of tiles corresponding to the 3 dots at the dotted line along the $(1, 2)$ direction in the sequence of tiles corresponding to the basis motif. The insertions of 3 dots in each of the four basis motifs and the corresponding tiling are shown on the right as examples. From these examples it is clear that we cannot write the 3 dots directly in the corresponding sequence of tiles. However, the mapping is still unambiguous.

to the number of tiles in the tilings that correspond to these motifs, we find that they exactly agree. Furthermore, the number of sites in a motif is given by three times the number of $S_1$ sites in a motif, since there are 2 $S_2$ sites for every $S_1$ site. On the other hand, for the tiles we find that the area of the diamond is 4 and the area of the square is 5. It is now easily verified that the number of fermions per site for the motifs is the same as the number of tiles per area for the corresponding tiling. Thus we find that, not only is the number of elements in the cohomology of $Q$ directly related to the number of tilings with the two tiles of figure 6.5(a), but also the number of fermions for each element corresponds to the number of tiles in the corresponding tiling.
One can verify that with these sequences of tiles, and the rules for concatenating them, one can obtain every possible tiling. Each tile can be preceded by a certain type of square and diamond and it can be followed by another type of square and diamond. In total this gives four possibilities for the surrounding neighbors. It can be checked that for each tile all four possibilities can be constructed with the given sequences of tiles and the rules for concatenating them.
Finally, the configurations with all zeroes or all dots account for the extra term in (5.1) in theorem 2 repeated here for convenience:

$$\Delta_i \equiv \begin{cases} -(-1)^{(\theta_m+1)p}\theta_d\theta_{d*} & \text{if } i = [2m/3]p \\ 0 & \text{otherwise.} \end{cases} \tag{6.10}$$

Remember that

$$\theta_d \equiv \begin{cases} 2 & \text{if } d = 3k, \text{ with } k \text{ integer} \\ -1 & \text{otherwise} \end{cases} \tag{6.11}$$

and with $\vec{v} = (1, 2)$ and $\vec{u} = (m, -m)$ we have $p = 1$, $d = \gcd(u_1 - u_2, v_1 - v_2) = \gcd(2m, -1) = 1$ and $d^* = \gcd(u_1 + u_2, v_1 + v_2) = \gcd(0, 3) = 3$. It follows that the extra term is $-2$ for $m = 3n$ and $+2$ otherwise.
Let us consider the configuration with all zeroes, which clearly has periodicity 1. If the number of zeroes is a multiple of three, i.e. $m = 3n$, the configuration accounts for 2 ground states, otherwise it accounts for 1 ground state. The number of fermions in this configuration is $i = [2m/3]$, i.e. the nearest integer to $2m/3$. From the mapping (fig. 6.7(a)) it is clear that the configuration corresponds to a tiling with periodicity 3 if $m = 3p$. If $m \neq 3p$, however, there is no corresponding tiling. Exactly the same holds for the configuration with all dots. It follows that for $m = 3p$ the tilings overcount the number of ground states by 2 and for $m \neq 3p$ the tilings fail to count 2 ground states.
Note that the choice of sublattices $S_1$ and $S_2$ has increased the number of tilings unrelated by a lattice symmetry by a factor of three (see fig. 6.5). Indeed when computing the number of ground states with the motifs given in step 2 it turns out that one discovers each tiling three times (given that the tiling is not completely uniform, that is all diamonds or all squares).

**Example 4** *Let us consider the case of example 3 again. So we have* $\vec{v} = (1, 2)$ *and* $\vec{u} = (10, -10)$. *One possibility is to cover the lattice with 6 squares. This tiling has a unit cell of size 5 and thus this tiling accounts for 5 ground states. The number of tiles is 6 and thus the ground states will have 6 fermions. We can also cover the lattice with 2 squares and 5 diamonds. The 2 squares can be placed between the diamonds in three independent ways. Each of these three tilings has a unit cell of size 30 and consists of 7 tiles, so they account for 90 ground states with 7 fermions.*
*We compare this with the 12 configurations found in example 3. The motif "*1000010000*" has periodicity 5 and accommodates 6 fermions, so this corresponds to the uniform tiling with all squares. The configurations with all zeroes and all dots account for two ground states with 7 fermions and have no corresponding tiling. Finally, there are 9 configurations with periodicity 10 and 7 fermions, which account for 90 ground states. Using the mapping given in figure 6.6, we find that these configurations can be split into three groups of three, each group corresponding to one of the tilings with 2 squares and 5 diamonds. For example the motifs "*1100000100*", "*1100110000*" and "*1100 1· ·100*" correspond to the tiling where the two squares are adjacent. They can be distinguished by considering for example the first of the two squares. In each motif it will be of a different type, where the three types are given in figure 6.5(b) (see fig. 6.8).*

### 6.5.2 The general case: $S_2$ consisting of $p$ chains

In the previous section we had $\vec{v} = (1, 2)$. In this section we relax this condition to $\vec{v} = (v_1, v_2)$ with $v_1 + v_2 = 3p$ with $p$ a positive integer. It follows that we get $p$ $S_2$ chains with their accompanying $S_1$ sites stacked on top of each other. For this situation we will prove theorem 2. The proof consists of 5 steps:

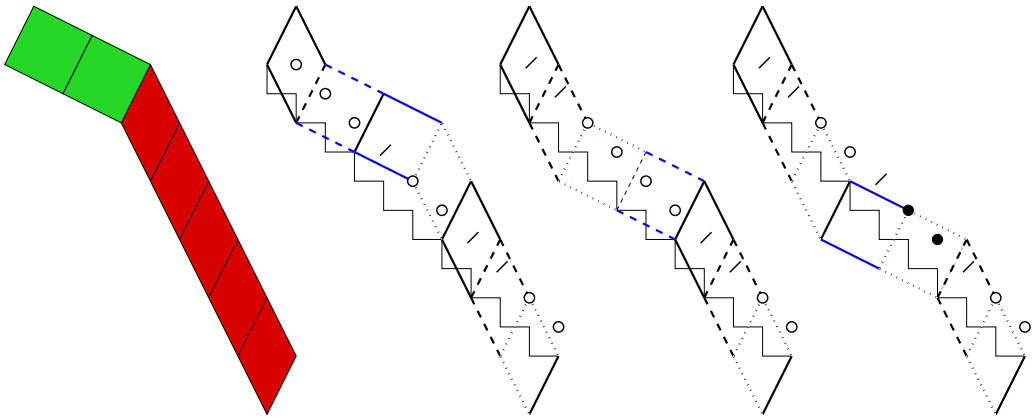

**Figure 6.8:** The square lattice with periodicities $\vec{v} = (1, 2)$ and $\vec{u} = (10, -10)$ can be tiled with 2 squares and 5 diamonds. One of these tilings, with the two squares adjacent is shown on the left. The choice of sublattices splits this tiling into three tilings. These three tilings and their corresponding motifs are shown on the right.

1. We compute $H_{Q_2}$.
2. We compute $H_{12} = H_{Q_1}(H_{Q_2})$.
3. We compute $H_Q$ starting from $H_{12}$ via the 'tic-tac-toe' procedure.
4. We relate the elements of $H_Q$ to tiling configurations by relating each motif to a small series of tiles.
5. We compute $\Delta_i$.

### Step 1

As in the previous section we shall start by computing the cohomology of $Q_2$. We will define two types of configurations that do not belong to $H_{Q_2}$ and then find that $H_{Q_2}$ consists of all configurations except these two types.

**Lemma 6** *A configuration that contains an occupied site $(k, l)$ on the $S_1$ lattice, such that the sites $(k+1, l+2)$ and $(k+2, l+1)$ and/or the sites $(k-1, l-2)$ and $(k-2, l-1)$ are empty, does not belong to $H_{Q_2}$.*

*Proof.* It is easily verified (see fig. 6.9) that in this configuration the $S_2$ sublattice contains the isolated site(s) $(k + 1, l + 1)$ and/or $(k - 1, l - 1)$. This site can be either occupied or empty, which leads to a vanishing $H_{Q_2}$. □

Note that in the previous section this situation never occurred because for each occupied site $(k, l)$, the sites $(k + 1, l + 2)$ and $(k - 1, l - 2)$ were automatically occupied due to the boundary condition set by $\vec{v} = (1, 2)$. The second type of configuration that does not belong to $H_{Q_2}$ follows from a generalization of lemma 2. Remember that occupying $S_1$ sites causes the $S_2$ chains to break into smaller open chains. The length of these open

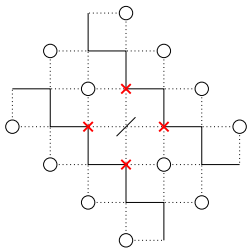

**Figure 6.9:** A configuration is shown where an occupied $S_1$ site is surrounded by empty sites. This sites isolates a site on the $S_2$ chains directly below and above the site.

chains now depends on the number of empty $S_1$ sites directly below and above the $S_2$ chain. For an example see figure 6.10.

**Lemma 7** *If, for a certain configuration, the sum of the number of empty $S_1$ sites directly below and above an open $S_2$ chain is $3s$, the configuration does not belong to $H_{Q_2}$.*

*Proof.* It is easily verified that the open $S_2$ chain corresponding to the $3s$ empty $S_1$ sites has length $3(s-1)+1$. This leads to a vanishing $H_{Q_2}$. □

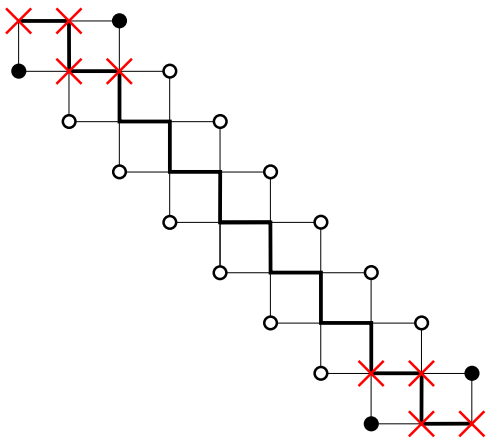

**Figure 6.10:** Part of a configuration is shown. The number of empty $S_1$ sites directly below and above the $S_2$ chain is 12. The $S_2$ sublattice thus contains an isolated chain of length 10. Consequently, this configuration does not belong to $H_{Q_2}$.

A configuration does not belong to $H_{Q_2}$ if it contains one or more isolated open chains on the sublattice $S_2$ with length $3p+1$. It is easy to see that all such configurations fall into the class of configurations described in lemma 6, or lemma 7, or both. It follows that all configurations that do not fall into either of these classes belong to $H_{Q_2}$.

### Step 2

As in the previous section, we will now compute $H_{12} = H_{Q_1}(H_{Q_2})$.

**Definition 3** *Define a row of $S_1$ sites as the set of $S_1$ sites directly above one $S_2$ chain.*

Note that the configurations in $H_{Q_2}$ again contain segments where $f_2$, the number of fermions on the $S_2$ sublattice, is zero and segments where it is non-zero.

**Lemma 8** *Lemma 4 for $H_{12}$ holds for each row of $S_1$ sites.*

That is, in the segments where $f_2 = 0$, the cohomology of $Q_1$ vanishes when the number of $S_1$ sites between any pair of bounding sites is $3p+1$ and it contains one element otherwise. The proof can be found in the previous section. It follows that, in the segments where $f_2 = 0$, two types of configurations on a row of $S_1$ sites are allowed. Using the notation of the previous section, the two types can be distinguished by containing $3s-1$ dots or $3s$ dots.

**Lemma 9** *The configurations in $H_{12}$ have spatially separated columnar segments where $f_2 = 0$ and segments where $f_2 > 0$. The width of a column in a segment where $f_2 = 0$ can vary between $3s+1$ and $3s+2$ $S_1$ sites, whereas the width of a column in a segment where $f_2 > 0$ can vary between $3p-1$ and $3p+1$ $S_1$ sites. In the latter case, two consecutive rows never both have width $3p$ and the difference in their widths is at most 1 (or -1).*

*Proof.* This follows from combining lemma's 6, 7 and 8. □

An example is shown in figure 6.11. From lemma 9 it follows that we only have to consider columns of width varying between 1 and 2 in the segments where $f_2 = 0$ separated by columns of width varying between 2 and 4 in the segments where $f_2 > 0$. All other configurations can be obtained from these configurations by inserting multiples of 3 dots in the segments where $f_2 = 0$ over the entire height of the columns, and, similarly, by inserting multiples of 3 zeroes in the segments where $f_2 > 0$ over the entire height of the columns.

We now turn to the segments where $f_2 > 0$. Remember that in the previous section this step was easy because all $S_1$ sites in the segment where $f_2 > 0$ were blocked by fermions on the $S_2$ chain. Here, however, that is not the case. The first thing we note in this case is the following.

**Lemma 10** *The $S_1$ sites within a column marking a segment where $f_2 > 0$ have to be empty if they are away from the boundaries with adjacent columns marking a segment where $f_2 = 0$.*

*Proof.* This follows directly from lemma 6. □

From this lemma it follows that we only have to consider the $S_1$ sites on the boundary between a segment where $f_2 > 0$ and a segment where $f_2 = 0$. In fact, we will argue that we only have to consider the boundary where the segment with $f_2 > 0$ is to the right of a segment with $f_2 = 0$ (and not the boundary on the other side).

First, however, we introduce a new notation where a configuration is fully characterized by the boundaries between the two types of segments ($f_2 = 0$ and $f_2 > 0$). From lemma 6 it follows that these boundaries are an arbitrary sequence of steps of $+(2,1)$ and $+(1,2)$. However, in the new notation we shall tilt the lattice by $-45°$, such that the rows of $S_1$ sites are horizontal. If we then draw the boundary as a collection of vertical lines between two $S_1$ sites that are to the left and to the right of the boundary, we find that

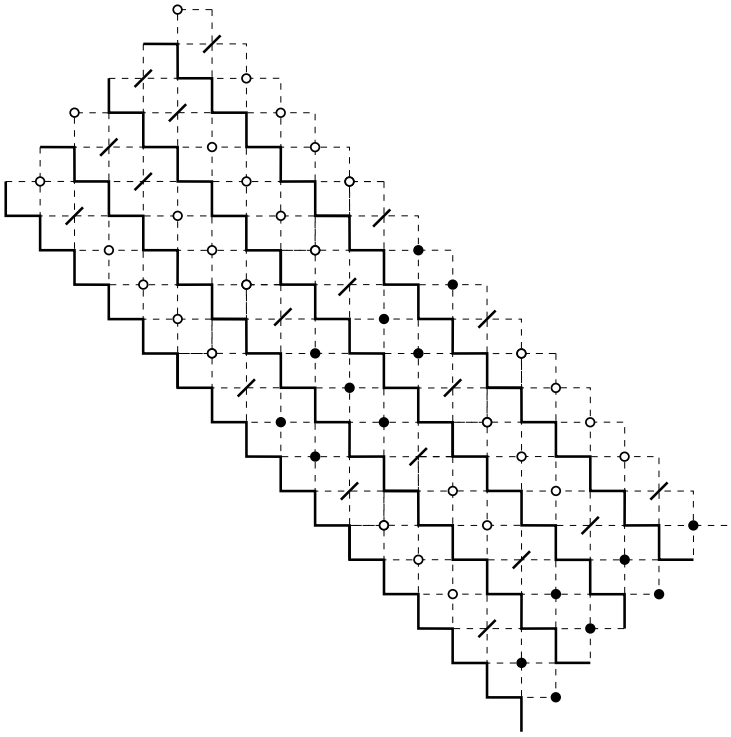

**Figure 6.11:** Part of a configuration is shown.

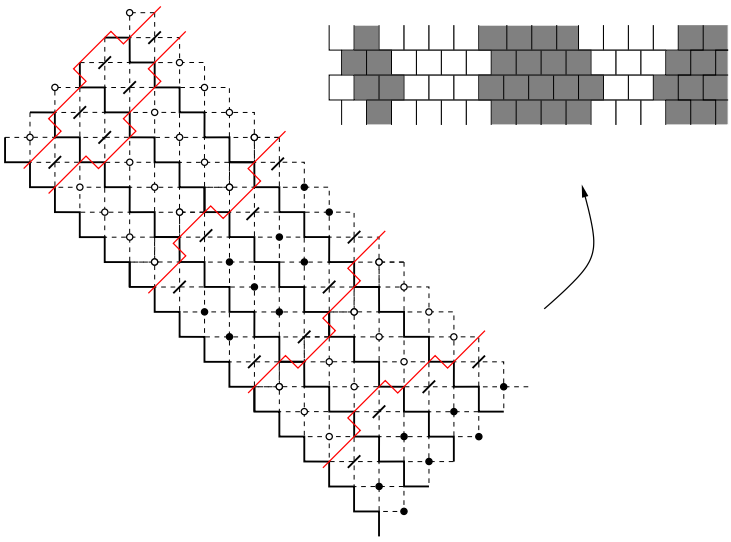

**Figure 6.12:** Part of a configuration is shown with a mapping to the new notation.

the boundaries have a zigzagged shape. The segments where $f_2 > 0$ will be white and the segments where $f_2 = 0$ will be grey. For an example see figure 6.12.

Suppose for a moment that we would have a completely disconnected graph, that is, just a collection of disconnected vertices. Then each site can be both empty and occupied. It is clear that each configuration with a least one empty site does not belong to the kernel of $Q$, whereas each configuration with at least one occupied site belongs to the image of $Q$. It follows that $H_Q$ vanishes at all grades. Here we do not have a disconnected graph, however, it turns out that the division in grey and white regions is similar to disconnecting the graph.
We define a special notation for a site that can be both empty and occupied. If this site is to the right of a grey region we shall denote this site with a dot, whereas when it is to the left of a grey region the site will be shaded. That is, suppose there are two configurations that both belong to $H_{Q_2}$ and obey lemma 9, such that these two configurations differ by one site only. Then we can summarize these two configurations in one picture by denoting this particular site by a dot if it is to the right of a grey region or by shading the site if it is to the left of a grey region. For an example see figure 6.13. Moreover, we can summarize $2^n$ configurations in one picture if the picture contains $n$ sites with dots or shaded sites. We make a distinction between sites to the left and to the right of the grey region, because we will argue that the configurations with a site with a dot do not belong to $H_{12}$. Clearly this is a choice, we could also have chosen to argue that the configurations with a shaded site do not belong to $H_{12}$.
Let us consider a boundary that separates a grey segment on the left from a white segment on the right. There are only a few such configurations that may have a site on the boundary with a dot.

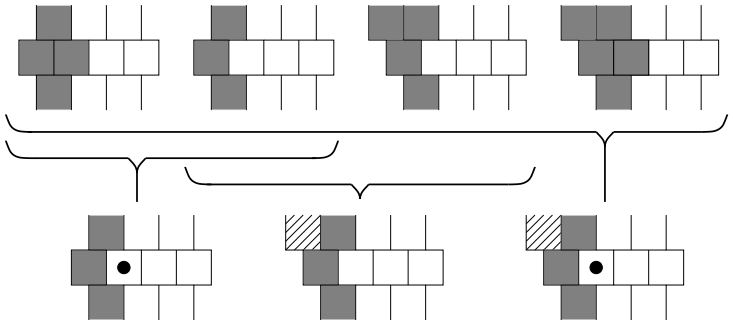

**Figure 6.13:** The big brackets indicate how the configurations at the top can be summarized using the notation introduced in the text. The two left-most configurations at the top differ by one site in the *right*-most boundary of the grey region, they can therefore be summarized by the left-most picture at the bottom by denoting this site with a dot. The middle two configurations at the top differ by one site in the *left*-most boundary of the grey region, they can therefore be summarized by the middle picture at the bottom by shading this site. Finally, all four configurations at the top can be summarized by the right-most picture at the bottom.

**Lemma 11** *There are 8 possible configurations with a site with a dot in a boundary that separates a grey segment on the left from a white segment on the right. The configurations are depicted in figure 6.14(c).*

*Proof.* The first restriction follows from lemma 6. That is, both when the site is empty as well as when it is occupied, the configuration should satisfy the lemma. This restriction

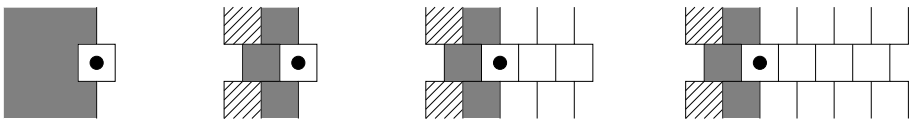


**Figure 6.14:** In three steps we find that there are 8 possible configurations with a site with a dot in a boundary that separates a grey segment on the left from a white segment on the right: (a) It follows from lemma 6 that a site with a dot must have occupied sites to the upper left and lower left and empty sites to the upper right and lower right. (b) There are four possibilities for the left-most boundary of the grey segment, following from the two shaded sites being empty or occupied. (c) There are two possibilities for the right-most boundary of the white segment.

is depicted in figure 6.14(a). Then the second restriction follows from lemma 8, that is, the width of a grey column varies between 1 and 2 modulo 3. It follows that next to the site with the dot there can only be one grey site (modulo 3). Combining this again with lemma 6, we find four possibilities for the left boundary of the grey segment. The four possibilities can be summarized in one picture with the notation defined above, see figure 6.14(b), the shaded sites can be both empty and occupied. Finally, it follows from lemma 7 that there are only two possible right most boundaries for the white segment, each modulo columns of width 3, see figure 6.14(c). □

From lemma 11 it follows that if there is more than one site with a dot in the same boundary, they are sufficiently far away to be independent. That is, each of these sites can be both empty and occupied independent of the configuration of the other dotted sites. Also note that if we select one of the 8 configurations with a dot from figure 6.14(c), the rest of the system can take on any configuration independent of the configuration of the dotted site. Note that this resembles a disconnected graph.
We are now ready to solve $H_{Q_1}(H_{Q_2})$.

**Lemma 12** *All configurations that contain a boundary between a grey segment to the left and a white segment to the right, such that this boundary contains one or more sites with a dot, do not belong to* $H_{Q_1}(H_{Q_2})$.

*Proof.* A site with a dot can be either empty or occupied. Suppose the site is empty and we act with $Q_1$ on the configuration. If $Q_1$ can act non-trivially only on the site under consideration we are done, since the configuration in which the site with the dot is empty does not belong to the kernel of $Q_1$ and the configuration in which it is occupied belongs to the image of $Q_1$. This proves the lemma for this case.
If, however, $Q_1$ can act non-trivially also on other sites, there are four scenarios: a) The other site is in the same boundary. b) The other site is in the left boundary of the grey region under consideration. c) The other site is in the right boundary of the white region under consideration. d) The other site is further away from the region under consideration than the first three cases.
For scenario a), we know that the other site is also a site with a dot. It follows that the configuration with both dotted sites empty does not belong to the kernel of $Q_1$. The sum of the configurations with one of the dotted sites empty belongs to the image of $Q_1$. The difference of the configurations with one of the dotted sites empty does not belong to

the kernel of $Q_1$, because it maps to the configuration with both dotted sites occupied. Clearly, the latter configuration belongs to the image of $Q_1$. So for this scenario the lemma is proven.
For scenario b) we distinguish two cases. First, the other site and the dotted site can be occupied simultaneously. In this case we can prove the lemma via the same argument as we did for scenario a). Second, the other site and the dotted site *cannot* be occupied simultaneously. This only happens when the other site is in the same row as the dotted site. In this case the sum of the configurations with one of them occupied is in the image of $Q_1$, but the difference belongs to the kernel of $Q_1$ and does not belong to the image of $Q_1$. The latter is thus an element of $H_{Q_1}(H_{Q_2})$. However, we have the freedom to decide to keep only the configuration in which the other site is occupied and the dotted site is empty as a representative of this element. At this point it becomes clear why we only consider configurations with a site with a dot, and not configurations with a shaded site.
For scenario c) we can again distinguish two cases. In the first case, the configuration of the other site and the dotted site are independent and the lemma is proven as for scenario a). In the second case, the other site and the dotted site *cannot* be occupied simultaneously. There are again three configurations under consideration. The configuration with both sites empty does not belong to $\ker Q_1$, the sum of the configurations with one of the two sites occupied belongs to Im $Q_1$ and, finally, the difference again is an element of $H_{Q_1}(H_{Q_2})$. And as under b), we choose to represent this element with the configuration where the dotted site is empty and the other site occupied.
Finally, for scenario d) it is clear that the configuration of the other site and the dotted site are always independent and the lemma is proven as for scenario a).
In the four scenarios we considered, there was just one other site on which $Q_1$ acts non-trivially. If there are more sites on which $Q_1$ acts non-trivially, the lemma clearly holds when these sites can again be empty or occupied independent of the dotted site. However, if they are not all independent, the proof is more lengthy, but analogous to the proofs of the second case in scenarios b) and c).

□

**Lemma 13** *All the configurations that belong to $H_{Q_1}(H_{Q_2})$ are a sequence of alternating grey and white columns subject to the conditions in lemma 9, such that the left-most boundary of all the white columns does not contain any sites with a dot.*

*Proof.* This is a direct consequence of lemma 12. □

As an example we consider the case where $\vec{v} = (6, 6)$ and $\vec{u} = (m, -m)$, that is, we stack four rows of $m$ $S_1$ sites separated by four $S_2$ chains. All configurations in $H_{12}$ can be obtained by concatenating the configurations depicted in figure 6.15, with eventual insertions of grey and/or white columns of width 3, such that the boundary conditions are satisfied[2]. That is, each row should in the end have width $m$ or, equivalently, the right-most boundary should fit with the left-most boundary. Finally, there is a configuration with all zeroes (one entirely white segment) and a configuration with all dots (one entirely grey segment).

[2]These configurations are obtained as follows. First consider all possible white segments satisfying the boundary condition in the $\vec{v}$-direction, then construct all possibilities for the grey segments to the left of these white segments.

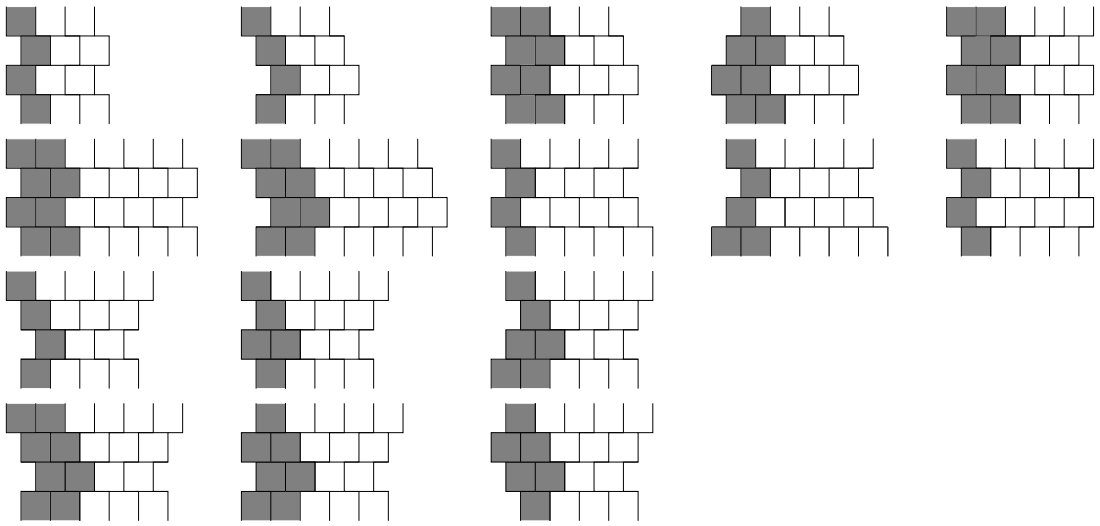

**Figure 6.15:** Building blocks of the configurations spanning $H_{Q_1}(H_{Q_2})$ for $\vec{v} = (6,6)$ and $\vec{u} = (m,-m)$, modulo insertions of grey and white columns of width 3.

### Step 3

In the previous step we have determined $H_{12}$. According to the 'tic-tac-toe' lemma, the cohomology of $Q$ is equal to or contained in $H_{12}$: $H_Q \subseteq H_{12}$. In the previous section we found that for $\vec{v} = (1,2)$, we have $H_Q = H_{12}$. For general $\vec{v}$, however, this is not the case. That is, within $H_{12}$, there are configurations that are not in the kernel of $Q$ and there are configurations that are in the image of $Q$. To find out which configurations do not belong to $H_Q$, we follow the 'tic-tac-toe' procedure [33] as described in step 3 of section 6.5.1.
In the previous section, we found via the 'tic-tac-toe' procedure that we could find for each element $|\psi_0\rangle$, that belongs to $H_{12}$, but not to $\ker Q$, an element $|\psi_n\rangle$ that does belong to $\ker Q$. In this section, however, we will find that for some elements $|\psi_0\rangle$, the 'tic-tac-toe' procedure leads to a corresponding element $|\tilde{\psi}\rangle$, that also belongs to $H_{12}$. We then say that $|\psi_0\rangle$ maps to $|\tilde{\psi}\rangle$ at the end of the 'tic-tac-toe' procedure and we conclude that neither $|\psi_0\rangle$ nor $|\tilde{\psi}\rangle$ belong to $H_Q$.
We now prove some rules for the 'tic-tac-toe' procedure specific to the configurations we obtained in the previous step.

**Lemma 14** *Let $Q$ act on an empty $S_1$ site $(k,l)$, such that for the preceding $S_1$ sites on that row we have: $(k-1,l+1)$ and $(k-3s-2,l+3s+2)$ are occupied and the intermediate sites are dotted. Then the new configuration with $(k,l)$ occupied, is also the image of $Q_1$ acting on the configuration with $(k,l)$ occupied and one less fermion in the preceding sites $(k-1,l+1)$ to $(k-3s-1,l+3s+1)$.*

*Proof.* For general $s$ we can denote the original configuration as "$1 \cdot_{3s} 10$", the new configuration is then "$1 \cdot_{3s} 11$". From lemma 4 we know that, if the number of $S_1$ sites between a bounding pair is $3s+1$, $H_{Q_1}$ vanishes. Consequently, each configuration that is in the kernel of $Q_1$ is also in the image of $Q_1$. Now, since the configuration "$1 \cdot_{3s} 11$" is in the kernel of $Q_1$ and the number of $S_1$ sites between the bounding pair is $3s+1$, it must also be in the image of $Q_1$. Thus, there is a configuration with one less fermion between the

bounding pair that maps to this configuration under the action of $Q_1$. □

**Example 5** *For $s = 0$ this is easily understood: the original configuration will have "110" on the $S_1$ sites $(k-2, l+2)$ through $(k, l)$. Acting on this with $Q$ gives "111", however, this can also be obtained by acting with $Q$ on -"101".*

**Lemma 15** *Acting with $Q$ on a white segment away from the boundary, gives zero.*

*Proof.* The proof is analogous to the proof of lemma 3. The length of the $S_2$ chains in the white region is $L = 3k$ or $L = 3k - 1$ each containing $k$ fermions. If $Q_1$ acts on a site above this chain and away from the boundary, it will cut the $S_2$ chain into 3 pieces. One of length 1 and two of lengths $L'_1$ and $L'_2$, such that $L'_1 + L'_2 = L - 3$. We will now argue that the new configuration with the smaller $S_2$ chains, always belongs to Im $Q_2$. This implies that we can always continue to the next step in the 'tic-tac-toe' procedure.
If the chain of length 1 contains a fermion, the new configuration clearly belongs to Im $Q_2$. If it is empty there are $k$ fermions on the other two chains. For $L = 3k$ their combined length is $L'_1 + L'_2 = 3(k-1)$, so $L'_1 = 3k_1$ and $L'_2 = 3k_2$ or $L'_1 = 3k_1 + 1$ and $L'_2 = 3k_2 - 1$, where in both cases $k_1 + k_2 = k - 1$. For the second case the cohomology vanishes for all fermion numbers because of the length $L'_1$. For the first case the cohomology is non-vanishing only if $f = k_1 + k_2 = k - 1$, however, there are $k$ fermions. So for both cases the new configuration belongs to Im $Q_2$ (since it belongs to $\ker Q_2$ and not to $H_{Q_2}$). For $L = 3k - 1$ we find $L'_1 = 3k_1$ and $L'_2 = 3k_2 - 1$ or $L'_1 = 3k_1 + 1$ and $L'_2 = 3k_2 - 2$, where in both cases $k_1 + k_2 = k - 1$. The rest of the argument is the same as before.
From the above it follows that we can always continue with the next step in the 'tic-tac-toe' procedure. Now suppose that in this next step we act with $Q_1$ on the same row as in the first step. Since there are no fermions between these two $S_1$ sites, this configuration will cancel against the configuration where the two $S_1$ sites are occupied in the reverse order. It follows that we only have to consider acting with $Q_1$ on each row just once.
It is now easily verified that, since there are as many $S_2$ chains as there are $S_1$ rows, we can always continue the 'tic-tac-toe' procedure until we get zero. □

In this lemma we restricted ourselves to $Q$ acting on $S_1$ sites away from the boundary. We will see in the following that if we allow $Q$ to act on sites at the boundary, the 'tic-tac-toe' procedure can map one configuration in $H_{12}$ to another configuration in $H_{12}$. The crucial point is that, when we act with $Q_1$ on a site at the boundary, the length of at least one of the $S_2$ chains below and above this site is reduced by 1. If the original length was $3k$, the new length is $3k - 1$ and both have non-vanishing cohomology for $f = k$. In that case we cannot use this $S_2$ chain to write the new configuration as $Q_2$ of some other configuration. It follows that to continue the 'tic-tac-toe' procedure, we have to use the other $S_2$ chain. However, if this chain was already used in a previous step, the 'tic-tac-toe' procedure could end. Before we continue with an example that illustrates this point, we will argue that it is enough to consider $Q$ acting only on sites at the boundary. This follows from lemma 9; if the 'tic-tac-toe' procedure ends because we have obtained a configuration that does not belong to Im $Q_2$ (nor to Im $Q_1$), this configuration must belong to $H_{12}$. From lemma 9 we know that configurations in $H_{12}$ have spatially separated columnar grey and white segments that do not branch. It follows that we can only map one configuration in $H_{12}$ to another by either creating a new grey column in a white column, or by (locally)

increasing the width of a grey column. Since the first possibility is excluded by lemma 15, we conclude that we can restrict $Q$ to act only on sites at the boundary. As in step 2 we will restrict ourselves to the left-most boundary to avoid overcounting.
Let us consider an example of a configuration that does belong to $H_{12}$, but does not belong to $H_Q$, i.e. it maps to another configuration in $H_{12}$ at the end of the 'tic-tac-toe' procedure.

**Example 6** *Consider the configuration shown on the left in figure 6.16. We label the three $S_2$ chains (not shown explicitly) between the four $S_1$ rows; chain 1, chain 2 and chain 3 ($c_1$, $c_2$ and $c_3$) from top to bottom. Similarly, we label the $S_1$ rows; row 1 to row 4 ($r_1$ to $r_4$) from top to bottom. The $S_2$ chains have lengths $L_{c_1} = 6$, $L_{c_2} = 5$ and $L_{c_3} = 3$ and thus contain 2, 2 and 1 particle respectively. Now consider the left-most, empty $S_1$ sites in the middle two rows. Occupying the left-most, empty $S_1$ site on row 2 reduces the length of $c_1$ from 6 to 5. There will still be 2 particles on $c_1$ and since the chain of length 5 has non-vanishing cohomology at grade 2, the configuration on this chain will in general not belong to Im $Q_2$. Occupying the left-most, empty $S_1$ site on row 3 reduces the length of $c_3$ from 3 to 2. Again the configuration on this chain will not belong to Im $Q_2$, since the chain of length 2 has non-vanishing cohomology at grade 1. It follows that if we occupy either of these $S_1$ sites in the 'tic-tac-toe' procedure, we have to use $c_2$ to write the new configuration as $Q_2$ of some other configuration. By definition this is always possible in the first step of the procedure. However, also by definition, we can do this only once since $Q^2 = 0$. It follows that, after two steps in the 'tic-tac-toe' procedure, we obtain a new configuration (see fig. 6.16 on the right) that has 2, 1 and 1 particles on the $S_2$ chains from top to bottom and belongs to $H_{12}$. Consequently, both the original as well as the final configuration do not belong to the cohomology of $Q$, although they do belong to $H_{12}$.*

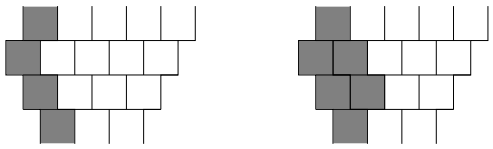

**Figure 6.16:** On the left we depict the configuration that does belong to $H_{12}$, but not to $H_Q$, since it does not belong to the kernel of $Q$. Instead it maps to the configuration depicted on the right under the 'tic-tac-toe' procedure. This configuration also belongs to $H_{12}$, but not to $H_Q$, since it belongs to Im $Q$. The configuration on the left has 4 particles on sublattice $S_1$ and 5 particles on sublattice $S_2$, divided as 2, 2, 1 over the $S_2$ chains from top to bottom. The configuration on the right has one more particle in total; it has 6 particles on $S_1$ and it has 4 particles on $S_2$, divided as 2, 1, 1 over the $S_2$ chains from top to bottom.

As we anticipated, the crucial point in this example is that the length of an $S_2$ chain is reduced from $3k$ to $3k-1$, since this limits the options to continue the 'tic-tac-toe' procedure. In fact, in the 'tic-tac-toe' procedure, we can only reach a configuration that is not in the image of $Q_2$ if the length of an $S_2$ chain is reduced from $3k$ to $3k-1$. To find the configurations in $H_{12}$ that map to another configuration in $H_{12}$ under the action

of $Q$ in the most efficient way[3], we will start the 'tic-tac-toe' procedure by occupying an $S_1$ site, such that this happens. It follows that we can then only use the other $S_2$ chain to continue the procedure. We will then, again for efficiency, continue the procedure by again occupying an $S_1$ site such that there is just one $S_2$ chain that we can use to continue the procedure. This means that we will act with $Q_1$ on consecutive rows, either moving upwards or downwards along the boundary.
In the previous step we constructed all possible configurations with a site *with a dot* in the left-most boundary of a white segment. Here we will construct all possible configurations with a site in the left-most boundary of a white segment, such that occupying this site reduces the length of an $S_2$ chain from $3k$ to $3k-1$. We shall call such sites 'critical reducer sites'. We start with the white segment and obtain the configurations depicted in figure 6.17. For these configurations occupying the left-most site of the middle row reduces the length of at least one of the adjacent $S_2$ chains from $3k$ to $3k-1$. For the two configurations on the left, occupying this site reduces the length of both $S_2$ chains to $3k-1$. It follows that the new configuration must belong to Im $Q_1$ (see lemma 14), otherwise it was a site with a dot in the previous step. So we do not have to consider these two configurations. This same reasoning tells us that the grey region to the left of the middle row should have width 1 modulo 3, otherwise the new configuration would belong to Im $Q_1$. This leads to the 12 possibilities in figure 6.18.

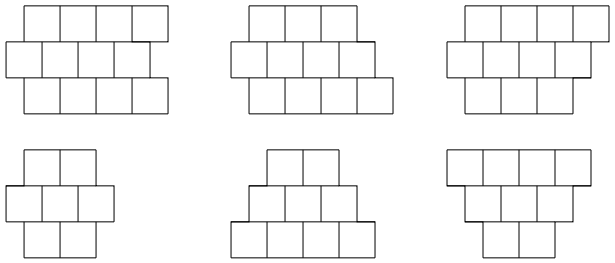

**Figure 6.17:** The possible boundaries of a white segment are shown, such that the left-most boundary contains a critical reducer site. That is, occupying this site reduces the length of at least one of the adjacent $S_2$ chains from $3k$ to $3k-1$.

Note that, indeed, occupying the critical reducer site at the boundary, leads to reducing the length of one of the $S_2$ chains from $3k$ to $3k-1$, for all these configurations. For efficiency we continue the 'tic-tac-toe' procedure either upwards or downwards, such that at every step in the procedure there is just one $S_2$ chain that we can use to continue the procedure. The direction we should follow, is indicated by the arrow in figure 6.19. Note that we dropped the two configurations for which the grey segment had width 2, because of lemma 14.
It is now clear that if we stack a configuration for which the 'tic-tac-toe' procedure goes downwards on top of a configuration for which it goes upwards, the 'tic-tac-toe' procedure ends. In particular, it maps the old configuration to a new configuration that is also in $H_{12}$. We can increase the number of steps necessary in the 'tic-tac-toe' procedure by stacking

[3]By 'the most efficient way' we mean the shortest sequence of occupying $S_1$ sites in the 'tic-tac-toe' procedure that maps one configuration in $H_{12}$ to another. This is the most efficient way, because as soon as this happens, we know that both configurations do not belong to $H_Q$, independent of all the other terms created under the action of $Q$.

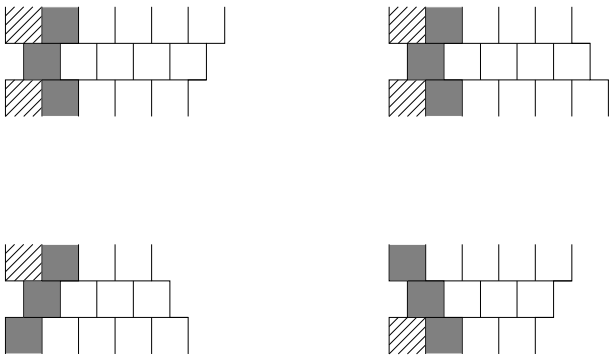

**Figure 6.18:** The 12 possible configurations such that the left-most site of the middle row is a critical reducer and occupying this site does not lead to a configuration that is in Im $Q_1$.

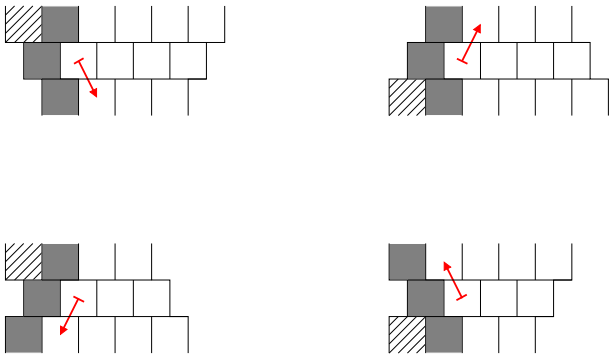

**Figure 6.19:** If the critical reducer site (the left-most site of the middle row) is occupied in the first step of the 'tic-tac-toe' procedure, the procedure should be continued in one direction only, as explained in the text. This direction is indicated by the arrow.

rows for which the grey segment has width 1 modulo 3 and the width of the white segment alternates between 3 and 4 modulo 3 (see fig. 6.20). Examples of the stacked configurations and the configurations they map to are shown in figure 6.21. Here the sites with connected dots can be either all empty or all occupied. The configuration with all the sites empty maps to the configuration with all the sites occupied under the 'tic-tac-toe' procedure. However, if the configurations on the left in figure 6.19 are not combined with one of the configurations on the right in figure 6.19, the 'tic-tac-toe' procedure will end with a state that is in the kernel of $Q$ (as long as we only let the sites on the left-most boundary participate).

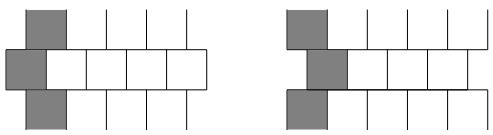

**Figure 6.20:** Stacking these configurations with the configurations of figure 6.19, increases the number of steps in the 'tic-tac-toe' procedure.

At this point we have identified a certain set of configurations that does belong to $H_{12}$, but

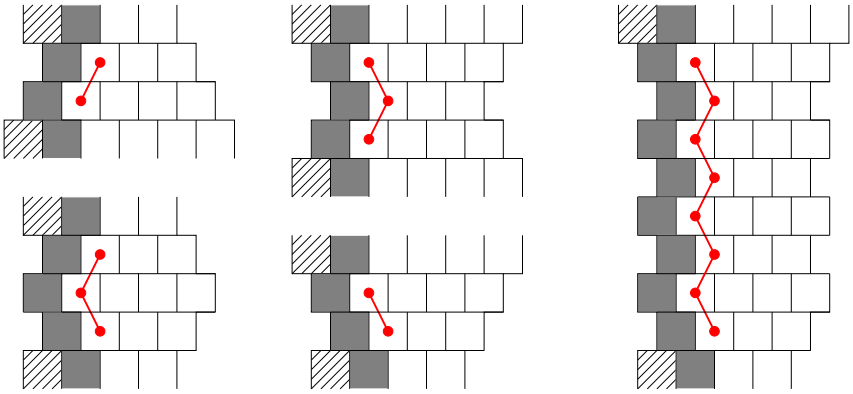

**Figure 6.21:** Some examples are shown of configurations that do belong to $H_{12}$, but not belong to $H_Q$. Here the sites with connected dots can be either all empty or all occupied.

does not belong to $H_Q$. However, we have to make a final step before we can identify all configurations in $H_Q$ with tiling configurations. This is due to the fact that certain parts of configurations seem to belong to $H_Q$, but they do not respect the boundary conditions. Note that, at this point, we have reduced all possible motifs to the following set:
"100"
"1100"
"10000"
"110000"
which can be separated by single insertions of the motifs:
"1000"
"11000"
all modulo insertions of three dots and three zeroes along an entire column. Each of the four basis motifs, comes with two directions, determined by whether the boundaries between the grey and white segments follows the direction $(-1,-2)$ or $(-2,-1)$.

**Definition 4** *We assign a letter to each of the four basis motifs:*
$A_i \equiv$"100"
$B_i \equiv$"1100"
$C_i \equiv$"10000"
$D_i \equiv$"110000"
*where the subscript $i$ is 1 or 2 when the direction of the motif is $(-1,-2)$ or $(-2,-1)$ respectively.*

Note that the direction of a motif is not defined if neither the motif directly above it nor the motif directly below it is the same. We will start, however, by considering cases in which this does not happen. At the end of step 4 we will encounter a case where this point needs some attention.
We now want to study whether a vertical sequence of a certain motif can be followed by a sequence of a different motif, eventually, with a insertion of one of the motifs with 3 zeroes: "1000" or "11000".

**Example 7** *As an example let us start with a sequence of motif $A_1$. This sequence could be followed by motifs $A_2$, $B_1$ and $C_2$. However, it cannot be followed by motif $B_2$, because*

*it would not belong to $H_{12}$. Nor can it be followed by motifs $C_1$ or $D_i$, because it would not belong to $H_Q$ (see fig. 6.22).*

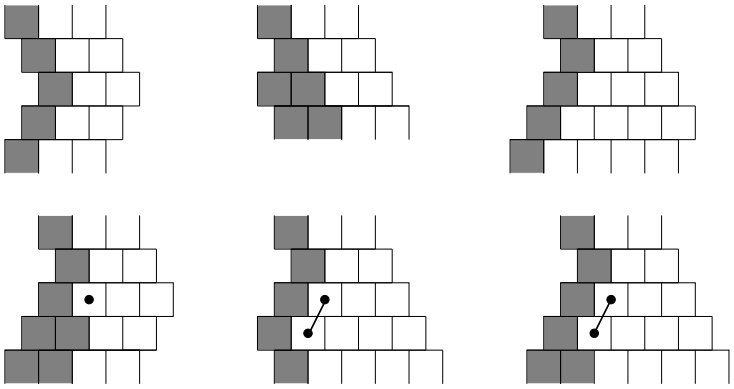

**Figure 6.22:** At the top, we show, from left to right, motif $A_1$ followed by the motifs $A_2$, $B_1$ and $C_2$. On the bottom-left, we see that a configuration in which $A_1$ is followed by $B_2$ contains a site with a dot in the left-most boundary of the white segment. The other two configurations on the bottom, show that configurations in which $A_1$ followed by $C_1$ or $D_i$ do not belong to $H_Q$. Here we used the notation of figure 6.21.

Similarly we find the following:

- motif $B_1$ can only be followed by motif $C_2$.
- motif $C_2$ can only be followed by motif $B_1$.
- motif $A_i$ can be followed by motifs $A_j$, $B_1$ and $C_2$.
- motif $D_i$ can be followed by motifs $D_j$, $B_1$ and $C_2$.
- motif $B_2$ can only follow after motif $C_1$.
- motif $C_1$ can only follow after motif $B_2$.

Finally, we know from lemma's 7 and 8 that grey and white columns cannot branch or have end points, since their width always oscillates between 1 and 2 modulo 3 or 2, 3 and 4 modulo 3 for the grey and white segments respectively. Consequently, grey and white columns may wind around the torus several times, but they will always close to form a loop.
Let us combine this observation with the rules we found for stacking motifs. Consider, for example, motif $A_1$, which can be followed by motifs $A_2$, $B_1$ and $C_2$. However, motifs $B_1$ and $C_2$ can only be followed by $C_2$ and $B_1$ respectively. Consequently, if motif $A_1$ is followed by either of these two motifs, we can never fulfill the boundary conditions, because the column cannot be closed to form a loop. Thus configurations in which motif $A_1$ is followed by motifs $B_1$ and $C_2$ do not belong to $H_Q$. In this same spirit we obtain the following lemma.

**Lemma 16** *For configurations that belong to $H_Q$ the following holds:*

- *motif $B_1$ can only be followed by motif $C_2$ and vice versa.*
- *motif $A_1$ can only be followed by motif $A_2$ and vice versa.*
- *motif $D_1$ can only be followed by motif $D_2$ and vice versa.*
- *motif $B_2$ can only be followed by motif $C_1$ and vice versa.*

For motifs $A_i$ and $D_i$ the width of the white segment does not change, thus the motif with direction 1 can follow directly below or above this same motif with direction 2. For the motifs $B_i$ and $C_i$, however, there is an intermediate motif of the type "1000" or "11000". Which of the two can be determined via the 'tic-tac-toe' procedure. If we read the motifs of the rows from top to bottom, we find that a sequence of $B_1$ motifs will be followed by "1000", to be followed by a sequence of $C_2$ motifs. Then the $C_2$ motifs will be followed by "11000", which is then to be followed by another sequence of $B_1$ motifs. On the other hand, a sequence of $B_2$ motifs will be followed by "11000", followed directly by a sequence of $C_1$ motifs. Finally, the $C_1$ motifs will be followed by "1000", followed directly by another sequence of $B_2$ motifs (see fig. 6.23). It is readily checked that any other choice gives a configuration that does belong to $H_{12}$, but not to $H_Q$.

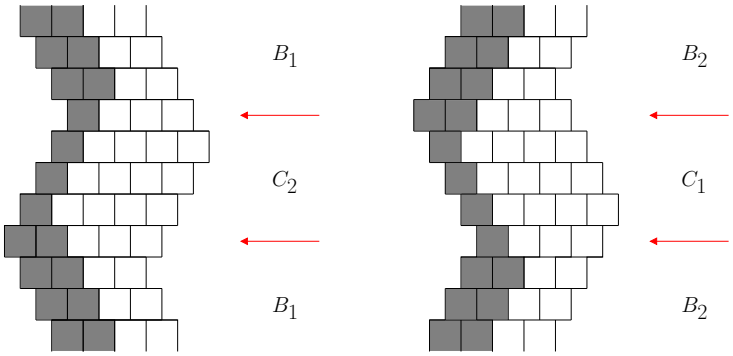


**Figure 6.23:** Two configurations are shown in which motif $B_i$ is followed by motif $C_j$ (where $i \neq j$) and vice versa, with the correct intermissions of the motifs "1000" and "11000" (indicated by the arrows).

### Step 4

We are now ready to make the identification with the tiles. For the four basis motifs $A_1$ through $D_1$ the identification is shown in figure 6.24 and $A_2$ through $D_2$ are identified with a tiling in figure 6.25. Note that to distinguish motif $X_1$ from $X_2$, where $X = A, B, C$ or $D$, one has to consider also the motif on the row above or below this motif. These motifs can be followed by an arbitrary threefold of zeroes. Let us define the motif $E \equiv$"000". For this motif we can also distinguish a direction, because its boundary will follow the left-most boundary of the white segment it is attached to. From figures 6.24 and 6.25 it is clear that the motifs $X_i$ can be followed by motif $E_i$, where the $i$ should be the same. For

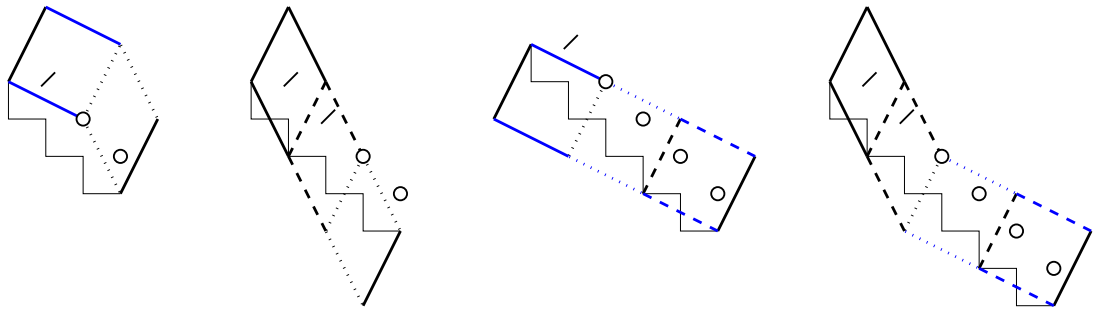

**Figure 6.24:** The motifs $X_1$ and the corresponding tilings. Note that this mapping was already found in section 6.5.1 (see fig. 6.6).

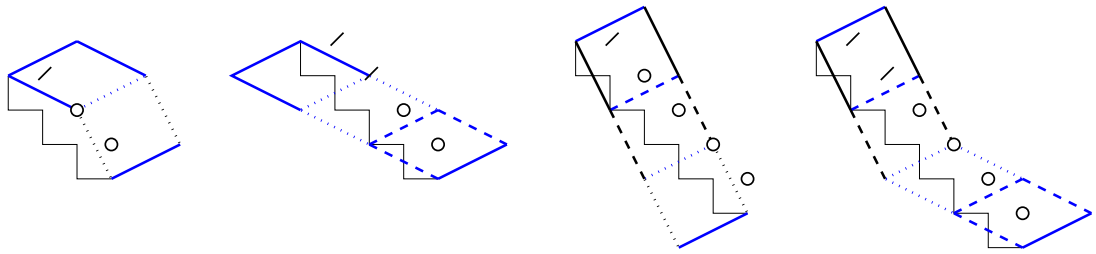

**Figure 6.25:** The motifs $X_2$ and the corresponding tilings.

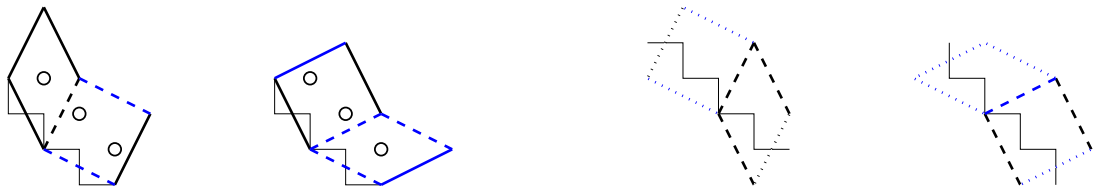

**Figure 6.26:** On the left the motifs $E_1$ (on the left) and $E_2$ (on the right) and the corresponding tilings. On the right the tilings corresponding to insertions of 3 dots into the motifs $X_1$ (on the left) and $X_2$ (on the right).

the motifs $B_1$ and $C_2$ there is an exception: when the motif above these motifs is "11000" and "1000" respectively, they are followed by $E_2$ and $E_1$ respectively.

There can also be insertions of multiples of three dots in the four basis motifs. How this translates into tilings is shown in figure 6.27. More precisely, note that each basis motif $X_1$ contains a dotted line, connecting two $S_1$ sites along the direction 1 (black) and equivalently, all basis motifs $X_2$ contain a dotted line with direction 2 (blue). An insertion of three dots in a basis motif corresponds to an insertion of two tiles, shown in figure 6.26, at this dotted line. Note that here we cannot easily write the motif of dots directly in the tiles, however, the mapping is still unambiguous.

Finally, we have the motifs "1000" and "11000". Which tilings these motifs correspond to depends on whether they occur between the motifs $B_1$ and $C_2$ or the motifs $B_2$ and $C_1$. In fact, in the first case, "1000" will correspond to the same sequence of tiles as $B_1$

and "11000" to the same tiling as $C_2$. Similarly, in the latter case, "1000" and $B_2$, on the one hand, and "11000" and $C_1$, on the other hand, correspond to the same tilings. For an example see figure 6.28.

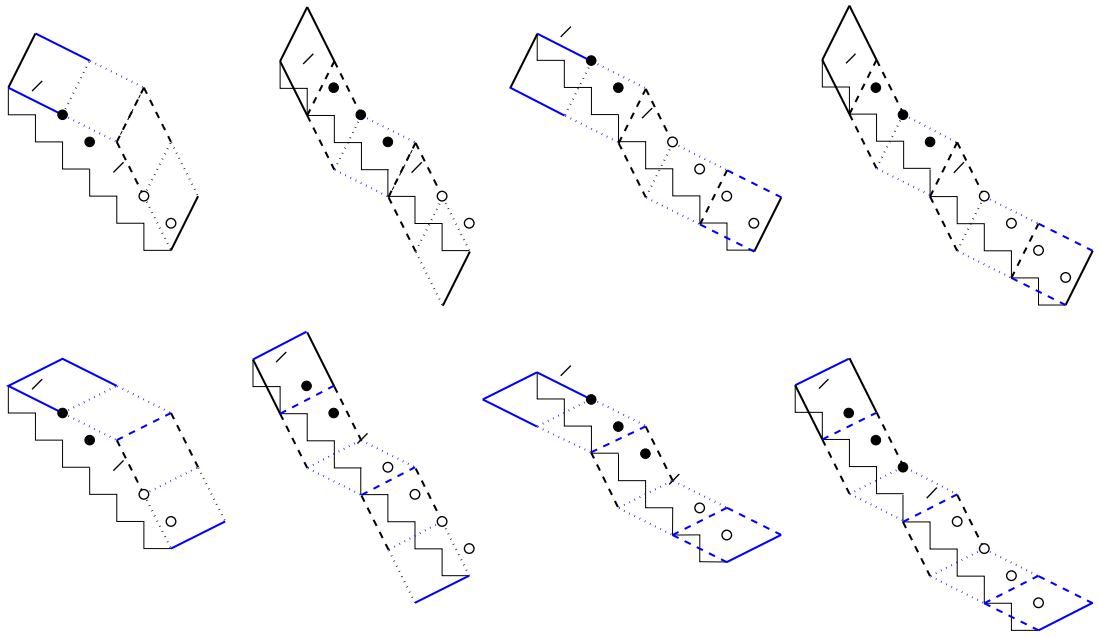

**Figure 6.27:** On the top (bottom), insertions of 3 dots into the motifs $X_1$ ($X_2$) and the corresponding tilings are shown.

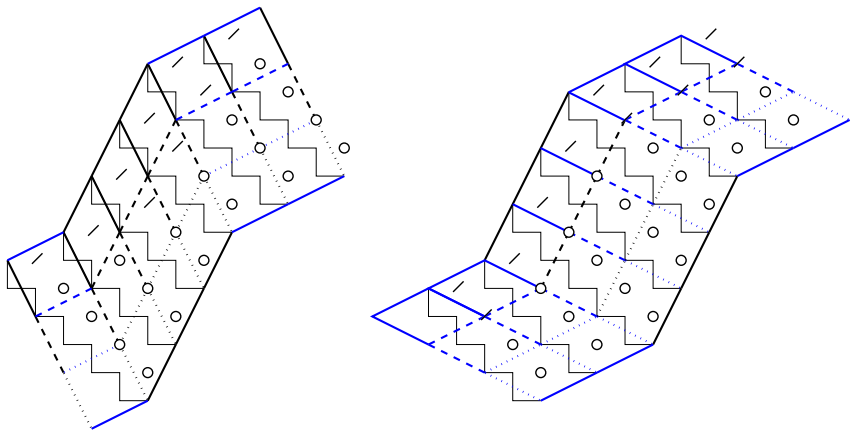

**Figure 6.28:** On the left (right), we show a configuration in which motifs $C_2$ and $B_1$ ($C_1$ and $B_2$) alternate with the corresponding tilings. Note that the motifs "1000" and "11000" correspond to different tilings on the left than on the right.

With these identifications there is one ambiguity, but it is easily dealt with. If there is a column in which the motifs alternate indefinitely between "1100" and "11000", we cannot determine whether the motif "1100" is of type $B_1$ or $B_2$. The same happens when the motifs "10000" and "1000" alternate indefinitely: the motif "10000" could be of type $C_1$ or $C_2$. Note that if we choose to identify the first with $B_1$ and the second with $C_2$, the

corresponding tilings would be indistinguishable. This also happens when we choose $B_2$ and $C_1$. So we conclude that we should either choose $B_1$ and $C_1$ or $B_2$ and $C_2$. The ambiguity is thus lifted by simply deciding that we will always choose, say, $B_1$ and $C_1$.
Finally, we note that again the number of fermions in a certain configuration is the same as the number of tiles in the corresponding tiling. For the four basis motifs and the motifs with 3 zeroes or 3 dots, this follows from the arguments in section 6.5.1. For the motifs "1000" and "11000", we should look at figure 6.28. If the motif "1000" sits between motifs $B_1$ and $C_2$, the number of fermions in these three rows is $3 * 3$ and the number of sites is 3 times the number of $S_1$ sites: $3 * (2 * 4 + 5)$. So 9 fermions on 39 sites. Compare this with the corresponding tiling: it contains 2 times 3 tiles of area 4 and once 3 tiles of area 5. So 9 tiles with total area 39. Similarly, if the motif "11000" sits between motifs $B_1$ and $C_2$, the number of fermions in these three rows is $3 * 3$ and the number of sites is $3 * (2 * 5 + 4)$. The corresponding tiling contains 2 times 3 tiles of area 5 and once 3 tiles of area 4. For the corners between motifs $B_2$ and $C_1$ the comparison is slightly more subtle. Following the same arguments as above, we find that in this case the number of fermions in the motifs "1000" and "11000" do not agree with the number tiles in the corresponding tiling. However, the discrepancy is minus one in one case and plus on in the other, and since the boundary conditions dictate that the number of "1000"-motifs equals the number of "11000"-motifs, the discrepancies exactly cancel.

### Step 5

The final step concerns the small correction $\Delta$ in equation (5.1). With the four basis motifs, horizontal insertions of multiples of three dots and three zeroes and vertical insertions of the motifs "1000" and "11000", we can represent all elements in $H_Q$. With the mappings given in the previous step, we find a corresponding tiling for each of these elements. On the other hand, each possible tiling can be constructed with the small sequences of tiles given in the previous step. Thus we find that for each possible tiling there is a corresponding element in $H_Q$. Furthermore, we found that the number of fermions and the number of tiles agree. So we find $N_i = t_i$, that is, the number of elements in $H_Q$ with $i$ fermions equals the number of tilings of the square lattice with $i$ tiles. However, there is a small discrepancy in this one-to-one relation for the configurations with all zeroes or all dots. For $\vec{u} = (m, -m)$ and $v_1 + v_2 = 3p$, it is readily verified that these configurations contain $i = [2m/3]p$ fermions. In the following we will first compute the number of elements of $H_Q$ that these configurations account for. We shall call this $N^{(a)}$, where $a$ stands for anomalous. We will then compute $t^{(a)}$, the number of tilings consisting only of the tiles that correspond to either all zeroes or all dots (see fig. 6.26). Combining these results we obtain $\Delta \equiv N^{(a)} - t^{(a)}$. Finally, since we found a one-to-one correspondence between tilings and elements of $H_Q$ for $i \neq [2m/3]p$, theorem 2 will then be established with $\Delta_i$ as in equation (5.2).
As we discussed in section 6.5.1 for $\vec{v} = (1, 2)$, the configurations with all dots and all zeroes actually correspond to multiple elements of the cohomology if there is a multiple of 3 $S_1$ sites per row, that is if $\vec{u} = (3n, -3n)$. This is a direct consequence of theorem 3, which says that a periodic chain with length $3j$ has two ground states. In fact, these configurations account for $2^p$ elements each, where $p = (v_1 + v_2)/3$ is the total number of $S_1$ rows or, equivalently, of $S_2$ chains. On the other hand, for $\vec{u} = (m, -m)$ with $m \neq 3n$

they each represent one element of the cohomology. So we find $N^{(a)} = 2^{p+1}$ for $m = 3n$ and $N^{(a)} = 2$ otherwise.
Now, let us look at the corresponding tilings. For $\vec{u} = (m, -m)$ with $m \neq 3n$ there is no corresponding tiling, thus there is a discrepancy of 2 between the number of tilings and the number of elements in the cohomology. That is $\Delta \equiv N^{(a)} - t^{(a)} = 2$ for $m \neq 3n$. For $\vec{u} = (3n, -3n)$ there are tilings corresponding to the configurations with all zeroes or all dots. Along the $\vec{u}$ direction these tilings have periodicity 3. The periodicity in the other direction is more involved. Given the boundary condition $\vec{v} = (2r + s, r + 2s)$ the tiling makes $r$ steps in the $(2, 1)$ direction and $s$ steps in the $(1, 2)$ direction, in arbitrary order. However, because of the periodicity of 3 in the $\vec{u}$ direction one can also end at $(2r + s + 3l, r + 2s - 3l)$, that is, $r + 3l$ steps in the $(2, 1)$ direction and $s - 3l$ steps in the $(1, 2)$ direction, again in arbitrary order. Thus we find

$$t^{(a)} = 2 * 3 \sum_{l \geq -r/3} \binom{r+s}{r+3l}.$$

If we define $r = 3k + c$, where $c \in 0, 1, 2$, we can write $t$ as:

$$\begin{aligned}
t^{(a)} &= 6 \sum_{l=0} \binom{r+s}{c+3l} \\
&= 6 \sum_{l=0} \left[ \binom{r+s-2}{c+3l-2} + 2\binom{r+s-2}{c+3l-1} + \binom{r+s-2}{c+3l} \right] \\
&= 6 \sum_{l=0} \left[ \binom{r+s-2}{l} + \binom{r+s-2}{c+3l-1} \right] \\
&= 6 * 2^{r+s-2} + 6 \sum_{l=0} \left[ \binom{r+s-2}{c+3l-1} \right].
\end{aligned}$$

Repeating these steps $d$ times, such that $2d \leq r + s$, we find

$$\begin{aligned}
t^{(a)} &= 6 \sum_{l=1}^{d} 2^{r+s-2l} + 6 \sum_{l=0} \binom{r+s-2d}{c+3l-d} \\
&= \sum_{l=0}^{2d-1} 2^{r+s-l} + 6 \sum_{l=0} \binom{r+s-2d}{c+3l-d} \\
&= \begin{cases} 2^{r+s+1} - 2 + 6 \sum_{l=0} \binom{0}{c+3l-d} & \text{if } r + s = 2d \\ 2^{r+s+1} - 4 + 6 \sum_{l=0} \binom{1}{c+3l-d} & \text{if } r + s = 2d + 1. \end{cases}
\end{aligned}$$

For the last term we find

$$\begin{aligned}
6 \sum_{l=0} \binom{0}{c+3l-d} &= \begin{cases} 6 & \text{if } d = 3b + c \\ 0 & \text{otherwise.} \end{cases} \\
6 \sum_{l=0} \binom{1}{c+3l-d} &= \begin{cases} 0 & \text{if } d = 3b + c + 1 \\ 6 & \text{otherwise.} \end{cases}
\end{aligned}$$

We now compare the expression for $t^{(a)}$ with the expression for the number of elements in the cohomology represented by the configurations with all zeroes and all dots, $N^{(a)}$. For

$\vec{v} = (2r + s, r + 2s)$ this is $N^{(a)} = 2 * 2^{(v_1+v_2)/3} = 2^{r+s+1}$. So we finally find

$$\Delta = N^{(a)} - t^{(a)} = \begin{cases} -4 & \text{if } r+s = 2d \text{ and } r-s = 6b \\ 2 & \text{if } r+s = 2d \text{ and } r-s = 6b \pm 2 \\ 4 & \text{if } r+s = 2d+1 \text{ and } r-s = 6b+3 \\ -2 & \text{if } r+s = 2d+1 \text{ and } r-s = 6b \pm 1. \end{cases}$$

Combining this with the result $\Delta = 2$ for $\vec{u} = (m, -m)$ with $m \neq 3n$, this can be cast in the compact form of equation (5.2).

## 6.6 Counting formula for tilings

In the previous sections we proved a theorem that expresses the number of ground states in terms of tiling configurations. In this section we derive a counting formula for the number of tilings of the plane with periodicities given by $\vec{u} = (m, -m)$ and $\vec{v} = (2\alpha + \beta, \alpha + 2\beta)$. An important property of the periodic tilings is that a given tiling can be specified completely by giving a collection of corners of tiles in the tiling that form a closed loop along a non-contractible direction of the torus when connected by edges of length $\sqrt{5}$. There is one constraint, namely that in the collection of edges between the corners at least one should be along the directions $(2, 1)$ or $(1, 2)$ and at least one should be along the directions $(2, -1)$ or $(1, -2)$.
Let us consider an example. Suppose we have the tiling shown in figure 6.29 with periodicities $\vec{u} = (6, 0)$ and $\vec{v} = (0, 6)$. It is not difficult to see that the set of corners $\{(0, 0), (1, 2), (3, 1), (5, 2)\}$ completely determines the tiling. However, the set $\{(0, 0), (1, 2), (3, 3), (4, 5)\}$ does not fully determine the tiling. Indeed in this case none of the edges between the corners is along the directions $(2, -1)$ or $(1, -2)$.
This property is the main reason why the number of tilings and thus the number of ground states of the doubly periodic square lattice does not grow exponentially with the 2D volume, but at most with the linear dimensions of the system.
In the following we will use this property to obtain a counting formula for the number of tilings of the plane with periodicities given by $\vec{u} = (m, -m)$ and $\vec{v} = (2\alpha+\beta, \alpha+2\beta)$. We will first consider the closed loop along the non-contractible direction of the torus given by $\vec{u} = (m, -m)$. Notice that a tiling with periodicity $\vec{u}$ will only exist if we can write

$$(m, -m) = r_1(1, -2) + s_1(2, -1) + r_2(2, 1) + s_2(1, 2),$$

where the $r_i$ and $s_i$ are integers. For $m$ positive we will have $r_1, s_1 \geq 0$ and $r_2, s_2$ will have the same sign. If we solve these equations for $r_2$ and $s_2$ we find

$$\begin{cases} r_2 = m - (4r_1 + 5s_1)/3 \\ s_2 = -m + (5r_1 + 4s_1)/3. \end{cases}$$

From this it follows that there are two regions in the parameter space of $r_1, s_1$ where $r_2, s_2$ have the same sign. These regions are bound by the lines

$$\begin{cases} r_2 = 0 & \rightarrow s_1 = (3m - 4r_1)/5 \\ s_2 = 0 & \rightarrow s_1 = (3m - 5r_1)/4. \end{cases}$$

The regions are shown in figure 6.30.

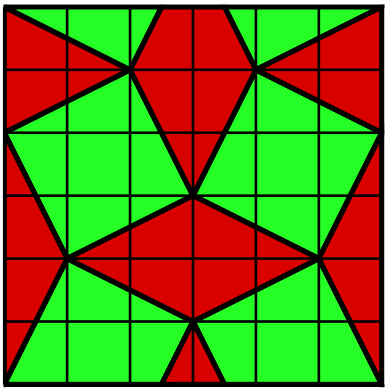

**Figure 6.29:** We show a tiling which obeys the periodicities $\vec{u} = (6, 0)$ and $\vec{v} = (0, 6)$.

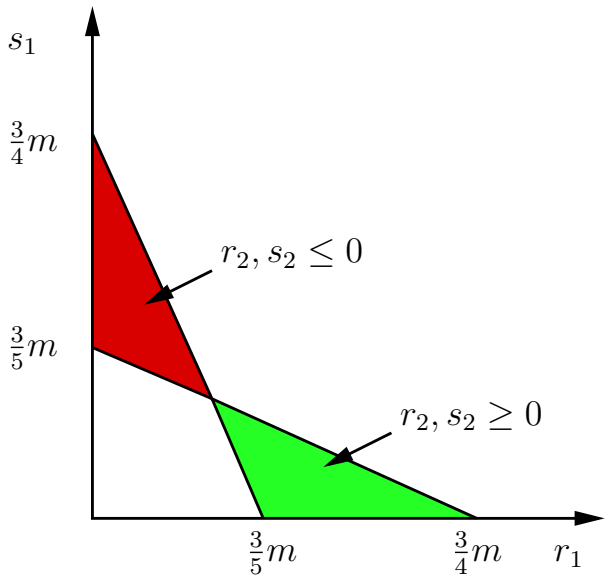


**Figure 6.30:** The lines $s_1 = (3m - 4r_1)/5$ and $s_1 = (3m - 5r_1)/4$ are shown and the region where $r_2, s_2$ have the same sign are indicated.

Now suppose we have $r_2 = \lambda$ and $s_2 = \mu$. Let us determine the constraints on $\lambda$ and $\mu$ set by $m$. First of all, we have

$$\begin{cases} r_1 = (m + 4\lambda + 5\mu)/3 \\ s_1 = (m - 5\lambda - 4\mu)/3 \end{cases}$$

and since $m$ is positive we have $r_1, s_1 \geq 0$ from which it follows that

$$\begin{cases} 5\lambda + 4\mu \leq m & \text{for } \lambda, \mu \geq 0 \\ 4|\lambda| + 5|\mu| \leq m & \text{for } \lambda, \mu \leq 0. \end{cases}$$

Furthermore, we find that, since $r_1$ and $s_1$ are integers, we must have

$$\begin{cases} m + 4\lambda + 5\mu = 3q_1 \\ m - 5\lambda - 4\mu = 3q_2, \end{cases}$$

with $q_1$ and $q_2$ positive integers. From this we find, with $q \in \mathbb{Z}$,

$$\lambda - \mu = \begin{cases} 3q & \text{for } m = 3p \\ 3q - 1 & \text{for } m = 3p + 1 \\ 3q + 1 & \text{for } m = 3p + 2. \end{cases}$$

Together with the condition that $\lambda$ and $\mu$ have the same sign, these are the conditions imposed by the periodicity $\vec{u}$. We now also impose the periodicity in the other direction, $\vec{v} = (2\alpha + \beta, \alpha + 2\beta)$. We only need consider the case where $\alpha$ and $\beta$ are both positive, since the other cases can be reduced to this case either by reflecting in $\vec{u}$ or translating by $\vec{u}$ or both. It is clear that the periodicity $\vec{v}$ imposes the following condition: either $\lambda = \mu = 0$ or

$$\lambda = \alpha/k \quad \text{and} \quad \mu = \beta/k,$$

with $k \in \mathbb{Z}$.
With all these condition in place, we can finally write down a counting formula. As we have emphasized at the start a tiling can be fully specified by a collection of corners that form a closed loop around an incontractible direction of the torus. Now suppose that we know that this loop contains $\kappa$ edges in the $(1, -2)$-direction, $\nu$ edges in the $(2, -1)$-direction, $\lambda$ edges in the $(2, 1)$-direction and $\mu$ edges in the $(1, 2)$-direction. Since the order of the edges in the directions $(2, 1)$ and $(1, 2)$ can be chosen independently from the order of the edges in the directions $(2, -1)$ and $(1, -2)$, it follows that the number of tilings specified by this collection of edges is

$$\frac{5(\kappa\lambda + \mu\nu) + 4(\kappa\mu + \lambda\nu)}{(\kappa + \nu)(\lambda + \mu)} \binom{\kappa + \nu}{\nu} \binom{\lambda + \mu}{\mu},$$

where the first factor is the total number of sites divided by the total number of tiles in the tiling.
Putting everything together we find that the number of tilings $R_{\vec{u},\vec{v}}$ for $\vec{u} = (m, -m)$ and $\vec{v} = (2\alpha + \beta, \alpha + 2\beta)$ with $m$ positive and $\alpha, \beta \in \mathbb{Z}_{\geq 0}$ is given by

$$R_{\vec{u},\vec{v}} = A_0 + A_k, \tag{6.12}$$

where

$$A_0 = \begin{cases} \frac{9}{2} \binom{\alpha+\beta}{\beta} \binom{2m/3}{m/3} & \text{for } m = 3p \\ 0 & \text{otherwise,} \end{cases} \tag{6.13}$$

and

$$A_k = \sum_k{}' \frac{5(\kappa\alpha + \nu\beta) + 4(\kappa\beta + \nu\alpha)}{(\kappa + \nu)(\alpha + \beta)} \binom{(\alpha + \beta)/|k|}{\beta/|k|} \binom{\kappa + \nu}{\nu},$$

with

$$\kappa = \frac{1}{3}(m + \frac{4\alpha}{k} + \frac{5\beta}{k}) \quad \text{and} \quad \nu = \frac{1}{3}(m - \frac{5\alpha}{k} - \frac{4\beta}{k}).$$

The prime denotes that the sum is restricted to run over integer values of $k$ such that

$$\begin{cases} (5\alpha + 4\beta)/m \leq k & \text{if } k > 0 \\ (4\alpha + 5\beta)/m \leq |k| & \text{if } k < 0, \end{cases}$$

furthermore we impose $\binom{a}{b} = 0$ if $a$ and/or $b$ is non-integer. Finally, we should have

$$\begin{cases} \frac{\alpha-\beta}{k} = 3q & \text{for } m = 3p \\ \frac{\alpha-\beta}{k} = 3q - 1 & \text{for } m = 3p + 1 \\ \frac{\alpha-\beta}{k} = 3q + 1 & \text{for } m = 3p + 2 \end{cases}$$

with $q \in \mathbb{Z}$.

Note that the counting formula derived here is consistent with the result for the growth behavior of the number of tilings (5.4) obtained in [38]. It is easily verified that for $m$ mod $3 = 0$ and $m$ and $\alpha = \beta$ large $A_0$ is the leading term in (6.12). Finally, writing $\alpha = \beta = \lambda q$ and $m = 3\mu q$ with $q$ large and using Stirling's approximation, one quickly recovers (5.4) from (6.13).

# Chapter 7
# The supersymmetric model on 2 and 3 leg ladders

## 7.1 Ladder models as a first step towards 2D systems

In the previous chapters, we have seen, first of all, that we have a detailed understanding of the supersymmetric model on the chain and second of all, that there are numerous results for counting ground states in two dimensional systems. Where the chain has only a doubly degenerate ground state, two dimensional systems typically enjoy an exponential degeneracy. For the chain, however, our understanding extends far beyond the ground state structure, whereas such understanding is lacking for the two dimensional systems. In this chapter we consider a variety of ladder models, which will bring these two results together. On the one hand, we will see that these ladder models also exhibit superfrustration, which we typically interpret as a feature of the two dimensional systems. On the other hand, however, many of the methods we used to study the chain, such as the spectral flow analysis and entanglement entropy computations, carry over to these ladder systems. In this chapter we focus on the analysis of the ladder models. In the next chapter, however, we will discuss an interpretation of these findings for the fully two dimensional systems (see also [34, 85]).
In the first section, we discuss the ground state structure of certain 2 and 3 leg ladders. We will show in particular that these ladders typically have an extensive ground state entropy and that the ground states are in one-to-one correspondence with tilings. In section 7.3 we discuss the results of the spectral flow analysis for these models [34] and present compelling evidence for criticality in these systems. In the final two sections, we discuss the zig-zag ladder and the square ladder in more detail. The zig-zag ladder is a very rich model, with zero energy ground states at all rational fillings between 1/5 and 1/4 filling. We build up a picture, where the system is in a gapped, charge ordered phase away from 2/9 filling, whereas at this critical filling the system shows a gapless phase. There will be a strong connection between this picture and the tilings corresponding to the ground states. The square ladder on the other hand, shows remarkable similarities to the model on the chain, but there also seem to be significant differences leading to some interesting open questions.

## 7.2 Ground states and tilings

In the previous chapter we have seen that for the square lattice there is an explicit relation between zero energy ground states of the supersymmetric model and tilings. This relation is not exclusive to the square lattice, but seems to be a more generic feature. In chapter 5, we discussed the work of Jonsson [39] which relates homology elements of $Q$ to tilings for the triangular and hexagonal lattice. Furthermore, we will see in this section that the ground states of the kagome ladder can also be related to tilings [21]. In the second part

of this section, we will discuss ladder realizations of the square lattice. We will show that theorem 2 also holds for these lattices, even though, their periodicities differ from the ones for which the proof was given. This is explicit support for the conjecture that theorem 2 holds for all periodicities on the square lattice.

### 7.2.1 Kagome ladder

In this section we consider the kagome ladder (see Fig. 7.1). This ladder has an extensive ground state entropy and the ground states can be related to tilings of the ladder. The cohomology can be computed exactly for open boundary conditions. We find a closed expression for the ground state partition function and a window of filling fraction for the supersymmetric ground states, which can both be interpreted in terms of tilings. For periodic boundary condition, the cohomology problem has not been solved, but we do have a conjecture for the ground state partition function.
Computing the cohomology in this case is slightly involved. First of all, we cannot choose the sublattice $S_2$ such that it consists of disconnected sites, which by themselves have zero cohomology. Instead the convenient choice for the sublattice $S_2$ is less trivial. The second complication arises because not all elements of the cohomology $H_{12}$ will have the same fermion-number, which was a sufficient condition for the tic-tac-toe lemma to hold. We compute the cohomology step by step. For each step there is a supporting picture in Fig. 7.2. **Step 1** is to map the kagome ladder with hard-core fermions to a square ladder with hard-core dimers. This mapping is one-on-one. In **Step 2** we define the sublattices $S_1$ and $S_2$. **Step 3** is to note that the cohomology of one square plus one additional edge vanishes. To do so, first note that if site 3 and 4 are both empty, we get zero cohomology due to site 5 which can now be both empty and occupied. The remaining four configurations are easily shown to be either $Q$ of something (exact) or not in the kernel of $Q$ (not closed). **Step 4** is to build up the ladder by consecutively adding blocks with 3 rungs (9 edges) to the ladder. From step 3 we now conclude that there are only two allowed configurations for the additional $S_1$-sites: they must be either both empty or both occupied, since if just one of them is occupied the remaining configurations on the additional $S_2$-sites are exactly the ones of step 3. A simple computation shows that if both sites on $S_1$ are occupied, $H_{Q_2}$ has one non-trivial element with one dimer and if both sites on $S_1$ are empty, $H_{Q_2}$ has two non-trivial elements, both with two dimers.
Now it is important to note that on the three additional rungs we find three non-trivial elements of the $H_{12}$, but two of them have $f_2 = 2$ and one has $f_2 = 1$. It can be shown that all three indeed belong to $H_Q$ by going through the spectral sequence step by step. This is a tedious computation, but it can be done.
Finally, we find the cohomology of the kagome ladder with open boundary conditions of length $n$, which corresponds to a ladder with $n + 1$ rungs and $3n + 1$ edges in total, by

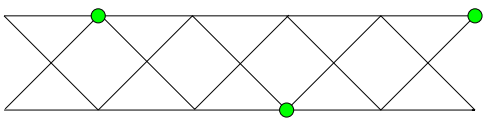

**Figure 7.1:** Hard-core fermions on the kagome ladder.

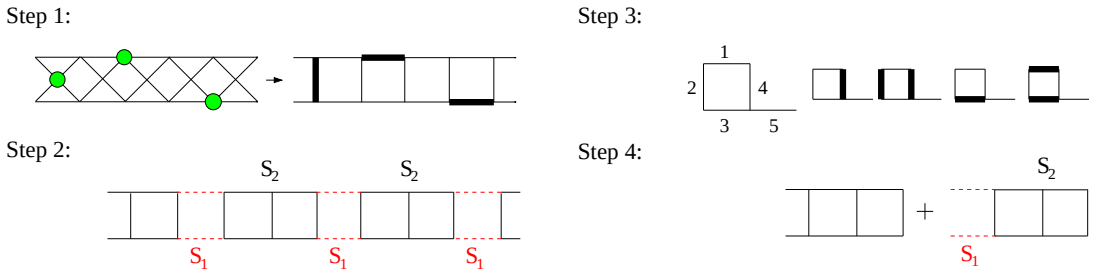


**Figure 7.2:** Step-by-step computation of the cohomology of the kagome ladder.

recursively adding rungs to the system. We thus obtain a recursion relation for the ground-state generating function $P_n(z) = \mathrm{tr}_{\mathrm{GS}}(z^F)$, which gives the Witten index for $z = -1$ and the total number of ground states for $z = 1$:

$$P_{n+3}(z) = 2z^2 P_n(z) + z^3 P_{n-1}(z),$$

with $P_0 = 0$, $P_1 = z$, $P_2 = 2z^2$, $P_3 = z^3$. If we introduce the following notation

$$A(n,m) = \begin{pmatrix} n-m \\ 3n-4m+1 \end{pmatrix} 2^{3n-4m+1}, \tag{7.1}$$

we can write the ground state partition sum in closed form

$$P_n(z) = \Sigma_m [A(n,m) + A(n+2, m+1)] z^m$$

Instead of drawing conclusions from here, let us picture the above in terms of tiles. From step 4 we conclude that we can cover the ladder with three tiles, two of size 9 (i.e. 9 edges) containing 2 dimers and one of size 12 containing 3 dimers. From this picture we obtain the same recursion relation provided that we allow four initial tiles corresponding to the initial conditions of the recursion relation above. Furthermore, we can see directly that the window of filling fraction of the tiles runs from 2/9 to 1/4. Using the recursion relation, we find that the ground state entropy is set by the largest solution $\lambda_{\max}$ of the characteristic polynomial $\lambda^4 - 2\lambda - 1 = 0$, giving $S_{\mathrm{GS}}/L = (\ln \lambda_{\max})/3 = 0.1110\ldots$.
For the case of periodic boundary conditions, the full cohomology problem has not been solved. However, we do conjecture an expression for the ground state partition sum, that has been verified numerically for systems up to 33 sites. First we compute the cohomology for an open ladder with an extra leg on the lower rung on each side. For this system, we prove that the ground state generating function satisfies

$$Q_n(z) = 2z^2 Q_{n-3}(z) + z^3 Q_{n-4}(z).$$

For the closed ladder of length $n$ (with $n$ rungs and $3n$ sites), we now naively constructed the following recursion relation

$$X_n(z) = P_{n-1}(z) + 2z Q_{n-3}(z) + z^2 P_{n-3}(z). \tag{7.2}$$

However upon comparison with the numerical data we conclude that it gives the Witten index correctly, but it overcounts the number of ground states. We conjecture that when

the first and second term in (7.2) differ by one power in $z$, these states are actually superpartners and similarly for the second and third term in (7.2). These terms should thus be subtracted. Using the definition (7.1), we can write

$$Q_n(z) = \Sigma_m A(n+4, m+2) z^m$$

and we find that the conjectured form of the ground state partition sum for the closed ladder is

$$\begin{aligned} X_n(z) = \Sigma_{m=0}^n [&A(n-1,m) + A(n+1,m+1) + 2zA(n+1,m+2) \\ &+ z^2 A(n-3,m) + z^2 A(n-1,m+1)] z^m \\ -\Sigma_{m=0}^n \mathrm{Min}[&A(n-1,m) + A(n+1,m+1), A(n+1,m+2)](z^m + z^{m+1}) \\ +\Sigma_{m=0}^n \mathrm{Min}[&A(n+1,m+2), A(n-3,m) + A(n-1,m+1)](z^{m+1} + z^{m+2}). \end{aligned}$$

### 7.2.2 Ladder realizations of the square lattice

As we mentioned in the beginning of this chapter, the main focus here is on ladder realizations of the square lattice. We construct ladders from the square lattice by choosing the periodicity $\vec{u} = (L, 0)$ in the horizontal direction, and for the periodicity $\vec{v}$ we consider the three cases $\vec{v} = (0, 2)$, $\vec{v} = (1, 2)$ and $\vec{v} = (3, 3)$ (see figure 7.3). The first two are 2 leg ladders, the first being the simple square ladder and the second turns out to be a zig-zag ladder. The third is a 3 leg ladder and is clearly the most two dimensional, in the sense that the particles can really hop past each other in this lattice.

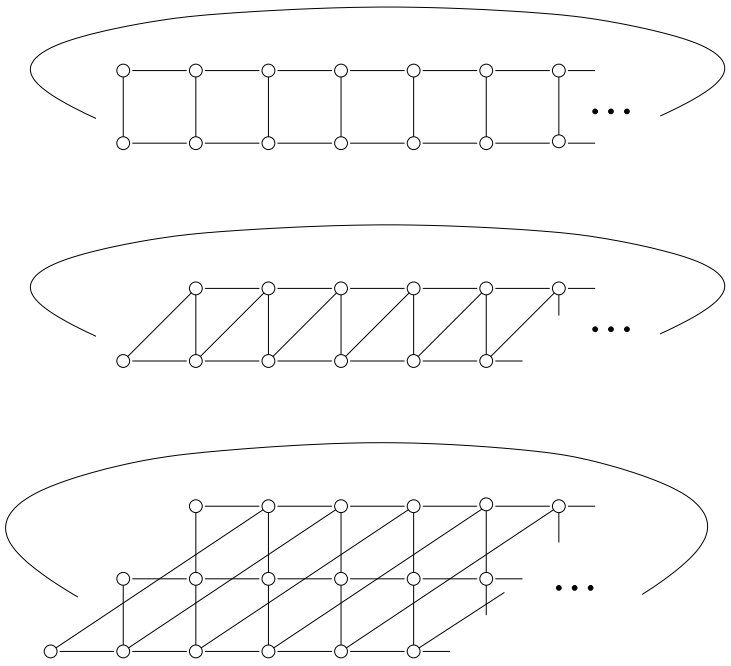

**Figure 7.3:** From top to bottom we show the square ladder, the zig-zag ladder and the 3 leg ladder, obtained from the square lattice by imposing the periodicities $\vec{u} = (L, 0)$ in the horizontal direction and $\vec{v} = (0, 2)$, $\vec{v} = (1, 2)$ and $\vec{v} = (3, 3)$ respectively in the vertical direction.

In the previous chapters, we discussed theorem 2 which relates ground states to tilings for the supersymmetric model on the square lattice with doubly periodic boundary conditions.

We strongly believe this theorem for all periodicities, however, a proof was given only for the case $\vec{u} = (m, -m)$ and $v_1 + v_2 = 3p$. It follows that the theorem has been proven only for zig-zag ladders of length $L = 3k$ and for the 3 leg ladder with length $L = 3k$. Although the square ladder falls outside the class of tori for which we prove the theorem, we can quite easily extend the proof for this case. Before we give the proof, we should mention that for all three ladders with up to 32-36 sites (depending on the model), the numerics are in precise agreement with the theorem. Clearly, this is very strong support for our belief that the theorem holds in general.

### Square ladder

For the square ladder ($\vec{u} = (L, 0)$ and $\vec{v} = (0, 2)$) the Witten index follows directly from Jonsson's theorem [37] (see theorem 1 in this thesis). For length $L = 4k$ we find that there are 4 tilings with $k$ tiles using just the diamonds, for length $L \neq 4k$ there are no tilings. Using the fact that $-(-1)^d \theta_d \theta_{d^*} = \pm 1$ for $L = 2k + 1$ and $L = 2k$ respectively, we find

$$W = \begin{cases} 3 & \text{for } L = 4k \\ -1 & \text{for } L = 4k + 2 \\ 1 & \text{for } L = 4k \pm 1 \end{cases}$$

For the case with $L = 4k$, we easily prove that there are 3 ground states with $2k$ fermions. The proof for the other cases is slightly more tedious. To compute the cohomology for $L = 4k$, we divide the lattice into two sublattices, where $S_1$ contains the isolated sites $(1 + 4m, 0)$ and $(3 + 4m, 1)$ with $m = 0, \ldots, k - 1$. The sublattice $S_2$ is then a periodic chain of length $2L - 2k = 6k$. It is easily seen that $H_{Q_2}$ is trivial unless the $S_1$ sites are all empty or all occupied. The first case corresponds to two non-trivial elements at grade $2k$ (the 2 ground states on the periodic chain with $2k$ particles). The second case gives the third non-trivial element at grade $2k$. To compute $H_{12}$ and $H_Q$ are now trivial steps and we conclude that there are 3 ground states with $2k$ fermions for $L = 4k$. For $L = 4k + 3$ we can choose the sublattices such that $S_1$ consists of $2k + 2$ disconnected sites and $S_2$ is an open chain of length $6k + 4$. It quickly follows that the only non-trivial element of $H_2$ has all sites on $S_1$ occupied and thus that there is a unique ground state with $2k + 2$ particles (in agreement with $W = +1$). For $L = 4k + 1$ we can choose the sublattices such that $S_1$ consists of $2k - 1$ disconnected sites and 2 connected sites and $S_2$ is a periodic chain of length $6k + 1$. The configuration with all $S_1$ sites empty gives one non-trivial element of $H_2$ at grade $2k$, all other allowed configurations on $S_1$ give trivial elements of $H_2$. It follows that there is a unique ground state with $2k$ particles (in agreement with $W = +1$). Finally, for $L = 4k + 2$ we can choose the sublattices such that $S_1$ consists of $2k + 1$ disconnected sites and $S_2$ is a periodic chain of length $6k + 2$, with one extra site connected to it. All configurations with at least on particle on $S_1$ are trivial elements of $H_2$. All $S_1$ sites empty gives rise to a periodic chain of length $6k + 2$, with one extra site connected to it. Using the 'tic-tac-toe' lemma for this case, where the extra site is considered as the $S_1$ sublattice one easily proves that there is one ground state with $2k+1$ particles. We conclude that for $L = 4k + 2$, there is a unique ground state with $2k + 1$ particles (in agreement with $W = -1$).

### Zig-zag ladder

For the zig-zag ladder ($\vec{u} = (L, 0)$ and $\vec{v} = (1, 2)$) the Witten index also follows from Jonsson's theorem. However, counting the number of tilings is less trivial than for the square ladder. The zig-zag ladder nicely accommodates tiling configurations. In the short direction the boundary condition is $\vec{v} = (1, 2)$, which is precisely along the edges of one of the diamonds and one of the squares. It follows that we can tile the zig-zag ladder with precisely one row of tiles, using just these two tiles that fit the boundary conditions. Imposing the periodicity $\vec{v} = (1, 2)$ changes the shape of the tiles. This is depicted in figure 7.4.

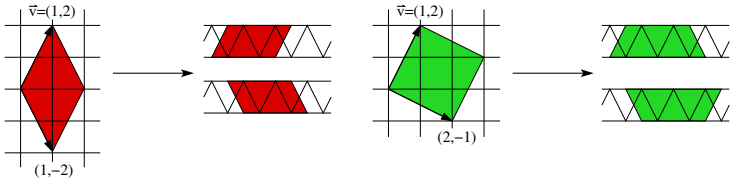


**Figure 7.4:** Two of the four allowed tiles nicely fit the periodicity imposed by $\vec{v} = (1, 2)$. We show what these tiles look like on the zig-zag ladder. Both the diamond as well as the square turn into two tiles on the zig-zag ladder differing in their orientation.

For the zig-zag ladder with $N$ sites and open boundary conditions the generating function for tiling configurations is

$$P^o_N(z) = zP^o_{N-4}(z) + zP^o_{N-5}(z), \tag{7.3}$$

with $P^o_1 = 0$, $P^o_2 = 0$, $P^o_3 = 0$ and $P^o_4 = z$. Interestingly, this recursion relation also seems to hold for the ground state generating function. This has been checked numerically for up to 22 sites. The only difference is that the first couple of values of $P^o$ are different: $P^o_1 = 0$, which is also true for the tilings, but $P^o_2 = z$, $P^o_3 = 2z$ and $P^o_4 = 2z$. It follows that the difference between the number of tilings and the number of ground states diverges as a function of $N$, due to a propagating different offset.
For the zig-zag ladder with periodic boundary conditions the generating function for tiling configurations obeys the same recursion relation (7.3). In this case, however, we also have an expression in closed form for the number of tilings

$$R_{\vec{u},\vec{v}}(z) = 4z^{L/2}(1-q) + \sum_{k=1}^{(L+5q)/10} z^{\tilde{L}-k+1} \frac{L}{2k-q} \begin{pmatrix} \tilde{L}-k \\ 4k-1-2q \end{pmatrix}$$

with $q = L \mod 2$ and $\tilde{L} = L/2 - 1 + q/2$, where $L$ is the length of the ladder (so the number of sites is $N = 2L$).
From theorem 2 we know that for $L = 3k$ the ground state partition function reads $Z_{\mathrm{GS}}(z) = R_{\vec{u},\vec{v}} + (-1)^{(\theta_{2k}+1)} 2z^{[4k/3]}$, with $[a]$ the nearest integer to $a$ and

$$\theta_d \equiv \begin{cases} 2 & \text{if } d = 3k, \text{ with } k \text{ integer} \\ -1 & \text{otherwise.} \end{cases} \tag{7.4}$$

Numerically we verified the following expression for general $L = N/2$ up to $N = 34$

$$Z_{\mathrm{GS}}(z) = R_{\vec{u},\vec{v}} - (-1)^{(\theta_{d^*}+[2N/9])} \theta_{d^*} z^{[2N/9]}, \tag{7.5}$$

with $d^* = \gcd(u_1 + u_2, v_1 + v_2) = \gcd(L, 3)$.

### 3 leg ladder

For the 3 leg ladder ($\vec{u} = (L, 0)$ and $\vec{v} = (3, 3)$) the theorem for the number of ground states is proven for $L = 3k$. The number of tilings can be expressed as

$$R_{\vec{u},\vec{v}}(z) = \sum_{s \geq L/9}^{2L/9} 9 \binom{L/3}{2L/3 - s} z^{2L/3},$$

with the restriction that $s$ is integer and that $\binom{a}{b} = 0$ if $a$ and/or $b$ are not positive integers. It follows that for $L \neq 3k$, there are no tilings. Furthermore, we see that for $L = 3k$ there are only tilings with $2L/3 = 2k$ tiles, more precisely with $k$ diamonds and $k$ squares.
From theorem 1 for the Witten index, we find

$$W = \begin{cases} -(-1)^L & \text{for } L \neq 3k \\ -(-1)^L 4 + R_{\vec{u},\vec{v}}(z = -1) & \text{for } L = 3k. \end{cases}$$

For $L \neq 3k$ we can thus quickly conjecture that $\Delta = 1$ in theorem 2, since the number of ground states must be positive. For $L = 3k$ we conjecture from comparison with numerical results for up to $L = 12$ that $\Delta = -(-1)^k 4$.

## 7.3 Spectral flow for ladder realizations of the square lattice

To investigate criticality of the supersymmetric model on ladder realizations of the square lattice, we investigated how the spectrum changes upon twisting the boundary condition along the $(L, 0)$-direction from periodic to anti-periodic [34]. This method was described and the results discussed for the supersymmetric model on the chain in section 4.8. It is a powerful way of distinguishing between critical and gapped states: for a gapped state, the correlation length is finite and a change in the boundary conditions will have an exponentially small effect on the energy. In contrast, for a critical state the change in the energy will be substantial since the correlation length goes to infinity. More specifically, the energy has a parabolic dependence on the boundary twist.
In addition to this, one can extract more quantitative properties from twisting the boundary condition. This is described in detail in section 4.8, but will be briefly summarized here for convenience. For a critical supersymmetric system in 1D with a Fermi surface, we expect that its continuum limit is described by an $\mathcal{N}$=2 superconformal field theory (SCFT). In such a theory, twisting the boundary condition corresponds to going from the Ramond to the Neveu-Schwarz sector. The twist can be carried out continuously and leads to a spectral flow [49]. If we define the twist parameter $\alpha$ to be integer in the Ramond sector and half-integer in the Neveu-Schwarz sector, the energy is a parabolic function of $\alpha$,

$$E_\alpha = E_{\alpha=0} + \alpha \tilde{Q}_{\alpha=0} + \alpha^2 c/3, \tag{7.6}$$

where $c$ is the central charge. $\tilde{Q}_\alpha \equiv q_L + q_R$ is the sum of the left- and right-moving U(1) charges and depends linearly on $\alpha$ [49, 43]. Their difference is conserved under the twist

and is related to the fermion number. In the lattice model, we can go from periodic to anti-periodic boundary conditions continuously by adding a phase to the terms that hop a particle over the boundary, e.g. $c_N^\dagger c_1 +$ h.c. is replaced by $e^{2\pi\imath\alpha} c_N^\dagger c_1 +$ h.c. The eigenvalues of the translation operator $p_\alpha$ will now depend linearly on the twist parameter:

$$T_\alpha^L |\psi\rangle \quad = \quad e^{2\pi\imath p_0 L} e^{2\pi\imath\alpha F} |\psi\rangle \equiv e^{2\pi\imath p_\alpha L} |\psi\rangle, \tag{7.7}$$

so $p_\alpha = p_0 + \alpha F/L$ where $L$ is the length of the system and $F$ is the total number of particles in the state $|\psi\rangle$.
We computed the spectrum for various values of the twist parameter via exact diagonalization. We find that the majority of states have a parabolic dependence on the twist parameter by fitting a parabola to the energy levels as a function of the twist parameter, or equivalently, as a function of $p_\alpha$. This clearly indicates that the system is critical. An example is shown in fig. 7.5.
For a critical system, the energy of the SCFT in (7.6) is related to the numerically obtained value of the energy via $E_{\text{num}} = 2\pi E_{\text{CFT}} v_F / L$, where $v_F$ is the Fermi velocity and $L$ the system size. So by comparing the parabolic fit to the numerics with equation (7.6), we can obtain the ratios $E_\alpha/c$ and $\tilde{Q}_\alpha/c$.

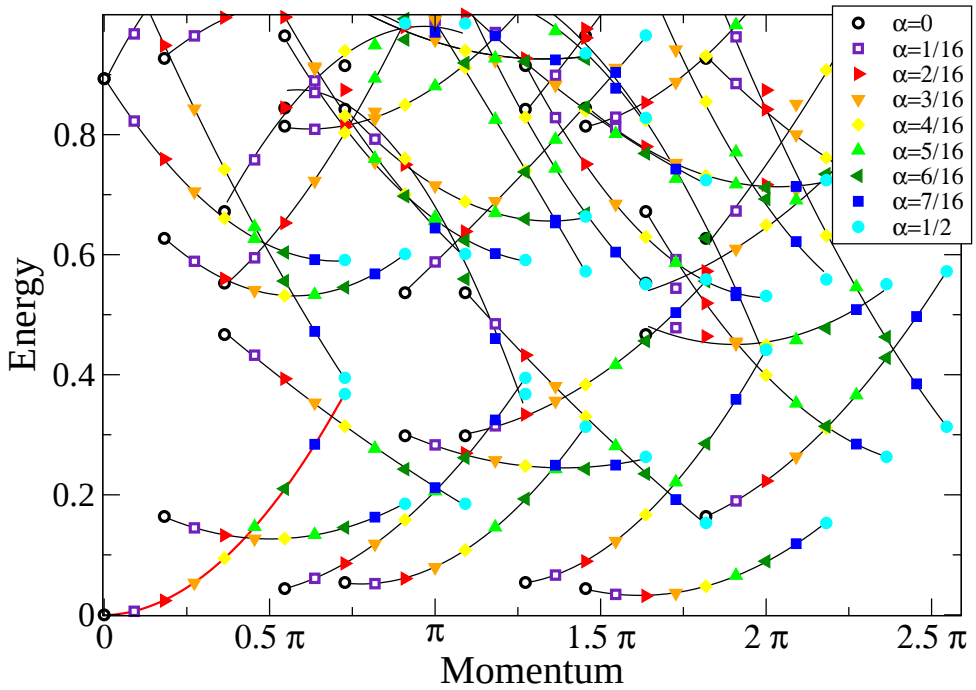


**Figure 7.5:** In the plot we show nine energy spectra as a function of momentum for increasing values of the twist parameter ($0 \leq \alpha \leq 1/2$, with steps of $1/16$) for a system with 33 sites ($\vec{u} = (11, 0)$ and $\vec{v} = (3, 3)$) and 8 fermions. The lines are parabolic fits to the numerical data. The results from the spectral flow analysis for the red line through the origin appear in red in table 7.1.

We extracted values for $E_\alpha/c$ and $\tilde{Q}_\alpha/c$ via the above described method for three models with up to 36 sites (see table 7.1). For the lowest energy levels, we typically find that $(E/c, \tilde{Q}/c)$ in the NS sector is either $(-1/12, 0)$, $(1/12, 1/3)$ or $(1/4, 2/3)$, all with an accuracy of within 10%. These values occur in the Kac table for the $k$-th minimal model

**Table 7.1:** Results from spectral flow analysis for three types of tori $(L,0)\times\vec{v}$ (and $(L,-1)\times(1,2)$ for the zig-zag ladder with odd number of sites wrapped on a Möbius strip). Here, $N$ denotes the number of sites and $F$ the number of fermions. We show the results for the lowest energy level for each system. The values for $E$ and $\tilde{Q}$ are given in the Neveu-Schwarz sector ($\alpha=1/2$) and $c$ is the central charge. For the level in red boldface the results are extracted from the red line in fig. 7.5.

| $N$ | $\vec{v}$ | $F$ | $E/c$ | $\tilde{Q}/c$ |
|---|---|---|---|---|
| 18 | $(3,3)$ | 4 | -0.0851 | 0.004 |
| 36 | $(3,3)$ | 8 | -0.0841 | -0.002 |
| 15 | $(3,3)$ | 4 | 0.0898 | 0.349 |
| 21 | $(3,3)$ | 4 | 0.0850 | 0.337 |
| 24 | $(3,3)$ | 5 | 0.0850 | 0.337 |
| 30 | $(3,3)$ | 7 | 0.0853 | 0.338 |
| **33** | **(3,3)** | **8** | **0.0855** | **0.338** |
| 9 | $(1,2)$ | 2 | -0.0858 | -0.005 |
| 18 | $(1,2)$ | 4 | -0.0842 | -0.002 |
| 27 | $(1,2)$ | 6 | -0.0839 | -0.001 |
| 17 | $(1,2)$ | 4 | 0.0844 | 0.336 |
| 26 | $(1,2)$ | 6 | 0.0840 | 0.335 |
| 35 | $(1,2)$ | 8 | 0.0839 | 0.335 |
| 14 | $(1,2)$ | 3 | 0.2666 | 0.701 |
| 23 | $(1,2)$ | 5 | 0.2458 | 0.657 |
| 32 | $(1,2)$ | 7 | 0.2432 | 0.652 |
| 16 | $(0,2)$ | 4 | -0.0897 | -0.014 |
| 24 | $(0,2)$ | 6 | -0.0889 | -0.012 |
| 32 | $(0,2)$ | 8 | -0.0885 | -0.011 |
| 12 | $(0,2)$ | 3 | 0.0911 | 0.350 |
| 20 | $(0,2)$ | 5 | 0.0900 | 0.348 |
| 28 | $(0,2)$ | 7 | 0.0894 | 0.347 |
| 14 | $(0,2)$ | 4 | 0.0855 | 0.338 |
| 22 | $(0,2)$ | 6 | 0.0849 | 0.337 |
| 30 | $(0,2)$ | 8 | 0.0847 | 0.336 |

of an $\mathcal{N}=(2,2)$ superconformal field theory with $k$ even [43]. This can be seen as follows. The possible values of the conformal dimensions and corresponding $U(1)$ charges of the superconformal minimal models are given in section 3.4. In the Neveu-Schwarz sector they read

$$h_{p,r}(k)=\frac{p(p+2)-r^2}{4(k+2)}\qquad q_r(k)=\frac{r}{k+2},$$

with $p=0,1,\ldots,k$ and $r=-p,-p+2,\ldots,p-2,p$. For a state with $h_L=h_R=h_{p,r}(k)$ and $q_L=q_R=q_r(k)$, we find

$$\begin{aligned}\frac{E}{c} &= \frac{2h_{p,r}(k)}{c}-\frac{1}{12}=\frac{p(p+2)-r^2-k/2}{6k}\\ \frac{\tilde{Q}}{c} &= \frac{2q_r(k)}{c}=\frac{2r}{3k}.\end{aligned}$$

One easily verifies that with $p = r = 0$, $p = r = k/2$ and $p = r = k$, we find $(E/c, Q/c) = (-1/12, 0)$, $(1/12, 1/3)$ and $(1/4, 2/3)$ respectively. The fact that we obtain these ratios from analyzing the spectral flow is very compelling evidence that each of these systems is quantum critical.

A few remarks are in order. The fits become less reliable for levels with higher energies, but also if there is an avoided level crossing as a function of the twist. This happens when the energy levels in the Ramond or NS sector are degenerate. For the chain, the avoided crossings vanish in the continuum limit (see section 4.8.1), so one would expect that for the other models this is also merely a finite size feature. For the square ladder ($\vec{u} = (L, 0)$ and $\vec{v} = (0, 2)$), however, the results from exact diagonalization suggest that the avoided crossing will prevail for large system sizes. We will discuss this issue in more detail in section 7.5.

For the zigzag ladder ($\vec{u} = (L, 0)$ or $\vec{u} = (L, 1)$ (Möbius strip) and $\vec{v} = (1, 2)$), we find that the energy depends parabolically on the boundary twist for filling fractions close to 2/9 filling. However, at 1/4 and 1/5 filling we find quite a different behavior; the energy of the states does not change or hardly changes as a function of the twist parameter. This suggests that away from 2/9 filling the system is gapped. In the section 7.4, we present further evidence for this observation. If we look more carefully at the spectral flow for this system one may even argue that only the extra or missing ground states, which are not related to tilings, but correspond to $\Delta$ in theorem 2, lead to critical modes. For a nice illustration of this idea see figure 7.6. Here we plot the spectral flow for the zig-zag ladder with 27 sites on a Möbius strip at 2/9 filling, that is $f = 6$. There are 90 possible tilings with 3 diamonds and 3 squares and the system realizes 88 zero energy ground states. In the plot we clearly see, that a few ground states show critical behavior under spectral flow, whereas the bulk of the ground states hardly reacts to the boundary twist. This is even more apparent upon comparison to the spectral flow of the 3 leg ladder with 36 sites and 8 fermions, where all 50 ground states clearly show a significant reaction to the boundary twist (see figure 7.7). Of course, it is difficult, if not impossible, to identify the critical modes in the zig-zag ladder with the *missing* ground states. However, from the proof of theorem 2 it follows that of the 9 tilings with diamonds and squares alternating, only 7 correspond to cohomology elements. It follows that the 9 cross-cycles corresponding to the tilings are not independent and one may argue that this leads to 7 extended states which show the critical behavior.

## 7.4 Zig-zag ladder

The zig-zag ladder nicely accommodates both the diamond- as well as the square-tile and thus has zero energy ground states for all rational fillings between 1/4 and 1/5. Consequently, this model forms an ideal testing ground for investigating the tiling-ground state relation beyond counting. In the previous section we saw that the spectral flow analysis for this model indicates the presence of critical modes, but only near 2/9 filling. In this section we present further evidence that the system has a gap at 1/4 and 1/5 filling due to charge ordering. In analogy with our studies of the supersymmetric model on the chain, we investigate the entanglement entropy and one-point functions for this model. For 1/4 filling we even prove the charge ordering explicitly, because we find an analytic expression for the ground states. We suspect, although we cannot prove this,

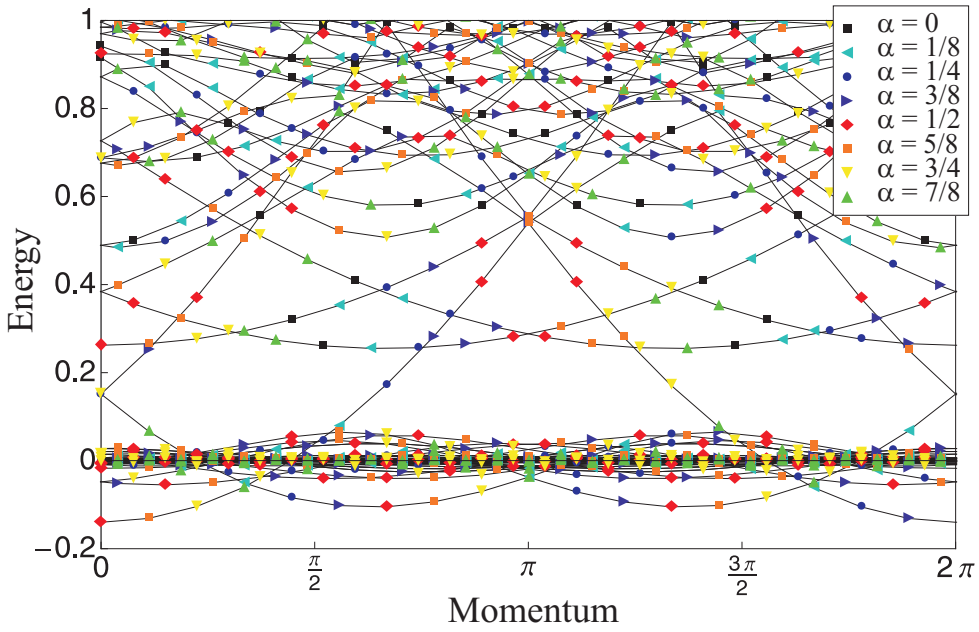


**Figure 7.6:** In the plot we show eight energy spectra as a function of momentum for increasing values of the twist parameter ($0 \leq \alpha \leq 7/8$, with steps of $1/8$) for the zig-zag ladder with 27 sites ($\vec{u} = (13, -1)$ and $\vec{v} = (1, 2)$) and 6 fermions. The lines connect the levels for different values of the twist parameter.

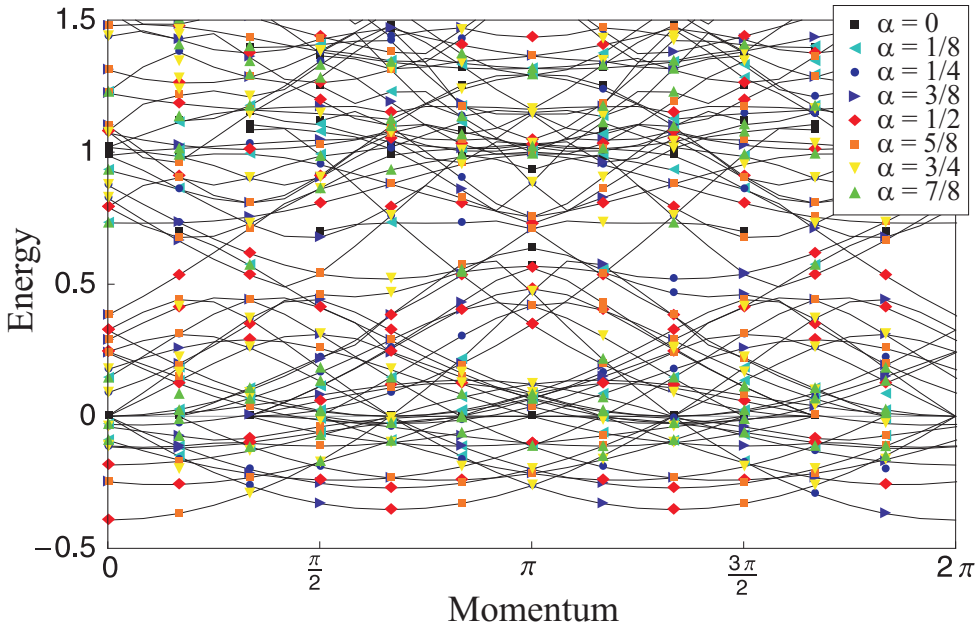


**Figure 7.7:** In the plot we show eight energy spectra as a function of momentum for increasing values of the twist parameter ($0 \leq \alpha \leq 7/8$, with steps of $1/8$) for a system with 36 sites ($\vec{u} = (12, 0)$ and $\vec{v} = (3, 3)$) and 8 fermions. The lines connect the levels for different values of the twist parameter.

that the spectrum of the model on the zig-zag ladder exhibits a gap everywhere except at 2/9 filling. On the one hand, this may be interpreted as a phase transition due to

competing orders (between the diamond and the squares), on the other hand, there are indications that only the extra or missing ground states, which are not related to tilings, but correspond to $\Delta$ in theorem 2, lead to critical modes. In the latter case the ground states that correspond to tilings would always exhibit a form of charge order and the critical modes arise independently.
Finally, we discuss a mapping from this model onto a spin chain. Since exploiting this relation could provide further insight in both the supersymmetric model as well as the spin chain, this may be an interesting future project.

### 7.4.1 Exact ground states at and near quarter filling

As we have seen in section 7.2.2 the zig-zag ladder is chosen such that it nicely accommodates tiling configurations (see figure 7.4). If the boundary condition in the horizontal direction is $\vec{u} = (2n, 0)$ with $n \in \mathbb{Z}_{\geq 1}$ there are always four tilings using only the diamonds. Now remember that one can associate a cross-cycle to a tiling (see section 5.4). It turns out that for the zig-zag ladder at quarter filling these cross-cycles are not just representatives of the homology of $Q$, but they are the actual ground states of the system at quarter filling[1]. A cross-cycles is a product state of one-particle-states with the particle resonating between two sites. To be precise, for general length $2n$ (boundary conditions $\vec{u} = (2n, 0)$ and $\vec{v} = (1, 2)$) the four ground states can be written as

$$\Psi_\alpha = \prod_{j=0}^{n-1} (c^\dagger_{4j+\alpha \mod 4n} - c^\dagger_{4j+\alpha+1 \mod 4n})|0\rangle, \tag{7.8}$$

where $\alpha = 0, 1, 2, 3$ and for the creation operators $c_i^\dagger$, $i = 0, \ldots, 4n-1$ with $i$ even (odd) labelling the sites of the lower (upper) rung of the ladder (see figure 7.8). These ground state can also be written in a translational invariant form and one finds that

- for $\vec{u} = (4m, 0)$ with $m \in \mathbb{Z}$ there are two ground states at momentum $p_1 = \pi/2$ and two ground states at momentum $p_2 = 3\pi/2$, and
- for $\vec{u} = (4m + 2, 0)$ with $m \in \mathbb{Z}$ there are two ground states at momentum $p_1 = 0$ and two ground states at momentum $p_2 = \pi$.

Interestingly, we can compute the effect of a boundary twist on these states analytically. The momenta of the states change linearly with the twist as expected. But we find that the twist has no effect on the energy of the states. This can be readily understood by remembering that the ground states are product states of one particle states with the particle resonating between two sites. A change in the boundary condition can thus be absorbed locally in the state of the particle that resonates across the boundary.
If we move away from quarter filling, the ground states correspond to tilings containing both diamonds and squares. It can be easily checked that the cross-cycles corresponding to tilings containing the square tile are annihilated by $Q^\dagger$, but not by $Q$. It follows that there is no analytic expression available for ground states at general filling. Nevertheless, there is more evidence that the relation between ground states and tilings is very robust.

[1] There is an exception for small chain lengths ($1 \leq n \leq 4$), where either not all four cross-cycles are independent ($n = 1$) or they do not constitute a complete representation of the cohomology ($n = 2, 3, 4$) at quarter filling. For $n > 4$ these subtleties do not occur.

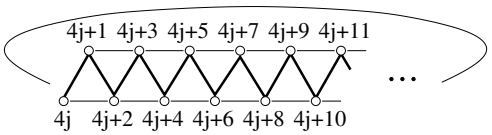


**Figure 7.8:** The zig-zag ladder can be obtained from the square lattice by imposing the periodicities $\vec{u} = (L, 0)$ and $\vec{v} = (1, 2)$. The sites on the lower (upper) rung are labelled by even (odd) integers.

First of all, the momenta of the ground states seem to nicely agree with the momenta one would expect from the tilings. For example at 1/5 filling the tilings are invariant under translations by 5 sites in the horizontal direction. Indeed we find that the 5 ground states at 1/5 filling have momenta $p_k = 2\pi k/5$ with $k = 1, \ldots, 5$.
Second of all, the tilings tell us that there are massless, fractionally charged defects in the system. Upon inspection of the tiles, one easily verifies that in a given tiling a sequence of 5 diamonds can be replaced by 4 squares. The new tiling has one charge less, however, since we can take the four squares apart, they can each be seen as a defect of charge $-1/4$. Note that these defects do not cost any energy.
Finally, we find an analytic expression for two states with zero energy for ladders with $\vec{u} = (4m - 1, 0)$, anti-periodic boundary conditions and $f = 2m - 1$. Clearly, this is just a curiosity (the ground state for these systems has negative energy), but for completeness we wish to mention it here. This state was found by considering the analytic ground state at quarter filling on a ladder with an odd number of rungs by leaving one rung empty. This can be seen as introducing a defect of charge $-1/2$ in the charge ordered state. We consider a ladder with $\vec{u} = (2n - 1, 0)$ and $f = n - 1$. By writing out the effect of the hamiltonian on this state (and handling the minus signs with care), one can show that for $\alpha = 0, 1$ the following states have zero energy

$$\Psi_\alpha = \sum_k (-1)^k T^k \prod_{j=0}^{n-2} (c^\dagger_{4j+\alpha} - c^\dagger_{4j+\alpha+1})|0\rangle, \tag{7.9}$$

where $T$ is the translation operator. We now see immediately that the translation eigenvalue is $t = -1$ and since $2n - 1$ is odd, we also have $t^{2n-1} = -1$. This is only the case if we have anti-periodic boundary conditions and an odd number of fermions, so $f = 2m - 1$ and thus $\vec{u} = (4m - 1, 0)$. Consequently, we have two zero energy states at momentum $p = \pi$. This is verified numerically for ladders of up to 30 sites.

### 7.4.2 Entanglement entropy

For a critical system of finite size $N$ the entanglement entropy between a subsystem $A$ and the rest of the system is given by (see section 4.10)

$$S(l_A) = \frac{c}{3} \log\left(\frac{N}{\pi} \sin\left(\frac{l_A \pi}{N}\right)\right) + b \tag{7.10}$$

where $b$ is some constant, $c$ is the central charge and $l_A$ is the size of the subsystem $A$.
From the spectral flow analysis, we found that the zig-zag ladder exhibits critical behavior near 2/9 filling. We have seen in section 4.10 that entanglement entropy computations are not reliable for degenerate states. Clearly for the zig-zag ladder this is a problem, since

near 2/9 filling the ground states are highly degenerate even if translational invariance is imposed. To overcome this problem we have computed the entanglement entropy in the Neveu-Schwarz sector. In particular, we select precisely the states which exhibit the critical behavior under spectral flow.
We computed the entanglement entropy for the zig-zag ladder with even ($\vec{u} = (L, 0)$ and $\vec{v} = (1, 2)$) and odd ($\vec{u} = (L, -1)$ and $\vec{v} = (1, 2)$) number of sites. For the states we selected using the spectral flow analysis we find a nice fit with the formula for the entanglement entropy using $b$ and $c$ as fit parameters (see figure 7.9). The inset in the figure shows the fitted values for $c$. The values suggest that the central charge is smaller than 3 which is in agreement with the minimal models for which $1 \leq c < 3$. However, the size of the studied systems is clearly too small to draw more quantitative conclusions on the value of the central charge.
We find that for the entanglement entropy of ground states at 1/4 and 1/5 filling, there is no good fit with (7.10). In fact, we find that the entanglement entropy saturates. This implies that the correlation length is finite and thus the ground states at 1/4 and 1/5 filling are not critical. Nice examples are shown in figures 7.10(b) and 7.10(a). Clearly, for the ground state at 1/4 filling, we know that the correlation length is finite, since the ground state is a product state. In particular, if we define $n_c$ as the number of resonating bonds that is cut by the boundary between subsystem $A$ and the rest of the system, we find that the entanglement entropy of the states $|\Psi_\alpha\rangle$ (7.8) reads

$$S_E = \begin{cases} 0 & \text{if } n_c = 0, \\ \ln 2 & \text{if } n_c = 1, \\ 2 \ln 2 & \text{if } n_c = 2. \end{cases}$$

In figure 7.10(b) we clearly see that, apart from the two boundary points, the entanglement entropy has one of two values, depending on whether the subsystem size is even or odd. Here the entanglement entropy is computed for one of the two translationally invariant ground states with momentum $p = \pi/2$. This state is a translationally invariant superposition of the states $|\Psi_\alpha\rangle$. Since not all $|\Psi_\alpha\rangle$ are completely orthogonal, it is not so easy to compute the entanglement entropy analytically for such a superposition. However, it is clear that in such a ground state the possibility to have zero entanglement entropy, drops out. Upon further inspection, one can probably explain the numerical result in more detail, however, it is not so clear what one learns from this.

### 7.4.3 Charge order at quarter and one fifth filling

The four ground states of the zig-zag ladder at quarter filling show a clear form of charge ordering. From the analytic expressions for the ground states (7.8) one easily obtains that the one-point functions, $< n_k >_\alpha \equiv \langle \Psi_\alpha | c_k^\dagger c_k | \Psi_\alpha \rangle$, read

$$< n_k >_\alpha = \begin{cases} 0 & \text{for } k - \alpha = 0 \mod 4 \text{ and } k - \alpha = 1 \mod 4, \\ 1/2 & \text{for } k - \alpha = 2 \mod 4 \text{ and } k - \alpha = 3 \mod 4, \end{cases}$$

where $\alpha = 0, 1, 2, 3$ labels the four ground states.
Both the spectral flow analysis as well as the entanglement entropy computations for the zig-zag ladder at 1/5 filling indicate that the system is also gapped in that regime. By numerically computing one-point functions for the zig-zag ladder, we investigate if

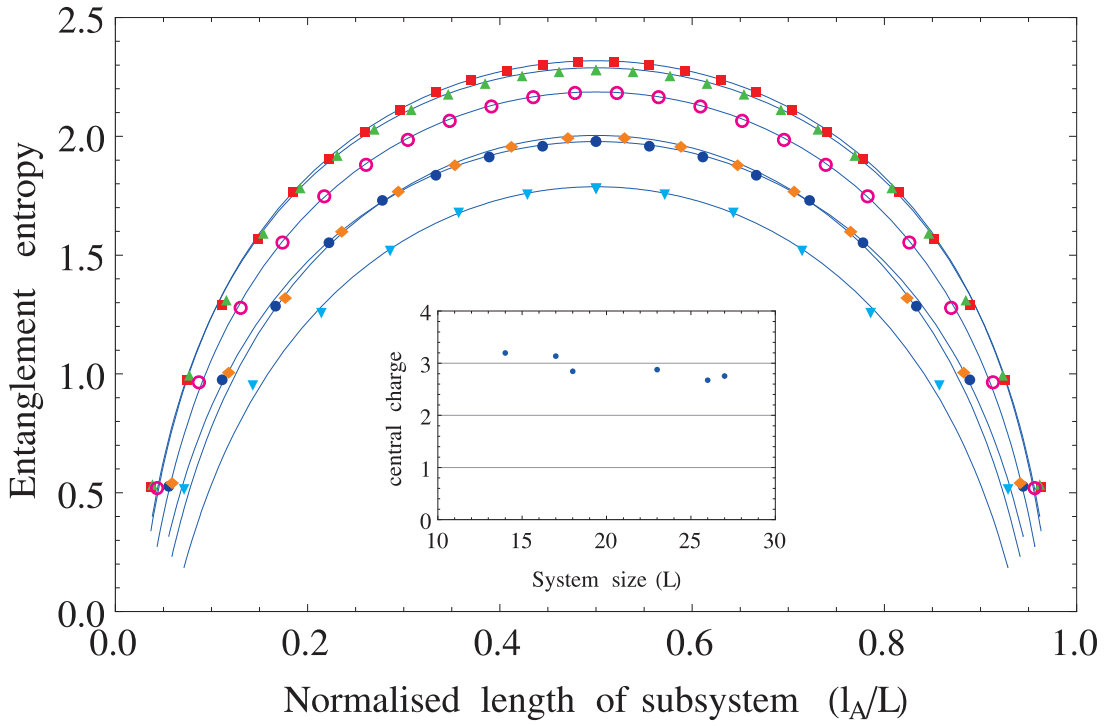


**Figure 7.9:** We plot the entanglement entropy for the states of the zig-zag ladder, which show critical behavior under spectral flow (see table 7.1). The entanglement entropy is plotted versus the number of sites ($l_A$) in the subsystem $A$ normalized by the total number of sites ($L$). The total number of sites ($L$) and the number of fermions ($f$) of the systems we investigated are: $L(f) = 14(3), 17(4), 18(4), 23(5), 26(6), 27(6)$. The corresponding plot markers are from the middle outwards: triangles, diamonds, circles, open circles, triangles and squares. The inset in the middle shows the values of the central charge extracted from the fits to the entanglement entropy versus the total number of sites.

the system also shows charge ordering at 1/5 filling. In figure 7.11(a) we plot the one-point function for the ground state of the zig-zag ladder of 25 sites with open boundary conditions and 5 particles[2]. At first glance the charge ordering seems very clear, but we have to be careful. Remember that the one-point function for the supersymmetric model on the chain also showed this substructure reminiscent of charge order, which was shown to vanish in the continuum limit (see section 4.9.2). Here we would like to see that the charge ordering persists in the continuum limit. Unfortunately, at this point we do not have enough data to claim this, since there is a -very small[3]- decay of the peak as one moves into the bulk. Nevertheless, combining these findings with the results presented in the previous sections, there is little room for a different conclusion than that the system is charge ordered also at 1/5 filling.

These findings suggest that the ground states are dominated by the tilings, that is the particles in the state are confined to quantum fluctuate within a certain area set by

[2]We choose open boundary conditions, since for periodic boundary conditions the ground state at 1/5 filling is 5-fold degenerate. A numerically obtained wavefunction, will be an arbitrary superposition of these states and the one-point function for such a state does not give much insight. We can distinguish between the five ground states by imposing translational invariance, but this destroys any structure in the one-point function.

[3]There is less than 2% decay from the outer peaks to the middle peak for the system with 25 sites.

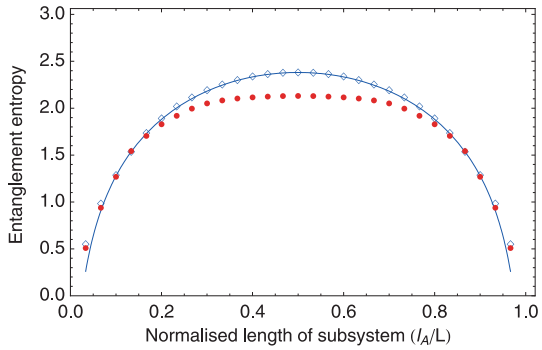


(a) $L = 30$, $f = 6$ (dots) and $f = 7$ (diamonds).

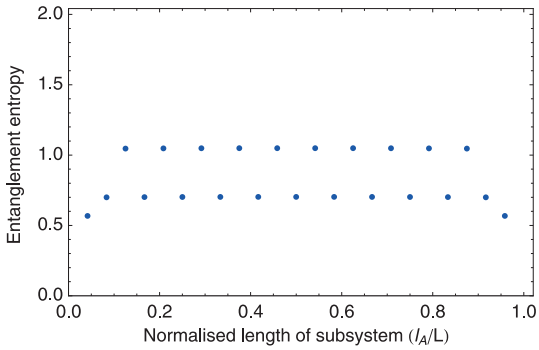


(b) $L = 24$, $f = 6$.

**Figure 7.10:** On the left we show the entanglement entropy (dots) for one of the 5 ground states of the zig-zag ladder with 30 sites at 1/5 filling ($f = 6$). For comparison we also plot the entanglement entropy (diamonds) of a ground state of the system with one extra fermion. Here the system is close to 2/9 filling and for the entanglement entropy there is a good fit with (7.10) (blue line). The zig-zag ladder with 30 sites and 7 particles has 92 zero energy ground states with periodic boundary conditions. To select one of these, we computed the entanglement entropy of the ground state for anti-periodic boundary conditions. On the right we plot the entanglement entropy for a ground state of the zig-zag ladder with 24 sites at 1/4 filling ($f = 6$). The ground states have momenta $p = \pi/2$ and $p = 3\pi/2$ and are both two-fold degenerate. It follows that we show the entanglement entropy of a certain superposition of the states $|\Psi_\alpha\rangle$ (7.8).

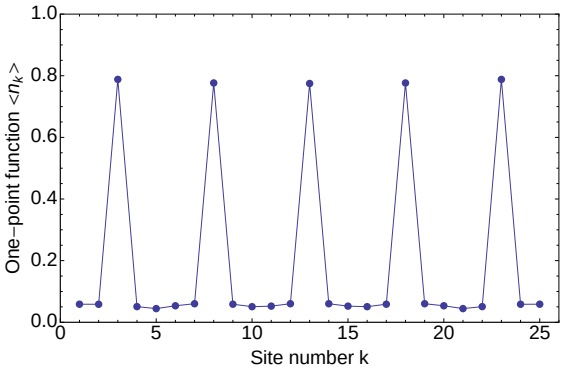


(a) $L = 25$, $f = 5$ and open boundary conditions.

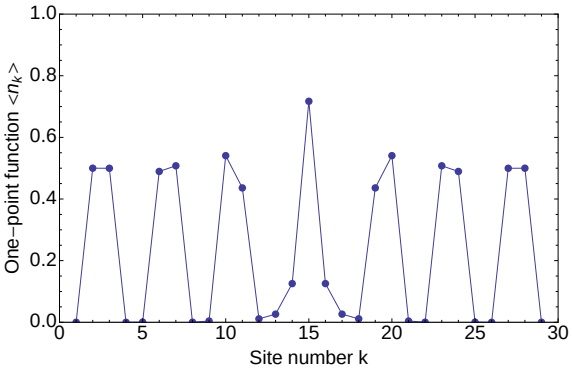


(b) $L = 29$, $f = 7$, periodic boundary conditions and perturbed hamiltonian.

**Figure 7.11:** On the left we plot the one-point function versus the site number for the ground state of the zig-zag ladder with 25 sites at 1/5 filling ($f = 5$) and open boundary conditions. On the right we plot the one-point function versus the site number for the ground state of the zig-zag ladder with 29 sites for $f = 7$ and periodic boundary conditions ($\vec{u} = (14, -1)$ and $\vec{v} = (1, 2)$). A small perturbation term is added to the supersymmetric hamiltonian: $H = \{Q, Q^\dagger\} - \epsilon c_{15}^\dagger c_{15}$, with $\epsilon = 0.01$, which favors site 15 to be occupied.

the tiles. To further test this idea, we compute the one-point function for the zig-zag ladder with 29 sites and 7 particles (see figure 7.11(b)). The tilings corresponding to the ground states of this system consist of 6 diamonds and one square. To select one specific tiling we add a small perturbation to the hamiltonian. By slightly changing the lattice

potential of one site, we favor this site to be occupied. This perturbation mildly breaks supersymmetry. From the one-point function of the ground state, we clearly see that this perturbation indeed seems to select the tiling with the square pinned to the perturbed site. Although, one should be careful interpreting this data, it is definitely in good agreement with the idea that the tiles set a certain area for the particles within which they can fluctuate. In particular, we can interpret the square tile as a defect in the charge ordered phase given by the diamonds. The fact that the one-point function corresponding to the quarter filled phase is recovered within a distance of 10 sites from the defect, suggests that this defect is indeed localized.

### 7.4.4 Flat band

For the zig-zag ladder there are zero-energy ground states at all rational filling fractions in the range between 1/5 and 1/4. For example, for a system with 30 sites there are 5 linearly independent ground states with 6 particles and 92 with 7 particles. In the previous sections we have seen that the tilings not only count, but indeed seem to dominate the actual ground states. From numerically inspecting one-point functions for specific ladder lengths, we have seen that the charge distribution of a ground state largely overlaps with that of the corresponding tiling. We can exploit this to gain physical insight. There are two uniform phases: all squares at 1/5 filling and all diamonds at 1/4 filling. One diamond in a phase with all squares is then a zero-energy defect with fractional charge 1/5. From counting the number of tilings with one such defect it follows that a defect can have any momentum. This is reminiscent of a flat band. Flat bands usually arise either from tuning the hopping terms of non-interacting particles on an exotic lattice, or from tuning potential terms for strongly interacting particles with negligible kinetic energy (see e.g. [86, 87] and references therein). Here, however, the flat band arises from tuning the potentials for particles with kinetic and potential energies of comparable size. Note that filling this flat band with defects is slightly subtle. Since defects cannot sit on top of each other and span over 4 sites, they obey a certain exclusion statistics.

### 7.4.5 Mapping to spin chain

In section 4.6.2 we briefly summarize the mapping between the supersymmetric model on the chain and the XXZ Heisenberg spin chain [23]. Borrowing these ideas, one can also find a mapping from the supersymmetric model on the zig-zag ladder to a spin chain. Similar to the chain, we map a site occupied by a fermion, including its four adjacent edges to a down-spin and the three edges between three empty sites to an up-spin (see figure 7.12). The length of the spin chain can therefore be written as $L = N - 2f$, where $N$ is the number of sites in the zig-zag ladder and $f$ the number of fermions. It follows from the mapping that a hop along a leg of the ladder corresponds to a spin flip between next-nearest neighbors, whereas a hop from one leg to the other corresponds to a spin flip between nearest neighbors. We thus find for the off-diagonal term in the supersymmetric model

$$\sum_i \left[ P_{<i>} \left( c_i^\dagger c_{i+1} + c_{i+1}^\dagger c_i \right) P_{<i+1>} \right]$$
$$\Longleftrightarrow$$
$$\sum_j \left[ \sigma_j^+ \sigma_{j+1}^- + \sigma_j^- \sigma_{j+1}^+ + \sigma_j^+ \sigma_{j+2}^- + \sigma_j^- \sigma_{j+2}^+ \right]$$

where the spin-flip operators are defined in terms of the usual Pauli matrices, $\sigma^{\pm} \equiv (\sigma^x \pm \imath\sigma^y)/2$. The diagonal term in the supersymmetric hamiltonian counts the number of empty next-nearest neighbor pairs, that is the number of sites (empty or occupied) surrounded by four empty sites. Under the mapping such a configuration either translates into a down-spin or into three neighboring up-spins. We thus find

$$\sum_i P_{<i>} \Longleftrightarrow \sum_j (1-\sigma_j^z)/2 + (1+\sigma_j^z)(1+\sigma_{j+1}^z)(1+\sigma_{j+2}^z)/8. \tag{7.11}$$

Working out the latter for a periodic spin chain of length $L$, we find

$$\sum_i P_{<i>} \Longleftrightarrow \frac{5L}{8} + \sum_{j=1}^{L} \left( -\frac{1}{4}\sigma_j^z + \frac{1}{4}\sigma_j^z\sigma_{j+1}^z + \frac{1}{8}\sigma_j^z\sigma_{j+2}^z + \frac{1}{8}\sigma_j^z\sigma_{j+1}^z\sigma_{j+2}^z \right). \tag{7.12}$$

Combining the results for the diagonal and off-diagonal terms we find that the supersymmetric model on the zig-zag ladder maps onto the following spin hamiltonian

$$\begin{aligned} H' &= \frac{1}{2}\sum_{j=1}^{L}\left[\sigma_j^x\sigma_{j+1}^x + \sigma_j^y\sigma_{j+1}^y + \frac{1}{2}\sigma_j^z\sigma_{j+1}^z\right] \\ &+ \frac{1}{2}\sum_{j=1}^{L}\left[\sigma_j^x\sigma_{j+2}^x + \sigma_j^y\sigma_{j+2}^y + \frac{1}{4}\sigma_j^z\sigma_{j+2}^z\right] \\ &- \frac{1}{4}\sum_{j=1}^{L}\sigma_j^z + \frac{1}{8}\sum_{j=1}^{L}\sigma_j^z\sigma_{j+1}^z\sigma_{j+2}^z + \frac{5L}{8}. \end{aligned} \tag{7.13}$$

We should warn the reader that this mapping is not one-to-one for the spectra. As for the chain the Hilbert spaces are not equal and one should account for the fermionic character of the particles in the supersymmetric model by imposing twisted boundary conditions in the spin chain.

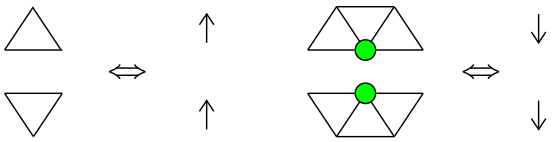

**Figure 7.12:** To map the supersymmetric model onto a spin chain, we identify a site occupied by a fermion, including its four adjacent edges to a down-spin and the three edges between three empty sites to an up-spin.

It is clear that the supersymmetric model on the zig-zag ladder maps to a rather involved and not very generic spin model. Nevertheless, it would be interesting to see if this relation can be exploited. In particular, it would be interesting to study the spin chain in the different sectors corresponding to different fillings in the supersymmetric model. In particular, the ground states at quarter filling map to a resonating valence bond state in the spin chain. These states are also known as the Majumdar-Ghosh states, which are known to be the ground states of a different, but related hamiltonian, namely the Majumdar-Ghosh hamiltonian [88]

$$H_{\mathrm{MG}} = \sum_i \left[ \vec{S}_i \cdot \vec{S}_{i+1} + \frac{1}{2}\vec{S}_i \cdot \vec{S}_{i+2} \right]. \tag{7.14}$$

Interestingly, quarter filling precisely corresponds to zero magnetic field ($\sum_{j=1}^{L} \sigma_j^z = 2f - L = 4f - N = 0$). The largest number of ground states occurs at 2/9 filling, which thus corresponds to optimal frustration in the spin chain. Based on the spectral flow analysis presented in the next section, we strongly believe that the model is quantum critical at this filling. Finally, at one fifth filling the system is expected to be gapped again. In the spin chain this may thus correspond to a phase transition as a function of the external magnetic field. There is clearly still a lot of room for a better understanding of this model and the mapping to the spin chain may provide a way to make progress and, at the same time, be an incentive to pursue these issues further.

## 7.5 Square ladder

Of the ladder realization of the square lattice considered here, the ground state structure of the square ladder is clearly the simplest. The number of ground states is 3 if the total number of sites is a multiple of 8 and the ground state is unique otherwise. Note that this periodic substructure resembles that of the chain. In this section we will try to explore this resemblance, by carrying out a further analysis of the square ladder, analogous to the analysis carried out for the supersymmetric model on the chain (see section 4.7).
Remember that for the superconformal models in the minimal series the Witten index reads $W_k = k+1$. From the fact that the Witten index is 3 (for ladder lengths $L = 4j$), a first guess for the continuum theory is the second ($k = 2$) superconformal minimal model. This guess is further supported by the fact that the supersymmetric model on the square ladder can also be seen as the plus-minus model on the chain. The plus-minus model is the supersymmetric model with two types of particles ("+" and "−"). The supercharge reads $Q = Q_+ + Q_-$, where $Q_+$ ($Q_-$) is a sum over all sites of the creation operators of the "+"-particle ("−"-particle). Clearly if we interpret the particles on the upper leg of the square ladder as "+"-particles and the particles on the lower leg of the square ladder as "−"-particles, the two models are identical. This picture agrees with the idea that the continuum theory has central charge $c = 3/2$. The bosonic part corresponds to the charge degrees of freedom and the fermionic part to the 'spin' degrees of freedom. Finally, entanglement entropy computations for the square ladder with open bc give $c \approx 1.5$ [66].
In the following we will test this first guess in more detail. We will see that we encounter a number of difficulties. It is not clear if these issues are finite size effects, or if our first guess is incorrect. In the last section we discuss the possibility that the continuum theory is a different $c = 3/2$ theory. Thus far this issue remains unresolved. We are optimistic, however, that further advanced numerical studies of the system can be successful in identifying the continuum theory. Clearly, the fact that the simplest guess seems too simple, makes this project all the more worthwhile.

### 7.5.1 First guess for the continuum theory

In this section we will discuss the second ($k = 2$) superconformal minimal model. The second superconformal minimal model has central charge $c = 3/2$, which means that it consists of a boson ($c = 1$) and a fermion ($c = 1/2$). The boson can be compactified on a circle with radius $R$. At $R = \sqrt{2}$ the conformal algebra is extended to an $\mathcal{N} = 2$ superconformal algebra. At this point the $c = 3/2$ conformal field theory precisely matches

the second superconformal minimal model [47, 89]. As explained above this is our first guess for the continuum limit of the supersymmetric model on the square ladder. In the following we will test this idea by comparing the spectrum of the continuum theory with finite size spectra for both periodic as well as open boundary conditions, just as we did for the chain (see section 4.7).

### Spectrum of the continuum theory

Let us start with the spectrum of the continuum theory. The partition function for the theory on the torus is composed of a bosonic part and a fermion part. The bosonic part for compactification radius $r$ reads

$$\Gamma(r) = \frac{1}{\eta\overline{\eta}} \sum_{m,n\in Z} q^{\frac{1}{2}(m/2r+nr)^2} \overline{q}^{\frac{1}{2}(m/2r-nr)^2}, \tag{7.15}$$

where $q = e^{2\pi\imath\tau}$ ($\tau$ is the modular parameter for the torus) and

$$\eta = q^{1/24} \prod_{n=1}^{\infty} (1-q^n). \tag{7.16}$$

The fermionic part is given by

$$Z_{\text{Ising}} = \frac{1}{2}\left(\left|\frac{\theta_3}{\eta}\right| + \left|\frac{\theta_4}{\eta}\right| + \left|\frac{\theta_2}{\eta}\right|\right), \tag{7.17}$$

where

$$\begin{aligned}
\sqrt{\frac{\theta_3}{\eta}} &= q^{-1/48} \prod_{n=1}^{\infty} (1+q^{n-1/2}) \\
\sqrt{\frac{\theta_4}{\eta}} &= q^{-1/48} \prod_{n=1}^{\infty} (1-q^{n-1/2}) \\
\sqrt{\frac{\theta_2}{\eta}} &= \sqrt{2} q^{1/24} \prod_{n=1}^{\infty} (1+q^n).
\end{aligned} \tag{7.18}$$

The partition function for $r = \sqrt{2}$ reads

$$\begin{aligned}
Z_{\text{circ}}(\sqrt{2}) &= \Gamma(\sqrt{2}) Z_{\text{Ising}} \\
&= (q^{-1/16} + q^{15/16} + \dots)\overline{q}^{-1/16} + (3 + 4q + \dots) + \\
&\quad (2q^{1/16} + \dots)\overline{q}^{1/16} + (2q^{3/16} + \dots)\overline{q}^{3/16} + \\
&\quad (2q^{1/4} + \dots)\overline{q}^{1/4} + (q^{7/16} + \dots)\overline{q}^{7/16} + \\
&\quad (q^{1/2} + \dots)\overline{q}^{1/2} + \dots
\end{aligned} \tag{7.19}$$

Due to the conventions used here the powers of $q$ and $\overline{q}$ correspond to the eigenvalues of $L_0 - 1/16$ and $\overline{L}_0 - 1/16$ respectively. The energy levels can thus be found from $Z_{\text{circ}}$ by summing the powers of $q$ and $\overline{q}$. We find the following energy levels

| Energy | degeneracy | sector |
|---|---|---|
| -1/8 | 1 | NS |
| 0 | 3 | R |
| 1/8 | 2 | NS |
| 3/8 | 2 | NS |
| 1/2 | 2 | R |
| 7/8 | 1 | NS |
| | ... | |

Let us check that this agrees with the spectrum of the second superconformal minimal model. The allowed conformal dimensions are (see section 3.4)

$$h = \frac{1}{16}, \frac{1}{16}, \frac{1}{16}, \frac{5}{16}, \frac{9}{16}, \frac{9}{16} \qquad \text{(R)}$$
$$h = 0, \frac{1}{8}, \frac{1}{8}, \frac{1}{4}, \frac{1}{4}, \frac{1}{2} \qquad \text{(NS)}.$$

For states with $h_L = h_R = h$ we thus find $E = 2h - 1/8$. For the first few values of the conformal dimensions this nicely reproduces the energies we obtained from the partition sum. The only subtlety is that the state with energy $E = 1/2$ is doubly degenerate in the Ramond sector, even though there is only one highest weight state with $h = 5/16$. The other state, however, can be obtained from this state using the supercharges. We also saw this for the first minimal model, where in the Ramond sector the non-zero energy highest weight state forms a quadruplet representation of the supersymmetry algebra (see section 4.7.1).

### Finite size scaling

We now consider the finite size spectra. We will consider the supersymmetric model on the square ladder of length $L = 4j$. For this length the system has three zero energy ground states when we impose periodic boundary conditions. These should correspond to the three Ramond vacua. For ladder lengths $L \neq 4j$ the system has only one zero energy ground state for periodic boundary conditions and, as for the chain, we expect these to correspond to twisted sectors of the continuum theory. For ladders of up to 32 sites we compute the spectra for periodic and anti-periodic boundary conditions. An example is shown in figure 7.14. Remember that the finite size scaling of the numerically obtained energy is given by

$$E_{\text{num}} = 2\pi v_F E_{\text{CFT}}/L + \mathcal{O}(1/L^2), \tag{7.20}$$

where $v_F$ is the Fermi velocity and $L$ is the length of the system. So we can extract $v_F$ from the energy of the Neveu-Schwarz vacuum for several system sizes and then determine the other energies, or conversely we can look at the ratios between the energy levels and the vacuum energy ($E_0$). We have computed the spectra for periodic and anti-periodic boundary conditions for ladders with 16, 24 and 32 sites and fitted each energy level as a function of the length to the function $E_{\text{num}} = a/L + b/L^3$ (an example is shown in figure 7.13). For the Neveu-Schwarz vacuum we obtain $a \approx -1.719$ which we define as $a_0$. For the other levels we show the results in table 7.2. Clearly, we do not find a good agreement.

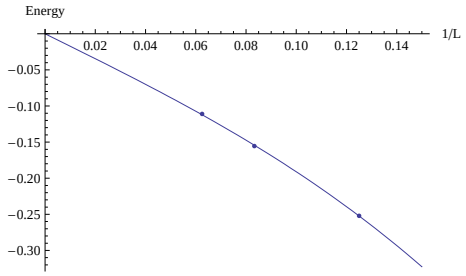


**Figure 7.13:** Energy of the NS vacuum plotted against $1/L$.

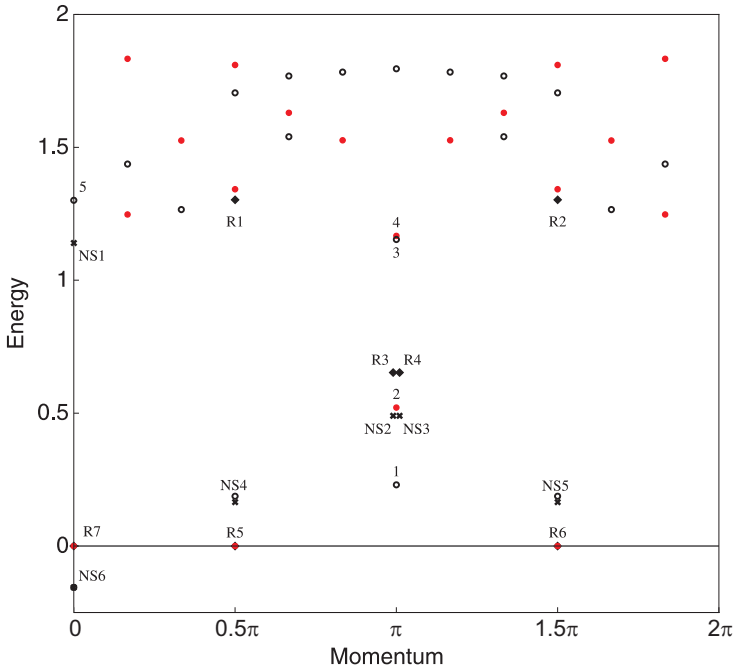


**Figure 7.14:** We show the spectra of the supersymmetric model on the square ladder with 24 sites and 6 particles for periodic and anti-periodic boundary conditions. The spectrum for (anti-) periodic boundary conditions is given by the red filled (black open) circles. The diamonds are highest weight states in the Ramond sector, the crosses are highest weight states in the NS sector (both are scaled with a fitted Fermi velocity according to (7.20))

### Spectral flow: avoided level crossings

Let us now look at the spectral flow analysis for the square ladder. In figure 7.15 we plot the spectra for twist parameter $\alpha$ between 0 and 1, with steps of 1/8. The discrepancy between the finite size scaling and the continuum spectrum can now be interpreted as an avoided level crossing as a function of the twist parameter. Remember that we also saw avoided crossings on the chain, however, in that case they were shown to vanish in the continuum limit (see section 4.8.1). Here the scaling analysis seems to suggest that the avoided crossing persists in the continuum limit.

**Table 7.2:** The first column gives the level labels corresponding to the labels in figure 7.14. The second column gives the ratio of the energy to the vacuum energy in the continuum theory (second superconformal minimal model). The third column gives the ratio of the fitted value for the energy to the fitted value for the vacuum energy. The last column gives the ratio of the energy to the vacuum energy in the continuum theory with $c = 3/2$, but now the orbifold line (see section 7.5.2).

| Label | Theory $E_{\mathrm{CFT}}/E_0$ ($r_{\mathrm{circ}} = \sqrt{2}$) | Fitted $a/a_0$ | Theory $E_{\mathrm{CFT}}/E_0$ ($r_{\mathrm{orb}} = 1$) |
|---|---|---|---|
| NS6 | 1 | 1 | 1 |
| NS4(=NS5) | -1 | -1.17 | -1 |
| 1 | -3 | -1.54 | -1 |
| 2 | -4 | -3.27 | -2 |
| 3 | -3 | -8.34 | -7 |
| 4 | -4 | -7.58 | -8 |
| 5 | -7 | -11.20 | -7 |

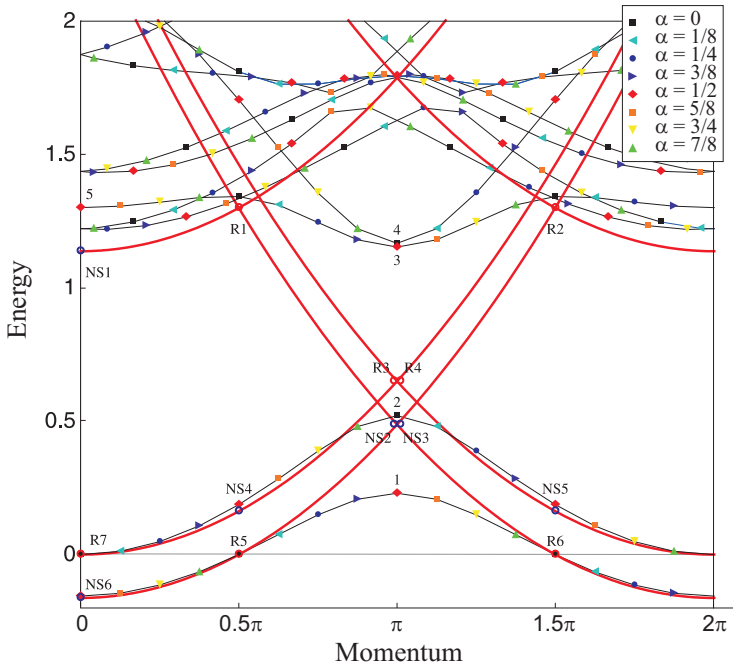


**Figure 7.15:** We plot the spectra for twist parameter $\alpha$ between 0 and 7/8, with steps of 1/8. The black line connects the levels for different values of the twist parameter. The red lines are the theoretical prediction for the spectral flow, open red circles correspond to the Ramond sector ($\alpha \in \mathbb{Z}$) and open blue circles correspond to the Neveu-Schwarz sector ($\alpha \in \mathbb{Z} + 1/2$).

### Open boundary conditions

For the square ladder with open boundary conditions we expect that the left- and right-moving modes are coupled, just as was found for the chain in section 4.9.1. In this section, we consider again our first guess for the continuum theory, namely the second superconformal minimal model. We first compute the spectrum of the continuum theory with coupled left- and right-moving modes and then compare this with the numerical analysis of the

finite size spectra of the lattice model. The boson compactified on a circle with radius $r = \sqrt{2}$ is represented by the operators

$$\Phi_m = e^{\imath m\phi/\sqrt{2}}, \tag{7.21}$$

with conformal dimension

$$h_m = m^2/4. \tag{7.22}$$

For the fermion we have the trivial representation 1, the fermion $\psi$ and the twist-field $\sigma$, with conformal dimensions $h_1 = 0$, $h_\psi = 1/2$ and $h_\sigma = 1/16$ respectively. The supercharges are given by

$$G^{\pm} = \psi e^{\pm\imath\sqrt{2}\phi}, \tag{7.23}$$

with conformal dimension $h = 1/2 + 1 = 3/2$.
Supersymmetry in the lattice model tells us that we are in the Ramond sector. There we have the following operator content: $\Phi_m$ and $\psi\Phi_m$ with $m \in Z+1/2$ and $\sigma\Phi_m$ with $m \in Z$. There are three highest weight states with zero energy, $\sigma\Phi_0$ and $\Phi_{\pm 1/2}$. The degeneracies of the levels generated from the highest weight states by the Virasoro algebra are given by

$$\begin{aligned}
\prod_{n=1}^{\infty}(1-q^n)^{-1}\prod_{j\geq 1}(1+q^j) &= 1 + 2q + 4q^2 + 8q^3 + 14q^4 + \ldots \text{ and} \\
\prod_{n=1}^{\infty}(1-q^n)^{-1}\prod_{j\geq 0}(1+q^{j+1/2}) &= 1 + q^{1/2} + q + 2q^{3/2} + 3q^2 + 4q^{5/2} + \ldots
\end{aligned} \tag{7.24}$$

in the sector with and without twistfield respectively. We can now construct the spectrum for $H = L_0 - c/24 = L_0 - 1/16$ as a function of $m$ (see figure 7.16).
Since the supercharge increases $m$ by two, we can make the following identification

$$\tilde{f} \equiv f - L/2 = (m + 1/2)/2, \tag{7.25}$$

where $L$ is the total number of rungs of the square ladder. In figure 7.17 we plot the sector for which $\tilde{f} = 0$, i.e. $m = 3/2 \mod 2$. The other sector present in the lattice model is $\tilde{f} = 1/2$, i.e. $m = 1/2 \mod 2$ (the blue spectrum in figure 7.16).
The sectors with twist field will probably correspond to the ladder with an odd number of sites. For $N = 4n + 1$, where $N$ is the number of sites, we find that the Witten index is zero. On the other hand, for $N = 4n - 1$ we find $|W| = 1$. If we compare this with (7.25), we find that the $m = 0$ sector (the black spectrum in figure 7.16) corresponds to $N = 4n - 1$ with $f = n$, whereas $m = 1$ and $m = -1$ (the yellow spectrum in figure 7.16) correspond to $N = 4n + 1$ with $f = n$ and $f = n + 1$ respectively.
In an unfinished study, we compared these finding to numerical data obtained with DMRG methods [66]. Preliminary results show similar issues as for periodic boundary conditions. In contrast with the results obtained for the chain with open boundary conditions (see figure 4.11), the spectra seem to contain various scales even for large system sizes. Furthermore, we investigated how the energy of the ground state depends on the fermion number.

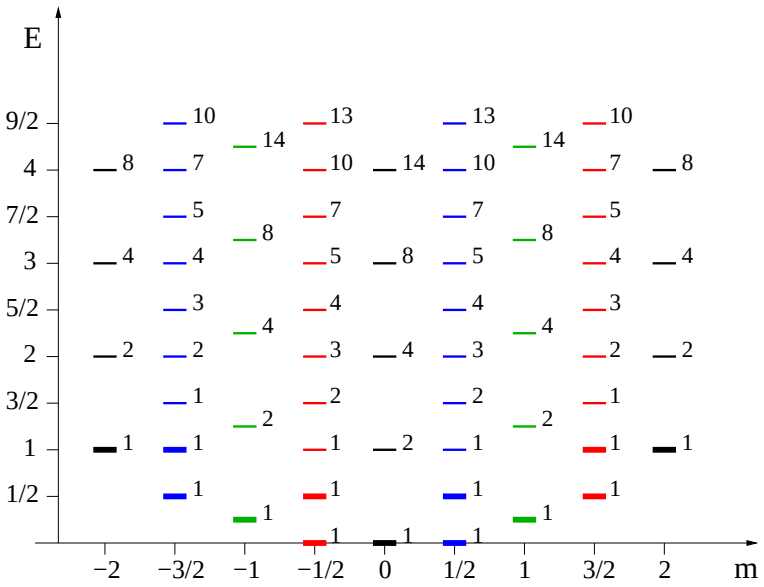


**Figure 7.16:** We show the spectrum of the second superconformal minimal model with $\mathcal{N} = 2$ supersymmetry. The energy $E = h - 1/16$ is plotted versus $m$. The level corresponding to the primary field and the levels that are generated from this field by the supercharge operators are indicated by a thick bar. The descendants are indicated by thinner bars. The label indicates the degeneracy of the levels. The color distinguishes sectors with different values for $m \mod 2$.

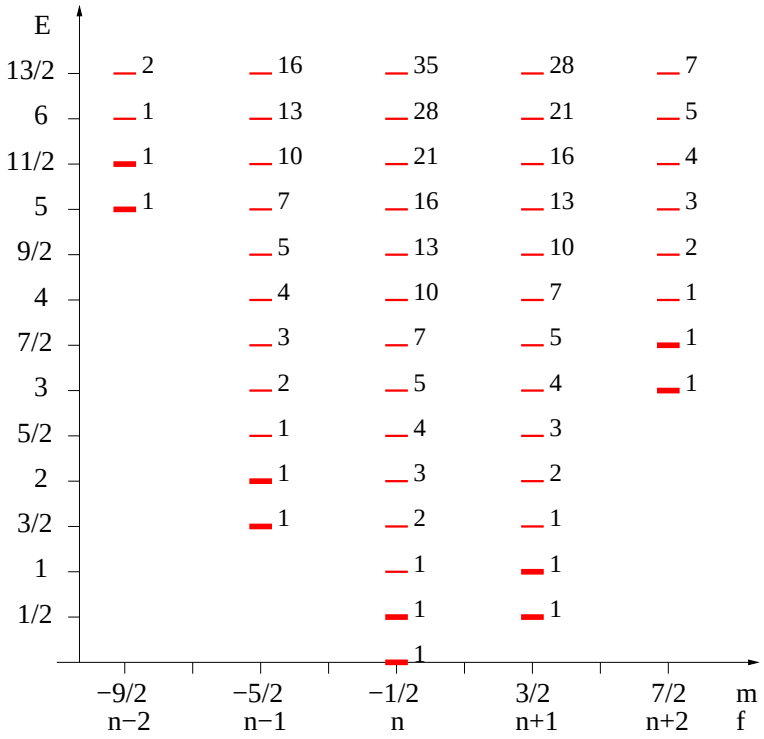


**Figure 7.17:** We show one sector of the spectrum of the second superconformal minimal model with $\mathcal{N} = 2$ supersymmetry.The energy $E = h - 1/16$ is plotted versus $m$ for $m = 3/2 \mod 2$, corresponding to a ladder with an even number of rungs $L = 2n$.

In the continuum theory we have $E = h_m - c/24 = m^2/(2r^2) - c/24$, which suggests a

parabolic dependence. Now let us define $m_0$ as follows: $m \equiv F - F_{GS} + m_0$, Since the energy is zero at $F = F_{GS}$, we find

$$\frac{m_0^2}{2r^2} = \frac{c}{24} \tag{7.26}$$

and thus

$$E_{GS}L = \frac{v_F \pi}{2r^2}\big((F - F_{GS})^2 + 2(F - F_{GS})m_0\big). \tag{7.27}$$

So $E_{GS}L$ should give a nice fit with $a(F - F_{GS})^2 + b(F - F_{GS})$. It follows that $b/a = 2m_0$, so we can extract $m_0$.
Upon comparison with the numerics, however, we find that such a fit does not seem to work well. Instead a much better fit is obtained when fitting $E$ for $F < F_{GS}$ and $F > F_{GS}$ separately. This is quite puzzling and suggests that the lack of a particle-hole symmetry in the lattice model may be at the source of all the discrepancies we find. To determine whether the lack of this symmetry just causes very persistent finite size effects or that the continuum theory is truly different is still an open question.

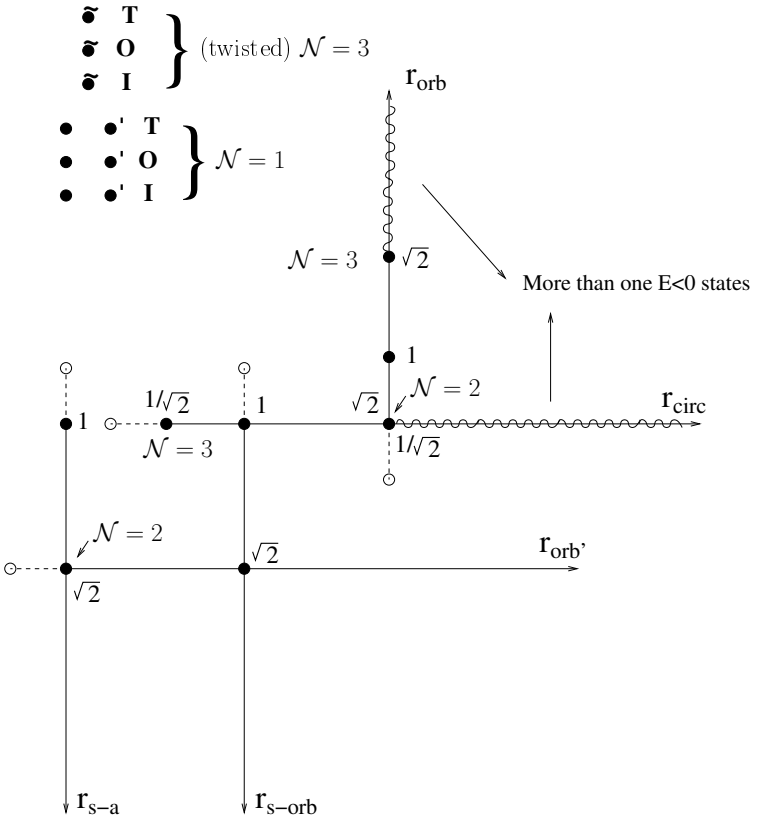


**Figure 7.18:** Survey of the $c = 3/2$ theories.

### 7.5.2 Other $c = 3/2$ theories

The superconformal minimal model with $k = 2$ is one of the theories with central charge $c = 3/2$. A survey of the $c = 3/2$ theories is given by Dixon, Ginsparg and Harvey in

[89] and is schematically depicted in figure 7.18. The second minimal model lies on the circle line at radius $r_{\text{circ}} = \sqrt{2}$. As we have seen, this theory is a promising candidate to describe the continuum limit of the square ladder, however, it runs into some trouble. Here we consider several other candidates and check a number of properties. The theory should have at least $\mathcal{N} = 2$ supersymmetry, three Ramond vacua and one negative energy state in the Neveu-Schwarz sector. Finally, for the theories on the orbifold line, we compare the higher energy states with the scaling analysis of the finite size spectra.
The following theories have at least $\mathcal{N} = 2$ supersymmetry.

- **The $\mathcal{N} = 2$ SUSY point on the super affine line**
  The $\mathcal{N} = 2$ supersymmtric point on the super affine line sits at $r = \sqrt{2}$. Its partition function is given in [89]. However, there are no zero energy states in the spectrum.
- **The $\mathcal{N} = 3$ SUSY point on the circle line at $r = 1/\sqrt{2}$**
  The $\mathcal{N} = 3$ supersymmtric point on the circle line at $r = 1/\sqrt{2}$ has just one zero energy state.
- **The (twisted) $\mathcal{N} = 3$ SUSY points $\tilde{T}$, $\tilde{O}$, $\tilde{I}$**
  The (twisted) $\mathcal{N} = 3$ supersymmtric points $\tilde{T}$, $\tilde{O}$ and $\tilde{I}$ have respectively 2, 3 and 2 zero-energy states and there are 3, 3 and 4 negative energy states respectively.
- **The (twisted) $\mathcal{N} = 3$ SUSY points on circle line with $r = n/\sqrt{2}$**
  The first two (twisted) $\mathcal{N} = 3$ supersymmtric points on the circle line sit at $r = 1/\sqrt{2}$, $r = \sqrt{2}$ and correspond to the second minimal model and its dual. For $n > 2$, we find $r^2/2 = n^2/4 > 1$ and thus there is more than one negative energy state (see the partition sum for the circle line (7.15)).

On the orbifold line there are three Ramond vacua, but the $\mathcal{N} = 2$ supersymmetry is broken to an $\mathcal{N} = 1$ supersymmetry. For certain values of the compactification radius, however, it is enhanced to $\mathcal{N} = 3$. The partition function on the orbifold line reads

$$Z_{\text{orb}}(r) = \frac{1}{2}(\Gamma(r) + \frac{|\theta_3\theta_4|}{\eta\overline{\eta}} + \frac{|\theta_2\theta_3|}{\eta\overline{\eta}} + \frac{|\theta_2\theta_4|}{\eta\overline{\eta}})Z_{\text{Ising}}. \tag{7.28}$$

The first terms of the $r$-independent part read

$$\begin{aligned}\frac{1}{2}(q\overline{q})^{-1/16} + \frac{5}{2} + 2(q\overline{q})^{1/16} + \frac{1}{2}(q\overline{q})^{7/16} + 4(q\overline{q})^{1/2} + \dots \\ -\frac{1}{2}(q^{15/16}\overline{q}^{-1/16} + h.c.) + 2(q + \overline{q}) + \dots\end{aligned} \tag{7.29}$$

The first terms of the $r$-dependent part read

$$\begin{aligned}\frac{1}{2}Z_{\text{Ising}}\Gamma(r) &= \Big(\frac{1}{2}(q\overline{q})^{-1/16} + \frac{1}{2} + \frac{1}{2}(q\overline{q})^{7/16} + \dots + \frac{1}{2}(q^{15/16}\overline{q}^{-1/16} + h.c.) \\ &\quad +(q + \overline{q}) + \dots\Big) * \sum_{m,n\in Z} q^{\frac{1}{2}(m/2r+nr)^2}\overline{q}^{\frac{1}{2}(m/2r-nr)^2} \\ &= \frac{1}{2}(q\bar{q})^{-1/16} + \frac{1}{2}(q\bar{q})^{0} + \frac{1}{2}(q\bar{q})^{7/16} \\ &\quad + \dots + \frac{1}{2}(q^{15/16}\overline{q}^{-1/16} + h.c.) + (q + \overline{q}) + \dots \\ &\quad +(q\bar{q})^{-1/16+1/(8r^2)} + (q\bar{q})^{1/(8r^2)} + (q\bar{q})^{7/16+1/(8r^2)} \\ &\quad +(q\bar{q})^{-1/16+r^2/2} + (q\bar{q})^{r^2/2} + (q\bar{q})^{7/16+r^2/2} + \dots\end{aligned}$$

So we obtain

$$\begin{aligned} Z_{\rm orb}(r) &= (q\bar{q})^{-1/16} + 3 + 2(q\bar{q})^{1/16} + (q\bar{q})^{7/16} + 4(q\bar{q})^{1/2} + \dots \\ &\quad +3(q+\bar{q}) + \dots + (q\bar{q})^{-1/16+1/(8r^2)} + (q\bar{q})^{1/(8r^2)} + (q\bar{q})^{7/16+1/(8r^2)} \\ &\quad +(q\bar{q})^{-1/16+r^2/2} + (q\bar{q})^{r^2/2} + (q\bar{q})^{7/16+r^2/2} + \dots \end{aligned} \tag{7.30}$$

We see that the levels that did not fit the finite size spectra are now $r$-dependent, except for the non-degenerate level with energy 7/8. The best fit follows from $r = 1$ (see table 7.2, last column), however there is just an $\mathcal{N} = 1$ SUSY at this point, which is not enough. The first $\mathcal{N} = 3$ SUSY point on the orbifold line occurs at $r = \sqrt{2}$, however there we find four Ramond vacua. For even larger radii there is more than one negative energy state. These negative energy states come from combining the first term in $Z_{\rm Ising}$ ($(q\bar{q})^{-1/48}$) with the first terms in $\Gamma(r)$, with $m$ small and $n = 0$ for larger values of $r$:

$$(q\bar{q})^{-1/48}(q\bar{q})^{-1/24} \sum_{m\in Z} q^{\frac{1}{2}(m/2r)^2} \bar{q}^{\frac{1}{2}(m/2r)^2}. \tag{7.31}$$

These have negative energy when $m^2 < r^2/2$.
We conclude that none of the theories considered in this section is a convincing candidate for the continuum theory of the square ladder. In particular, none of them seems to do better than our first guess, the theory on the circle line with $r_{\rm circ} = \sqrt{2}$. Identifying the low energy continuum theory of the supersymmetric model on the square ladder thus stands as an open problem.

# Chapter 8

# Discussion and outlook

## 8.1 Quantum criticality

We have seen that for a variety of one dimensional lattices, the model shows quantum critical behavior. For the chain this is in fact an exact result [22]. Here the model is integrable and in the continuum limit one can derive the thermodynamic Bethe Ansatz equations. From this is was found that the low energy spectrum in the continuum limit is described by the massless free boson at the $\mathcal{N} = 2$ supersymmetric point. In chapter 4 we investigate the continuum limit in great detail. Combining numerical and analytic results, we relate operators and sectors in the continuum theory, on the one hand, to lattice operators and chains with different boundary conditions on the other hand. Furthermore, the chain serves as a good model to test and develop the spectral flow analysis [34]. By relating a boundary twist in the lattice model to a spectral flow in the continuum theory, we can extract important parameters in the continuum theory from the numerics. This technique has several important pros. First of all, it tells us on a qualitative level that if the energy of a state has a parabolic dependence on the twist parameter, this is clear evidence of quantum criticality. Second of all, the analysis can be carried out in a single system, that is, no scaling of the size of the system is necessary. This is very useful in particular for systems with oscillations as a function of the number of sites (for the chain these oscillation have a period of only 3 sites, but for example for the 3 leg ladder discussed in chapter 7 this is 18 sites!). Finally, we find that the quantitative results extracted from the spectral flow analysis are quite accurate already in very small systems, at least for the lowest energy state. The only true con of the spectral flow analysis, is that it only gives ratios, consequently, it cannot be used to extract the value of the central charge.

In chapter 7 we apply the spectral flow analysis on various ladder models and find convincing evidence for critical modes in these systems. The ubiquity of criticality in the supersymmetric model on one dimensional lattices may suggest a deep relation with the imposed supersymmetry. Since quantum criticality usually occurs in an isolated point in the parameter space of interactions, it typically requires fine tuning. Here it seems that imposing supersymmetry, which indeed leads to fine tuning of the interactions, is a sufficient condition for criticality. In [90] this question is addressed for a specific lattice. It is argued that by tuning to the supersymmetric point, one lands on a multi-critical point, representing a phase transition between at least three different types of order. Although the reported results are very suggestive, further investigations are needed to confirm this hypothesis. Finally, there are also a few counter examples, where the supersymmetric model on a one dimensional lattice is gapped (the zig-zag ladder at quarter filling for example).

## 8.2 Ground states and tilings

The numerous results on the number of zero-energy ground states of the supersymmetric model, discussed in this thesis, suggest that there is a profound connection with tilings. For the square lattice there is an explicit relation between zero energy ground states of the supersymmetric model and tilings. However, this relation is not exclusive to the square lattice, but seems to be a more generic feature. In chapter 5, we discussed the work of Jonsson [39] which relates homology elements of $Q$ to tilings for the triangular and hexagonal lattice. In chapter 7, we encountered the kagomé ladder as yet another example. Moreover, there is compelling evidence from the zig-zag ladder that the tilings not only count, but indeed seem to dominate the actual ground states. In this section we wish to exploit this relation and discuss various possible implications for two dimensional systems.

### 8.2.1 Edge modes in the square lattice

For the square lattice we can exploit the effective geometric description of the space of ground states by comparing periodic and free boundary conditions [34]. This comparison suggests the existence of critical edge modes in the system. For the square lattice wrapped around the torus with $\vec{u} = (m, -m)$ and $\vec{v} = (n, n)$ the number of ground states grows exponentially with the linear system size, i.e. as $2^{2(n+m)/3}$ [38]. On the cylinder, however, if one cuts the torus open along the $(m, -m)$-direction only $2^{2n/3}$ ground states remain. Finally, if one also cuts the cylinder open along the $(n, n)$-direction one is left with a unique ground state on the plane.
What happens to this vast number of ground states that disappear upon changing the boundary conditions? Consider the picture in fig. 8.1. If one identifies the dotted, zig-zagged boundaries both in the horizontal as well as in the vertical direction, one finds that both the tiling with the drawn lines as well as the one with the dashed lines represent ground states. However, if one only identifies the left and right boundaries, then the tiling with the drawn lines no longer represents a ground state. Instead it has two defects at the edges, which can propagate along the edge. The only available scale for the energy of the edge mode is one over the length of the edge, which suggests that the edge modes are gapless.
Further evidence for the existence of these gapless edge modes comes from the spectral flow analysis of the ladder realizations of the square lattice. In all three cases compelling evidence for critical modes was found. The fact that the ladders are rather confined in one direction, suggests that they essentially probe the edge modes and we have thus confirmed that they are gapless. Whether there are also gapless modes in the bulk remains unclear from this analysis.
While the physical understanding of the quantum phase on the square lattice remains far from complete, we speculate on the following picture. The ground state corresponding to a given tiling has fermions that are confined to the area set by an individual tile, but quantum fluctuating within that space. Explicit support for this picture comes from the ground states of the zig-zag ladder at quarter filling (see section 7.4.1). The tiling based physical picture of the ground state wavefunctions is reminiscent of electrons in a filled magnetic Landau level, each of them effectively occupying an area set by the strength of the magnetic field. Critical edge modes naturally fit into a picture of this sort. In the

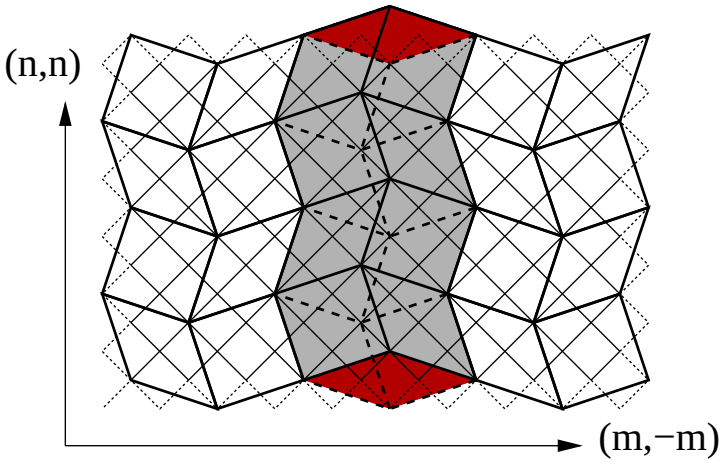


**Figure 8.1:** Edge modes.

next section, we briefly discuss the octagon-square lattice, which we propose as a suitable model to test these ideas.

### 8.2.2 Octagon-square lattice

As discussed in section 5.2.2, the octagon-square lattice is another 2D lattice where the supersymmetric model displays sub-extensive ground state entropy. The growth behavior of the numbers of ground states on the plane, cylinder and torus is similar to that of the square lattice. A big difference, however, is that here all ground states reside at 1/4 filling. This hugely simplifies the computation of the degeneracies. For the plane we find that the ground state is unique. For the cylinder with $M \times L$ square plaquettes, where $M$ is the number of square plaquettes along the periodic, horizontal direction and $L$ along the open, vertical direction, the number of ground states is $2^L$. Finally, for the torus the number of ground states is $2^M + 2^L - 1$ [21].
There is again a relatively simple physical picture which we propose as a basis for further analysis of physical properties [85]. This picture reflects the systematics uncovered by the analysis of the associated cohomology problem as well as results for small system sizes. The basic building block of the many-body ground states is the 1-fermion ground state on an isolated square plaquette. The unique many-body ground state on the plane essentially has individual fermions occupying this lowest 1-plaquette orbital, again allowing the analogy with a filled Landau level. Closing boundaries leads to the possibility that electrons on horizontal or vertical rows of plaquettes 'shift' into a second 1-fermion state, this way building up the total of $2^M + 2^L - 1$ ground states. This picture can be further substantiated by allowing defects, which can be brought in by adding diagonal links in individual plaquettes. The diagonal link in a plaquette could be interpreted as an additional magnetic flux through the plaquette. Indeed the effect of the defect on the number of ground states seems reminiscent of the effect of adding holes in a filled Landau level. In particular, the cohomology picture of these ground states suggests that these defects may have non-trivial braid properties.

At this point, these ideas are highly speculative and it is unclear whether the cohomology elements can truly reveal so much of the physics of the model. Among the key issues that are presently on the agenda for further study are: the existence of energy gaps, the presence of bulk or edge critical modes, and interactions and braiding properties of defects. Currently, we have joined forces with J. Vala and N. Moran to address some of these questions.

### 8.2.3 Bulk criticality

On a rather speculative note one may argue that the results for the square lattice suggest the existence of bulk critical modes for the triangular and hexagonal lattice. The argument goes as follows. For the square lattice the properties of the tilings tell us that to go from one tiling to another, one has to change (at least) all the tiles along a line that wraps around one direction of the torus. This statement in equivalent to the observation that the number of tiling grows exponentially with the linear size of the system. In contrast, for the triangular and hexagonal lattice there is compelling evidence that the number of ground states grows exponentially with the (two dimensional) volume of the system. Furthermore, also here, there is a relation between the ground states and tilings. If indeed all ground states can be represented by tilings, one would find that the different tilings are related via local moves of the tiles in order to account for the extensive ground state entropy. In analogy with the square lattice, we can then speculate that a local defect can drastically reduce the number of ground states, leading to a bulk critical mode. Whether this picture is correct, is obviously an extremely difficult question.

## 8.3 Extensions of the supersymmetric model

The models discussed in this thesis are all described by the same supersymmetric hamiltonian for hardcore spinless fermions. By considering different underlying lattices a whole class of models is generated, exhibiting a rich variety of properties, ranging from broken to unbroken supersymmetry to an exponential ground state degeneracy and from quantum critical to gapped to possibly topological phases.
However, there are many other ways to adjust the supersymmetric model, some of which we would like to mention here. Possibly the simplest generalization of the model is to allow for site-dependent coefficients in the definition of the supercharges:

$$Q = \sum_i \alpha_i c_i^\dagger \prod_{j \text{ next to } i} (1 - n_j) \quad Q^\dagger = \sum_i \alpha_i c_i \prod_{j \text{ next to } i} (1 - n_j), \tag{8.1}$$

with the $\alpha_i$ real numbers. It is easily verified that these generalized supercharges are still nilpotent. Also the hamiltonian constructed from these operators still consists of the same local terms. The parameters of the kinetic and potential terms, however, now depend on the coefficients $\alpha_i$. The hopping term from site $i$ to site $j$ next to $i$ is parametrized by $t_{ij} = \alpha_i \alpha_j$, the chemical potential becomes site dependent, $\mu_i = \alpha_i^2$ and also the two-body repulsive terms (and three- or four-body terms for D>1 dimensional lattices) acquire a similar site dependence. An interesting choice for the $\alpha_i$ is inspired by the chemical potential: choosing $\alpha_i = \alpha$ for $i \mod p = 0$ for some value of $p$ and setting $\alpha_i$ to unity for all other $i$, creates a lattice potential with a periodic staggering for the fermions.

For the one dimensional chain, for example, it is interesting to choose $p = 3$, since the ground states then take a very simple form in the limits $\alpha \to 0$ and $\alpha \to \infty$. Exploring such staggered versions of the supersymmetric model holds the promise of interesting new insights, especially if they are combined with our understanding of the ground states in terms of cohomology elements.
Since the supersymmetric model is motivated by the wish to understand phases of strongly correlated electrons, a natural generalization of the model is to incorporate spin. This was first considered in [91]. Insisting on an $SU(2)$ spin symmetry leads to an algebraic structure with $\mathcal{N} = 4$ rather than $\mathcal{N} = 2$ supersymmetry. They show that an $\mathcal{N} = 4$ supersymmetric model for itinerant spin-1/2 fermions in D=1 dimension can be constructed and the results indicate that this system describes a hole doped antiferromagnet. Unfortunately, the construction is rather involved and an extension to D>1 dimensions is still an open challenge. An intermediate step between spinless fermions and spin-1/2 fermions with a full $SU(2)$ symmetry, is to consider the supersymmetric model with two types of particles, suggestively called "+" and "−". This model is studied in [90] both on the D=1 dimensional chain[1] and on the D=2 dimensional copper-oxide lattice, which is the square lattice with one additional site on each link. Various (non-supersymmetric) limits of the model are investigated, leading to a very intriguing conjectured phase diagram.
Finally, we mention another $\mathcal{N} = 2$ supersymmetric model constructed from supercharges quite different from the ones considered in this thesis [92]. In this one dimensional model the lattice particles and their interactions are such that the excitations are cooper pairs with zero energy and free particles obeying exclusion statistics. This integrable model is closely related to the Haldane-Shastry chain [93], which is a variant of the Heisenberg model with long-range interactions. The degrees of freedom are two types of spinless free fermions with a non-trivial exchange statics between the two types. Each type of fermion is restricted to move on a chain, but the two chains are coupled to form a zig-zag ladder. Now the supercharges change a particle of type 1 into a particle of type 2 taking into account their mutual statistics. The model is analyzed in detail via Bethe ansatz, however, a number of the derived properties can be easily understood exploiting the supersymmetry. This leads to the idea that a supersymmetry preserving deformation of the model can be used to gap out the exclusons, while preserving the cooper pairs, resulting in a truly superconducting system.
Clearly, there are numerous other generalizations one may think of and it is reasonable to expect that the study of supersymmetric models in their various guises will lead to further interesting developments.

## 8.4 Superfrustration and black holes

The focus of the research presented in this thesis has been on the square lattice. We have found that this system only shows a sub-extensive ground state entropy. Nevertheless, we believe that the findings presented here may also have implications for the truly extensive cases. It is likely that we were able to obtain especially the exact result in D = 2, precisely because the square lattice is special and therefore simpler.
Recent developments in a seemingly unrelated field are the reason that we wish to make

[1] The "+/−" model on the chain is equivalent to the spinless model on the square ladder, see section 7.5.

some closing remarks on the superfrustrated systems. As was mentioned before an extensive ground state entropy, is in contradiction with the third law of thermodynamics, which says that as the temperature goes to zero, the entropy vanishes. Experimentally, indications for a developing zero temperature entropy have recently been observed in highly pure $Sr_3Ru_2O_7$ single crystals at magnetic field strengths for which the compound is believed to have a zero temperature quantum critical point [79] (see also [80] for a nice perspective). In [94], J. Zaanen relates this feature to observations in theoretical studies of condensed matter systems using the AdS/CFT-correspondence [95].
The AdS/CFT correspondence [96] is a conjectured -but generally accepted- mapping between a D dimensional theory with (quantum) gravity and a D-1 dimensional quantum field theory without gravity. The power of the correspondence is that it constitutes a duality between a strongly coupled theory on one side of the correspondence and a weakly coupled theory on the other side, thus providing a way to access the strong coupling regime of a quantum field theory. The rapidly growing field of AdS/CMT, which applies the AdS/CFT correspondence to condensed matter systems, has seen some recent successes. In particular, there is substantial evidence that the correspondence can be employed to describe a condensed matter system in the Fermi liquid phase [97, 98].
Interestingly, in trying to get AdS/CMT to work, physicists face the obstacle that the best understood examples of the AdS/CFT correspondence have supersymmetric large N gauge theories on the boundary, which are rather different from the theories one usually encounters in condensed matter theory. Furthermore, one typically finds an extremal black hole on the gravity side of the correspondence, which has the property that their mass and charge are equal. Additionally, these extremal black holes have a finite zero-temperature entropy, which translates into an extensive ground state entropy for the (supersymmetric) quantum field theory. The observed superfrustration in the supersymmetric model for lattice fermions indicates that the continuum theory of these systems should also exhibit this feature. It would be very interesting to investigate if the continuum theory of the supersymmetric lattice model could be a quantum field theory for which a weakly coupled gravitational dual exists. Clearly, if such a connection can be made and the supersymmetric lattice model can serve as a toy model to explore AdS/CMT, this would be quite spectacular.

# Bibliography


[1] L.D. Landau. The theory of a Fermi liquid. *Sov. Phys. JETP*, 3:920, 1956.

[2] P.W. Anderson. *Basic notions in condensed matter physics.* Benjamin, 1984.

[3] D. C. Tsui, H. L. Stormer, and A. C. Gossard. Two-dimensional magnetotransport in the extreme quantum limit. *Phys. Rev. Lett.*, 48(22):1559–1562, 1982.

[4] R. de Picciotto, M. Reznikov, M. Heiblum, V. Umansky, G. Bunin, and D. Hahalu. Direct observation of a fractional charge. *Nature*, 389:162, 1997.

[5] L. Saminadayar, D. C. Glattli, Y. Jin, and B. Etienne. Observation of the $e/3$ fractionally charged laughlin quasiparticle. *Phys. Rev. Lett.*, 79(13):2526–2529, 1997.

[6] Z.-X. Shen, D. S. Dessau, B. O. Wells, D. M. King, W. E. Spicer, A. J. Arko, D. Marshall, L. W. Lombardo, A. Kapitulnik, P. Dickinson, S. Doniach, J. DiCarlo, T. Loeser, and C. H. Park. Anomalously large gap anisotropy in the a-b plane of $Bi_2Sr_2CaCu_2O_{8+\delta}$. *Phys. Rev. Lett.*, 70(10):1553–1556, 1993.

[7] A. Damascelli, Z. Hussain, and Z.-X. Shen. Angle-resolved photoemission studies of the cuprate superconductors. *Rev. Mod. Phys.*, 75(2):473–541, 2003.

[8] V. J. Emery and S. A. Kivelson. Superconductivity in bad metals. *Phys. Rev. Lett.*, 74(16):3253–3256, 1995.

[9] C. Honerkamp and P. A. Lee. Staggered flux vortices and the superconducting transition in the layered cuprates. *Phys. Rev. Lett.*, 92(17):177002, 2004.

[10] S. Chakravarty, R. B. Laughlin, D. K. Morr, and C. Nayak. Hidden order in the cuprates. *Phys. Rev. B*, 63(9):094503, 2001.

[11] S. Martin, A. T. Fiory, R. M. Fleming, L. F. Schneemeyer, and J. V. Waszczak. Normal-state transport properties of $Bi_{2+x}Sr_{2-y}CuO_{6+\delta}$ crystals. *Phys. Rev. B*, 41(1):846–849, 1990.

[12] A. V. Puchkov, D. N. Basov, and T. Timusk. The pseudogap state in high-$T_c$ superconductors: an infrared study. *J. Phys.: Condens. Matter*, 8(48):10049–10082, 1996.

[13] C. M. Varma, P. B. Littlewood, S. Schmitt-Rink, E. Abrahams, and A. E. Ruckenstein. Phenomenology of the normal state of Cu-O high-temperature superconductors. *Phys. Rev. Lett.*, 63(18):1996–1999, 1989.

[14] J. Zaanen and O. Gunnarsson. Charged magnetic domain lines and the magnetism of high-$T_c$ oxides. *Phys. Rev. B*, 40(10):7391–7394, 1989.

[15] M. Troyer and U.-J. Wiese. Computational complexity and fundamental limitations to fermionic Quantum Monte Carlo simulations. *Phys. Rev. Lett.*, 94(17):170201, 2005.

[16] J. Zaanen, F. Krüger, J.-H. She, D. Sadri, and S. I. Mukhin. Pacifying the Fermi-liquid: battling the devious fermion signs. *Ir. J. Phys. Res.*, 8(2):39, 2008.

[17] S. Sachdev and M. Müller. Quantum criticality and black holes. *J. Phys.: Condens. Matter*, 21(16):164216, 2009.

[18] C. L. Henley and N.-G. Zhang. Spinless fermions and charged stripes at the strong-coupling limit. *Phys. Rev. B*, 63(23):233107, 2001.

[19] N. G. Zhang and C. L. Henley. Stripes and holes in a two-dimensional model of spinless fermions or hardcore bosons. *Phys. Rev. B*, 68(1):014506, 2003.

[20] U. Hizi and C. L. Henley. Hole on a stripe in a spinless fermion model. *Europhys. Lett.*, 65(2):228–234, 2004.

[21] P. Fendley and K. Schoutens. Exact results for strongly-correlated fermions in 2+1 dimensions. *Phys. Rev. Lett.*, 95:046403, 2005.

[22] P. Fendley, K. Schoutens, and J. de Boer. Lattice models with $\mathcal{N} = 2$ supersymmetry. *Phys. Rev. Lett.*, 90:120402, 2003.

[23] P. Fendley, B. Nienhuis, and K. Schoutens. Lattice fermion models with supersymmetry. *J. Phys. A*, 36:12399, 2003.

[24] L. Huijse and K. Schoutens. Superfrustration of charge degrees of freedom. *EPJ B*, 64:543–550, 2008.

[25] S. Sachdev. *Quantum phase transitions.* Cambridge University Press, 1999.

[26] For a review see M. R. Norman and C. Pepin. The electronic nature of high temperature cuprate superconductors. *Rep. Prog. Phys.*, 66(10):1547–1610, 2003.

[27] For a review see G. R. Stewart. Heavy-fermion systems. *Rev. Mod. Phys.*, 56(4):755–787, 1984.

[28] Th. Giamarchi. *Quantum physics in one dimension.* Oxford university press, 2004.

[29] H. Mutka. Proceedings of the Highly Frustrated Magnetism 2003 Conference. *J. Phys: Condens. Matter*, 16(11), 2004.

[30] E. Runge and P. Fulde. Charge degrees of freedom in frustrated lattice structures. *Phys. Rev. B*, 70(24):245113, 2004.

[31] J. Bagger, S. Duplij, and W. Siegel, editors. *Concise Encyclopedia of SUPERSYMMETRY and noncommutative structures in mathematics and physics.* Kluwer Academic Publishers, Dordrecht, 2003.

[32] E. Witten. Constraints on supersymmetry breaking. *Nucl. Phys. B*, 202(2):253–316, 1982.

[33] R. Bott and L.W. Tu. *Differential Forms in Algebraic Topology.* Springer Verlag, New York, 1982.

[34] L. Huijse, J. Halverson, P. Fendley, and K. Schoutens. Charge frustration and quantum criticality for strongly correlated fermions. *Phys. Rev. Lett.*, 101:146406, 2008.

[35] L. Huijse and K. Schoutens. Supersymmetry, lattice fermions, independence complexes and cohomology theory. *Adv. Theor. Math. Phys.*, 14.2, 2010. Preprint [ArXiv:0903.0784].

[36] P. Fendley, K. Schoutens, and H. van Eerten. Hard squares at negative activity. *J. Phys. A*, 38:315, 2005.

[37] J. Jonsson. Hard squares with negative activity and rhombus tilings of the plane. *Electr. J. Comb.*, 13(1):#R67, 2006.

[38] J. Jonsson. Hard squares on grids with diagonal boundary conditions. Preprint, 2006.

[39] J. Jonsson. Certain homology cycles of the independence complex of grid graphs. *Discrete Comput. Geom.*, 2010.

[40] R.J. Baxter. Hard hexagons: exact solution. *J. Phys. A: Math. Gen.*, 13:L61–L70, 1980.

[41] N. P. Warner. $\mathcal{N} = 2$ supersymmetric integrable models and topological field theories. In *High Energy Physics and Cosmology*, E. Gava, K. Narain, S. Randjbar-Daemi, E. Sezgin, and Q. Shafi (Eds.), page 143, 1993.

[42] Ph. Di Francesco, P. Mathieu, and D. Sénéchal. *Conformal field theory.* Springer Verlag, 1997.

[43] W. Boucher, D. Friedan, and A. Kent. Determinant formulae and unitarity for the $\mathcal{N} = 2$ superconformal algebras in two dimensions or exact results on string compactification. *Phys. Lett. B*, 172(3-4):316–322, 1986.

[44] P. Di Vecchia, J. L. Petersen, and H. B. Zheng. $\mathcal{N} = 2$ extended superconformal theories in two dimensions. *Phys. Lett. B*, 162(4-6):327–332, 1985.

[45] B. L. Feigin and D. B. Fuchs. Skew-symmetric differential operators on the line and Verma modules over the Virasoro algebra. *Functs. Anal. Prilozhen*, 16:47, 1982.

[46] B. L. Feigin and D. B. Fuchs. Verma modules over the Virasoro algebra. In *Topology, Proceedings of Leningrad conference, 1982, Lecture Notes in Mathematics*, L. D. Faddeev and A. A. Malcev (Eds.), volume 1060. Springer, New York, 1985.

[47] D. Friedan, Z. Qiu, and S. Shenker. Conformal invariance, unitarity, and critical exponents in two dimensions. *Phys. Rev. Lett.*, 52(18):1575–1578, 1984.

[48] Z.-A. Qiu. Nonlocal current algebra and $\mathcal{N} = 2$ superconformal field theory in two-dimensions. *Phys. Lett. B*, 188:207, 1987.

[49] A. Schwimmer and N. Seiberg. Comments on the $\mathcal{N} = 2, 3, 4$ superconformal algebras in two dimensions. *Phys. Lett. B*, 184(2-3):191–196, 1987.

[50] W. Lerche, C. Vafa, and N. P. Warner. Chiral rings in $\mathcal{N} = 2$ superconformal theories. *Nucl. Phys. B*, 324(2):427–474, 1989.

[51] M. Beccaria and G. F. De Angelis. Exact ground state and finite size scaling in a supersymmetric lattice model. *Phys. Rev. Lett.*, 94:100401, 2005.

[52] H. B. Thacker. Exact integrability in quantum field theory and statistical systems. *Rev. Mod. Phys.*, 53(2):253–285, 1981.

[53] D. Friedan and A. Kent. Supersymmetric critical phenomena and the two dimensional gaussian model. In Conformal Invariance and Applications to Statistical Mechanics, eds. C. Itzykson, H. Saleur, and J.B. Zuber (World Scientific, Singapore, 1988), pp. 578–579, 1988.

[54] G. Waterson. Bosonic construction of an $\mathcal{N} = 2$ extended superconformal theory in two dimensions. *Phys. Lett. B*, 171:77–80, 1986.

[55] I. Affleck. Field theory methods and quantum critical phenomena. In *Fields, strings, critical phenomena: proceedings of Les Houches Summer School in Theoretical Physics 1988.*, E. Brezin and J. Zinn-Justin (Eds.), volume Session 49. North-Holland, 1990.

[56] G. Veneziano and J. Wosiek. Planar quantum mechanics: an intriguing supersymmetric example. *JHEP*, 2006(01):156, 2006.

[57] G. Veneziano and J. Wosiek. A supersymmetric matrix model: III. hidden susy in statistical systems. *JHEP*, 2006(11):030, 2006.

[58] X. Yang and P. Fendley. Non-local spacetime supersymmetry on the lattice. *J. Phys. A: Math. Gen.*, 37(38):8937, 2004.

[59] G. Veneziano and J. Wosiek. A supersymmetric matrix model: II. exploring higher-fermion-number sectors. *JHEP*, 2006(10):033, 2006.

[60] A. Armoni, M. Shifman, and G. Veneziano. Exact results in non-supersymmetric large n orientifold field theories. *Nucl. Phys. B*, 667(1-2):170–182, 2003.

[61] P. Korcyl. Detailed study of a transition point in the Veneziano-Wosiek model of planar quantum mechanics. *Acta Phys. Pol.*, B38:3169–3180, 2007.

[62] M. Beccaria. On the supersymmetric vacua of the Veneziano-Wosiek model. *JHEP*, 2007(03):117, 2007.

[63] H. W. J. Blöte, J. L. Cardy, and M. P. Nightingale. Conformal invariance, the central charge, and universal finite-size amplitudes at criticality. *Phys. Rev. Lett.*, 56(7):742–745, 1986.

[64] I. Affleck. Universal term in the free energy at a critical point and the conformal anomaly. *Phys. Rev. Lett.*, 56(7):746–748, 1986.

[65] N. Yu and M. Fowler. Twisted boundary conditions and the adiabatic ground state for the attractive XXZ Luttinger liquid. *Phys. Rev. B*, 46(22):14583–14593, 1992.

[66] M. Campostrini. Private communication.

[67] C. Holzhey, F. Larsen, and F. Wilczek. Geometric and renormalized entropy in conformal field theory. *Nucl. Phys. B*, 424(3):443–467, 1994.

[68] G. Vidal, J. I. Latorre, E. Rico, and A. Kitaev. Entanglement in quantum critical phenomena. *Phys. Rev. Lett.*, 90(22):227902, 2003.

[69] P. Calabrese and J. Cardy. Entanglement entropy and quantum field theory. *J. Stat. Mech.*, 2004(06):P06002, 2004.

[70] V. E. Korepin. Universality of entropy scaling in one dimensional gapless models. *Phys. Rev. Lett.*, 92(9):096402, 2004.

[71] S. R. White. Density matrix formulation for quantum renormalization groups. *Phys. Rev. Lett.*, 69(19):2863–2866, 1992.

[72] S. R. White. Density-matrix algorithms for quantum renormalization groups. *Phys. Rev. B*, 48(14):10345–10356, 1993.

[73] U. Schollwöck. The density-matrix renormalization group. *Rev. Mod. Phys.*, 77(1):259–315, 2005.

[74] R.J. Baxter. Hard squares for $z = -1$. Preprint, 2007.

[75] M. Bousquet-Melou, S. Linusson, and E. Nevo. On the independence complex of square grids. *J. Alg. Comb.*, 27:423–450, 2008.

[76] A. Engström. Upper bounds on the Witten index for supersymmetric lattice models by discrete Morse theory. *Eur. J. Comb.*, 30(2):429–438, 2009.

[77] P. Csorba. Subdivision yields Alexander duality on independence complexes. *Electr. J. Comb.*, 16(2):#R11, 2009.

[78] H. van Eerten. Extensive ground state entropy in supersymmetric lattice models. *J. Math. Phys.*, 46:123302, 2005.

[79] A. W. Rost, R. S. Perry, J.-F. Mercure, A. P. Mackenzie, and S. A. Grigera. Entropy landscape of phase formation associated with quantum criticality in $Sr_3Ru_2O_7$. *Science*, 325(5946):1360–1363, 2009.

[80] Z. Fisk. The thermodynamics of quantum critical points. *Science*, 325:1348–1349, 2009.

[81] A. Sütö. Models of superfrustration. *Zeit. Phys. B Cond. Matt.*, 44(1):121–127, 1981.

[82] P. W. Kasteleyn. Dimer statistics and phase transitions. *J. Math. Phys.*, 4:287–293, 1963.

[83] F. Y. Wu. Remarks on the modified Potassium Dihydrogen Phosphate model of a ferroelectric. *Phys. Rev.*, 168(2):539–543, 1968.

[84] J. Jonsson. Hard squares with negative activity on cylinders with odd circumference. *Electr. J. Comb.*, 16(2):#R5, 2009.

[85] L. Huijse and K. Schoutens. Quantum phases of supersymmetric lattice models. In *XVITH International congress on mathematical physics*, P. Exner (Ed.), pages 635–639. World Scientific, 2010.

[86] D. L. Bergman, C. Wu, and L. Balents. Band touching from real-space topology in frustrated hopping models. *Phys. Rev. B*, 78(12):125104, 2008.

[87] M. E. Zhitomirsky and H. Tsunetsugu. Exact low-temperature behavior of a kagomé antiferromagnet at high fields. *Phys. Rev. B*, 70(10):100403, 2004.

[88] C. K. Majumdar and D. K. Ghosh. On next-nearest-neighbor interaction in linear chain. *J. Math. Phys.*, 10(8):1388–1398, 1969.

[89] L. Dixon, P. Ginsparg, and J. Harvey. superconformal field theory. *Nucl. Phys. B*, 306(3):470–496, 1988.

[90] L. van der Noort. Supersymmetric lattice models and quantum criticality. master thesis, 2007.

[91] R. Santachiara and K. Schoutens. Supersymmetric model of spin-1/2 fermions on a chain. *J. Phys. A: Math. Gen.*, 38(24):5425, 2005.

[92] P. Fendley and K. Schoutens. Cooper pairs and exclusion statistics from coupled free-fermion chains. *J. Stat. Mech.*, 2007(02):P02017, 2007.

[93] F. D. M. Haldane. Exact Jastrow-Gutzwiller resonating-valence-bond ground state of the spin-1/2 antiferromagnetic Heisenberg chain with $1/r^2$ exchange. *Phys. Rev. Lett.*, 60(7):635–638, 1988.

[94] J. Zaanen. A theoretical physicist journeys to a hairy black hole's horizon. Nature's journal club, 2009.

[95] S. A. Hartnoll, C. P. Herzog, and G. T. Horowitz. Holographic superconductors. *JHEP*, 2008(12):015, 2008.

[96] O. Aharony, S.S. Gubser, J. Maldacena, H. Ooguri, and Y. Oz. Large n field theories, string theory and gravity - the rac. *Phys. Rep.*, 323:183–386(204), 2000.

[97] M. Cubrovic, J. Zaanen, and K. Schalm. String theory, quantum phase transitions, and the emergent fermi liquid. *Science*, 325(5939):439–444, 2009.

[98] T. Faulkner, H. Liu, J. McGreevy, and D. Vegh. Emergent quantum criticality, fermi surfaces, and AdS2. Preprint [ArXiv:0907.2694v1 (hep-th)], 2009.

# Summary

In the past decades the study of solid state materials with strongly interacting electrons has become a major area of research. These materials exhibit exotic effects such as high temperature superconductivity and giant magnetoresistance. While extensively studied in the lab, these systems challenge our theoretical understanding, since traditional condensed matter techniques fail when analyzing strongly interacting electrons. Due to the strong interactions, these systems are truly governed by many-body effects, rendering descriptions based on perturbation theory unreliable. It is well known that for fermionic particles, such as electrons, the analysis of many-body physics is plagued by sign problems.

This thesis describes a lattice model for itinerant spin-less fermions with strong repulsive interactions. A judicious tuning of the kinetics and the interactions of the fermions leads to models possessing supersymmetry. Quite remarkably, the notion of supersymmetry, which was developed in the context of high energy physics, turns out to be a powerful tool in the analysis of strongly correlated itinerant fermions. In the model discussed here, the supersymmetry induces a subtle competition between the kinetics, on the one hand, and the strong repulsive interactions, on the other hand. As a result the system realizes its lowest energy states in a regime where both the kinetics as well as the interactions play an important role. It is precisely this regime that is unaccessible via traditional techniques. Supersymmetry, however, provides us with a rich mathematical structure that can be employed to derive rigorous results for some of the key features of the model.

The supersymmetric model was first introduced by P. Fendley, K. Schoutens and J. de Boer in 2003 [22]. A variety of results for this model on one and two dimensional lattices was known at the time the research for this thesis started. In 1D it was shown that the supersymmetric model on the chain is quantum critical, with the low energy continuum limit described by an $\mathcal{N} = (2, 2)$ superconformal field theory. On 2D lattices one generically finds superfrustration, a strong form of quantum charge frustration leading to an extensive ground state entropy. A heuristic understanding of superfrustration was given by the "3-rule": to minimize the energy, fermions prefer to be mostly 3 sites apart. For generic two dimensional lattices the 3-rule can be satisfied in an exponential number of ways. This picture was supported by a remarkable relation found by J. Jonsson between quantum ground states of the supersymmetric model and tilings of the lattice.

The main subject of this thesis is the supersymmetric model on the square lattice. First of all, inspired by the work of J. Jonsson, we establish a rigorous mathematical result which relates quantum ground states to certain tiling configurations on the square lattice. Due to supersymmetry, the quantum ground states of the model are in one-to-one correspondence with cohomology elements. To compute the cohomology is in general very difficult, however, using a spectral sequencing technique this problem can be cut into several smaller problems. For the square lattice with periodic boundary conditions all these sub-problems

turn out to be non-trivial, rendering the proof of the ground state-tiling theorem rather involved. From this theorem, however, we obtain a closed expression for the total number of ground states on the square lattice and the number of particles in each ground state. For periodic boundary conditions we find that the number of ground states grows exponentially with the linear dimensions of the system, leading to a sub-extensive ground state entropy. We furthermore find that the ground states occur for densities between $1/5$ and $1/4$.

Second of all, we find substantial analytic and numerical evidence that for the square lattice with open boundary conditions the system has gapless edge modes. For this result we built on the understanding of the supersymmetric model on the 1D chain. Numerical studies of this system provide a detailed relation between the lattice model on the one hand, and its continuum description, a superconformal field theory, on the other hand. In particular, we relate a boundary twist in the lattice model to a spectral flow in the superconformal field theory. This relation is not exclusive to the chain. Consequently, the analysis of a boundary twist, or spectral flow analysis, is an important new technique to investigate the supersymmetric model. By applying this spectral flow analysis to ladder realizations of the square lattice, we find compelling evidence for quantum criticality in these systems. Furthermore, by combining the ground state-tiling relation with our findings for the ladder models, we arrive at a picture in which the tilings not only count the number of ground states, but actually dominate the ground state wavefunctions. This picture allows us to propose the existence of critical edge modes in the supersymmetric model on the two dimensional square lattice with a boundary.

Finally, combining these two results, the ground state-tiling relation on the one hand, and the results for the ladders on the other hand, we conclude that the supersymmetric model on the square lattice exhibits a novel phase. This phase is characterized by a sub-extensive ground state entropy and edge criticality. The work in this thesis underlines the intricate relation between supersymmetry on the one hand, and criticality and quantum charge frustration on the other hand, thereby making the supersymmetric model a promising system for future research.

# Samenvatting

De meeste materialen om ons heen zijn goed begrepen. Ze zijn onder te verdelen in elektrisch geleidende en isolerende materialen, zoals bijvoorbeeld koper en plastic, en halfgeleiders, zoals silicium. In de vaste fase zijn de atomen, waaruit het materiaal is opgebouwd, gekristalliseerd en worden de materiaaleigenschappen gedomineerd door de elektronen die het zwakst aan de atoomkern gebonden zijn. Materialen kunnen dus beschreven worden door slechts te kijken naar deze elektronen. De atoomkernen worden vrijwel volledig buiten beschouwing gelaten, ze vormen slechts een achtergrond waarin de elektronen kunnen bewegen en wisselwerken. Zo'n versimpelde weergave van een materiaal, dat een complex geheel is van atoomkernen en elektronen die allerlei krachten op elkaar uitoefenen, noemen we een roostermodel, of kortweg, model. Gewone materialen, zoals koper, aluminium en silicium, kunnen worden beschreven met een model waarin de elektronen nauwelijks krachten op elkaar uitoefenen. In de afgelopen decennia zijn er echter verschillende materialen ontdekt met bijzondere eigenschappen, die theoretisch nog slecht begrepen zijn. De oorzaak voor dit achterblijvende begrip ligt in het feit dat de elektronen in deze materialen elkaar sterk afstoten en dus sterk wisselwerken. Dit proefschrift beschrijft een model voor elektronen met sterke wisselwerking.

Het begrijpen van elektronen met sterke wisselwerking is niet alleen belangrijk vanuit het perspectief van de fundamentele natuurkunde, maar maakt uiteindelijk ook de weg vrij voor technologische vooruitgang. Een mooi voorbeeld is de ontdekking van het GMR-effect (voor *giant magnetoresistance*), waarvoor in 1997 de Nobelprijs voor de natuurkunde is uitgereikt. Dit effect -een grote verandering in elektrische weerstand zodra een sterk magneetveld wordt aangelegd- wordt veroorzaakt door de sterke wisselwerking van de elektronen in het materiaal. De commerciële toepassing van dit effect heeft geleid tot een dramatische toename in de opslagcapaciteit van harde schijven. Een ander voorbeeld is supergeleiding; het verschijnsel dat de elektrische weerstand van sommige materialen beneden een bepaalde temperatuur opeens helemaal verdwijnt. Supergeleiding treedt bij de meeste materialen pas op wanneer ze worden afgekoeld tot nabij het absolute nulpunt (-273 graden Celcius). Er zijn echter materialen die bij een relatief hoge temperatuur supergeleidend zijn. Het record ligt momenteel rond -140 graden Celcius. Deze materialen bestaan uit een gelaagde structuur van onder andere koperoxide vlakken. In deze koperoxide vlakken is de wisselwerking tussen de elektronen zeer sterk. Supergeleiders vinden nu al hun toepassing in, bijvoorbeeld, telecommunicatie, waar ze worden gebruikt om de capaciteit van het netwerk te vergroten. Het moge duidelijk zijn dat de ontdekking van een materiaal dat bij kamertemperatuur supergeleidt, een technologische revolutie tot gevolg zal hebben.

Er zijn veel verschillende materialen waarvan de eigenschappen niet goed begrepen zijn, elk materiaal heeft zijn eigen details, maar de grote gemene deler is steeds dat de elek-

tronen in die materialen sterk met elkaar wisselwerken. Deze eigenschap moet dus zeker in een model, dat dit soort materialen beschrijft, terugkomen. Het probleem is echter dat traditionele technieken om aan modellen te rekenen niet werken wanneer de elektronen sterk wisselwerken. Het is dus van belang nieuwe technieken te verkennen. In 2003 hebben P. Fendley, K. Schoutens en J. de Boer een nieuw model voorgesteld voor elektron-achtige deeltjes met sterke wisselwerking. Dit model heeft een bijzondere eigenschap die het mogelijk maakt buiten de gebaande paden te treden. Deze eigenschap is supersymmetrie, een symmetrie die oorspronkelijk is geïntroduceerd in de deeltjesfysica. Door het introduceren van een symmetrie wordt het vaak makkelijker om een probleem te benaderen. Het is bijvoorbeeld een stuk makkelijker om je weg te vinden op Manhattan dan in het centrum van Rome. Het stratennetwerk van Mahattan is ontworpen als een grid met veel symmetrie, terwijl in Rome alle straten kris-kras door elkaar lopen. In het model van Fendley et al. leidt supersymmetrie tot een aantal bijzondere eigenschappen en vergroot het de mogelijkheden voor theoretische analyse. Hoewel het bestuderen van dit model zeker kan bijdragen aan een beter begrip van materialen waarin de elektronen sterk wisselwerken, is het belangrijk om op te merken dat het een zeer specifiek model is. De elektron-achtige deeltjes zijn bijvoorbeeld geen echte elektronen, maar een soort cartoon voorstelling daarvan. Bovendien is de wisselwerking tussen deze deeltjes op een bepaalde manier gekozen en dus niet heel generiek.

Dit proefschrift beschrijft het model van Fendley et al. voor het geval dat de deeltjes zich bewegen in een vierkant rooster (een grid net zoals ruitjes papier). Dit rooster ontstaat door de (zeer zwakke) wisselwerking van de elektronen met de atoomkernen in het kristalrooster. Het is belangrijk om het vierkante rooster te bestuderen, omdat het in materialen een veel voorkomende kristalstructuur is. We hebben in het bijzonder gekeken naar de toestanden met de laagste energie. Deze zogenaamde grondtoestand bepaalt voor een groot deel de eigenschappen van het materiaal. Voor een skater in een halfpipe is de laagste energie toestand, de toestand waarin de skater in het midden van de halfpipe stilstaat. Wanneer er echter heel veel skaters zijn, zodat ze niet meer allemaal in het midden passen, dan wordt het al ingewikkelder om te bepalen wat precies de laagste energie toestand is. Stel nu dat die skaters ook nog hard beginnen te duwen als iemand te dichtbij komt (een soort sterke wisselwerking) dan wordt het nog complexer. In het model dat wij bestuderen is er bovendien nóg een complicatie, de elektronen zijn namelijk kwantummechanische deeltjes, waardoor hun plaats en snelheid niet precies bepaald zijn. Hier biedt de supersymmetrie echter uitkomst: deze zorgt er namelijk voor dat de grondtoestanden gevonden kunnen worden door geavanceerde technieken uit de wiskunde te gebruiken.

Eén van de belangrijkste resultaten van dit proefschrift is het bewijs van een stelling die het lastige, kwantummechanische probleem van het vinden van de grondtoestand van dit model vertaalt naar een veel simpeler probleem. Stel dat de elektronen bewegen in een vierkant rooster van een bepaalde grootte, tien bij tien hokjes bijvoorbeeld, dan zegt de stelling dat het aantal grondtoestanden voor dit geval gevonden kan worden door te tellen op hoeveel mogelijke manieren je dit rooster van tien bij tien hokjes kan betegelen. Voor het maken van een betegeling mogen slechts vier soorten tegels gebruikt worden, deze staan weergegeven op de omslag van dit proefschrift. Verder werkt het net als het betegelen van een badkamer: de tegels mogen niet overlappen en er mogen ook geen spleten tussen zitten. Het vinden van een betegeling en zeker het aftellen van alle mogelijkheden is dus even puzzelen, maar vele malen simpeler dan het oorspronkelijke probleem uit de kwantummechanica. Dit is precies de kracht van de stelling. Bovendien blijkt uit deze

stelling, dat dit model een zeer bijzonder materiaal beschrijft dat niet één unieke grondtoestand heeft, zoals verre weg de meeste materialen, maar eindeloos veel laagste energie toestanden. Dit is een bijzondere vorm van frustratie; de sterke afstotende wisselwerking van de deeltjes zorgt ervoor dat er heel veel manieren zijn waarop de laagste energie bereikt kan worden.
Naast het bewijs van deze stelling, beschrijft dit proefschrift ook een numerieke analyse van de supersymmetrische modellen. Door gebruik te maken van computersimulaties van het model enerzijds, en begrip uit de deeltjesfysica anderzijds, hebben we kunnen aantonen dat het model een materiaal beschrijft dat in bepaalde gevallen zeer goed stroom geleidt. Dit is het geval wanneer het rooster waarop de deeltjes bewegen in één richting heel smal is, waarbij de deeltjes dus eigenlijk op een lijn bewegen. Door deze resultaten te combineren met de stelling voor de grondtoestanden, die niet alleen geldt wanneer de deeltjes op een lijn bewegen, maar ook wanneer ze in het vlak bewegen, kunnen we concluderen dat het model waarschijnlijk een materiaal beschrijft dat nog een bijzondere eigenschap heeft. Niet alleen heeft het materiaal heel veel grondtoestanden, bovendien is het waarschijnlijk zo dat als je een elektrische stroom door het materiaal wil laten lopen, deze stroom niet in het materiaal kan doordringen, maar wel langs de rand kan lopen. Dit is een bijzondere eigenschap die experimenteel voor verschillende materialen, waarin de elektronen sterk wisselwerken, is waargenomen.
De bevindingen in dit proefschrift laten duidelijk zien dat sterke wisselwerking tussen de elektronen inderdaad kan leiden tot bijzondere materiaaleigenschappen. Voor het behalen van deze resultaten was het ontwikkelen van nieuwe technieken essentieel. Of het bestudeerde model ook daadwerkelijk een materiaal beschrijft dat we op een bepaald moment in onze hand kunnen houden (of misschien al eens gehad hebben!) zal nog moeten blijken.

# Dankwoord

In de vier jaar dat ik aan dit proefschrift heb gewerkt, zijn er heel veel mensen geweest die me hebben geïnspireerd, gemotiveerd, gesteund en geholpen. Op deze laatste pagina's wil ik hen hiervoor graag bedanken.

In de eerste plaats wil ik mijn promotor, Kareljan Schoutens, bedanken. Kareljan, ik kan met volle overtuiging zeggen dat ik me geen betere begeleider zou kunnen wensen. Je hebt me geïntroduceerd in een fascinerend vakgebied en me aangestoken met je enthousiasme. Vanaf het allereerste moment heb je me volledig serieus genomen als onderzoeker, zelfs toen ik dat zelf nog totaal niet deed. Dit heeft mij enorm gestimuleerd om zelfstandig te werken en mijn intuïtie voor natuurkunde te ontwikkelen. Op conferenties heb je geen gelegenheid voorbij laten gaan om me aan collega's voor te stellen. Het netwerk dat ik hierdoor heb kunnen opbouwen, is voor mij van onschatbare waarde. Tenslotte heb ik enorme bewondering voor je professionaliteit. Je hebt het, zeker sinds je directeur bent, vaak onzettend druk en ook wel eens met vervelende dingen, maar chagerijnig heb ik je nooit gezien. Ik heb heel veel van je geleerd en genoten van onze samenwerking, dank je wel!

In the second place, I would like to thank Paul Fendley. During the past four years we have met on several occasions, the first time being even before I started my PhD as I passed through Charlottesville on a road trip. Soon after that we started discussing via e-mail. You taught me many things and handed me various interesting ideas. Your replies were almost instant and always very illuminating. During our visit to Oxford, I experienced your energy and enthusiasm "live". These interactions have been of great value and inspiration for me. They also led to a fruitful collaboration. On the last day of our visit, you challenged me to take all the responsibility for writing the paper if I wanted to be first author. I thank you for giving me this opportunity.

I would also like to thank Jim Halverson for his contribution to this collaboration. It was a pleasure exchanging ideas and data with you. I hope we will have the chance to meet in person one time.

Then I would like to thank Jakob Jonsson. Thank you for thoroughly reading the proof of the ground state-tiling theorem. Your comments definitely improved the manuscript. Thank you also for hosting me at your group seminar and for the inspiring discussions about the triangular lattice. I really wonder if this case will ever be cracked, I'm sure we will be in touch about this.

Closer to home, at least at the start of this period, I would like to thank Pasquale Calabrese. Thank you for your advise on practical matters, your suggestions for my research, in particular on entanglement entropy and of course, the yellow pages, the caciocavallo and many other things. In het laatste jaar van mijn promotie was Thomas Quella mijn vraagbaak voor vragen over CFT. Thomas, bedankt voor je interesse in onze modellen en

voor je vele heldere antwoorden op mijn vragen. Ook Bernard Nienhuis wil ik bedanken voor menig verhelderende discussie. In de eerste plaats natuurlijk over de susy modellen en betegelingen, maar ook over vele andere dingen, van studenten tot magnetische bolletjes. Je hebt me meer dan eens ergens een compleet andere kant van doen inzien. Erik Verlinde wil ik bedanken voor het meedenken over de éénpuntsfuncties. Onze discussies hebben me veel inzicht gegeven en hebben bovendien geleid tot een leuk resultaat. Jesper Romers wil ik bedanken voor de leuke samenwerking aan een voor mij totaal nieuw onderwerp in mijn laatste jaar.
Balt van Rees en Bahar Mehmani, bedankt dat jullie mijn partners in crime waren bij het opzetten van de social club. Ook de leden van de andere social clubs wil ik bedanken voor een leuke samenwerking: Antje Ludewig, Joost Overtoom, Alessia Gasparini, Richard Newell, en de rest. Balt, niet alleen als Sinterklaas, maar ook als kamergenoot, was je erg goed gezelschap. Naast de nodige afleiding op z'n tijd, heb ik ook veel gehad aan onze gesprekken over natuurkunde.
Dan wil ik Jesper Romers en Johannes Oberreuter bedanken voor de strakke en inspirerende samenwerking bij het organiseren van de CFT cursus. Erik Verlinde, Jan de Boer, Thomas Quella en Kareljan Schoutens, bedankt voor het geven van een serie steengoeie colleges. Eddy Ardonne, bedankt voor het meedenken op de achtergrond (en natuurlijk, geheel ongerelateerd, voor ons fantastische bezoek aan Stockholm).
Het bestuur van de LOTN wil ik bedanken voor een leerzame periode als lid van het promovendi-overleg. De andere leden van het overleg, bedankt voor de leuke samenwerking bij het organiseren van de PhD-Days.
Verder wil ik de vele collega's bedanken, die van de afgelopen jaren een leuke, interessante tijd hebben gemaakt: Alessia, Alex, Antje, Antoine, Aron, Bahar, Balazs, Balt, Benoit, Dolf, Guillaume, Jean-Sébastien, Jesper, Johannes, Joost, Jorn, Keiichi, Laura, Lotte, Marc, Michiel, Milosz, Raoul, Richard, Rob, Salima, Salvo, Sander, Sasha, Shanna, Sheer, Thomas, Tom, Vincent, Wieteke, Xerxes. Ook voor de gezelligheid en voor de ondersteuning bij personeels en administratieve zaken, bedankt Yocklang, Bianca, Sandra, Jonneke, Paula en Lottie.
Af en toe ontspannen en alles van een afstandje bekijken is natuurlijk essentieel geweest in deze periode. Vrijmibo's waren vaste prik. Michelangelo en Nienke als harde kern, regelmatig aangevuld met andere graaggeziene gasten, zeeverkenners, haarlemmerdijkgangers, de nerds, de meisjes, klimmers-soms allang niet meer-, kunstenaars en natuurlijk altijd veel Barleanen en heel veel oeverloos gelul. Op vakantie naar Normandië, wandelen en skiën in Zwitserland met bijkomen in Basel, eten in Naarden of toch uit in Amsterdam, Olstival, zeilen in Friesland, standaard naar de sneak, eten op de Atalanta, haken op de bank, dancing with the girls, op het bootje door de grachten, paardrijden in Olst en natuurlijk Pom en Mees. Etentjes bij Eric met al Tom z'n vrienden en soms Tom zelf, waarbij een zak chips noodzaak is, omdat het -altijd heerlijke- eten nooit voor elf uur op tafel staat. Mijn paranimfen Marieke en Maurice. Hoewel heel verschillend, hebben jullie met elkaar gemeen dat ik jullie allebei al heel lang ken en dat ik altijd bij jullie terecht kan. En dan natuurlijk Michiel, in Olst, in Delft, in Amsterdam, in Groningen, altijd anders, soms heel inspirerend en leuk, soms ook niet, maar dat kan als broer en zus. Bedankt voor jullie gezelligheid, steun en interesse in waar ik mee bezig was!
Pauline en Frits, lieve jongens, zonder jullie was het natuurlijk nooit zover gekomen. Van kleins af aan hebben jullie me gestimuleerd en tegelijk vrij gelaten om mijn eigen weg te vinden. Ik heb genoten van onze vele gesprekken over dit proefschrift en alles eromheen,

van waardevolle adviezen en serieuze pogingen de inhoud te behappen tot vreselijke slappe lach om ... ja, wat niet eigenlijk? Maar het belangrijkste is dat jullie er altijd voor me zijn.
Tot slot, Tobias, jij weet als geen ander dat ik het zonnetje *uit* huis ben. Thuis kwam alle stress, spanning en onzekerheid eruit. Soms moest je troosten, soms met rust laten, dan weer tot de orde manen, geen makkelijke taak. Maar ik heb ontzettend veel aan je steun gehad. Dankzij jou heb ik meer bereikt en gedaan en dan ik zelf had gedurft. Dank je, m'n lief!